INAUGURAL – DISSERTATION
zur
Erlangung der Doktorwürde
der Naturwissenschaftlich-Mathematischen Gesamtfakultät
der
Ruprecht – Karls – Universität
Heidelberg

vorgelegt von

Master of Science:	Simon Gawlok
aus:	Lübeck
Tag der mündlichen Prüfung:	.....

Numerical Methods for Compressible Flow with Meteorological Applications

Betreuer: Professor Dr. Vincent Heuveline

Zusammenfassung

In dieser Arbeit werden die kompressiblen Navier-Stokes-Gleichungen, welche die Dynamik in einer trockenen Atmosphäre beschreiben, hergeleitet. Basierend auf einer Skalenanalyse für Strömungen bei kleiner Mach-Zahl wird die Low-Mach-Approximation der kompressiblen Navier-Stokes-Gleichungen hergeleitet, indem der hydrodynamische Anteil des Druckes, der im Vergleich zu den hydrostatischen und thermodynamischen Anteilen klein ist, im Gesetz für ideale Gase vernachlässigt wird. Beide Modelle werden mit Finiten Elementen im Raum und Finiten Differenzen in der Zeit diskretisiert, wobei alle gemeinsamen Diskretisierungsparameter identisch gewählt werden, um Einflüsse auf die diskreten Lösungen durch die jeweilige Diskretisierung zu minimieren. Für beide Modelle wird ein Lösungsansatz basierend auf einem inexakten Newton-Verfahren vorgestellt, wobei die linearen Löser und ihre Vorkonditionierer an das jeweilige Modell angepasst sind. Im Falle des Low-Mach-Modells wird eine Vorkonditionierungstechnik vorgeschlagen, die auf geschachtelten Schur-Komplementen basiert. Als Benchmark-Problem wird ein Szenario zweier interagierender tropischer Wirbelstürme beschrieben, anhand dessen die Lösungen der beiden Modelle hinsichtlich numerischer und physikalischer Aspekte verglichen werden. Die gewonnenen numerischen Ergebnisse zeigen die Skalierbarkeit und Robustheit des Lösungsansatzes. Für das betrachtete Szenario zeigen die vorhergesagten Sturmtrajektorien des Low-Mach-Modells eine sehr gute Übereinstimmung mit denen des kompressiblen Navier-Stokes-Modells, bei signifikant geringeren Kosten bezüglich der Rechenzeit, so dass die Low-Mach-Approximation für diesen Fall als gültig angesehen werden kann.

Abstract

In this work, the compressible Navier-Stokes equations describing the dynamics of a dry atmosphere are derived. Based on a scale analysis for Low-Mach number flows, the Low-Mach approximation is derived from the compressible Navier-Stokes equations by neglecting the hydrodynamic part of pressure, which is small compared to the hydrostatic and thermodynamic parts, in the ideal gas law. Both models are discretised by finite elements in space and finite differences in time, where all common parameters of the discretisations are chosen identically in order to minimise influences on the discrete solutions due to differences in the respective discretisation. A solution strategy for both models based on an inexact Newton method is presented, where the linear solvers and preconditioners are adapted to the respective model. In case of the Low-Mach model, a preconditioning technique based on nested Schur complement iterations is proposed. A scenario of two interacting tropical cyclones is presented as benchmark problem in order to compare the solutions of the two models in terms of numerical as well as physical properties. The obtained numerical results show the scalability and robustness of the solution approach. For the considered scenario, the predicted tracks of the cyclones, which are computed by the Low-Mach model, show very good coincidence with those of the Compressible Navier-Stokes model at significantly smaller computational costs, such that the Low-Mach approximation can be regarded as valid in this case.

Acknowledgements

First and foremost I want to thank my advisor Prof. Dr. Vincent Heuveline. It has been a great honour for me to be his Ph.D. student at the Faculty of Mathematics and Computer Science at Heidelberg University. I am very happy, that he gave me the chance to work on topics at the interface of mathematics and meteorology, which has been a great dream of mine since I attended my first numerics lectures. I want to express my deepest thankfulness for his kind support, his motivation and his patience. I have always enjoyed our fruitful scientific and visionary discussions.

Great thanks are further dedicated to the Faculty of Mathematics and Computer Science and the Interdisciplinary Centre for Scientific Computing at Heidelberg University for their infrastructural and professional support. This work was partly funded by the BMBF project HD(CP)^2. I want to thank all the collaborators for the excellent cooperation and the chance to have an insight into their research. Furthermore, I want express my gratitude towards the Jülich Supercomputing Centre (JSC) (grants HKA14 and HKA15) as well as the Heidelberg University Computing Centre (URZ) for the granted computing resources on their clusters. Without these resources it would not have been possible to achieve the results of this thesis.

I owe my colleagues of the Engineering Mathematics and Computing Lab (EMCL) a big "Thank you". Their company, open ears, good ideas and great social spirit helped me through all phases of the challenge Ph.D. Big thanks are further devoted to Mrs Mehra for pulling the strings behind the scenes and having all organisational and formal aspects always in mind.

Finally, I want to express my special thanks to those who supported and motivated me beyond the world of science: My family, my friends and, especially, my wife Judith.

To my family.

Contents

List of Figures

List of Tables

1. Introduction

The formation of clouds and precipitation processes occupy a central role in current research about climate change. Compared to the temporal and spatial scales of global climatic phenomena, e.g., the gulf stream – several thousand kilometres in space and months in time –, these processes often occur on small scales, i.e., a few hundred meters in space and some minutes or hours in time. Among these processes shower or weak tornadoes are typical examples. Another example, where local weather forecasts with high precision in space and time are needed, are severe storms like tropical cyclones. Based on precise and fast numerical forecasts, emergency management has the chance to evacuate precisely affected regions in time for saving human lives.

In order to fulfil these demands in a computer-aided forecast, extremely fine scales with respect to both space and time are needed compared to the current state of the art [24]. The cells in the discrete spatial grid have to be small enough such that single clouds are covered by at least one whole cell, for example, see Figure 1.1. The increase in spatial resolution leads to a proportional rise in the demands of compute power. Consequently, the usage of supercomputers becomes inevitable. To exploit the provided compute power optimally, appropriate parallel algorithms have to be developed. Recent studies [10] show, that with an increasing number of used processor cores in a supercomputer the main part of the overall consumed computing time is spend in communication between the nodes of the cluster, whereas the local computations on each node consume less time with an increasing number of processor cores and new generations of processors. Therefore, the solution process for atmospheric dynamics needs to be based on methods, which provide the solution with a minimum effort in terms of communication, while featuring excellent mathematical properties in terms of robustness and rate of convergence, for example.

Furthermore, it has to be noticed, that the applied algorithms and solution schemes are highly demanding with respect to the spatial and temporal resolutions themselves in order to provide accurate results in a stable and robust way. *Stable* in the context of this thesis means, that the solution remains bounded for bounded given data, i.e., initial and boundary data as well as parameters. These demands arise due to the mathematical properties of the underlying physical model. Especially, the spatial and temporal resolutions are coupled in the sense, that the size of the discrete time-step may not exceed a certain value, which decreases with increasing wind-speed and decreasing size of the spatial cells. Therefore, high-resolution simulations, as for the scenarios mentioned above, lead to a significant increase of the required number of time-steps, while simultaneously the computational costs per time-step grow notably, too. The precise value and the strength the described coupling depends strongly on the applied time-stepping scheme.

In current models for numerical weather and climate prediction a main source for restrictions on the time-step size is the fact, that the underlying simulation of the fluid dynamics is based on the compressible Navier-Stokes equations [24, 25]. These equations are valid for all Mach numbers and they consider all sources of compressibility, i.e., changes in density due to both temperature and pressure variations. Therefore, these equations do not only resolve the velocity field of interest, but also the sound of wind, which is caused by density variations on very small temporal and spatial scales. These variations are mainly caused by changes in the pressure. But for many relevant atmospheric fluid flows, only the velocity field at Mach numbers much smaller

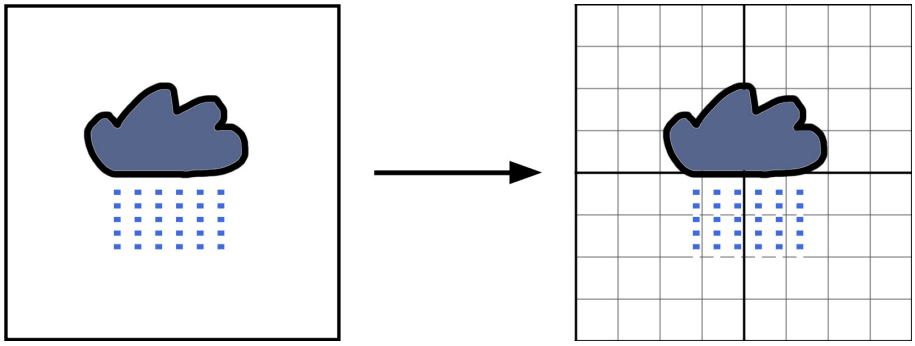

Figure 1.1.: Resolving a cloud in a numerical simulation by sufficiently refining the computational grid.

than one is of interest and not the acoustic modes of the fluid flow. A scale analysis for flows at Mach numbers smaller than one shows, that density variations are mainly due to temperature differences and that certain parts of the pressure are negligible in the equation for the density. This leads to the so called *Low-Mach number approximation*. Equations of these type have been studied since the 1980s [3, 4, 13, 40, 52].

Considering the above demands and the induced problems, the objective of this thesis is defined as follows. Based on the fully compressible Navier-Stokes equations for the dry atmosphere, a Low-Mach model based on the Low-Mach number approximation is derived. Both models for flows in a dry atmosphere are discretised by finite elements in space and a finite difference scheme in time, which is a mixture of the implicit Euler and Crank-Nicolson time-stepping schemes. The spatial finite element discretisations as well as the weights in the time-stepping scheme are chosen identically in order to minimise differences between the respective solutions due to the spatial and temporal discretisations. Both models are compared for the case of two interacting tropical cyclones on a domain with a horizontal extent of several thousand kilometres. The key question is, how many times larger the time-step size for the Low-Mach model can be chosen compared to the fully Compressible Navier-Stokes model and, consequently, which factor in the number of time-steps can be saved in order to simulate a certain period of time. Of course, the time to compute one time-step of the Low-Mach model needs to be at least less than the time for one time-step of the fully Compressible Navier-Stokes model times the factor in the time-step sizes in order to provide the desired solution in less overall simulation time. The respective solutions are then analysed in terms of numerical aspects, i.e., the needed computational costs, as well as physical aspects, i.e. the predicted storm tracks. Ideally, the Low-Mach model is by factors faster than the fully Compressible Navier-Stokes model and would, therefore, allow either finer resolutions at the same computational costs or yield the result of a simulation for a fixed problem size in a shorter time span, by simultaneously providing a very good approximation without significant differences in the predicted solutions.

A similar comparison for a moist atmosphere was recently published in [26], but for different scenarios and on smaller spatial scales. To the best of the knowledge of the author, this thesis provides the first comparison of these specific models for a scenario of two interacting tropical cyclones on a large domain with a size of several thousand kilometres in the horizontal. Furthermore, in contrast to [26], the spatial discretisation is based on finite elements (finite volumes in [26]) and a fully implicit time-stepping scheme (predictor-corrector scheme in [26]) is applied. Typically, implicit schemes allow larger time-steps than explicit or semi-implicit methods, but

robust and efficient non-linear as well as linear solvers are needed to resolve the implicit description of the solution at the next time-step. The resulting non-linear algebraic equations describing the dynamics from one time-step to the next one are solved by a Newton method. To solve the arising linear systems in each Newton iteration, a preconditioned (Flexible) Generalized Minimum Residual ((F)GMRES) method is used, where in the case of the Low-Mach model a preconditioning technique based on nested Schur complements is proposed. This preconditioner – to the best of the knowledge of the author – has not been reported in the context of Low-Mach number approximations so far in the literature. The proposed preconditioners are combined of components where the necessary scaling properties, see the above discussion, have been reported in the literature, namely parallel algebraic multigrid techniques [30, 32, 33, 55, 77, 78], which ideally provide convergence rates independently of the spatial resolution. Therefore, the presented solvers promise to be scalable solution approaches, if the configurations of all components are optimized properly.

The remainder of this thesis is organised as follows: In Chapter 2, the fully compressible Navier-Stokes equations for dry atmospheric dynamics are derived from basic conservation principles and their discretisation based on finite elements in space and finite differences in time is described. Subsequently, the Low-Mach approximation is applied to the fully compressible Navier-Stokes equations in Chapter 3, yielding the Low-Mach equations of dry atmospheric dynamics. Furthermore, the discretisation of the Low-Mach model is described. The solution methodology for both models is presented in Chapter 4. Chapter 5 contains the description of the considered benchmark scenario, namely the interaction of two tropical cyclones. Then, the obtained numerical results are discussed and analysed in Chapter 6. Finally, the findings of this thesis are summarized in Chapter 7 and an outlook on possible further research, that evolves from this thesis, is given.

2. Compressible Navier-Stokes equations

Contents

The dynamics of atmospheric flows of air are described by the fully compressible Navier-Stokes equations in most current state-of-the-art numerical models for weather forecasting and climate prediction [24, 25]. Based on the conservation of momentum and mass, the thermodynamic energy equation and the ideal gas law, these equations model the dynamic evolution of wind velocity as well as density, temperature and pressure of air. Due to the ideal gas law, variations of density are coupled to variations in both temperature and pressure. Especially, these equations are valid for all Mach numbers. Therefore, also fast acoustic modes, which are physically irrelevant in many meteorological scenarios of interest, are resolved. As a consequence, the maximum discrete time-step size in a numerical solver is limited, because the stability conditions of the applied time-stepping scheme have to be met under the constraint, that fast acoustic modes may appear in a flow at hand. This fact motivates the Low-Mach number approximation, which is described in the next Chapter.

As there is no assumption made on the considered wind speeds – i.e., in contrast to the Low-Mach models the derivation of the fully compressible Navier-Stokes equations is valid for *all* wind speeds –, the solutions of the fully compressible Navier-Stokes equations will serve as *reference solutions* against which those of the Low-Mach model have to compete. Furthermore, the equations, as they are introduced here, provide an idealised description of atmospheric dynamics, because they are only valid for dry processes, i.e., moist processes, heating due to radiation as well as chemical reactions, for example, are neglected. On the one hand, this allows a clearer presentation and, on the other hand, minimises influences on the fluid dynamics due to external effects. Therefore, the characteristic property of the equations – the presence of acoustic modes – is preserved and differences between the models are purely due to the underlying model for the fluid dynamics.

In Section 2.1, the fully compressible Navier-Stokes equations are derived from the aforementioned basic physical principles. Subsequently, these equations are put to a weak setting in Section 2.2. On this basis, a discretisation based on finite elements in space and finite differences in time is introduced in Section 2.3.

2.1. Derivation

In this section, the system of compressible Navier-Stokes equations is derived on the basis of the textbook [46]. [46] provides excellent descriptions of the underlying physical processes and quantities. Therefore, the precise physical descriptions given there are adopted here. The derivation is restricted to the case of dry atmosphere. For further details, see [46]. The derivation of the material derivative is based on [27], and the derivation of the continuity equation on [51].

2.1.1. Momentum equation

The momentum equation is derived from *Newton's second law of motion*

$$F = ma,$$

where F is a force ($[N]$) acting on a body with mass m ($[kg]$) and a is the acceleration ($\left[\frac{m}{s^2}\right]$) of the body. When applying it to the atmosphere and fixing a parcel of air, Newton's second law of motion can be written in vector valued form as

$$\mathbf{a}_i = \frac{1}{m_a} \sum \mathbf{F}, \tag{2.1}$$

where $\mathbf{a}_i$ is the *total or inertial acceleration*, m_a is the mass of the parcel of air, and $\sum \mathbf{F}$ is the sum of the forces exerted on the fixed parcel. Inertial acceleration describes the rate of change of velocity of a parcel of air relative to a coordinate system fixed in space (outside the Earth-atmosphere system), i.e., in Eulerian coordinates.

The mathematical definition of inertial acceleration is

$$\mathbf{a}_i := \frac{\mathrm{d}\mathbf{v}_A}{\mathrm{d}t} + \boldsymbol{\Omega} \times \mathbf{v}_A, \tag{2.2}$$

where $\mathbf{v}_A$ denotes the *absolute velocity* of a body near the Earth's surface and is given by

$$\mathbf{v}_A = \mathbf{v} + \boldsymbol{\Omega} \times \mathbf{R}_e, \tag{2.3}$$

where $\mathbf{v} := (u, v, w)^\top$ is the local velocity of a body relative to the surface of the Earth, $\mathbf{\Omega}$ is the angular velocity vector for Earth, $\mathbf{R}_e$ is the radius vector for the Earth, and $\mathbf{\Omega} \times \mathbf{R}_e$ is the rate of change in position of the body due to the Earth's rotation.

$\mathbf{\Omega}$ is independent of time and the total derivative of $\mathbf{R}_e$ is

$$\frac{\mathrm{d}\mathbf{R}_e}{\mathrm{d}t} = R_e \frac{\mathrm{d}\mathbf{k}_r}{\mathrm{d}t} \approx \mathbf{v}, \tag{2.4}$$

where R_e is the Earth's radius (m) and $\mathbf{k}_r$ is the corresponding unit vector.

Remark 2.1 (Time derivatives of unit vectors)
The conversions between the increments of horizontal distance in Cartesian coordinates and increments of horizontal distance in spherical coordinates are given as follows (cf. [46]). The conversion in west-east direction is given by

$$\mathrm{d}x = (R_e \cos\varphi)\, \mathrm{d}\lambda_e \tag{2.5}$$

and the conversion in south-north direction by

$$\mathrm{d}y = R_e \mathrm{d}\varphi, \tag{2.6}$$

respectively. $\mathrm{d}\lambda_e$ denotes the west-east longitude increment in radians, $\mathrm{d}\varphi$ denotes the south-north latitude increment in radians, and $R_e \cos\varphi$ is the distance from the Earth's axis of rotation to the surface of the Earth at latitude φ. Furthermore, the following derivatives of the unit vectors in spherical coordinates can be derived (cf. [46]):

$$\begin{aligned}
&\frac{\partial \mathbf{i}_\lambda}{\partial \lambda_e} = \mathbf{j}_\varphi \sin\varphi - \mathbf{k}_r \cos\varphi, && \frac{\partial \mathbf{i}_\lambda}{\partial \varphi} = 0, && \frac{\partial \mathbf{i}_\lambda}{\partial z} = 0,\\
&\frac{\partial \mathbf{j}_\varphi}{\partial \lambda_e} = -\mathbf{i}_\lambda \sin\varphi, && \frac{\partial \mathbf{j}_\varphi}{\partial \varphi} = -\mathbf{k}_r, && \frac{\partial \mathbf{j}_\varphi}{\partial z} = 0,\\
&\frac{\partial \mathbf{k}_r}{\partial \lambda_e} = \mathbf{i}_\lambda \cos\varphi, && \frac{\partial \mathbf{k}_r}{\partial \varphi} = \mathbf{j}_\varphi, && \frac{\partial \mathbf{k}_r}{\partial z} = 0.
\end{aligned} \tag{2.7}$$

Substituting (2.5) into (2.19) gives the *total* or *material derivative in spherical-altitude coordinates*:

$$\frac{\mathrm{d}}{\mathrm{d}t} = \partial_t + \frac{u}{R_e \cos\varphi}\partial_{\lambda_e} + \frac{v}{R_e}\partial_\varphi + w\partial_z. \tag{2.8}$$

Applying (2.8) to $\mathbf{i}_\lambda$ gives

$$\frac{\mathrm{d}}{\mathrm{d}t}\mathbf{i}_\lambda = \partial_t \mathbf{i}_\lambda + \frac{u}{R_e \cos\varphi}\partial_{\lambda_e}\mathbf{i}_\lambda + \frac{v}{R_e}\partial_\varphi \mathbf{i}_\lambda + w\partial_z \mathbf{i}_\lambda. \tag{2.9}$$

It holds $\partial_t \mathbf{i}_\lambda = 0$, because $\mathbf{i}_\lambda$ does not change in time at any location. Substituting this observation as well as terms from (2.7) into (2.9) and into like expressions for $\frac{\mathrm{d}}{\mathrm{d}t}\mathbf{j}_\varphi$ and $\frac{\mathrm{d}}{\mathrm{d}t}\mathbf{k}_r$, respectively, yields

$$\begin{aligned}
\frac{\mathrm{d}}{\mathrm{d}t}\mathbf{i}_\lambda &= \mathbf{j}_\varphi \frac{u\tan\varphi}{R_e} - \mathbf{k}_r \frac{u}{R_e},\\
\frac{\mathrm{d}}{\mathrm{d}t}\mathbf{j}_\varphi &= -\mathbf{i}_\lambda \frac{u\tan\varphi}{R_e} - \mathbf{k}_r \frac{v}{R_e},\\
\frac{\mathrm{d}}{\mathrm{d}t}\mathbf{k}_r &= \mathbf{i}_\lambda \frac{u}{R_e} + \mathbf{j}_\varphi \frac{v}{R_e}.
\end{aligned} \tag{2.10}$$

The last equality in (2.10) yields the approximative equality in (2.4).

Thus, substituting (2.3) into (2.2) yields

$$\mathbf{a}_i = \frac{\mathrm{d}\mathbf{v}}{\mathrm{d}t} + 2\boldsymbol{\Omega} \times \mathbf{v} + \boldsymbol{\Omega} \times (\boldsymbol{\Omega} \times \mathbf{R}_e) = \mathbf{a}_l + \mathbf{a}_c + \mathbf{a}_r, \tag{2.11}$$

where

$$\mathbf{a}_l := \frac{\mathrm{d}\mathbf{v}}{\mathrm{d}t}, \quad \mathbf{a}_c := 2\boldsymbol{\Omega} \times \mathbf{v}, \quad \mathbf{a}_r := \boldsymbol{\Omega} \times (\boldsymbol{\Omega} \times \mathbf{R}_e) \tag{2.12}$$

are *local*, *Coriolis* and Earth's centripetal accelerations, respectively.

Local acceleration is the rate of change of velocity of a parcel of air in motion relative to a coordinate system fixed on earth. *Coriolis acceleration* is the rate of change of velocity of a parcel due to the rotation of a spherical Earth underneath the parcel. *Earth's centripetal acceleration* is the inward-directed rate of change of velocity of a parcel due to its motion around the Earth's axis.

The terms on the right hand side of (2.1) are so called *real forces*. The local acceleration of a parcel of air is affected by the gravitational force (*true gravitational force*), the force arising from local differences in the pressure of air (*pressure-gradient force*) and the force arising from air molecules exchanging momentum with each other (*viscous force*). Substituting (2.11) into (2.1) and expanding the right hand side yields

$$\mathbf{a}_l + \mathbf{a}_c + \mathbf{a}_r = \frac{1}{m_a}\left(\mathbf{F}_g^* + \mathbf{F}_p + \mathbf{F}_v\right), \tag{2.13}$$

where $\mathbf{F}_g^*$ represents true gravitational force, $\mathbf{F}_p$ is the pressure gradient force, and $\mathbf{F}_v$ denotes the viscous force. Atmospheric models are usually based on expressions for local acceleration, because local acceleration can be expressed directly by the time-derivative of the velocity field. Therefore, the momentum equation is written in a reference frame fixed on the surface of the Earth instead of a coordinate system fixed outside the Earth-atmosphere system. Consequently, only local acceleration is treated as an acceleration, whereas the Coriolis acceleration and centripetal forces are considered as *apparent forces*, i.e., these only appear like forces due to the choice of the coordinate system. Thus, the Coriolis acceleration is regarded as Coriolis force per unit mass ($\mathbf{a}_c = \frac{\mathbf{F}_c}{m_a}$), and the Earth's centripetal acceleration is considered as centrifugal (i.e. negative centripetal) force per unit mass ($\mathbf{a}_r = -\frac{\mathbf{F}_r}{m_a}$). Substituting these terms into (2.13) yields the *momentum equation from a reference frame fixed on Earth's surface*

$$\mathbf{a}_l = \frac{1}{m_a}\left(\mathbf{F}_r - \mathbf{F}_c + \mathbf{F}_g^* + \mathbf{F}_p + \mathbf{F}_v\right). \tag{2.14}$$

2.1.1.1. Material derivative

A point of material can be described by its position X in a *reference configuration* $\Omega \subset \mathbb{R}^d$. Assume, that Ω is open and connected. The course of a point $X \in \Omega$ in time is described by the mapping

$$t \mapsto x(t, X), \tag{2.15}$$

where t is the variable of time and x is the position of X at time t. Let the mapping x fulfil the following reasonable assumption:

1. $x(0, X) = X$, i.e., the point is identified by its position at the time $t = 0$.
2. The mapping $(t, X) \mapsto x(t, X)$ is continuously differentiable.

3. For every $t \geq 0$ the mapping $\Omega \ni X \mapsto x(t, X)$ can be inverted.

4. The determinant of the Jacobian matrix

$$J(t, X) = \det \left(\frac{\partial x_j}{\partial X_k}(t, X) \right)_{j,k=1}^{d}$$

is positive for all $t \geq 0$, $X \in \Omega$.

X is called *Lagrangian* or *material* coordinate and x is called *Eulerian* coordinate.

Let $\Phi(t, X)$ denote some variable in Lagrangian coordinates and $\varphi(t, x)$ denote the same variable in Eulerian coordinates. Then the following relationship holds:

$$\varphi\left(t, x(t, X)\right) = \Phi(t, X). \tag{2.16}$$

From (2.16) it follows with the chain rule that

$$\partial_t \Phi(t, X) = \partial_t \varphi\left(t, x(t, X)\right) + \nabla_x \varphi\left(t, x(t, X)\right) \cdot \partial_t x(t, X). \tag{2.17}$$

Denote by

$$\mathbf{V}(t, X) = \partial_t x(t, X), \quad \mathbf{v}(t, x) = \mathbf{V}\left(t, x(t, X)\right), \tag{2.18}$$

the velocity of a point of material X in Lagrangian and Eulerian coordinates, respectively.

Definition 2.2 (Material derivative)
The expression

$$\frac{\mathrm{d}}{\mathrm{d}t}\varphi(t, x) = \partial_t \varphi(t, x) + \mathbf{v}(t, x) \cdot \nabla \varphi(t, x) \tag{2.19}$$

is called *material derivative* of φ with respect to t.

Remark 2.3
The material derivative is often written in the form

$$\frac{\mathrm{d}}{\mathrm{d}t}\varphi = \partial_t \varphi + \left(\mathbf{v} \cdot \nabla\right) \varphi$$

and the associated operator as

$$\frac{\mathrm{d}}{\mathrm{d}t} = \partial_t + \left(\mathbf{v} \cdot \nabla\right).$$

In the case of vector valued variables, the material derivative is applied per coordinate.

2.1.1.2. Local acceleration

The local acceleration, i.e., the total or material derivative of velocity, expands with (2.19) to

$$\mathbf{a}_l = \frac{\mathrm{d}\mathbf{v}}{\mathrm{d}t} = \partial_t \mathbf{v} + \left(\mathbf{v} \cdot \nabla\right) \mathbf{v}, \tag{2.20}$$

i.e., the local acceleration along the motion of a parcel equals the local acceleration at a fixed point plus changes in local acceleration because of fluxes of velocity gradients.

2.1.1.3. Coriolis force

The Coriolis term in (2.14) expands in spherical-altitude coordinates to

$$\frac{\mathbf{F}_c}{m_a} = 2\boldsymbol{\Omega} \times \mathbf{v} = \mathbf{i}_\lambda 2\Omega \left(w\cos\varphi - v\sin\varphi\right) + \mathbf{j}_\varphi 2\Omega u \sin\varphi - \mathbf{k}_r 2\Omega u\cos\varphi, \tag{2.21}$$

where $\mathbf{i}_\lambda$ denotes the unit vector with respect to spherical coordinates in west-east direction, $\mathbf{j}_\varphi$ the unit vector in south-north direction, and $\mathbf{k}_r$ the vertical unit vector.

Because the vertical velocity component w is by orders of magnitude smaller than the horizontal velocity components u and v, i.e., $|w| \ll |u|, |v|$, the term $\mathbf{i}_\lambda 2\Omega w\cos\varphi$ may be neglected in (2.21). Similarly, the vertical component of the Coriolis force is smaller by orders of magnitude than other terms in the vertical momentum equation (gravity and pressure-gradient-terms, for example). Thus, the term $\mathbf{k}_r 2\Omega u\cos\varphi$ may also be neglected. Consequently, the *Coriolis force vector* per unit mass in spherical-altitude coordinates reduces to

$$\frac{\mathbf{F}_c}{m_a} = 2\boldsymbol{\Omega} \times \mathbf{v} \approx -\mathbf{i}_\lambda 2\Omega v\sin\varphi + \mathbf{j}_\varphi 2\Omega u\sin\varphi. \tag{2.22}$$

Let

$$f := 2\Omega\sin\varphi \tag{2.23}$$

denote the *Coriolis parameter*, where

$$\Omega \approx 7.2921 \cdot 10^{-5}. \tag{2.24}$$

Then, the term describing the Coriolis force can be written equivalently as

$$\frac{\mathbf{F}_c}{m_a} = 2\boldsymbol{\Omega} \times \mathbf{v} \approx -\mathbf{i}_\lambda fv + \mathbf{j}_\varphi fu = f\mathbf{k}_r \times \mathbf{v}_{hor}, \tag{2.25}$$

where $\mathbf{v}_{hor} := (u, v, 0)^\top$ denotes the horizontal velocity components.

In the case, that the curved surface of the earth is approximated by a plane, the following approximation of the Coriolis term is used. Coordinates on the plane are given in Cartesian (x, y) coordinates, where x denotes the position in west-east direction and y the position in south-north direction. First, the radial unit vector $\mathbf{k}_r$ reduces to the third Cartesian unit vector

$$\mathbf{e}_3 := (0, 0, 1)^\top, \tag{2.26}$$

which is orthogonal to the approximating plane. Second, if large-scale phenomena at the mid-latitudes are investigated, the Coriolis parameter f is often approximated based on a Taylor series about a reference latitude Φ_0:

$$f(y) \approx f\left(\Phi_0\right) + \beta y, \quad \beta := \frac{2\Omega\cos\left(\Phi_0\right)}{R_e}, \tag{2.27}$$

where

$$R_e \approx 6.371 \cdot 10^6 m \tag{2.28}$$

denotes the radius of the earth. This approximation is usually known as the *mid-latitude β-plane approximation*:

$$\frac{\mathbf{F}_c}{m_a} \approx f\mathbf{e}_3 \times \mathbf{v} = \left(-fv, fu, 0\right)^\top. \tag{2.29}$$

2.1.1.4. Gravitational and centrifugal force

Gravity is one of the real forces that act on a parcel of air. The gravity that is experienced by an observer on the earth is in fact a combination of true gravitational force and the Earth's apparent centrifugal force. *True gravitational force* acts towards the centre of the Earth, whereas the Earth's *apparent centrifugal force*, which acts away from the axis of rotation of Earth, alters the direction and magnitude of the true gravitational force marginally. Adding the true gravitational and apparent centrifugal force vectors yields the *effective gravitational force vector*.

The *true gravitational force vector* per unit mass is given by

$$\frac{\mathbf{F}_g^*}{m_a} = -\mathbf{k}_r^* g^*, \tag{2.30}$$

where g^* is the *true gravitational acceleration*. The vectors $\mathbf{i}_\lambda^*, \mathbf{j}_\varphi^*, \mathbf{k}_r^*$ denote the unit vectors in spherical coordinates on a true sphere, whereas the vectors $\mathbf{i}_\lambda, \mathbf{j}_\varphi, \mathbf{k}_r$ denote the unit vectors in spherical coordinates on the Earth, which is an oblate spheroid; see also above.

Assuming a true sphere, the apparent centrifugal force per unit mass can be expressed as

$$\frac{\mathbf{F}_r}{m_a} = -\mathbf{a}_r = -\boldsymbol{\Omega} \times (\boldsymbol{\Omega} \times \mathbf{R}_e) = -\mathbf{j}_\varphi^* R_e \Omega^2 \cos\varphi \sin\varphi + \mathbf{k}_r^* R_e \Omega^2 \cos^2\varphi, \tag{2.31}$$

where

$$\boldsymbol{\Omega} = \mathbf{j}_\varphi^* \Omega \cos\varphi + \mathbf{k}_r^* \Omega \sin\varphi, \quad \mathbf{R}_e = \mathbf{k}_r^* R_e,$$

denote the angular velocity vector and the radius vector of the Earth.

Adding (2.31) to (2.30) gives the *effective gravitational force vector* per unit mass on the Earth as

$$\frac{\mathbf{F}_g}{m_a} = \frac{\mathbf{F}_g^*}{m_a} + \frac{\mathbf{F}_r}{m_a} = -\mathbf{k}_r g, \tag{2.32}$$

where $\mathbf{k}_r$ is the unit vector normal to the oblate spheroid surface of the Earth, and

$$g = \left[\left(R_e \Omega^2 \cos\varphi \sin\varphi \right)^2 + \left(g^* - R_e \Omega^2 \cos^2\varphi \right)^2 \right]^{\frac{1}{2}}, \tag{2.33}$$

is the magnitude of the gravitational force per unit mass, or *effective gravitational acceleration* (effective gravity). The value of g at sea level varies slightly from $g = 9.799 \frac{m}{s^2}$ at the Equator and $g = 9.833 \frac{m}{s^2}$ at the poles. In the context of the idealised setting within this thesis, g is assumed to be constant and is fixed to the value

$$g = 9.80665 \frac{m}{s^2}. \tag{2.34}$$

In the case of a β-plane approximation (cf. (2.29)), (2.32) reduces to

$$\frac{\mathbf{F}_g}{m_a} = -\mathbf{e}_3 g. \tag{2.35}$$

2.1.1.5. Pressure-gradient force

The *pressure-gradient force*, which results from pressure differences in space, is a real force, which induces air to move from regions of high pressure to regions of low pressure.

Assume a parcel of air with cubic form, which has the volume $\Delta x \Delta y \Delta z$. Furthermore, assume that the air pressure only changes in x direction. Then, the air pressures, that are exerted on

the right and left sides of the parcel from outside, are given approximately by a Taylor series expansion of first order as

$$F_{p,r} = -\left(p_c + \frac{\Delta x}{2}\partial_x p\right)\Delta y \Delta z, \quad F_{p,l} = \left(p_c - \frac{\Delta x}{2}\partial_x p\right)\Delta y \Delta z, \tag{2.36}$$

where p_c denotes the pressure at the centre of the cell. Adding these forces, dividing the result by the mass $m_a = \rho_a \Delta x \Delta y \Delta z$ of the parcel and taking the limit $\Delta x, \Delta y, \Delta z \to 0$ yields the pressure-gradient force per unit mass in the direction of the x coordinate

$$\frac{F_{p,x}}{m_a} = -\frac{1}{\rho_a}\partial_x p_a, \tag{2.37}$$

where ρ_a denotes the density of air.

Generalizing this derivation to three space dimensions yields the vector valued pressure-gradient force

$$\frac{\mathbf{F}_p}{m_a} = -\frac{1}{\rho_a}\nabla p_a. \tag{2.38}$$

2.1.1.6. Viscous force

Molecular viscosity is a measure for the viscidity of a fluid. An increase in its viscosity makes a fluid more resistant to motion. This resistance is caused by other reasons in liquids than in gases.

In liquids, viscosity arises when molecules of the fluid approach each other and stick shortly together, e.g., by van der Waals forces. To break the bond between the molecules, kinetic energy needs to be converted, which slows the motion of the liquid down. Therefore, viscosity is an internal friction.

In gases, momentum is transferred between molecules when they collide. This transfer is viscosity in gases. In general, molecules of gases do not bond to each other, which results in a little net loss of energy due to a collision. When a molecule moving at a higher speed bumps into one moving at a lower speed, the faster molecule is slowed down, whereas the motion of the slower one is sped up. During this process, both molecules change their direction of motion.

As a consequence of these different reasons of viscosity, increasing the temperature leads to a decrease of viscosity in liquids, whereas an increase in temperature increases the viscosity of a gas.

A measure to quantify the molecular viscosity of air is the *dynamic viscosity of air*

$$\eta_a = \frac{5}{16 A d_a^2}\sqrt{\frac{M_a R^* T}{\pi}} \quad \left[\frac{kg}{ms}\right]. \tag{2.39}$$

This expression is based on gas kinetic theory and can be extended to any gas, where M_a denotes the molecular weight of air ($28.966\frac{g}{mol}$), R^* is the universal gas constant ($8314.51\frac{g}{m^2 s^2 K\ mol}$), T denotes the absolute temperature ($[K]$), A is Avogadro's number (molecules per mol), and d_a is the *average diameter of an air molecule* ($[m]$).

A related parameter is the *kinematic viscosity of air*

$$\nu_a = \frac{\eta_a}{\rho_a} \quad \left[\frac{m^2}{s}\right], \tag{2.40}$$

which is a molecular diffusion coefficient for air.

The *viscous force* is caused by viscous interactions between the different air molecules when they slide over each other. *Wind shear* denotes the change of velocity with altitude, i.e., $\partial_z u$. Because different layers of air slip over each other at different velocities because of wind shear, each layer exerts a *viscous* or *shearing stress*, which can be interpreted as a force per unit area, on the others. Consider a cubic parcel of air. This parcel experiences viscous stress in x-direction at its top and bottom due to shearing stress caused by the velocity component u, which denotes the velocity in x-direction. Therefore, if a force is exerted in x-direction per unit area of the $x-y$-plane by wind shear in the z-direction, the caused shearing stress is given by

$$\tau_{zx} = \eta_a \partial_z u \quad \left[\frac{N}{m^2}\right]. \tag{2.41}$$

In this case, the *net viscous force* on the cubic parcel of air equals the difference of shearing stress on the top of the parcel and the shearing stress on the bottom times the area on which the stress acts. Analogously to the derivation of the pressure gradient force, if τ_{zx} denotes the shearing stress in the middle of the parcel of air and $\partial_z \tau_{zx}$ is the derivative of shearing stress with respect to the vertical coordinate z, a first order Taylor series expansion yields the approximate shearing stresses at the top and bottom of the parcel:

$$\tau_{zx,top} = \tau_{zx} + \frac{\Delta z}{2}\partial_z \tau_{zx}, \quad \tau_{zx,bot} = \tau_{zx} - \frac{\Delta z}{2}\partial_z \tau_{zx}. \tag{2.42}$$

Computing the net viscous force with these approximations and dividing by the mass $m_a = \rho_a \Delta x \Delta y \Delta z$ of the parcel and taking the limit $\Delta x, \Delta y, \Delta z \to 0$ yields the net viscous force per unit mass

$$\frac{F_{\mathbf{v},zx}}{m_a} = \frac{1}{\rho_a}\partial_z \tau_{zx}. \tag{2.43}$$

Substituting (2.41) into (2.43) and assuming that η_a is invariant with altitude gives

$$\frac{\mathbf{F}_{\mathbf{v},zx}}{m_a} = \frac{\eta_a}{\rho_a}\partial_z^2 u. \tag{2.44}$$

Generalizing (2.44) to all three coordinate directions and all three velocity components finally yields the *viscous force vector* per unit mass

$$\frac{\mathbf{F}_\mathbf{v}}{m_a} = \frac{\eta_a}{\rho_a}\Delta \mathbf{v} = \nu_a \Delta \mathbf{v}. \tag{2.45}$$

In the context of the idealised setting within this thesis, ν_a is assumed to be constant and is fixed to the value

$$\nu_a = 1.47 \cdot 10^{-5} \frac{m^2}{s}. \tag{2.46}$$

2.1.1.7. The complete momentum equation

Substituting (2.20), (2.25), (2.32), (2.38) and (2.45) into (2.14) yields

$$\partial_t \mathbf{v} + (\mathbf{v} \cdot \nabla)\,\mathbf{v} + \frac{1}{\rho_a}\nabla p_a - \nu_a \Delta \mathbf{v} + f\mathbf{k} \times \mathbf{v}_{hor} + g\mathbf{k} = 0. \tag{2.47}$$

Table 2.1 lists the terms in the momentum equation and their typical horizontal and vertical scales.

[a] Low value for large-scale motions, high value for small-motions ($< 3km$)
[b] Low value for free atmosphere, high value for air adjacent to the surface

Term	**Acceleration or force/mass expression**	**Horizontal acceleration** $\left(\frac{m}{s^2}\right)$	**Vertical acceleration** $\left(\frac{m}{s^2}\right)$
Local acceleration	$\partial_t \mathbf{v} + (\mathbf{v} \cdot \nabla)\,\mathbf{v}$	10^{-4}	[a]$10^{-7} - 1$
Coriolis force per unit mass	$\frac{\mathbf{F}_c}{m_a} = f\mathbf{k} \times \mathbf{v}$	10^{-3}	0
Effective gravitational force per unit mass	$\frac{\mathbf{F}_g}{m_a} = -\mathbf{k}_r g$	0	10
Pressure-gradient force per unit mass	$\frac{\mathbf{F}_p}{m_a} = -\frac{1}{\rho_a}\nabla p_a$	10^{-3}	10
Viscous force per unit mass	$\frac{\mathbf{F}_v}{m_a} = \nu_a \Delta \mathbf{v}$	[b]$10^{-12} - 10^{-3}$	[b]$10^{-15} - 10^{-5}$

Table 2.1.: Vertical and horizontal scales of terms in the momentum equation

2.1.2. Equation of state

The *equation of state* describes, how pressure, volume and absolute temperature are related in a real gas. The *ideal gas law* is the equation of state for an ideal gas. A gas is called an *ideal gas*, if the product of the pressure and volume is proportional to the absolute temperature. Under typical atmospheric temperature and pressure conditions, the ideal gas law gives approximately an expanded equation of state with a relative error of less than 0.2 percent for dry air. Therefore, the ideal gas law is a reasonable approximation of the equation of state in the case of atmospheric scenarios.

The ideal gas law is expressed as a combination of *Boyle's law*

$$p \propto \frac{1}{V} \quad \text{at constant temperature,} \tag{2.48}$$

Charles' law

$$V \propto T \quad \text{at constant pressure,} \tag{2.49}$$

and *Avogadro's law*

$$V \propto n \quad \text{at constant pressure and temperature.} \tag{2.50}$$

p is the pressure exerted on the gas ($[hPa]$), V is the volume enclosed by the gas ($[m^3]$), T is the (absolute) temperature of the gas ($[K]$) and n denotes the number of gas moles. The symbol $\propto$ states proportionality between the expressions on its left and right hand sides, i.e., doubling the volume V in (2.48) reduces the pressure p by one-half. All gases exhibit the same number of molecules per mole. This constant number is given by *Avogadro's number*

$$A = 6.0221367 \cdot 10^{23} \frac{molec.}{mol}. \tag{2.51}$$

Combining Boyle's, Charles' and Avogadro's laws yields the *ideal gas law* or *simplified equation of state*

$$p = \frac{nR^*T}{V} = Nk_BT, \tag{2.52}$$

where

$$R^* = 0.0831451 \frac{m^3\ hPa}{K\ mol} \tag{2.53}$$

is the *universal gas constant*,

$$N = \frac{nA}{V} \tag{2.54}$$

is the number concentration of gas molecules and

$$k_B = \frac{R^*}{A} = 1.380658 \cdot 10^{-25} \frac{m^3\ hPa}{K\ molec.} \tag{2.55}$$

is *Boltzmann's constant*.

For dry air, (2.52) can be stated in the form

$$p_d = \rho_d R' T, \tag{2.56}$$

where

$$\rho_d = \frac{n_d M_d}{V}, \quad R' = \frac{R^*}{M_d} = 2.8704 \frac{m^3\ hPa}{K\ kg}, \tag{2.57}$$

are the dry-air mass density and dry-air gas constant, respectively,

$$M_d = 28.966 \frac{g}{mol} \tag{2.58}$$

is the standard value for the *molecular weight of dry air* and p_d ($[hPa]$) is dry-air partial pressure.

2.1.3. Continuity equation

The continuity equation describes the conservation of mass. Let V denote some volume of air, then the rate of change of mass in the volume V must equal the net mass flux across ∂V

$$\frac{\mathrm{d}}{\mathrm{d}t} \int_V \rho \mathrm{d}x = - \int_{\partial V} (\rho \mathbf{v}) \cdot \mathbf{n} \mathrm{d}\sigma, \tag{2.59}$$

where $\mathbf{n}$ denotes the outward pointing normal unit vector to ∂V. The integration theorem by Gauß A.1Integration theorysatz.A.1 thus implies

$$\int_V (\partial_t \rho + \operatorname{div}\ (\rho \mathbf{v}))\, \mathrm{d}x = 0. \tag{2.60}$$

If all the variables are continuous, shrinking V to a point gives

$$\partial_t \rho + \operatorname{div}\ (\rho \mathbf{v}) = 0, \tag{2.61}$$

the continuity equation of air.

2.1.4. Thermodynamic energy equation

Air temperature changes due to the transfer of energy and work. To derive an equation, which describes energy changes in the atmosphere, the first law of thermodynamics and the continuity equation for air are combined.

2.1.4.1. Potential and potential virtual temperature

First, an expression for specific humidity (kilograms of water vapour per kilogram of moist air) is given by

$$q_v = \frac{\rho_v}{\rho_a}, \tag{2.62}$$

where $\rho_a = \rho_d + \rho_v$ ($\left[\frac{kg}{m^3}\right]$) denotes the mass density of moist air, ρ_d ($\frac{kg}{m^3}$) the mass density of dry air, and ρ_v ($\frac{kg}{m^3}$) is the mass density of water vapour. In the case of dry air, it holds

$$q_v = 0. \tag{2.63}$$

Furthermore, *virtual temperature* ($[K]$) is defined as

$$T_v = T\left(1 + 0.608 q_v\right), \tag{2.64}$$

where T ($[K]$) denotes the absolute temperature of air, and *potential virtual temperature* ($[K]$) is defined as

$$\theta_v = T\left(1 + 0.608 q_v\right)\left(\frac{1000\ hPa}{p_a}\right)^{\kappa} = T_v\left(\frac{1000\ hPa}{p_a}\right)^{\kappa}, \tag{2.65}$$

where

$$\kappa = \frac{R'}{c_{p,d}} = 0.286, \quad c_{p,d} = 1004.67 \frac{m^2}{s^2 K}, \tag{2.66}$$

$c_{p,d}$ denotes the specific heat of dry air at constant pressure, and $p_a = p_d + p_v$ ($[hPa]$) is the pressure of air and p_v ($[hPa]$) the partial pressure exerted by water vapour. The value of 1000 hPa is the *reference* value for the pressure of air at the Earth's surface.

In the case of dry air, it holds

$$T_v = T, \quad \theta_v = T\left(\frac{1000\ hPa}{p_d}\right)^{\kappa}. \tag{2.67}$$

2.1.4.2. First law of thermodynamics

Applying the *first law of thermodynamics* to the atmosphere yields

$$\mathrm{d}Q^* = \mathrm{d}U^* + \mathrm{d}W^*, \tag{2.68}$$

where $\mathrm{d}Q^*$ denotes the *diabetic heating term*, which is the *energy* ($[J]$) transferred between an air parcel and its environment, $\mathrm{d}U^*$ is the change in *internal energy* of the parcel, and $\mathrm{d}W^*$ is the *work* ($[J]$) done by or on the parcel. Norming all three terms to m_a, i.e. the mass of a parcel of air ($[kg]$) consisting of dry air mass m_d and water vapour mass m_v,

$$\mathrm{d}Q = \frac{\mathrm{d}Q^*}{m_a}, \quad \mathrm{d}U = \frac{\mathrm{d}U^*}{m_a}, \quad \mathrm{d}W = \frac{\mathrm{d}W^*}{m_a}, \tag{2.69}$$

yields the first law of thermodynamics in terms of energy per unit mass of air ($\left[\frac{J}{kg}\right]$) as

$$\mathrm{d}Q = \mathrm{d}U + \mathrm{d}W. \tag{2.70}$$

In the case of a dry atmosphere, i.e. $m_v = 0$, the terms occurring in (2.70) can be expanded to

$$\mathrm{d}W = p_d \mathrm{d}\alpha_d, \quad \alpha_d = \frac{1}{\rho_d}, \tag{2.71}$$

where α_d denotes the *specific volume of dry air*,

$$\mathrm{d}U = c_{v,d}\mathrm{d}T, \quad c_{v,d} = 717.63\frac{J}{kg\ K}, \tag{2.72}$$

$c_{v,d}$ the *specific heat of dry air at constant volume*. Substituting (2.72) and (2.71) into (2.70) yields the *first law of thermodynamics for the dry atmosphere*

$$\mathrm{d}Q = c_{v,d}\mathrm{d}T + p_d\mathrm{d}\alpha_d. \tag{2.73}$$

Dividing (2.56) by ρ_d gives $p_d\alpha_d = R'T$, which can be differentiated and yields

$$\mathrm{d}(p_d\alpha_d) = \alpha_d\mathrm{d}p_d + p_d\mathrm{d}\alpha_d = R'\mathrm{d}T = \mathrm{d}(R'T). \tag{2.74}$$

Substitution of (2.74) into (2.73) gives

$$\mathrm{d}Q = (c_{v,d} + R')\mathrm{d}T - \alpha_d\mathrm{d}p_d = c_{p,d}\mathrm{d}T - \alpha_d\mathrm{d}p_d. \tag{2.75}$$

2.1.4.3. Thermodynamic energy equation

(2.75) is equivalent to

$$\mathrm{d}T = \frac{\mathrm{d}Q}{c_{p,d}} + \frac{1}{\rho_d c_{p,d}}\mathrm{d}p_d \tag{2.76}$$

and differentiating (2.76) with respect to time yields

$$\frac{\mathrm{d}T}{\mathrm{d}t} = \frac{1}{c_{p,d}}\frac{\mathrm{d}Q}{\mathrm{d}t} + \frac{1}{\rho_d c_{p,d}}\frac{\mathrm{d}p_d}{\mathrm{d}t}. \tag{2.77}$$

Differentiating (2.65) with respect to time and using (2.56), (2.66) and (2.77) gives

$$\begin{aligned}
\frac{\mathrm{d}\theta_v}{\mathrm{d}t} &= \frac{\mathrm{d}}{\mathrm{d}t}\left(T\left(\frac{1000\ hPa}{p_d}\right)^k\right) \\
&= \left(\frac{1000\ hPa}{p_d}\right)^k\frac{\mathrm{d}T}{\mathrm{d}t} + \kappa T\left(\frac{1000\ hPa}{p_d}\right)^{k-1}\left(-\frac{1000\ hPa}{p_d^2}\right)\frac{\mathrm{d}p_d}{\mathrm{d}t} \\
&= \frac{\theta_v}{T}\frac{\mathrm{d}T}{\mathrm{d}t} - \frac{\kappa\theta_v}{p_d}\frac{\mathrm{d}p_d}{\mathrm{d}t} \\
&= \frac{\theta_v}{Tc_{p,d}}\frac{\mathrm{d}Q}{\mathrm{d}t} + \frac{\theta_v}{T\rho_d c_{p,d}}\frac{\mathrm{d}p_d}{\mathrm{d}t} - \frac{R'\theta_v}{c_{p,d}p_d}\frac{\mathrm{d}p_d}{\mathrm{d}t} \\
&= \frac{\theta_v}{Tc_{p,d}}\frac{\mathrm{d}Q}{\mathrm{d}t} + \left(\frac{R'\theta_v}{c_{p,d}p_d} - \frac{R'\theta_v}{c_{p,d}p_d}\right)\frac{\mathrm{d}p_d}{\mathrm{d}t} \\
&= \frac{\theta_v}{Tc_{p,d}}\frac{\mathrm{d}Q}{\mathrm{d}t}.
\end{aligned}$$

Expanding the total time derivative of θ_v according to (2.19) yields the thermodynamic energy equation

$$\partial_t\theta_v + (\mathbf{v}\cdot\nabla)\,\theta_v = \frac{\theta_v}{Tc_{p,d}}\frac{\mathrm{d}Q}{\mathrm{d}t}. \tag{2.78}$$

2.1.5. Reference states for thermodynamic variables

In absence of any wind, i.e., $\mathbf{v} \equiv 0$ everywhere, the momentum, continuity, thermodynamic energy and ideal gas law equations should be balanced and the equation systems should stay at the current steady, i.e., there is no velocity induced by imbalances in the relations of density, temperature or pressure.

In order to achieve this, density, pressure and temperature are each split into a given reference state, which only depends on the vertical coordinate, and a perturbation of the reference state:

$$\rho = \rho_0(z) + \rho^*, \quad p = p_0(z) + p^*, \quad \theta_v = \theta_{v,0}(z) + \theta_v^*. \tag{2.79}$$

The reference states ρ_0, p_0 and $\theta_{v,0}$ shall form a stable atmosphere, i.e., in the absence of any velocity field ($\mathbf{v} = 0$) also all three perturbations ρ^*, p^* and θ_v^* shall equal zero.

To this end, assume that the following relations

$$\partial_z \theta_{v,0} = \theta_z = const., \quad \partial_z p_0 = -g\rho_0 \tag{2.80}$$

as well as the equation of state (2.56) hold for the reference states. The first relation assumes a linear vertical profile for potential virtual temperature

$$\theta_{v,0}(z) = \theta_0 + \theta_z z, \tag{2.81}$$

where θ_0 denotes the reference temperature at the Earth's surface. The second relation is the hydrostatic balance which assumes that the downward force of gravity per unit volume of air ($-g\rho_0$) exactly balances an upward pressure gradient force per unit volume ($\partial_z p_0$). The latter is precisely the remainder of the momentum equation in the case $\mathbf{v} \equiv 0$.

Remark 2.4 (Vertical profile of reference temperature)
The choice of (2.81) is meaningful, because it can be derived (cf. [46]), that the atmosphere is stably stratified in vertical direction, if it holds

$$\partial_z \theta_v > 0.$$

Therefore, if a value $\theta_z > 0$ is prescribed, the reference state of the atmosphere, as it is introduced here, fulfils this condition.

For the derivation of closed expressions for the reference states, substitution of (2.80) and (2.56) into (2.65) yields

$$\theta_{v,0} = \theta_0 + \theta_z z = T_0 \left(\frac{1000\ hPa}{p_0}\right)^{\kappa} = \frac{p_0}{R'\rho_0}\left(\frac{1000\ hPa}{p_0}\right)^{\kappa} = -\frac{g p_0}{R'\partial_z p_0}\left(\frac{1000\ hPa}{p_0}\right)^{\kappa}. \tag{2.82}$$

Inverting (2.82)

$$\frac{1}{\theta_0 + \theta_z z} = -\frac{R'}{g p_0}\partial_z p_0 \left(\frac{p_0}{1000\ hPa}\right)^{\kappa} = -\frac{R'}{g \cdot 1000\ hPa}\partial_z p_0 \left(\frac{p_0}{1000\ hPa}\right)^{\kappa-1} \tag{2.83}$$

and integrating from the Earth's surface ($z = 0$) to some height $z \geq 0$ gives (by applying the substitution rule of integration)

$$\begin{aligned}
& \int_0^z \frac{1}{\theta_0 + \theta_z z'} \mathrm{d}z' = -\frac{R'}{g \cdot 1000\ hPa} \int_{1000\ hPa}^{p_0} \left(\frac{p'}{1000\ hPa}\right)^{\kappa-1} \mathrm{d}p' \\
\Leftrightarrow \quad & \left[\frac{1}{\theta_z}\ln\left(\theta_0 + \theta_z z'\right)\right]_0^z = -\frac{R'}{g\,(1000\ hPa)^{\kappa}}\left[\frac{1}{\kappa}\left(p'\right)^{\kappa}\right]_{1000\ hPa}^{p_0} \\
\Leftrightarrow \quad & \frac{1}{\theta_z}\ln\left(1 + \frac{\theta_z z}{\theta_0}\right) = -\frac{R'}{g\kappa\,(1000\ hPa)^{\kappa}}\left(p_0^{\kappa} - (1000\ hPa)^{\kappa}\right).
\end{aligned}$$

Parameter	θ_0	θ_z
Value	$300\ K$	$3 \cdot 10^{-3} \frac{K}{m}$

Table 2.2.: Parameters of reference states of density, temperature and pressure for the numerical results in Chapter 6.

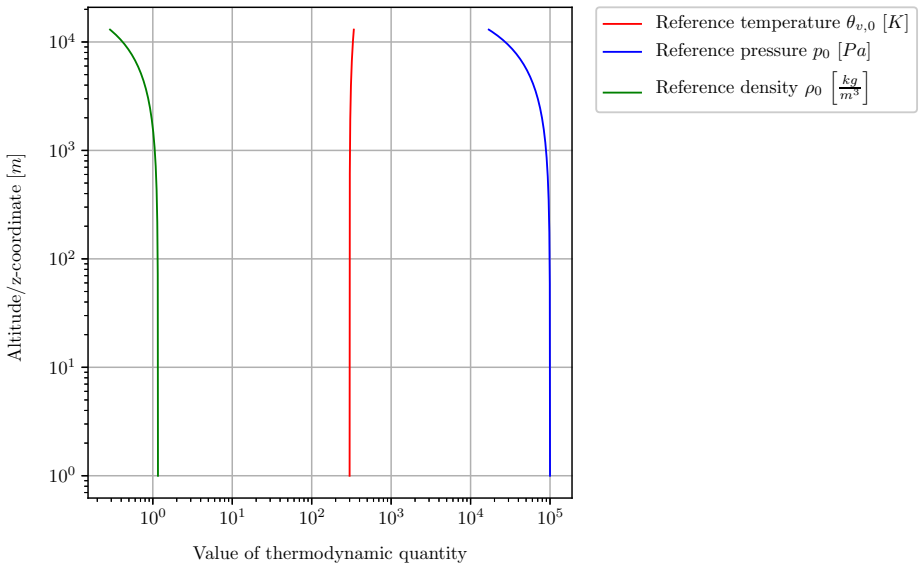

Figure 2.1.: Reference states of temperature, pressure and density

Solving the last equation for p_0 yields

$$p_0(z) = 1000\ hPa \left[-\frac{g\kappa}{R'\theta_z} \ln\left(1 + \frac{\theta_z z}{\theta_0}\right) + 1 \right]^{\frac{1}{\kappa}}. \tag{2.84}$$

With (2.56) it follows that

$$\rho_0(z) = \frac{p_0(z)}{R'T(z)} = \frac{1000\ hPa}{R'\theta_{v,0}(z)} \left[-\frac{g\kappa}{R'\theta_z} \ln\left(1 + \frac{\theta_z z}{\theta_0}\right) + 1 \right]^{\frac{1}{\kappa}-1}. \tag{2.85}$$

For the scenario of interacting tropical cyclones in Chapter 5, the parameters of this subsection are chosen according to Table 2.2. The resulting reference states for all three thermodynamic variables are depicted in Figure 2.1.

Remark 2.5 (Vertical derivatives of reference states)
In the following, the derivatives of the reference states for the thermodynamic variables with respect to the vertical coordinate z are needed extensively. Therefore, these derivatives are given here for later reference.

1. Reference potential virtual temperature:

$$\partial_z \theta_{v,0}(z) = \theta_z. \tag{2.86}$$

2. Reference pressure:

$$\partial_z p_0(z) = -\frac{1000\ hPa \cdot g}{R'\theta_{v,0}(z)} \left[-\frac{g\kappa}{R'\theta_z} \ln\left(1 + \frac{\theta_z z}{\theta_0}\right) + 1 \right]^{\frac{1}{\kappa}-1}. \tag{2.87}$$

3. Reference density:

$$\begin{aligned} \partial_z \rho_0(z) = &-\frac{1000\ hPa}{R'\left(\theta_{v,o}(z)\right)^2} \left[-\frac{g\kappa}{R'\theta_z} \ln\left(1 + \frac{\theta_z z}{\theta_0}\right) + 1 \right]^{\frac{1}{\kappa}-2} \\ &\cdot \left[\theta_z \left[-\frac{g\kappa}{R'\theta_z} \ln\left(1 + \frac{\theta_z z}{\theta_0}\right) + 1 \right] + \frac{g(1-\kappa)}{R'} \right]. \end{aligned} \tag{2.88}$$

2.1.6. The complete system of compressible Navier-Stokes equations

The complete system of compressible Navier-Stokes equations consists of (2.47), (2.61), (2.78) and (2.56):

$$\partial_t \mathbf{v} + (\mathbf{v} \cdot \nabla)\,\mathbf{v} + \frac{1}{\rho_d}\nabla p_d - \nu_a \Delta \mathbf{v} + f\mathbf{k} \times \mathbf{v} + g\mathbf{k} = 0 \tag{2.89}$$

$$\partial_t \rho_d + \operatorname{div}\ (\rho_d \mathbf{v}) = 0 \tag{2.90}$$

$$\partial_t \theta_v + (\mathbf{v} \cdot \nabla)\,\theta_v = \frac{\theta_v}{T c_{p,d}} \frac{\mathrm{d}Q}{\mathrm{d}t} \tag{2.91}$$

$$\left(\rho_d R' \theta_v\right)^{\frac{1}{1-\kappa}} (1000hPa)^{\frac{-\kappa}{1-\kappa}} = p_d \tag{2.92}$$

Equations (2.89)-(2.92) can be expressed in terms of the perturbation variables introduced in Subsection 2.1.5. Furthermore, in the considered idealised setting $\frac{\mathrm{d}Q}{\mathrm{d}t} = 0$ is assumed as well as a β-plane approximation (2.29), (2.35), i.e., the domain Ω is defined as

$$\begin{aligned} \Omega &:= (x_{min}, x_{max}) \times (y_{min}, y_{max}) \times (z_{min}, z_{max}) \subset \mathbb{R}^3, \\ &x_{min} < x_{max},\ y_{min} < y_{max},\ z_{min} < z_{max}, \\ \Gamma &:= \{(x, y, z) \in \partial\Omega : \quad z \in \{z_{min}, z_{max}\}\}, \end{aligned} \tag{2.94}$$

an axis-aligned rectangular cuboid and Γ denotes its top and bottom boundaries, respectively. Then, with (2.79) and (2.80) the problem of solving the compressible Navier-Stokes equations can be stated as follows:

Problem 2.6 (Compressible Navier-Stokes model)
Let $\Omega \subset \mathbb{R}^3$ be as in (2.94) and $T \geq 0$ a final point in time. Find a velocity field $\mathbf{v} := (u, v, w)^\top : [0, T) \times \Omega \to \mathbb{R}^3$, a density perturbation $\rho^* : [0, T) \times \Omega \to \mathbb{R}$, a temperature perturbation $\theta_v^* : [0, T) \times \Omega \to \mathbb{R}$ and a pressure perturbation $p^* : [0, T) \times \Omega \to \mathbb{R}$ satisfying

$$\partial_t \mathbf{v} + (\mathbf{v} \cdot \nabla)\mathbf{v} + \frac{1}{\rho}\nabla p^* - \nu_a \Delta \mathbf{v} = \left(fv, -fu, -\frac{\rho^*}{\rho} g \right)^\top \tag{2.95}$$

$$\partial_t \rho^* + w \partial_z \rho_0 + \mathbf{v} \cdot \nabla \rho^* + \rho \operatorname{div}\ \mathbf{v} = 0 \tag{2.96}$$

$$\partial_t \theta_v^* + w \partial_z \theta_{v,0} + (\mathbf{v} \cdot \nabla)\,\theta_v^* = 0 \tag{2.97}$$

$$\left[\frac{\left(-\frac{g\kappa}{\theta_z} \ln\left(1 + \frac{\theta_z z}{\theta_0}\right) + R' \right) \rho^* \left(\theta_v^* + \theta_{v,0}\right)}{p_0} + 1 + \frac{\theta_v^*}{\theta_{v,0}} \right]^{\frac{1}{1-\kappa}} p_0 - p_0 = p^* \tag{2.98}$$

$$w = 0 \quad \text{on} \quad [0, T] \times \Gamma \tag{2.99}$$

$$\mathbf{v}(0, x) = \mathbf{v}_0(x), \quad \rho^*(0, x) = \rho_0^*(x), \quad \theta_v^*(0, x) = \theta_{v,0}^*(x), \quad p^*(0, x) = p_0^*(x) \tag{2.100}$$

as well as periodic boundary conditions in both horizontal directions for all variables $\mathbf{v}$, ρ^*, θ_v^* and p^*, where the subscript d has been omitted for better readability,

$$p_0^* := \left(\left(\rho_0^* + \rho_0\right) R' \left(\theta_{v,0}^* + \theta_0\right)\right)^{\frac{1}{1-\kappa}} \left(1000 hPa\right)^{\frac{-\kappa}{1-\kappa}} - p_0$$

and

$$\rho := \rho^* + \rho_0.$$

Equations (2.95)-(2.98) are required to hold on $(0,T) \times \Omega$ and (2.100) is asked to hold on $\{t = 0\} \times \Omega$.

Remark 2.7 (Boundary conditions for thermodynamic variables)
Observe, that the thermodynamic quantities ρ^*, θ_v^* and p^* are not equipped with boundary conditions. ρ^* and θ_v^* are governed by the pure transport (equations (2.96) and (2.97)) due to the velocity field $\mathbf{v}$ and the initial conditions ρ_0^* and $\theta_{v,0}^*$, respectively, and are, therefore, uniquely determined by these data. The pressure p^* is computed via the purely algebraic relation (2.98) and, therefore, inherits its values on the boundary due to this relation from density and temperature.

Remark 2.8 (Problem 2.6)
In the absence of vacuum in the atmosphere as well as mass sinks, it holds $\rho(x) > 0$ for all $x \in \Omega$. Therefore, (2.95) is well defined if enough regularity of all functions is assumed, see Subsection 2.2 below.

Remark 2.9 (Stability of ideal gas law)
The numerical evaluation of (2.92) is numerically unstable for small perturbations ρ^*, θ_v^* and p^*. Especially, it does not hold $p^* = 0$ if $\theta_v^* = \rho^* = 0$. To stabilise the evaluation, (2.92) is rewritten as follows: First, define

$$b_p(z) := \left[-\frac{g\kappa}{R'\theta_z} \ln\left(1 + \frac{\theta_z z}{\theta_0}\right) + 1 \right].$$

Then, it follows from (2.84), that

$$b_p = \left(\frac{p_0}{1000\ hPa}\right)^{\kappa}. \tag{2.101}$$

Consequently, (2.82) can be expressed as

$$\theta_{v,0} = \frac{p_0}{R'\rho_0 b_p}. \tag{2.102}$$

Inserting (2.101) and (2.102) into (2.92) yields (2.98):

$$
\begin{aligned}
p^* &= \left[\left(\rho^* + \rho_0\right) R' \left(\theta_v^* + \theta_{v,0}\right) \left(1000\ hPa\right)^{-\kappa}\right]^{\frac{1}{1-\kappa}} - p_0 \\
&= \left[\left(\rho^* R'\theta_v^* + \rho^* R'\theta_{v,0} + \frac{p_0}{R'\theta_{v,0} b_p} R'\theta_v^* + \frac{p_0}{R'\theta_{v,0} b_p} R'\theta_{v,0}\right) \left(1000\ hPa\right)^{-\kappa}\right]^{\frac{1}{1-\kappa}} - p_0 \\
&= \left[\left(\rho^* R'\theta_v^* + \rho^* R'\theta_{v,0}\right) \left(1000\ hPa\right)^{-\kappa} + p_0 \frac{\theta_v^* + \theta_{v,0}}{\theta_{v,0} b_p} (1000\ hPa)^{-\kappa}\right]^{\frac{1}{1-\kappa}} - p_0 \\
&= \left[\left(\rho^* R'\theta_v^* + \rho^* R'\theta_{v,0}\right) p_0^{-\kappa} b_p + p_0 \frac{\theta_v^* + \theta_{v,0}}{\theta_{v,0} b_p} p_0^{-\kappa} b_p\right]^{\frac{1}{1-\kappa}} - p_0 \\
&= \left[\left(\rho^* R'\theta_v^* + \rho^* R'\theta_{v,0}\right) \frac{p_0^{1-\kappa}}{p_0} b_p + \frac{\theta_v^* + \theta_{v,0}}{\theta_{v,0}} p_0^{1-\kappa}\right]^{\frac{1}{1-\kappa}} - p_0 \\
&= \left[\frac{b_p R' \rho^* \left(\theta_v^* + \theta_{v,0}\right)}{p_0} + 1 + \frac{\theta_v^*}{\theta_{v,0}}\right]^{\frac{1}{1-\kappa}} p_0 - p_0.
\end{aligned}
$$

2.2. Weak formulation

In order to apply the finite element method (FEM) for the discretisation of the system of compressible Navier-Stokes equations (Problem 2.6), a weak formulation is given in this Section. To the best knowledge of the author, the question of existence and uniqueness of solutions for the full compressible Navier-Stokes equations is still open in two and three space dimensions, especially, when large initial data are considered. Results for special cases like the so called barotropic case in which pressure depends on the density only and, therefore, the thermodynamic energy equation is decoupled from the remaining ones, can be found in [59, 60], for example. However, the numerical results in Chapter 6, which are obtained by the discretisation described in Subsection 2.3, which itself is based on Problem 2.10, indicate that Problem 2.10 is well-posed for the flow which is considered in the scenario of two interacting tropical cyclones, see Chapter 5. Therefore, in the remainder of this thesis it is assumed that a unique weak solution to Problem 2.10 exists and fulfils the demanded regularity assumptions for the considered flow.

Problem 2.10 (Weak formulation of Problem 2.6)
Let $\Omega \subset \mathbb{R}^3$ be as in (2.94) and $T \geq 0$ a final point in time. Then the weak formulation of Problem 2.6 is as follow: Find a tuple

$$
(\mathbf{v}, \rho^*, \theta_v^*, p^*) : (0,T) \times \Omega \to \mathbb{R}^3 \times \mathbb{R} \times \mathbb{R} \times \mathbb{R}, \quad \mathbf{v} := (u, v, w)^\top,
$$

such that the following conditions are satisfied:

1. The variables satisfy

$$
\mathbf{v} \in \left(L^2\left(0, T; H^1\left(\Omega\right)\right)\right)^3, \tag{2.103}
$$

$$
\partial_t \mathbf{v} \in \left(L^2\left(0, T; H^{-1}\left(\Omega\right)\right)\right)^3, \tag{2.104}
$$

$$
w = 0 \quad \text{on} \quad [0,T] \times \Gamma, \tag{2.105}
$$

$$
\rho^*, \theta_v^*, p^* \in L^2\left(0, T; H^1\left(\Omega\right)\right), \tag{2.106}
$$

$$
\partial_t \rho^*, \partial_t \theta_v^* \in L^2\left(0, T; H^{-1}\left(\Omega\right)\right), \tag{2.107}
$$

   as well as periodic boundary conditions in both horizontal directions.

2. The integral identity

$$\langle \partial_t \mathbf{v}, \varphi_{\mathbf{v}} \rangle + \left((\mathbf{v} \cdot \nabla)\mathbf{v} + \frac{1}{\rho}\nabla p^* + \left(-fv, fu, \frac{\rho^*}{\rho} g \right)^\top, \varphi_{\mathbf{v}} \right) + (\nu_a \nabla \mathbf{v}, \nabla \varphi_{\mathbf{v}}) = 0, \quad (2.108)$$

where

$$\rho := \rho^* + \rho_0,$$

$(\cdot,\cdot)$ denotes the inner product in $L^2(\Omega)$ and $\langle \cdot, \cdot \rangle$ the dual pairing between $H^{-1}(\Omega)$ and $H_0^1(\Omega)$, holds for all $\varphi_{\mathbf{v}} \in \left(H_0^1(\Omega)\right)^3$ and almost every (a.e.) $t \in [0,T]$. Furthermore, it holds

$$(\mathbf{v}(0) - \mathbf{v}_0, \psi_{\mathbf{v}}) = 0 \quad \text{for all } \psi_{\mathbf{v}} \in \left(H^1(\Omega)\right)^3. \quad (2.109)$$

3. The integral identity

$$\langle \partial_t \rho^*, \varphi_\rho \rangle + (w\partial_z \rho_0 + \mathbf{v} \cdot \nabla \rho^* + \rho \text{div } \mathbf{v}, \varphi_\rho) = 0, \quad (2.110)$$

where

$$\rho := \rho^* + \rho_0,$$

holds for all $\varphi_\rho \in H_0^1(\Omega)$ and a.e. $t \in [0,T]$. Furthermore, it holds

$$(\rho^*(0) - \rho_0^*, \psi_\rho) = 0 \quad \text{for all } \psi_\rho \in H^1(\Omega). \quad (2.111)$$

4. The integral identity

$$\langle \partial_t \theta_v^*, \varphi_\theta \rangle + (w\partial_z \theta_{v,0} + (\mathbf{v} \cdot \nabla)\, \theta_v^*, \varphi_\theta) = 0 \quad (2.112)$$

holds for all $\varphi_\theta \in H_0^1(\Omega)$ and a.e. $t \in [0,T]$. Furthermore, it holds

$$\left(\theta_v^*(0) - \theta_{v,0}^*, \psi_\theta\right) = 0 \quad \text{for all } \psi_\theta \in H^1(\Omega). \quad (2.113)$$

5. The integral identity

$$(p^*, \varphi_p) = \left(\left[\frac{\left(-\frac{g\kappa}{\theta_z} \ln\left(1 + \frac{\theta_z z}{\theta_0}\right) + R' \right) \rho^* \left(\theta_v^* + \theta_{v,0}\right)}{p_0} + 1 + \frac{\theta_v^*}{\theta_{v,0}} \right]^{\frac{1}{1-\kappa}} p_0 - p_0, \varphi_p \right) \quad (2.114)$$

holds for all $\varphi_p \in H_0^1(\Omega)$ and a.e. $t \in [0,T]$. Furthermore, it holds

$$(p^*(0) - p_0^*, \psi_p) = 0 \quad \text{for all } \psi_p \in H^1(\Omega). \quad (2.115)$$

2.3. Discretisation

In this section, the weak formulation (Problem 2.10) of the system of the compressible Navier-Stokes equations (Problem 2.6) is discretised with finite elements in space and finite differences in time. The discretisation is done by the method of lines, i.e., the finite element discretisation in space is done first and the finite difference discretisation in time afterwards.

The presented scheme is formulated quite generally. The concrete choices of finite element spaces and coefficients in the time-stepping scheme that are used for the numerical tests in Chapter 6, are given in Section 4.1.

2.3.1. Discretisation in space

The Finite Element Method (FEM) is based on the following idea: The space is discretised by "elements" which allow a flexible approximation of the domain of interest. On each of these elements, *trial functions* are defined and the approximate solution is intended to be a linear combination of them. To get the corresponding coefficients for the linear combination, this trial is put into the weak formulation of the PDE. As test functions appropriate functions from a finite-dimensional test space are chosen and the integrals are evaluated *exactly* up to the precision of the applied quadrature rule. Both test and trial functions form finite dimensional spaces spanned by themselves. Due to the linear nature of these spaces it is sufficient to test only with the basis functions of the test space in the weak formulation. Thus the quality of the approximation is mainly influenced by the approximation of the infinite dimensional spaces by the finite dimensional ones.

If the locally defined trial functions are extended to functions that are globally defined on the whole domain, the FEM is a special variant of the *Petrov-Galerkin* approximation.

Let Ω be defined as in (2.94). Let $\mathscr{T}_h \subset \mathbb{R}^3$ be a triangulation of Ω with the properties

$$\bigcup_{K \in \mathscr{T}_h} = \Omega, \quad K \neq \emptyset \ (\forall K \in \mathscr{T}_h), \quad \overset{\circ}{K}_i \cap \overset{\circ}{K}_j = \emptyset \ (\forall K_i, K_j \in \mathscr{T}_h, i \neq j), \tag{2.116}$$

where $\overset{\circ}{K}$ denotes the interior of a subset $K \subset \mathbb{R}^3$.

Let $V_h \subset H^1(\Omega)$ a finite dimensional subspace for the velocity components u, v, w, $X_h \subset H_0^1(\Omega)$ a finite dimensional subspace for the test functions of velocity, $Q_h \subset H^1(\Omega)$ a finite dimensional subspace for density ρ^* and temperature θ_v^*, $Y_h \subset H_0^1(\Omega)$ a finite dimensional subspace for the test functions of density and temperature, $P_h \subset H^1(\Omega)$ a finite dimensional subspace for the pressure p^*, as well as $Z_h \subset H_0^1(\Omega)$ a finite dimensional subspace for the test functions of pressure, where $V_h, Q_h, P_h, X_h, Y_h, Z_h$ are spaces of continuous and piecewise polynomial functions defined on $\mathscr{T}_h$. Details are given in Subsection 4.1.

With the above notations, the semi-discrete, i.e., discrete in space and continuous in time, problem to the Problem 2.10 reads:

Problem 2.11 (Semi-discrete problem of Problem 2.10)
Let $\Omega \subset \mathbb{R}^3$ be as in (2.94), $\mathscr{T}_h$ a triangulation of Ω as in (2.116) and $T \geq 0$ a final point in time. Find

$$\mathbf{v}_h \in \left(C^1\left([0,T]; V_h\right)\right)^3, \quad \rho_h^*, \theta_{v,h}^* \in C^1\left([0,T]; Q_h\right), \quad p_h^* \in C\left([0,T]; P_h\right), \tag{2.117}$$

where

$$\mathbf{v}_h := \left(u_h, v_h, w_h\right)^\top,$$

such that the following conditions are satisfied:

1. The variables satisfy

$$w_h = 0 \quad \text{on} \quad [0,T] \times \Gamma, \tag{2.118}$$

as well as periodic boundary conditions in both horizontal directions.

2. The integral identity

$$\begin{aligned} 0 = &(\partial_t \mathbf{v}_h, \varphi_{\mathbf{v},h}) \\ &+ \left((\mathbf{v}_h \cdot \nabla)\mathbf{v}_h + \frac{1}{\rho_h}\nabla p_h^* + \left(-fv_h, fu_h, \frac{\rho_h^*}{\rho_h} g\right)^\top, \varphi_{\mathbf{v},h} \right) \\ &+ (\nu_a \nabla \mathbf{v}_h, \nabla \varphi_{\mathbf{v},h}), \end{aligned} \tag{2.119}$$

where

$$\rho_h := \rho_h^* + \rho_0,$$

holds for all $\varphi_{\mathbf{v},h} \in (X_h)^3$ and all $t \in [0,T]$. Furthermore, it holds

$$(\mathbf{v}_h(0) - \mathbf{v}_0, \psi_{\mathbf{v},h}) = 0 \quad \forall \psi_{\mathbf{v},h} \in (V_h)^3. \tag{2.120}$$

3. The integral identity

$$(\partial_t \rho_h^*, \varphi_{\rho,h}) + (w_h \partial_z \rho_0 + \mathbf{v}_h \cdot \nabla \rho_h^* + \rho_h \text{div } \mathbf{v}_h, \varphi_{\rho,h}) = 0, \tag{2.121}$$

where

$$\rho_h := \rho_h^* + \rho_0,$$

holds for all $\varphi_{\rho,h} \in Y_h$ and all $t \in [0,T]$. Furthermore, it holds

$$(\rho_h^*(0) - \rho_0^*, \psi_{\rho,h}) = 0 \quad \forall \psi_{\rho,h} \in Q_h. \tag{2.122}$$

4. The integral identity

$$\left(\partial_t \theta_{v,h}^*, \varphi_{\theta,h}\right) + \left(w_h \partial_z \theta_{v,0} + (\mathbf{v} \cdot \nabla)\, \theta_{v,h}^*, \varphi_{\theta,h}\right) = 0 \tag{2.123}$$

holds for all $\varphi_{\theta,h} \in Y_h$ and all $t \in [0,T]$. Furthermore, it holds

$$\left(\theta_{v,h}^*(0) - \theta_{v,0}^*, \psi_{\theta,h}\right) = 0 \quad \forall \psi_{\theta,h} \in Q_h. \tag{2.124}$$

5. The integral identity

$$\begin{aligned} (p_h^*, \varphi_{p,h}) = &\left(\left[\frac{\left(-\frac{g\kappa}{\theta_z} \ln\left(1 + \frac{\theta_z z}{\theta_0}\right) + R'\right) \rho_h^* \left(\theta_{v,h}^* + \theta_{v,0}\right)}{p_0} + 1 + \frac{\theta_{v,h}^*}{\theta_{v,0}} \right]^{\frac{1}{1-\kappa}} p_0, \varphi_{p,h} \right) \\ &- (p_0, \varphi_{p,h}) \end{aligned} \tag{2.125}$$

holds for all $\varphi_{p,h} \in Z_h$ and all $t \in [0,T]$. Furthermore, it holds

$$(p_h^*(0) - p_0^*, \psi_{p,h}) = 0 \quad \forall \psi_{p,h} \in P_h. \tag{2.126}$$

Remark 2.12 (Semi-discrete problem of Problem 2.10)
Problem 2.11 forms a system of ordinary differential-algebraic equations, where the occurring ordinary differential equations (2.119), (2.121) and (2.123) are of first order. The semi-discrete ideal gas law (2.125) forms the algebraic constraint.

2.3.2. Stabilisation

Finite element computations of flow phenomena comprise two main sources of potential numerical instabilities which are linked to the Galerkin or Petrov-Galerkin formulation of the problem. The first source is induced by the presence of advection terms in the PDE, which can result in spurious node-to-node oscillations in the transported quantities [72]. These oscillations can be observed especially in advection-dominated flows, where the Reynolds number is high, and in flows with sharp layers or steep gradients in the solution. The second source of instability arises in flows, which are governed by equation sets with saddle-point structure, where inappropriate combinations of finite-element interpolations are used for the velocity and pressure components, see Subsection 3.3.4.

In the case of compressible flows governed by the compressible Navier-Stokes equations (Problem 2.10), only the first source of instabilities is relevant [43, 74]. An overview about stabilisation techniques for compressible flows is given in [43, 74] and for incompressible flows in [1, 16, 17, 72, 73], for example. In the following, only residual based stabilisation techniques are considered. These methods are constructed by adding an appropriately weighted multiple of the residual of the strong problem formulation (Problem 2.6), evaluated for the semi-discrete solution of Problem 2.11, element-wise to the residual form of the semi-discrete solution of Problem 2.11. These additional terms can be interpreted as an element-wise penalty term and, therefore, they penalise the violation of the underlying conservation law on the element level. Consequently, the conservation property is not only demanded globally over the whole domain, but also to a certain extend per element. Thus, node-to-node oscillations are avoided effectively without introducing excessive numerical dissipation and the resulting scheme is consistent, i.e., if the continuous solution of Problem 2.6 or Problem 2.10, respectively, is inserted in the stabilised formulation, the additional stabilisation terms vanish and, therefore, the continuous solution still solves the stabilised problem.

Problem 2.13 (Stabilised semi-discrete problem of Problem 2.10)
Let $\Omega \subset \mathbb{R}^3$ be as in (2.94), $\mathscr{T}_h$ a triangulation of Ω as in (2.116) and $T \geq 0$ a final point in time. Furthermore, let the residual operators of the momentum, continuity and thermodynamic energy equation, respectively, be defined as

$$\mathscr{R}_{\mathbf{v}}(\mathbf{u}, r, q) = \partial_t \mathbf{u} + (\mathbf{u} \cdot \nabla)\mathbf{u} + \frac{1}{\rho_0 + r}\nabla q - \nu_a \Delta \mathbf{u} - \left(fv, -fu, -\frac{r}{\rho_0 + r} g \right)^\top, \tag{2.127}$$

$$\mathscr{R}_{\rho}(\mathbf{u}, r) = \partial_t r + w \partial_z \rho_0 + \mathbf{u} \cdot \nabla r + (\rho_0 + r) \operatorname{div} \mathbf{u}, \tag{2.128}$$

$$\mathscr{R}_{\theta}(\mathbf{u}, s) = \partial_t s + w \partial_z \theta_{v,0} + (\mathbf{u} \cdot \nabla) s, \tag{2.129}$$

where

$$\mathbf{u} := (u, v, w)^\top.$$

Let $\bar{\mathbf{v}} \in (V_h)^3$ be a reference velocity field. Find

$$\mathbf{v}_h \in \left(C^1([0,T]; V_h) \right)^3, \quad \rho_h^*, \theta_{v,h}^* \in C^1([0,T]; Q_h), \quad p_h^* \in C([0,T]; P_h), \tag{2.130}$$

where

$$\mathbf{v}_h := (u_h, v_h, w_h)^\top,$$

such that the following conditions are satisfied:

1. The variables satisfy

$$w_h = 0 \quad \text{on} \quad [0,T] \times \Gamma, \tag{2.131}$$

as well as periodic boundary conditions in both horizontal directions.

2. The integral identity

$$\begin{aligned} 0 = &(\partial_t \mathbf{v}_h, \varphi_{\mathbf{v},h}) \\ &+ \left((\mathbf{v}_h \cdot \nabla)\mathbf{v}_h + \frac{1}{\rho_h}\nabla p_h^* + \left(-f v_h, f u_h, \frac{\rho_h^*}{\rho_h} g \right)^\top, \varphi_{\mathbf{v},h} \right) \\ &+ (\nu_a \nabla \mathbf{v}_h, \nabla \varphi_{\mathbf{v},h}) \\ &+ \sum_{K \in \mathscr{T}_h} \tau_{\mathbf{v},K} \left(\mathscr{R}_{\mathbf{v}} \left(\mathbf{v}_h, \rho_h^*, p_h^* \right), \left(\bar{\mathbf{v}} \cdot \nabla \right) \varphi_{\mathbf{v},h} - \nu_a \Delta \varphi_{\mathbf{v},h} \right)_K , \end{aligned} \tag{2.132}$$

where

$$\rho_h := \rho_h^* + \rho_0,$$

holds with $\tau_{\mathbf{v},K} \geq 0$ for all $\varphi_{\mathbf{v},h} \in (X_h)^3$ and all $t \in [0,T]$, where

$$\rho_h := \rho_h^* + \rho_0.$$

Furthermore, it holds

$$(\mathbf{v}_h(0) - \mathbf{v}_0, \psi_{\mathbf{v},h}) = 0 \quad \forall \psi_{\mathbf{v},h} \in (V_h)^3. \tag{2.133}$$

3. The integral identity

$$\begin{aligned} 0 = &(\partial_t \rho_h^*, \varphi_{\rho,h}) + (w_h \partial_z \rho_0 + \mathbf{v}_h \cdot \nabla \rho_h^* + \rho_h \text{div } \mathbf{v}_h, \varphi_{\rho,h}) \\ &+ \sum_{K \in \mathscr{T}_h} \tau_{\rho,K} \left(\mathscr{R}_\rho \left(\mathbf{v}_h, \rho_h^* \right), \bar{\mathbf{v}} \cdot \nabla \varphi_{\rho,h} \right)_K , \end{aligned} \tag{2.134}$$

where

$$\rho_h := \rho_h^* + \rho_0,$$

holds with $\tau_{\rho,K} \geq 0$ for all $\varphi_{\rho,h} \in Y_h$ and all $t \in [0,T]$, where

$$\rho_h := \rho_h^* + \rho_0.$$

Furthermore, it holds

$$(\rho_h^*(0) - \rho_0^*, \psi_{\rho,h}) = 0 \quad \forall \psi_{\rho,h} \in Q_h. \tag{2.135}$$

4. The integral identity

$$\begin{aligned} 0 = &\left(\partial_t \theta_{v,h}^*, \varphi_{\theta,h} \right) + \left(w_h \partial_z \theta_{v,0} + (\mathbf{v} \cdot \nabla) \theta_{v,h}^*, \varphi_{\theta,h} \right) \\ &+ \sum_{K \in \mathscr{T}_h} \tau_{\theta,K} \left(\mathscr{R}_\theta \left(\mathbf{v}_h, \theta_{v,h}^* \right), \bar{\mathbf{v}} \cdot \nabla \varphi_{\theta,h} \right)_K , \end{aligned} \tag{2.136}$$

holds with $\tau_{\theta,K} \geq 0$ for all $\varphi_{\theta,h} \in Y_h$ and all $t \in [0,T]$. Furthermore, it holds

$$\left(\theta_{v,h}^*(0) - \theta_{v,0}^*, \psi_{\theta,h} \right) = 0 \quad \forall \psi_{\theta,h} \in Q_h. \tag{2.137}$$

5. The integral identity

$$(p_h^*, \varphi_{p,h}) = \left(\left[\frac{\left(-\frac{g\kappa}{\theta_z} \ln\left(1 + \frac{\theta_z z}{\theta_0}\right) + R' \right) \rho_h^* \left(\theta_{v,h}^* + \theta_{v,0}\right)}{p_0} + 1 + \frac{\theta_{v,h}^*}{\theta_{v,0}} \right]^{\frac{1}{1-\kappa}} p_0, \varphi_{p,h} \right) - (p_0, \varphi_{p,h}) \tag{2.138}$$

holds for all $\varphi_{p,h} \in Z_h$ and all $t \in [0,T]$. Furthermore, it holds

$$(p_h^*(0) - p_0^*, \psi_{p,h}) = 0 \quad \forall \psi_{p,h} \in P_h. \tag{2.139}$$

Remark 2.14 (Stabilised semi-discrete problem of Problem 2.10)

1. The choice of the reference velocity $\bar{\mathbf{v}}$ is made precise in the next subsection in the context of the discretisation in time. Basically, the reference velocity shall be "close" to the actual velocity field $\mathbf{v}_h$.

2. If the reference velocity and the gradient of the corresponding test function are perpendicular to each other, then the scalar product of both is zero and, therefore, does not contribute to the stabilisation. If the two vectors are parallel, the scalar product of both takes its maximum value and the stabilisation is strongest. Consequently, this part of the stabilisation only acts in the direction of the reference velocity field.

3. The stabilisation term of the momentum equation is additionally stabilised by the Laplace of the test functions times the diffusion coefficient of air. Therefore, this term always adds a certain amount of stabilisation independent of the reference velocity field.

4. The element-wise defined non-negative parameters $\tau_{\mathbf{v},K}$, $\tau_{\rho,K}$ and $\tau_{\theta,K}$ are called *stabilisation parameters* and a precise definition of their values is given in the next subsection in the context of the discretisation in time.

5. Remark 2.12 also holds true in the situation of Problem 2.13.

2.3.3. Discretisation in time

Let

$$0 =: t_0 < t_1 < t_2 < \ldots < t_M := T \tag{2.140}$$

be an equidistant discretisation of the interval $[0,T]$, i.e., all intervals $I_i := (t_{i-1}, t_i)$, $i = 1, \ldots, M$, have the same length $\Delta t := t_i - t_{i-1} = const.$

Let $\theta \in [0,1]$. The time derivative of a quantity $q \in C^1(0,T;\mathbb{R})$ is discretised by

$$\frac{q(t_{n+1}) - q(t_n)}{\Delta t} = \theta \partial_t q(t_{n+1}) + (1-\theta)\partial_t q(t_n) + O\left(\left(\frac{1}{2} - \theta\right) \cdot \Delta t, \Delta t^2\right), \tag{2.141}$$

This scheme is called the *θ-family of time discretisation methods*. For $\theta = 0$ this scheme is called *explicit Euler method*, for $\theta = \frac{1}{2}$ *Crank-Nicolson method* and for $\theta = 1$ *implicit Euler method*, respectively, see, e.g., [61].

According to Remark 2.14, Problem 2.13 forms a system of ordinary differential-algebraic equations, where the differential part is of first order. Therefore, every discretisation scheme for

a system of ordinary differential-algebraic equations of first order can be applied to Problem 2.13 like Runge-Kutta methods, multistep methods etc., see, e.g., [70].

Applying (2.141) to Problem 2.13 yields the following fully discrete formulation of Problem 2.6.

Problem 2.15 (Discrete problem of Problem 2.10)
Let $\Omega \subset \mathbb{R}^3$ be as in (2.94), $\mathscr{T}_h$ a triangulation of Ω as in (2.116) and $T \geq 0$ a final point in time. Furthermore, let t_i, $i = 0, \ldots, M$ be a an equidistant discretisation of the interval $[0, T]$ as defined in (2.140). Let $\bar{\mathbf{v}} \in (V_h)^3$ be a reference velocity field and $\theta_j \in [0, 1]$, $j = 1, \ldots, 12$ such that

$$\theta_j + \theta_{j+6} = 1, \quad j = 1, \ldots, 6.$$

Find

$$\mathbf{v}_h^{(n)} \in V_h^3, \quad (\rho_h^*)^{(n)}, \left(\theta_{v,h}^*\right)^{(n)} \in Q_h, \quad (p_h^*)^{(n)} \in P_h, \quad \forall\, n = 1, \ldots, M, \tag{2.142}$$

where

$$\mathbf{v}_h^{(n)} := \left(u_h^{(n)}, v_h^{(n)}, w_h^{(n)}\right)^\top,$$

such that the following conditions are satisfied:

1. The variables satisfy

$$w_h^{(n)} = 0 \quad \text{on } \Gamma, \quad \forall\, n = 0, \ldots, M, \tag{2.143}$$

as well as periodic boundary conditions in both horizontal directions.

2. The integral identity

$$
\begin{aligned}
0 = &\left(\left(\mathbf{v}_h^{(n+1)} - \mathbf{v}_h^{(n)}\right) + \Delta t\theta_1 \left(\mathbf{v}_h^{(n)} \cdot \nabla\right) \mathbf{v}_h^{(n)} + \Delta t\theta_7 \left(\mathbf{v}_h^{(n+1)} \cdot \nabla\right) \mathbf{v}_h^{(n+1)}, \varphi_{\mathbf{v},h}\right) \\
&+ \left(\Delta t\theta_2 \frac{1}{\rho_h^{(n)}} \nabla (p_h^*)^{(n)} - \Delta t\theta_4 \left(f v_h^{(n)}, -f u_h^{(n)}, -\frac{(\rho_h^*)^{(n)}}{\rho_h^{(n)}} g\right)^\top, \varphi_{\mathbf{v},h}\right) \\
&+ \left(\Delta t\theta_8 \frac{1}{\rho_h^{(n+1)}} \nabla (p_h^*)^{(n+1)} - \Delta t\theta_{10} \left(f v_h^{(n+1)}, -f u_h^{(n+1)}, -\frac{(\rho_h^*)^{(n+1)}}{\rho_h^{(n+1)}} g\right)^\top, \varphi_{\mathbf{v},h}\right) \\
&+ \left(\Delta t\theta_3 \nu \nabla \mathbf{v}_h^{(n)} + \Delta t\theta_9 \nu \nabla \mathbf{v}_h^{(n+1)}, \nabla \varphi_{\mathbf{v},h}\right) \\
&+ \sum_{K \in \mathscr{T}_h} \tau_{\mathbf{v},K} \left(\mathbf{v}_h^{n+1} - \mathbf{v}_h^n, (\bar{\mathbf{v}} \cdot \nabla) \varphi_{\mathbf{v},h} - \nu_a \Delta \varphi_{\mathbf{v},h}\right)_K \\
&+ \sum_{K \in \mathscr{T}_h} \tau_{\mathbf{v},K} \left(\Delta t\theta_1 \left(\mathbf{v}_h^{(n)} \cdot \nabla\right) \mathbf{v}_h^{(n)}, (\bar{\mathbf{v}} \cdot \nabla) \varphi_{\mathbf{v},h} - \nu_a \Delta \varphi_{\mathbf{v},h}\right)_K \\
&+ \sum_{K \in \mathscr{T}_h} \tau_{\mathbf{v},K} \left(\Delta t\theta_7 \left(\mathbf{v}_h^{(n+1)} \cdot \nabla\right) \mathbf{v}_h^{(n+1)}, (\bar{\mathbf{v}} \cdot \nabla) \varphi_{\mathbf{v},h} - \nu_a \Delta \varphi_{\mathbf{v},h}\right)_K \\
&+ \sum_{K \in \mathscr{T}_h} \tau_{\mathbf{v},K} \left(\Delta t\theta_2 \frac{1}{\rho_h^{(n)}} \nabla (p_h^*)^n, (\bar{\mathbf{v}} \cdot \nabla) \varphi_{\mathbf{v},h} - \nu_a \Delta \varphi_{\mathbf{v},h}\right)_K \\
&- \sum_{K \in \mathscr{T}_h} \tau_{\mathbf{v},K} \left(\Delta t\theta_4 \left(f v_h^{(n)}, -f u_h^{(n)}, -\frac{(\rho_h^*)^{(n)}}{\rho_h^{(n)}} g\right)^\top, (\bar{\mathbf{v}} \cdot \nabla) \varphi_{\mathbf{v},h} - \nu_a \Delta \varphi_{\mathbf{v},h}\right)_K \\
&+ \sum_{K \in \mathscr{T}_h} \tau_{\mathbf{v},K} \left(\Delta t\theta_8 \frac{1}{\rho_h^{(n+1)}} \nabla (p_h^*)^{(n+1)}, (\bar{\mathbf{v}} \cdot \nabla) \varphi_{\mathbf{v},h} - \nu_a \Delta \varphi_{\mathbf{v},h}\right)_K \\
&- \sum_{K \in \mathscr{T}_h} \tau_{\mathbf{v},K} \left(\Delta t\theta_{10} \left(f v_h^{(n+1)}, -f u_h^{(n+1)}, -\frac{(\rho_h^*)^{(n+1)}}{\rho_h^{(n+1)}} g\right)^\top, (\bar{\mathbf{v}} \cdot \nabla) \varphi_{\mathbf{v},h} - \nu_a \Delta \varphi_{\mathbf{v},h}\right)_K \\
&- \sum_{K \in \mathscr{T}_h} \tau_{\mathbf{v},K} \left(\Delta t\theta_3 \nu \Delta \mathbf{v}_h^{(n)}, (\bar{\mathbf{v}} \cdot \nabla) \varphi_{\mathbf{v},h} - \nu_a \Delta \varphi_{\mathbf{v},h}\right)_K \\
&- \sum_{K \in \mathscr{T}_h} \tau_{\mathbf{v},K} \left(\Delta t\theta_9 \nu \Delta \mathbf{v}_h^{(n+1)}, (\bar{\mathbf{v}} \cdot \nabla) \varphi_{\mathbf{v},h} - \nu_a \Delta \varphi_{\mathbf{v},h}\right)_K
\end{aligned}
\tag{2.144}
$$

holds with $\tau_{\mathbf{v},K} \geq 0$ for all $\varphi_{\mathbf{v},h} \in (X_h)^3$ and all $n = 0, \ldots, M-1$, where

$$\rho_h^{(i)} := (\rho_h^*)^{(i)} + \rho_0.$$

Furthermore, it holds

$$\left(\mathbf{v}_h^{(0)} - \mathbf{v}_0, \psi_{\mathbf{v},h}\right) = 0 \quad \forall \psi_{\mathbf{v},h} \in (V_h)^3. \tag{2.145}$$

3. The integral identity

$$\begin{aligned}
0 = &\left((\rho_h^*)^{(n+1)} - (\rho_h^*)^{(n)}, \varphi_{\rho,h}\right) \\
&+ \left(\Delta t\theta_5 \left(w_h^{(n)}\partial_z\rho_0 + \mathbf{v}_h^{(n)} \cdot \nabla(\rho_h^*)^{(n)} + \rho_h^{(n)}\text{div } \mathbf{v}_h^{(n)}\right), \varphi_{\rho,h}\right) \\
&+ \left(\Delta t\theta_{11} \left(w_h^{(n+1)}\partial_z\rho_0 + \mathbf{v}_h^{(n+1)} \cdot \nabla(\rho_h^*)^{(n+1)} + \rho_h^{(n+1)}\text{div } \mathbf{v}_h^{(n+1)}\right), \varphi_{\rho,h}\right) \\
&+ \sum_{K\in\mathscr{T}_h} \tau_{\rho,K} \left((\rho_h^*)^{(n+1)} - (\rho_h^*)^{(n)}, \bar{\mathbf{v}} \cdot \nabla\varphi_{\rho,h}\right)_K \\
&+ \sum_{K\in\mathscr{T}_h} \tau_{\rho,K} \left(\Delta t\theta_5 \left(w_h^{(n)}\partial_z\rho_0 + \mathbf{v}_h^{(n)} \cdot \nabla(\rho_h^*)^{(n)} + \rho_h^{(n)}\text{div } \mathbf{v}_h^{(n)}\right), \bar{\mathbf{v}} \cdot \nabla\varphi_{\rho,h}\right)_K \\
&+ \sum_{K\in\mathscr{T}_h} \tau_{\rho,K} \left(\Delta t\theta_{11} \left(w_h^{(n+1)}\partial_z\rho_0 + \mathbf{v}_h^{(n+1)} \cdot \nabla(\rho_h^*)^{(n+1)}\right), \bar{\mathbf{v}} \cdot \nabla\varphi_{\rho,h}\right)_K \\
&+ \sum_{K\in\mathscr{T}_h} \tau_{\rho,K} \left(\Delta t\theta_{11}\rho_h^{(n+1)}\text{div } \mathbf{v}_h^{(n+1)}, \bar{\mathbf{v}} \cdot \nabla\varphi_{\rho,h}\right)_K
\end{aligned} \tag{2.146}$$

holds with $\tau_{\rho,K} \geq 0$ for all $\varphi_{\rho,} \in Y_h$ and all $n = 0, \ldots, M-1$, where

$$\rho_h^{(i)} := (\rho_h^*)^{(i)} + \rho_0.$$

Furthermore, it holds

$$\left((\rho_h^*)^{(0)} - \rho_0^*, \psi_{\rho,h}\right) = 0 \quad \forall\psi_{\rho,h} \in Q_h. \tag{2.147}$$

4. The integral identity

$$\begin{aligned}
0 = &\left((\theta_{v,h}^*)^{(n+1)} - (\theta_{v,h}^*)^{(n)}, \varphi_{\theta,h}\right) \\
&+ \left(\Delta t\theta_6 \left(w_h^{(n)}\partial_z\theta_{v,0} + \mathbf{v}_h^{(n)} \cdot \nabla(\theta_{v,h}^*)^{(n)}\right), \varphi_{\theta,h}\right) \\
&+ \left(\Delta t\theta_{12} \left(w_h^{(n+1)}\partial_z\theta_{v,0} + \mathbf{v}_h^{(n+1)} \cdot \nabla(\theta_{v,h}^*)^{(n+1)}\right), \varphi_{\theta,h}\right) \\
&+ \sum_{K\in\mathscr{T}_h} \tau_{\theta,K} \left((\theta_{v,h}^*)^{(n+1)} - (\theta_{v,h}^*)^{(n)}, \bar{\mathbf{v}} \cdot \nabla\varphi_{\theta,h}\right)_K \\
&+ \sum_{K\in\mathscr{T}_h} \tau_{\theta,K} \left(\Delta t\theta_6 \left(w_h^{(n)}\partial_z\theta_{v,0} + \mathbf{v}_h^{(n)} \cdot \nabla(\theta_{v,h}^*)^{(n)}\right), \bar{\mathbf{v}} \cdot \nabla\varphi_{\theta,h}\right)_K \\
&+ \sum_{K\in\mathscr{T}_h} \tau_{\theta,K} \left(\Delta t\theta_{12} \left(w_h^{(n+1)}\partial_z\theta_{v,0} + \mathbf{v}_h^{(n+1)} \cdot \nabla(\theta_{v,h}^*)^{(n+1)}\right), \bar{\mathbf{v}} \cdot \nabla\varphi_{\theta,h}\right)_K
\end{aligned} \tag{2.148}$$

holds with $\tau_{\theta,K} \geq 0$ for all $\varphi_\theta \in Y_h$ and all $n = 0, \ldots, M-1$. Furthermore, it holds

$$\left(\left(\theta_{v,h}^*\right)^{(0)} - \theta_{v,0}^*, \psi_{\theta,h}\right) = 0 \quad \forall\psi_{\theta,h} \in Q_h. \tag{2.149}$$

5. The integral identity

$$\begin{aligned}
0 = &\left((p_h^*)^{(n+1)} + p_0, \varphi_{p,h}\right) \\
&- \left(\left[\frac{\left(-\frac{g\kappa}{\theta_z}\ln\left(1 + \frac{\theta_z z}{\theta_0}\right) + R'\right)(\rho_h^*)^{(n+1)}\theta_{v,h}^{(n+1)}}{p_0} + 1 + \frac{(\theta_{v,h}^*)^{(n+1)}}{\theta_{v,0}}\right]^{\frac{1}{1-\kappa}} p_0, \varphi_{p,h}\right)
\end{aligned} \tag{2.150}$$

holds for all $\varphi_{p,h} \in Z_h$ and all $n = 0, \ldots, M-1$, where

$$\theta_{v,h}^{(n+1)} := (\theta_{v,h}^*)^{(n+1)} + \theta_{v,0}.$$

Furthermore, it holds

$$\left((p_h^*)^{(0)} - p_0^*, \psi_{p,h}\right) = 0 \quad \forall \psi_{p,h} \in P_h. \tag{2.151}$$

2.3.3.1. Choice of stabilisation parameters

With the notion of a time-discrete solution of Problem 2.15 and the corresponding notation of the time discretisation, the precise choice of the stabilisation parameters $\tau_{\mathbf{v},K}$, $\tau_{\rho,K}$ and $\tau_{\theta,K}$ is stated next.

The question how to choose the *optimal* stabilisation parameters in the context of compressible and incompressible flows is, to the best of the knowledge of the author, open and an active field of research. Many choices are proposed in the literature, see, e.g., [1, 16, 17, 43, 72–74] and the references therein, which are often based on heuristic arguments and observations. The choice given here can be found in, e.g., [13, 17, 40], and for a derivation of the parameters refer to these references.

Let $h_K > 0$ denote the diameter of the cell $K \in \mathscr{T}_h$, $\Delta t > 0$ the time-step size and

$$\|\mathbf{u}\|_{\infty,K} := \max\left\{\sqrt{\mathbf{u}(\mathbf{x})^\top \mathbf{u}(\mathbf{x})} : \quad \mathbf{x} \in K\right\},$$

i.e., the point-wise maximum of the vector field $\mathbf{u}$ on K in the Euclidean norm. The stabilisation parameters in Problem 2.15 are chosen as follows:

$$\begin{aligned} \tau_{\mathbf{v},K} &= \delta_0 \left[\frac{1}{\Delta t} + \frac{\nu_a}{h_K^2} + \frac{\|\bar{\mathbf{v}}\|_{\infty,K}}{h_K}\right]^{-1}, \\ \tau_{\rho,K} = \tau_{\theta,K} &= \|\bar{\mathbf{v}}\|_{\infty,K}^2 \cdot \tau_{\mathbf{v},K}, \\ \delta_0 &= 0.2, \end{aligned}$$

where

$$\bar{\mathbf{v}} := \mathbf{v}_h^{(n)},$$

i.e., in the time-step for the computation of the quantities at the next point in time t_{n+1}, the velocity field at the last time-step $\mathbf{v}_h^{(n)}$ is taken as reference velocity.

3. Low-Mach approximation

Contents

A characteristic property of the fully Compressible Navier-Stokes model, which was derived in the previous chapter, is the possible presence of acoustic waves. Whenever modes travelling at the speed of sound arise in the dynamics of the considered application scenario, they are the motion with the highest speed in the domain.

Considering a numerical discretisation of the governing equations, the maximum time-step size, that can be chosen for a stable simulation of the dynamics in time, depends on the ratio of the minimum grid spacing to the speed of the fastest motion in the domain. For explicit schemes, the time-step size *necessarily* has to be smaller than this ratio, whereas in the case implicit schemes the time-step size may be chosen larger, depending on the applied time-stepping method. Therefore, the presence of acoustic waves limits the maximum possible stable choice of the time-step size. Particularly, this issue arises for acoustic modes, which travel in vertical direction, as the grid spacing in the vertical is usually considerably finer than in the horizontal [46].

But for many relevant atmospheric fluid flows, only the velocity field at Mach numbers much smaller than one is of interest and not the sound produced by the fluid flow. Therefore, filtering out the acoustic waves as a solution to the governing equations, i.e., modifying these equations on the modelling level, is a feasible approach in order to relax the demands on the time-stepping method in terms of the maximum possible time-step size. As the described problem is in particular relevant in vertical direction, there are basically two well-known possibilities to remove vertical acoustic modes [46]. One possibility is to remove the total derivative $\frac{\mathrm{d}w}{\mathrm{d}t}$ from the vertical momentum equation. The other possible approach is to remove the local derivative $\partial_t \rho$ from the continuity equation.

The first approach yields the so called *hydrostatic approximation* and the second one the so called *anelastic approximation*. The popular *Boussinesq approximation* is a special case of the anelastic approximation in the case of a shallow flow. Therefore, a model, which solves the full vertical momentum equation, is called a *non-hydrostatic model*. Furthermore, a non-hydrostatic model can be *anelastic*, i.e., the anelastic continuity equation is solved, or *elastic*, i.e., the full continuity equation is solved. Therefore, the fully Compressible Navier-Stokes model presented in Chapter 2 is an elastic non-hydrostatic model. Observe, that the incompressible Navier-Stokes

equations are a special case of an anelastic model in this context. Both approximations, hydrostatic and anelastic, require further modifications or even new equations in order to obtain all solution components, i.e., velocity, density, temperature and pressure, see, [42, 46], for example. It has to be emphasized, that in both hydrostatic and anelastic models acoustic waves, which propagate in horizontal directions, may still be present.

In this chapter, another approach to filter out acoustic waves from the solution of the governing equations is considered. Based on a scale analysis of the pressure for flows at Low-Mach numbers it can be derived, that certain parts of the total pressure are negligible small compared to the others. Therefore, it is justifiable to neglect these parts in the ideal gas law and, therefore, decouple density from these small parts of pressure. The result is the so called *Low-Mach number approximation*. It turns out, that this leads to a removal of acoustic modes from the solution of the governing system of equations in *all* spatial directions. Furthermore, the resulting model is still both non-hydrostatic and elastic. Approximations of this type have been studied since the 1980s, see references [52, 56, 57], for example.

The remainder of this chapter is organised as follows: In Section 3.1, the Low-Mach number approximation is applied to the fully compressible Navier-Stokes equations. The applied splitting of the pressure introduces a new part of pressure, which needs an additional equation to determine its evolution in time. The required equation is derived in Section 3.2. The discretisation of the resulting governing system of equations by means of finite elements in space and finite differences in time is described in Section 3.3.

3.1. Derivation

In order to filter out acoustic waves from the compressible Navier-Stokes equations by means of the Low-Mach number approximation, the *total pressure* p is split in three parts [15],

$$p(x,t) := p_{th}(t) + p_0(x) + p^*(x,t), \tag{3.1}$$

where p_{th} denotes the *thermodynamic pressure*, which is constant in space, p_0 is the *hydrostatic pressure* and corresponds to the pressure reference state derived in (2.84), and p^* is the *hydrodynamic pressure*. In the Low-Mach number flow regime, it holds [15, 56, 57]

$$|p^*(x,t)| \ll |p_{th}(t) + p_0(x)|$$

and, therefore, the hydrodynamic part of the pressure may be neglected in the ideal gas law. Consequently, density is decoupled from the hydrodynamic pressure part, which implies the filtering of acoustic modes. A rigorous theoretical scale analysis is given in [57].

Remark 3.1 (Pressure splitting)
The scale analysis in [57] leads to a splitting

$$p(x,t) = p_{th}(t) + \tilde{p}(x,t)$$

with

$$|\tilde{p}(\cdot,t)| \ll |p_{th}(t)|\,.$$

In atmospheric dynamics, the pressure reference state $p_0(x)$ holds an important role for the stability of the stratification of the atmosphere, see Subsection 2.1.5. Therefore, it is separately considered and, as it is constant in time and does not account for acoustic modes, is treated in the ideal gas law like the thermodynamic pressure part p_{th}.

Consequently, the ideal gas law becomes an equation for the density,

$$\rho = \frac{(1000\ hPa)^{\kappa}\,(p_{th}(t) + p_0(x))^{1-\kappa}}{R\theta_v}. \tag{3.2}$$

Inserting (3.2) into (2.90) and using (2.97) yields

$$\begin{aligned}
0 &= \partial_t \rho + \operatorname{div}\ \rho\mathbf{v} \\
&\overset{(3.2)}{=} \partial_t \left(\frac{(1000\ hPa)^{\kappa}\,(p_{th}+p_0)^{1-\kappa}}{R\theta_v} \right) + \operatorname{div}\ \left(\frac{(1000\ hPa)^{\kappa}\,(p_{th}+p_0)^{1-\kappa}}{R\theta_v} \cdot \mathbf{v} \right) \\
&= \frac{(1000\ hPa)^{\kappa}\, R\theta_v(1-\kappa)\partial_t p_{th}(p_{th}+p_0)^{-\kappa} - (1000\ hPa)^{\kappa}\,(p_{th}+p_0)^{1-\kappa} R\partial_t\theta_v^*}{R^2\theta_v^2} \\
&+ \left(\frac{(1000\ hPa)^{\kappa}\,(p_{th}+p_0)^{1-\kappa}}{R\theta_v} \right) \operatorname{div}\ \mathbf{v} \\
&+ \mathbf{v} \cdot \left(\frac{R\theta_v\,(1000\ hPa)^{\kappa}\,(1-\kappa)(p_{th}+p_0)^{-\kappa}}{R^2\theta_v^2} \nabla p_0 - \frac{(1000\ hPa)^{\kappa}\,(p_{th}+p_0)^{1-\kappa} R}{R^2\theta_v^2} \nabla\theta_v \right) \\
&= \frac{(1000\ hPa)^{\kappa}\,(1-\kappa)(p_{th}+p_0)^{-\kappa}}{R\theta_v} \left(\partial_t p_{th} + \mathbf{v}\cdot\nabla p_0\right) \\
&+ \left(\frac{(1000\ hPa)^{\kappa}\,(p_{th}+p_0)^{1-\kappa}}{R\theta_v} \right) \operatorname{div}\ \mathbf{v} \\
&- \frac{(1000\ hPa)^{\kappa}\,(p_{th}+p_0)^{1-\kappa} R}{R^2\theta_v^2} \left(\partial_t\theta_v^* + \mathbf{v}\cdot\nabla\theta_v\right) \\
&\overset{(2.97)}{=} \frac{(1000\ hPa)^{\kappa}\,(1-\kappa)(p_{th}+p_0)^{-\kappa}}{R\theta_v} \left(\partial_t p_{th} + \mathbf{v}\cdot\nabla p_0\right) \\
&+ \left(\frac{(1000\ hPa)^{\kappa}\,(p_{th}+p_0)^{1-\kappa}}{R\theta_v} \right) \operatorname{div}\ \mathbf{v}.
\end{aligned}$$

Multiplying both sides by

$$\frac{R\theta_v}{(1000\ hPa)^{\kappa}\,(p_{th}+p_0)^{-\kappa}(1-\kappa)} \tag{3.3}$$

finally yields the continuity equation

$$\partial_t p_{th} + \mathbf{v}\cdot\nabla p_0 + \frac{p_{th}+p_0}{1-\kappa} \operatorname{div}\ \mathbf{v} = 0 \tag{3.4}$$

of the Low-Mach number approximation.

Remark 3.2
The multiplication by (3.3) is allowed since in the considered Low-Mach regime it holds

$$p_{th} + p_0 > 0 \quad \text{and} \quad \theta_v > 0 \quad \text{for all } x \in \Omega,\ t \in [0,T].$$

Observe, that p^* is only determined up to an additive constant in the Low-Mach number approximation because only its gradient occurs in the momentum equation and there is no algebraic law or instationary partial differential equation that determines the pressure uniquely. Therefore, the hydrodynamic part of the pressure p^* is required to fulfil the condition

$$\int_{\Omega} p^* \mathrm{d}x = 0. \tag{3.5}$$

at any time $t \in [0,T]$.

So the system of the Low-Mach number approximation reads in analogy to Problem 2.6:

Problem 3.3 (Low-Mach model, without p_{th})
Let $\Omega \subset \mathbb{R}^3$ be as in (2.94) and $T \geq 0$ a final point in time. Find a velocity field $\mathbf{v} := (u,v,w)^\top : [0,T) \times \Omega \to \mathbb{R}^3$, a density perturbation $\rho^* : [0,T) \times \Omega \to \mathbb{R}$, a temperature perturbation $\theta_v^* : [0,T) \times \Omega \to \mathbb{R}$ and a pressure perturbation $p^* : [0,T) \times \Omega \to \mathbb{R}$, which fulfils (3.5), satisfying

$$\partial_t \mathbf{v} + (\mathbf{v} \cdot \nabla)\mathbf{v} + \frac{1}{\rho}\nabla p^* - \nu_a \Delta \mathbf{v} + \left(-fv, fu, \frac{\rho^*}{\rho} g\right)^\top = 0 \tag{3.6}$$

$$\partial_t p_{th} + w \partial_z p_0 + \frac{p_{th} + p_0}{1-\kappa} \text{div } \mathbf{v} = 0 \tag{3.7}$$

$$\partial_t \theta_v^* + w \partial_z \theta_{v,0} + (\mathbf{v} \cdot \nabla)\, \theta_v^* = 0 \tag{3.8}$$

$$\frac{\left(\frac{p_0}{p_{th}+p_0}\right)^\kappa p_{th}\theta_{v,0} + \left[\left(\frac{p_0}{p_{th}+p_0}\right)^\kappa - 1\right] p_0 \theta_{v,0} - p_0 \theta_v^*}{\left(-\frac{g\kappa}{R'\theta_z} \ln\left(1 + \frac{\theta_z z}{\theta_0}\right) + 1\right) R'\,(\theta_{v,0} + \theta_v^*)\,\theta_{v,0}} = \rho^* \tag{3.9}$$

$$w = 0 \quad \text{on} \quad [0,T] \times \Gamma \tag{3.10}$$

$$\mathbf{v}(0,x) = \mathbf{v}_0(x), \quad \rho^*(0,x) = \rho_0^*(x), \quad \theta_v^*(0,x) = \theta_{v,0}^*(x), \quad p^*(0,x) = p_0^*(x) \tag{3.11}$$

as well as periodic boundary conditions in both horizontal directions for all variables $\mathbf{v}$, ρ^*, θ_v^* and p^*,

$$\rho_0^* := \frac{(1000\ hPa)^\kappa\,(p_{th}(t) + p_0(x))^{1-\kappa}}{R'\left(\theta_{v,0}^* + \theta_0\right)} - \rho_0$$

and

$$\rho := \rho^* + \rho_0.$$

Equations (3.6)-(3.9) are required to hold on $(0,T) \times \Omega$ and (3.11) is asked to hold on $\{t = 0\} \times \Omega$.

Remark 3.4 (Stability of ideal gas law)
In analogy to Remark 2.9 the ideal gas law (3.2) is reformulated towards (3.9) in order to increase the stability of its numerical evaluation for small perturbations and small thermodynamic pressure as follows. As in Remark 2.9, (2.101) and (2.102) are inserted into (3.2)

$$\begin{aligned}
\rho^* &= \frac{(1000\ hPa)^\kappa (p_{th}+p_0)^{1-\kappa}}{R'\,(\theta_v^* + \theta_{v,0})} - \rho_0 \\
&= \frac{p_0^\kappa (p_{th}+p_0)^{1-\kappa}}{b_p R'\,(\theta_v^* + \theta_{v,0})} - \frac{p_0}{R'\theta_{v,0} b_p} \\
&= \frac{\left(\frac{p_0}{p_{th}+p_0}\right)^\kappa (p_{th}+p_0)}{b_p R'\,(\theta_v^* + \theta_{v,0})} - \frac{p_0}{R'\theta_{v,0} b_p} \\
&= \frac{\left(\frac{p_0}{p_{th}+p_0}\right)^\kappa (p_{th}+p_0)\theta_{v,0} - p_0\,(\theta_v^* + \theta_{v,0})}{b_p R'\,(\theta_v^* + \theta_{v,0})\,\theta_{v,0}} \\
&= \frac{\left(\frac{p_0}{p_{th}+p_0}\right)^\kappa p_{th}\theta_{v,0} + \left[\left(\frac{p_0}{p_{th}+p_0}\right)^\kappa - 1\right] p_0\theta_{v,0} - p_0\theta_v^*}{b_p R'\,(\theta_v^* + \theta_{v,0})\,\theta_{v,0}},
\end{aligned}$$

which is (3.9).

3.2. Determination of the thermodynamic pressure

With the splitting of the pressure described above, the thermodynamic part of the pressure has been introduced as additional unknown function of time and has to be determined independently of (3.6)-(3.9).

The continuity equation (3.7) shall hold at any time $t \in [0, T)$ and at all points in Ω. Therefore, the integral of (3.7) over Ω has to vanish at any time t:

$$\int_\Omega \left(\partial_t p_{th} + w \partial_z p_0 + \frac{p_{th} + p_0}{1 - \kappa} \text{div } \mathbf{v} \right) \mathrm{d}x = 0. \tag{3.12}$$

Since $\partial_t p_{th}$ does not depend on the spatial location x, it can be extracted from the integral expression (3.12) due to the linearity of integration. This yields the equation

$$\partial_t p_{th} = -\frac{\int_\Omega \left((1-\kappa) w \partial_z p_0 + (p_{th} + p_0) \text{div } \mathbf{v} \right) \mathrm{d}x}{(1-\kappa) \left| \Omega \right|}, \tag{3.13}$$

where

$$|\Omega| := \int_\Omega 1 \mathrm{d}x$$

denotes the volume of the domain Ω.

Remark 3.5 (Role of thermodynamic pressure p_{th})
Since the dynamic behaviour of p_{th} in time is derived from (3.7), the role of p_{th} in the Low-Mach model can be interpreted as the quantity, which balances thermodynamic effects in the conservation of mass in the course of time. Therefore, at $t = 0$, where everything is balanced and the dynamics of the system just start,

$$p_{th}(0) = 0$$

can be chosen.

The integral in the numerator of (3.13) can be simplified as follows: The boundary conditions of Problem 3.3, together with the definition of Ω and its boundary (2.94), yield the following identity:

$$\begin{aligned}
\int_\Omega \left((1-\kappa) w \partial_z p_0 + (p_{th} + p_0) \text{div } \mathbf{v} \right) \mathrm{d}x &= \int_\Omega \left((1-\kappa) w \partial_z p_0 + \sum_{i=1}^{3} (p_{th} + p_0) \partial_i \mathbf{v}_i \right) \mathrm{d}x \\
&= \int_\Omega \left((1-\kappa) w \partial_z p_0 - \sum_{i=1}^{3} \partial_i (p_{th} + p_0) \mathbf{v}_i \right) \mathrm{d}x \\
&\quad + \underbrace{\int_\Gamma (p_{th} + p_0) \mathbf{n}_i \mathbf{v}_i \mathrm{d}s}_{=0} \\
&= \int_\Omega \left((1-\kappa) w \partial_z p_0 - w \partial_z p_0 \right) \mathrm{d}x \\
&= -\int_\Omega \kappa w \partial_z p_0 \mathrm{d}x.
\end{aligned}$$

Consequently, the full system of the Low-Mach number approximation reads:

Problem 3.6 (Low-Mach model)
Let $\Omega \subset \mathbb{R}^3$ be as in (2.94) and $T \geq 0$ a final point in time. Find a velocity field $\mathbf{v} := (u, v, w)^\top : [0, T) \times \Omega \to \mathbb{R}^3$, a density perturbation $\rho^* : [0, T) \times \Omega \to \mathbb{R}$, a temperature perturbation $\theta_v^* : [0, T) \times \Omega \to \mathbb{R}$, a pressure perturbation $p^* : [0, T) \times \Omega \to \mathbb{R}$ and a thermodynamic pressure $p_{th} : [0, T) \to \mathbb{R}$, which fulfils (3.5), satisfying

$$\partial_t \mathbf{v} + (\mathbf{v} \cdot \nabla)\mathbf{v} + \frac{1}{\rho}\nabla p^* - \nu_a \Delta \mathbf{v} + \left(-fv, fu, \frac{\rho^*}{\rho} g\right)^\top = 0 \tag{3.14}$$

$$\partial_t p_{th} + w \partial_z p_0 + \frac{p_{th} + p_0}{1 - \kappa} \text{div } \mathbf{v} = 0 \tag{3.15}$$

$$\partial_t \theta_v^* + w \partial_z \theta_{v,0} + (\mathbf{v} \cdot \nabla)\, \theta_v^* = 0 \tag{3.16}$$

$$\frac{\left(\frac{p_0}{p_{th}+p_0}\right)^\kappa p_{th} \theta_{v,0} + \left[\left(\frac{p_0}{p_{th}+p_0}\right)^\kappa - 1\right] p_0 \theta_{v,0} - p_0 \theta_v^*}{\left(-\frac{g\kappa}{R'\theta_z} \ln\left(1 + \frac{\theta_z z}{\theta_0}\right) + 1\right) R'\left(\theta_{v,0} + \theta_v^*\right) \theta_{v,0}} = \rho^* \tag{3.17}$$

$$\partial_t p_{th} - \frac{\int_\Omega \kappa w \partial_z p_0 \mathrm{d}x}{(1 - \kappa)\,|\Omega|} = 0 \tag{3.18}$$

$$w = 0 \quad \text{on} \quad [0, T] \times \Gamma \tag{3.19}$$

$$\mathbf{v}(0, x) = \mathbf{v}_0(x), \quad \rho^*(0, x) = \rho_0^*(x), \quad \theta_v^*(0, x) = \theta_{v,0}^*(x), \quad p^*(0, x) = p_0^*(x), \quad p_{th}(0) = 0 \tag{3.20}$$

as well as periodic boundary conditions in both horizontal directions for all variables $\mathbf{v}$, ρ^*, θ_v^* and p^*,

$$\rho_0^* := \frac{(1000\ hPa)^\kappa \left(p_{th}(t) + p_0(x)\right)^{1-\kappa}}{R'\left(\theta_{v,0}^* + \theta_0\right)} - \rho_0$$

and

$$\rho := \rho^* + \rho_0.$$

Equations (3.14)-(3.17) are required to hold on $(0, T) \times \Omega$ and (3.20) is asked to hold on $\{t = 0\} \times \Omega$.

3.3. Discretisation

The discrete formulation of the Low-Mach model is derived in a different way than the one for the Compressible Navier-Stokes model above, see Section 2.3. First, Problem 3.6 is semi-discretised in time, which yields a sequence of systems of stationary partial differential equations (Subsection 3.3.1). The resulting sequence is formulated as a sequence of weak problems afterwards (Subsection 3.3.2). Subsequently, a finite element discretisation is applied in space (Subsection 3.3.3) and, finally, stabilised (Subsection 3.3.4).

3.3.1. Discretisation in time

Problem 3.6 is discretised in time with the so called θ-scheme as above for the Compressible Navier-Stokes model, see Subsection 2.3.3. With the temporal grid and the notations, that have been introduced above, the semi-discrete formulation of Problem 3.6 reads as follows:

Problem 3.7 (Semi-discrete formulation of Problem 3.6)
Let $\Omega \subset \mathbb{R}^3$ be as in (2.94) and $T \geq 0$ a final point in time. Furthermore, let t_i, $i = 0, \ldots, M$ be a an equidistant discretisation of the interval $[0, T]$ as defined in (2.140). Let $\theta_j \in [0, 1]$,

$j = 1, \dots, 12$ be such that

$$\theta_j + \theta_{j+6} = 1, \quad j = 1, \dots, 6,$$

as well as $\theta_{13}, \theta_{14} \in [0, 1]$ such that

$$\theta_{13} + \theta_{14} = 1.$$

Find

$$\mathbf{v}^{(n)} \in \left(C^2(\Omega)\right)^3, \quad (\rho^*)^{(n)}, (\theta_v^*)^{(n)} \in C^1(\Omega), \quad (p^*)^{(n)} \in C^1(\Omega), \quad p_{th}^{(n)} \in \mathbb{R} \quad \forall\, n = 1, \dots, M, \tag{3.21}$$

where

$$\mathbf{v}^{(n)} := \left(u^{(n)}, v^{(n)}, w^{(n)}\right)^\top$$

and p^* fulfils (3.5), such that the following conditions are satisfied:

1. The variables satisfy

$$w^{(n)} = 0 \quad \text{on } \Gamma, \quad \forall\, n = 0, \dots, M, \tag{3.22}$$

as well as periodic boundary conditions in both horizontal directions.

2. The partial differential equation

$$\begin{aligned} 0 = {} & \mathbf{v}^{(n+1)} - \mathbf{v}^{(n)} + \Delta t \theta_1 (\mathbf{v}^{(n)} \cdot \nabla)\mathbf{v}^{(n)} + \Delta t \theta_7 (\mathbf{v}^{(n+1)} \cdot \nabla)\mathbf{v}^{(n+1)} \\ & + \Delta t \theta_2 \frac{1}{\rho^{(n)}} \nabla (p^*)^{(n)} + \Delta t \theta_8 \frac{1}{\rho^{(n+1)}} \nabla (p^*)^{(n+1)} \\ & + \Delta t \theta_4 \left(-f v^{(n)}, f u^{(n)}, \frac{(\rho^*)^{(n)}}{\rho^{(n)}} g\right)^\top + \Delta t \theta_{10} \left(-f v^{(n+1)}, f u^{(n+1)}, \frac{(\rho^*)^{(n+1)}}{\rho^{(n+1)}} g\right)^\top \\ & - \Delta t \theta_3 \nu_a \Delta \mathbf{v}^{(n)} - \Delta t \theta_9 \nu_a \Delta \mathbf{v}^{(n)} \end{aligned} \tag{3.23}$$

holds in Ω for all $n = 0, \dots, M-1$. Furthermore, it holds

$$\mathbf{v}^{(0)} = \mathbf{v}_0 \quad \text{in } \Omega.$$

3. The partial differential equation

$$\begin{aligned} 0 = {} & \frac{p_{th}^{(n+1)} - p_{th}^{(n)}}{p_{th}^{(n+1)} + p_0} + \frac{\Delta t \theta_5}{p_{th}^{(n+1)} + p_0} \left(w^{(n)} \partial_z p_0 + \frac{p_{th}^{(n)} + p_0}{1 - \kappa} \operatorname{div} \mathbf{v}^{(n)}\right) \\ & + \frac{\Delta t \theta_{11}}{1 - \kappa} \operatorname{div} \mathbf{v}^{(n+1)} + \frac{\Delta t \theta_{11}}{p_{th}^{(n+1)} + p_0} w^{(n+1)} \partial_z p_0 \end{aligned} \tag{3.24}$$

holds in Ω for all $n = 0, \dots, M-1$. Furthermore, it holds

$$(p^*)^{(0)} = p_0^* \quad \text{in } \Omega.$$

4. The partial differential equation

$$\begin{aligned} 0 = {} & (\theta_v^*)^{(n+1)} - (\theta_v^*)^{(n)} + \Delta t \theta_6 \left(w^{(n)} \partial_z \theta_{v,0} + \left(\mathbf{v}^{(n)} \cdot \nabla\right) (\theta_v^*)^{(n)}\right) \\ & + \Delta t \theta_{12} \left(w^{(n+1)} \partial_z \theta_{v,0} + \left(\mathbf{v}^{(n+1)} \cdot \nabla\right) (\theta_v^*)^{(n+1)}\right) \end{aligned} \tag{3.25}$$

holds in Ω for all $n = 0, \dots, M-1$. Furthermore, it holds

$$(\theta_v^*)^{(0)} = \theta_{v,0}^* \quad \text{in } \Omega.$$

5. The identity

$$\frac{\left(\frac{p_0}{p_{th}^{(n+1)}+p_0}\right)^{\kappa} p_{th}^{(n+1)}\theta_{v,0} + \left[\left(\frac{p_0}{p_{th}^{(n+1)}+p_0}\right)^{\kappa} - 1\right] p_0\theta_{v,0} - p_0\left(\theta_v^*\right)^{(n+1)}}{\left(-\frac{g\kappa}{R'\theta_z}\ln\left(1+\frac{\theta_z z}{\theta_0}\right)+1\right) R'\left(\theta_{v,0}+\left(\theta_v^*\right)^{(n+1)}\right)\theta_{v,0}} = \left(\rho^*\right)^{(n+1)} \tag{3.26}$$

holds in Ω for all $n = 0, \ldots, M-1$. Furthermore, it holds

$$\left(\rho^*\right)^{(0)} = \rho_0^* \quad \text{in } \Omega.$$

6. The identity

$$p_{th}^{(n+1)} - p_{th}^{(n)} - \Delta t\theta_{13}\frac{\int_\Omega \kappa w^{(n)}\partial_z p_0 \mathrm{d}x}{(1-\kappa)|\Omega|} - \Delta t\theta_{14}\frac{\int_\Omega \kappa w^{(n+1)}\partial_z p_0 \mathrm{d}x}{(1-\kappa)|\Omega|} = 0 \tag{3.27}$$

holds for all $n = 0, \ldots, M-1$. Furthermore, it holds

$$p_{th}^{(0)} = 0.$$

Remark 3.8 (Semi-discrete formulation of continuity equation)
The direct application of the θ-scheme to (3.15) leads to the semi-discrete equation

$$\begin{aligned} 0 &= p_{th}^{(n+1)} - p_{th}^{(n)} \\ &+ \Delta t\left(\theta_5\left(w^{(n)}\partial_z p_0 + \frac{p_{th}^{(n)}+p_0}{1-\kappa}\operatorname{div}\mathbf{v}^{(n)}\right) + \theta_{11}\left(w^{(n+1)}\partial_z p_0 + \frac{p_{th}^{(n+1)}+p_0}{1-\kappa}\operatorname{div}\mathbf{v}^{(n+1)}\right)\right). \end{aligned}$$

Dividing the whole equation by $\left(p_{th}^{(n+1)}+p_0\right)$ yields (3.24). This step is done in order to ensure that the factors in front of div $\mathbf{v}^{(n+1)}$ in (3.24) and $\frac{1}{\rho^{(n+1)}}\nabla\left(p^*\right)^{(n+1)}$ in (3.23), respectively, have the same order of magnitude. Otherwise, the condition number of the resulting Jacobian matrix of the fully discrete system in Section 4.3 would be significantly increased and, consequently, the convergence rate of the linear solver for the computation of the Newton step deteriorates, see Chapter 4 for details about the solution process.

3.3.2. Weak formulation of semi-discrete problem

The weak formulation is quite similar to the compressible case, except, that the continuity equation is tested with the test functions of the hydrodynamic pressure and the ideal gas law with those of the density variable, see [13, 40, 52], for example. Therefore, it is even closer to the case of the incompressible Navier-Stokes equations and, especially, inherits the saddle-point structure of the weak formulation as it contains the Stokes system as a special case.

Problem 3.9 (Weak formulation of Problem 3.7)
Let $\Omega \subset \mathbb{R}^3$ be as in (2.94) and $T \geq 0$ a final point in time. Furthermore, let t_i, $i = 0, \ldots, M$ be a an equidistant discretisation of the interval $[0, T]$ as defined in (2.140). Let $\theta_j \in [0, 1]$, $j = 1, \ldots, 12$ be such that

$$\theta_j + \theta_{j+6} = 1, \quad j = 1, \ldots, 6,$$

as well as $\theta_{13}, \theta_{14} \in [0, 1]$ such that

$$\theta_{13} + \theta_{14} = 1.$$

Find

$$\mathbf{v}^{(n)} \in \left(H^1(\Omega)\right)^3, \quad (\rho^*)^{(n)}, (\theta_v^*)^{(n)}, (p^*)^{(n)} \in H^1(\Omega), \quad p_{th}^{(n)} \in \mathbb{R} \quad \forall\, n = 1, \ldots, M, \tag{3.28}$$

where

$$\mathbf{v}^{(n)} := \left(u^{(n)}, v^{(n)}, w^{(n)}\right)^\top$$

and p^* fulfils (3.5), such that the following conditions are satisfied:

1. The variables satisfy

$$w^{(n)} = 0 \quad \text{on } \Gamma, \quad \forall\, n = 0, \ldots, M, \tag{3.29}$$

as well as periodic boundary conditions in both horizontal directions.

2. The integral identity

$$\begin{aligned} 0 = &\left(\mathbf{v}^{(n+1)} - \mathbf{v}^{(n)} + \Delta t\theta_1(\mathbf{v}^{(n)} \cdot \nabla)\mathbf{v}^{(n)} + \Delta t\theta_7(\mathbf{v}^{(n+1)} \cdot \nabla)\mathbf{v}^{(n+1)}, \varphi_{\mathbf{v}}\right) \\ &+ \left(\Delta t\theta_2 \frac{1}{\rho^{(n)}} \nabla\, (p^*)^{(n)} + \Delta t\theta_8 \frac{1}{\rho^{(n+1)}} \nabla\, (p^*)^{(n+1)}, \varphi_{\mathbf{v}}\right) \\ &+ \left(\Delta t\theta_4 \left(-fv^{(n)}, fu^{(n)}, \frac{(\rho^*)^{(n)}}{\rho^{(n)}} g\right)^\top + \Delta t\theta_{10} \left(-fv^{(n+1)}, fu^{(n+1)}, \frac{(\rho^*)^{(n+1)}}{\rho^{(n+1)}} g\right)^\top, \varphi_{\mathbf{v}}\right) \\ &+ \left(\Delta t\theta_3 \nu_a \nabla \mathbf{v}^{(n)} + \Delta t\theta_9 \nu_a \nabla \mathbf{v}^{(n)}, \nabla \varphi_{\mathbf{v}}\right) \end{aligned} \tag{3.30}$$

holds for all $\varphi_{\mathbf{v}} \in \left(H_0^1(\Omega)\right)^3$ and for all $n = 0, \ldots, M-1$. Furthermore, it holds

$$\left(\mathbf{v}^{(0)} - \mathbf{v}_0, \psi_{\mathbf{v}}\right) = 0 \quad \text{for all} \quad \psi_{\mathbf{v}} \in \left(H^1(\Omega)\right)^3.$$

3. The integral identity

$$\begin{aligned} 0 = &\left(\frac{p_{th}^{(n+1)} - p_{th}^{(n)}}{p_{th}^{(n+1)} + p_0} + \frac{\Delta t\theta_5}{p_{th}^{(n+1)} + p_0} \left(w^{(n)} \partial_z p_0 + \frac{p_{th}^{(n)} + p_0}{1-\kappa} \text{div } \mathbf{v}^{(n)}\right), \varphi_p\right) \\ &+ \left(\frac{\Delta t\theta_{11}}{1-\kappa} \text{div } \mathbf{v}^{(n+1)} + \frac{\Delta t\theta_{11}}{p_{th}^{(n+1)} + p_0} w^{(n+1)} \partial_z p_0, \varphi_p\right) \end{aligned} \tag{3.31}$$

holds for all $\varphi_p \in H_0^1(\Omega)$ and for all $n = 0, \ldots, M-1$. Furthermore, it holds

$$\left((p^*)^{(0)} - p_0^*, \psi_p\right) = 0 \quad \text{for all } \psi_p \in H^1(\Omega).$$

4. The integral identity

$$\begin{aligned} 0 = &\left((\theta_v^*)^{(n+1)} - (\theta_v^*)^{(n)} + \Delta t\theta_6 \left(w^{(n)} \partial_z \theta_{v,0} + \left(\mathbf{v}^{(n)} \cdot \nabla\right) (\theta_v^*)^{(n)}\right), \varphi_\theta\right) \\ &+ \left(\Delta t\theta_{12} \left(w^{(n+1)} \partial_z \theta_{v,0} + \left(\mathbf{v}^{(n+1)} \cdot \nabla\right) (\theta_v^*)^{(n+1)}\right), \varphi_\theta\right) \end{aligned} \tag{3.32}$$

holds for all $\varphi_\theta \in H_0^1(\Omega)$ and for all $n = 0, \ldots, M-1$. Furthermore, it holds

$$\left((\theta_v^*)^{(0)} - \theta_{v,0}^*, \psi_\theta\right) = 0 \quad \text{for all } \psi_\theta \in H^1(\Omega).$$

5. The integral identity

$$0 = \left((\rho^*)^{(n+1)}, \varphi_\rho\right) - \left(\frac{\left(\frac{p_0}{p_{th}^{(n+1)}+p_0}\right)^\kappa p_{th}^{(n+1)}\theta_{v,0} + \left[\left(\frac{p_0}{p_{th}^{(n+1)}+p_0}\right)^\kappa - 1\right] p_0\theta_{v,0} - p_0\left(\theta_v^*\right)^{(n+1)}}{\left(-\frac{g\kappa}{R'\theta_z}\ln\left(1+\frac{\theta_z z}{\theta_0}\right)+1\right) R'\left(\theta_{v,0} + \left(\theta_v^*\right)^{(n+1)}\right)\theta_{v,0}}, \varphi_\rho \right) \tag{3.33}$$

holds for all $\varphi_\rho \in H_0^1(\Omega)$ and for all $n = 0, \dots, M-1$. Furthermore, it holds

$$\left((\rho^*)^{(0)} - \rho_0^*, \psi_\rho\right) = 0 \quad \text{for all} \quad \psi_\rho \in H^1(\Omega).$$

6. The identity

$$p_{th}^{(n+1)} - p_{th}^{(n)} - \Delta t\theta_{13}\frac{\int_\Omega \kappa w^{(n)}\partial_z p_0 \mathrm{d}x}{(1-\kappa)|\Omega|} - \Delta t\theta_{14}\frac{\int_\Omega \kappa w^{(n+1)}\partial_z p_0 \mathrm{d}x}{(1-\kappa)|\Omega|} = 0 \tag{3.34}$$

holds for all $n = 0, \dots, M-1$. Furthermore, it holds

$$p_{th}^{(0)} = 0.$$

3.3.3. Discretisation in space

Problem 3.9 is discretised in space with the finite element method analogously to Subsection 2.3.1. With the same notation as for the finite element discretisation of the Compressible Navier-Stokes model, the fully discrete formulation of Problem 3.6 reads:

Problem 3.10 (Discrete formulation of Problem 3.9)
Let $\Omega \subset \mathbb{R}^3$ be as in (2.94), $\mathscr{T}_h$ a triangulation of Ω as in (2.116) and $T \geq 0$ a final point in time. Furthermore, let t_i, $i = 0, \dots, M$ be a an equidistant discretisation of the interval $[0, T]$ as defined in (2.140). Let $\theta_j \in [0,1]$, $j = 1, \dots, 12$ be such that

$$\theta_j + \theta_{j+6} = 1, \quad j = 1, \dots, 6,$$

as well as $\theta_{13}, \theta_{14} \in [0,1]$ such that

$$\theta_{13} + \theta_{14} = 1.$$

Find

$$\mathbf{v}_h^{(n)} \in (V_h)^3, \quad (\rho_h^*)^{(n)}, \left(\theta_{v,h}^*\right)^{(n)} \in Q_h, \quad (p_h^*)^{(n)} \in P_h, \quad p_{th}^{(n)} \in \mathbb{R} \quad \forall\, n = 1, \dots, M, \tag{3.35}$$

where

$$\mathbf{v}_h^{(n)} := \left(u_h^{(n)}, v_h^{(n)}, w_h^{(n)}\right)^\top$$

and p_h^* fulfils (3.5), such that the following conditions are satisfied:

1. The variables satisfy

$$w_h^{(n)} = 0 \quad \text{on } \Gamma, \quad \forall\, n = 0, \dots, M, \tag{3.36}$$

as well as periodic boundary conditions in both horizontal directions.

2. The integral identity

$$\begin{aligned}
0 = &\left(\mathbf{v}_h^{(n+1)} - \mathbf{v}_h^{(n)} + \Delta t\theta_1(\mathbf{v}_h^{(n)}\cdot\nabla)\mathbf{v}_h^{(n)} + \Delta t\theta_7(\mathbf{v}_h^{(n+1)}\cdot\nabla)\mathbf{v}_h^{(n+1)}, \varphi_{\mathbf{v},h}\right)\\
&+\left(\Delta t\theta_2\frac{1}{\rho_h^{(n)}}\nabla\left(p_h^*\right)^{(n)} + \Delta t\theta_8\frac{1}{\rho_h^{(n+1)}}\nabla\left(p_h^*\right)^{(n+1)}, \varphi_{\mathbf{v},h}\right)\\
&+\left(\Delta t\theta_4\left(-fv_h^{(n)}, fu_h^{(n)}, \frac{\left(\rho_h^*\right)^{(n)}}{\rho_h^{(n)}}g\right)^\top, \varphi_{\mathbf{v},h}\right)\\
&+\left(\Delta t\theta_{10}\left(-fv_h^{(n+1)}, fu_h^{(n+1)}, \frac{\left(\rho_h^*\right)^{(n+1)}}{\rho_h^{(n+1)}}g\right)^\top, \varphi_{\mathbf{v},h}\right)\\
&+\left(\Delta t\theta_3\nu_a\nabla\mathbf{v}_h^{(n)} + \Delta t\theta_9\nu_a\nabla\mathbf{v}_h^{(n)}, \nabla\varphi_{\mathbf{v},h}\right)
\end{aligned} \tag{3.37}$$

holds for all $\varphi_{\mathbf{v}} \in (X_h)^3$ and for all $n = 0, \ldots, M-1$. Furthermore, it holds

$$\left(\mathbf{v}_h^{(0)} - \mathbf{v}_0, \psi_{\mathbf{v},h}\right) = 0 \quad \text{for all} \quad \psi_{\mathbf{v},h} \in (V_h)^3.$$

3. The integral identity

$$\begin{aligned}
0 = &\left(\frac{p_{th}^{(n+1)} - p_{th}^{(n)}}{p_{th}^{(n+1)} + p_0} + \frac{\Delta t\theta_5}{p_{th}^{(n+1)} + p_0}\left(w_h^{(n)}\partial_z p_0 + \frac{p_{th}^{(n)} + p_0}{1-\kappa}\text{div }\mathbf{v}_h^{(n)}\right), \varphi_{p,h}\right)\\
&+\left(\frac{\Delta t\theta_{11}}{1-\kappa}\text{div }\mathbf{v}_h^{(n+1)} + \frac{\Delta t\theta_{11}}{p_{th}^{(n+1)} + p_0}w_h^{(n+1)}\partial_z p_0, \varphi_{p,h}\right)
\end{aligned} \tag{3.38}$$

holds for all $\varphi_p \in Z_h$ and for all $n = 0, \ldots, M-1$. Furthermore, it holds

$$\left(\left(p_h^*\right)^{(0)} - p_0^*, \psi_{p,h}\right) = 0 \quad \text{for all } \psi_{p,h} \in P_h.$$

4. The integral identity

$$\begin{aligned}
0 = &\left(\left(\theta_{v,h}^*\right)^{(n+1)} - \left(\theta_{v,h}^*\right)^{(n)} + \Delta t\theta_6\left(w_h^{(n)}\partial_z\theta_{v,0} + \left(\mathbf{v}_h^{(n)}\cdot\nabla\right)\left(\theta_{v,h}^*\right)^{(n)}\right), \varphi_{\theta,h}\right)\\
&+\left(\Delta t\theta_{12}\left(w_h^{(n+1)}\partial_z\theta_{v,0} + \left(\mathbf{v}_h^{(n+1)}\cdot\nabla\right)\left(\theta_{v,h}^*\right)^{(n+1)}\right), \varphi_{\theta,h}\right)
\end{aligned} \tag{3.39}$$

holds for all $\varphi_{\theta,h} \in Y_h$ and for all $n = 0, \ldots, M-1$. Furthermore, it holds

$$\left(\left(\theta_{v,h}^*\right)^{(0)} - \theta_{v,0}^*, \psi_{\theta,h}\right) = 0 \quad \text{for all } \psi_{\theta,h} \in Q_h.$$

5. The integral identity

$$\begin{aligned}
0 = &\left(\left(\rho_h^*\right)^{(n+1)}, \varphi_{\rho,h}\right)\\
&-\left(\frac{\left(\frac{p_0}{p_{th}^{(n+1)}+p_0}\right)^\kappa p_{th}^{(n+1)}\theta_{v,0} + \left[\left(\frac{p_0}{p_{th}^{(n+1)}+p_0}\right)^\kappa - 1\right]p_0\theta_{v,0} - p_0\left(\theta_{v,h}^*\right)^{(n+1)}}{\left(-\frac{g\kappa}{R'\theta_z}\ln\left(1+\frac{\theta_z z}{\theta_0}\right)+1\right)R'\left(\theta_{v,0} + \left(\theta_{v,h}^*\right)^{(n+1)}\right)\theta_{v,0}}, \varphi_{\rho,h}\right)
\end{aligned} \tag{3.40}$$

holds for all $\varphi_{\rho,h} \in Y_h$ and for all $n = 0, \dots, M-1$. Furthermore, it holds

$$\left((\rho_h^*)^{(0)} - \rho_0^*, \psi_{\rho,h} \right) = 0 \quad \text{for all} \quad \psi_{\rho,h} \in Q_h.$$

6. The identity

$$p_{th}^{(n+1)} - p_{th}^{(n)} - \Delta t \theta_{13} \frac{\int_\Omega \kappa w_h^{(n)} \partial_z p_0 \mathrm{d}x}{(1-\kappa)\,|\Omega|} - \Delta t \theta_{14} \frac{\int_\Omega \kappa w_h^{(n+1)} \partial_z p_0 \mathrm{d}x}{(1-\kappa)\,|\Omega|} = 0 \tag{3.41}$$

holds for all $n = 0, \dots, M-1$. Furthermore, it holds

$$p_{th}^{(0)} = 0.$$

3.3.4. Stabilisation

Analogously to the case of the Compressible Navier-Stokes model, the space-discretisation of the Low-Mach model is stabilised. Additionally to the stabilisation of the transport operators above, the so called *grad-div* stabilisation [17] is applied in order to allow equal-order interpolation of the velocity and pressure finite element spaces, respectively.

Problem 3.11 (Stabilised discrete problem of Problem 3.6)
Let $\Omega \subset \mathbb{R}^3$ be as in (2.94), $\mathscr{T}_h$ a triangulation of Ω as in (2.116) and $T \geq 0$ a final point in time. Furthermore, let t_i, $i = 0, \dots, M$ be a an equidistant discretisation of the interval $[0, T]$ as defined in (2.140). Let $\bar{\mathbf{v}} \in (V_h)^3$ be a reference velocity field and $\theta_j \in [0,1]$, $j = 1, \dots, 12$ be such that

$$\theta_j + \theta_{j+6} = 1, \quad j = 1, \dots, 6,$$

as well as $\theta_{13}, \theta_{14} \in [0,1]$ such that

$$\theta_{13} + \theta_{14} = 1.$$

Find

$$\mathbf{v}_h^{(n)} \in (V_h)^3, \quad (\rho_h^*)^{(n)}, \left(\theta_{v,h}^*\right)^{(n)} \in Q_h, \quad (p_h^*)^{(n)} \in P_h, \quad p_{th}^{(n)} \in \mathbb{R} \quad \forall\, n = 1, \dots, M, \tag{3.42}$$

where

$$\mathbf{v}_h^{(n)} := \left(u_h^{(n)}, v_h^{(n)}, w_h^{(n)} \right)^\top$$

and p_h^* fulfils (3.5), such that the following conditions are satisfied:

1. The variables satisfy

$$w_h^{(n)} = 0 \quad \text{on } \Gamma, \quad \forall\, n = 0, \dots, M, \tag{3.43}$$

as well as periodic boundary conditions in both horizontal directions.

2. The integral identity

$$
\begin{aligned}
0 = &\left(\left(\mathbf{v}_h^{(n+1)} - \mathbf{v}_h^{(n)}\right) + \Delta t\theta_1 \left(\mathbf{v}_h^{(n)} \cdot \nabla\right) \mathbf{v}_h^{(n)} + \Delta t\theta_7 \left(\mathbf{v}_h^{(n+1)} \cdot \nabla\right) \mathbf{v}_h^{(n+1)}, \varphi_{\mathbf{v},h}\right) \\
&+ \left(\Delta t\theta_2 \frac{1}{\rho_h^{(n)}} \nabla (p_h^*)^{(n)} - \Delta t\theta_4 \left(f v_h^{(n)}, -f u_h^{(n)}, -\frac{(\rho_h^*)^{(n)}}{\rho_h^{(n)}} g\right)^\top, \varphi_{\mathbf{v},h}\right) \\
&+ \left(\Delta t\theta_8 \frac{1}{\rho_h^{(n+1)}} \nabla (p_h^*)^{(n+1)} - \Delta t\theta_{10} \left(f v_h^{(n+1)}, -f u_h^{(n+1)}, -\frac{(\rho_h^*)^{(n+1)}}{\rho_h^{(n+1)}} g\right)^\top, \varphi_{\mathbf{v},h}\right) \\
&+ \left(\Delta t\theta_3 \nu \nabla \mathbf{v}_h^{(n)} + \Delta t\theta_9 \nu \nabla \mathbf{v}_h^{(n+1)}, \nabla \varphi_{\mathbf{v},h}\right) \\
&+ \sum_{K \in \mathscr{T}_h} \tau_{\mathbf{v},K} \left(\mathbf{v}_h^{n+1} - \mathbf{v}_h^n, (\bar{\mathbf{v}} \cdot \nabla) \varphi_{\mathbf{v},h} - \nu_a \Delta \varphi_{\mathbf{v},h} + \nabla \varphi_{p,h}\right)_K \\
&+ \sum_{K \in \mathscr{T}_h} \tau_{\mathbf{v},K} \left(\Delta t\theta_1 \left(\mathbf{v}_h^{(n)} \cdot \nabla\right) \mathbf{v}_h^{(n)}, (\bar{\mathbf{v}} \cdot \nabla) \varphi_{\mathbf{v},h} - \nu_a \Delta \varphi_{\mathbf{v},h} + \nabla \varphi_{p,h}\right)_K \\
&+ \sum_{K \in \mathscr{T}_h} \tau_{\mathbf{v},K} \left(\Delta t\theta_7 \left(\mathbf{v}_h^{(n+1)} \cdot \nabla\right) \mathbf{v}_h^{(n+1)}, (\bar{\mathbf{v}} \cdot \nabla) \varphi_{\mathbf{v},h} - \nu_a \Delta \varphi_{\mathbf{v},h} + \nabla \varphi_{p,h}\right)_K \\
&+ \sum_{K \in \mathscr{T}_h} \tau_{\mathbf{v},K} \left(\Delta t\theta_2 \frac{1}{\rho_h^{(n)}} \nabla (p_h^*)^n, (\bar{\mathbf{v}} \cdot \nabla) \varphi_{\mathbf{v},h} - \nu_a \Delta \varphi_{\mathbf{v},h} + \nabla \varphi_{p,h}\right)_K \\
&- \sum_{K \in \mathscr{T}_h} \tau_{\mathbf{v},K} \left(\Delta t\theta_4 \left(f v_h^{(n)}, -f u_h^{(n)}, -\frac{(\rho_h^*)^{(n)}}{\rho_h^{(n)}} g\right)^\top, (\bar{\mathbf{v}} \cdot \nabla) \varphi_{\mathbf{v},h} - \nu_a \Delta \varphi_{\mathbf{v},h} + \nabla \varphi_{p,h}\right)_K \\
&+ \sum_{K \in \mathscr{T}_h} \tau_{\mathbf{v},K} \left(\Delta t\theta_8 \frac{1}{\rho_h^{(n+1)}} \nabla (p_h^*)^{(n+1)}, (\bar{\mathbf{v}} \cdot \nabla) \varphi_{\mathbf{v},h} - \nu_a \Delta \varphi_{\mathbf{v},h} + \nabla \varphi_{p,h}\right)_K \\
&- \sum_{K \in \mathscr{T}_h} \tau_{\mathbf{v},K} \left(\Delta t\theta_{10} \left(f v_h^{(n+1)}, -f u_h^{(n+1)}, -\frac{(\rho_h^*)^{(n+1)}}{\rho_h^{(n+1)}} g\right)^\top, (\bar{\mathbf{v}} \cdot \nabla) \varphi_{\mathbf{v},h} - \nu_a \Delta \varphi_{\mathbf{v},h}\right)_K \\
&- \sum_{K \in \mathscr{T}_h} \tau_{\mathbf{v},K} \left(\Delta t\theta_{10} \left(f v_h^{(n+1)}, -f u_h^{(n+1)}, -\frac{(\rho_h^*)^{(n+1)}}{\rho_h^{(n+1)}} g\right)^\top, \nabla \varphi_{p,h}\right)_K \\
&- \sum_{K \in \mathscr{T}_h} \tau_{\mathbf{v},K} \left(\Delta t\theta_3 \nu \Delta \mathbf{v}_h^{(n)}, (\bar{\mathbf{v}} \cdot \nabla) \varphi_{\mathbf{v},h} - \nu_a \Delta \varphi_{\mathbf{v},h} + \nabla \varphi_{p,h}\right)_K \\
&- \sum_{K \in \mathscr{T}_h} \tau_{\mathbf{v},K} \left(\Delta t\theta_9 \nu \Delta \mathbf{v}_h^{(n+1)}, (\bar{\mathbf{v}} \cdot \nabla) \varphi_{\mathbf{v},h} - \nu_a \Delta \varphi_{\mathbf{v},h} + \nabla \varphi_{p,h}\right)_K
\end{aligned}
\tag{3.44}
$$

holds with $\tau_{\mathbf{v},K} \geq 0$ for all $\varphi_{\mathbf{v},h} \in (X_h)^3$, all $\varphi_{p,h} \in Z_h$ and all $n = 0, \ldots, M-1$, where

$$\rho_h^{(i)} := (\rho_h^*)^{(i)} + \rho_0.$$

Furthermore, it holds

$$\left(\mathbf{v}_h^{(0)} - \mathbf{v}_0, \psi_{\mathbf{v},h}\right) = 0 \quad \text{for all} \quad \psi_{\mathbf{v},h} \in (V_h)^3.$$

3. The integral identity

$$
\begin{aligned}
0 = &\left(\frac{p_{th}^{(n+1)} - p_{th}^{(n)}}{p_{th}^{(n+1)} + p_0} + \frac{\Delta t \theta_5}{p_{th}^{(n+1)} + p_0}\left(w_h^{(n)} \partial_z p_0 + \frac{p_{th}^{(n)} + p_0}{1-\kappa} \text{div } \mathbf{v}_h^{(n)}\right), \varphi_{p,h}\right) \\
&+ \left(\frac{\Delta t \theta_{11}}{1-\kappa} \text{div } \mathbf{v}_h^{(n+1)} + \frac{\Delta t \theta_{11}}{p_{th}^{(n+1)} + p_0} w_h^{(n+1)} \partial_z p_0, \varphi_{p,h}\right) \\
&+ \sum_{K \in \mathscr{T}_h} \tau_{\rho,K} \left(\frac{p_{th}^{(n+1)} - p_{th}^{(n)}}{p_{th}^{(n+1)} + p_0}, \text{div } \varphi_{\mathbf{v},h}\right)_K \\
&+ \sum_{K \in \mathscr{T}_h} \tau_{\rho,K} \left(\frac{\Delta t \theta_5}{p_{th}^{(n+1)} + p_0}\left(w_h^{(n)} \partial_z p_0 + \frac{p_{th}^{(n)} + p_0}{1-\kappa} \text{div } \mathbf{v}_h^{(n)}\right), \text{div } \varphi_{\mathbf{v},h}\right)_K \\
&+ \sum_{K \in \mathscr{T}_h} \tau_{\rho,K} \left(\frac{\Delta t \theta_{11}}{1-\kappa} \text{div } \mathbf{v}_h^{(n+1)} + \frac{\Delta t \theta_{11}}{p_{th}^{(n+1)} + p_0} w_h^{(n+1)} \partial_z p_0, \text{div } \varphi_{\mathbf{v},h}\right)_K,
\end{aligned}
\tag{3.45}
$$

holds with $\tau_{\rho,K} \geq 0$ for all $\varphi_{p,h} \in Z_h$, all $\varphi_{\mathbf{v},h} \in (X_h)^3$ and all $n = 0, \ldots, M-1$. Furthermore, it holds

$$
\left((p_h^*)^{(0)} - p_0^*, \psi_{p,h}\right) = 0 \quad \text{for all } \psi_{p,h} \in P_h.
$$

4. The integral identity

$$
\begin{aligned}
0 = &\left((\theta_{v,h}^*)^{(n+1)} - (\theta_{v,h}^*)^{(n)}, \varphi_{\theta,h}\right) \\
&+ \left(\Delta t \theta_6 \left(w_h^{(n)} \partial_z \theta_{v,0} + \mathbf{v}_h^{(n)} \cdot \nabla (\theta_{v,h}^*)^{(n)}\right), \varphi_{\theta,h}\right) \\
&+ \left(\Delta t \theta_{12} \left(w_h^{(n+1)} \partial_z \theta_{v,0} + \mathbf{v}_h^{(n+1)} \cdot \nabla (\theta_{v,h}^*)^{(n+1)}\right), \varphi_{\theta,h}\right) \\
&+ \sum_{K \in \mathscr{T}_h} \tau_{\theta,K} \left((\theta_{v,h}^*)^{(n+1)} - (\theta_{v,h}^*)^{(n)}, \bar{\mathbf{v}} \cdot \nabla \varphi_{\theta,h}\right)_K \\
&+ \sum_{K \in \mathscr{T}_h} \tau_{\theta,K} \left(\Delta t \theta_6 \left(w_h^{(n)} \partial_z \theta_{v,0} + \mathbf{v}_h^{(n)} \cdot \nabla (\theta_{v,h}^*)^{(n)}\right), \bar{\mathbf{v}} \cdot \nabla \varphi_{\theta,h}\right)_K \\
&+ \sum_{K \in \mathscr{T}_h} \tau_{\theta,K} \left(\Delta t \theta_{12} \left(w_h^{(n+1)} \partial_z \theta_{v,0} + \mathbf{v}_h^{(n+1)} \cdot \nabla (\theta_{v,h}^*)^{(n+1)}\right), \bar{\mathbf{v}} \cdot \nabla \varphi_{\theta,h}\right)_K
\end{aligned}
\tag{3.46}
$$

holds with $\tau_{\theta,K} \geq 0$ for all $\varphi_\theta \in Y_h$ and all $n = 0, \ldots, M-1$. Furthermore, it holds

$$
\left(\left(\theta_{v,h}^*\right)^{(0)} - \theta_{v,0}^*, \psi_{\theta,h}\right) = 0 \quad \text{for all } \psi_{\theta,h} \in Q_h.
$$

5. The integral identity

$$
\begin{aligned}
0 = &\left((\rho_h^*)^{(n+1)}, \varphi_{\rho,h}\right) \\
&- \left(\frac{\left(\frac{p_0}{p_{th}^{(n+1)} + p_0}\right)^\kappa p_{th}^{(n+1)} \theta_{v,0} + \left[\left(\frac{p_0}{p_{th}^{(n+1)} + p_0}\right)^\kappa - 1\right] p_0 \theta_{v,0} - p_0 \left(\theta_{v,h}^*\right)^{(n+1)}}{\left(-\frac{g\kappa}{R' \theta_z} \ln\left(1 + \frac{\theta_z z}{\theta_0}\right) + 1\right) R'\left(\theta_{v,0} + \left(\theta_{v,h}^*\right)^{(n+1)}\right) \theta_{v,0}}, \varphi_{\rho,h}\right)
\end{aligned}
\tag{3.47}
$$

holds in for all $\varphi_{\rho,h} \in Y_h$ and for all $n = 0, \ldots, M-1$. Furthermore, it holds

$$\left((\rho_h^*)^{(0)} - \rho_0^*, \psi_{\rho,h}\right) = 0 \quad \text{for all} \quad \psi_{\rho,h} \in Q_h.$$

6. The identity

$$p_{th}^{(n+1)} - p_{th}^{(n)} - \Delta t \theta_{13} \frac{\int_\Omega \kappa w_h^{(n)} \partial_z p_0 \mathrm{d}x}{(1-\kappa)\,|\Omega|} - \Delta t \theta_{14} \frac{\int_\Omega \kappa w_h^{(n+1)} \partial_z p_0 \mathrm{d}x}{(1-\kappa)\,|\Omega|} = 0 \tag{3.48}$$

holds for all $n = 0, \ldots, M-1$. Furthermore, it holds

$$p_{th}^{(0)} = 0.$$

The stabilisation parameters and the reference velocity are chosen as in the case of the Compressible Navier-Stokes model, see Subsection 2.3.3.1.

4. Solver

Contents

The discretisation approaches for both the Compressible Navier-Stokes model and the Low-Mach model lead to non-linear algebraic systems of equations, see Problems 2.15 and 3.11, respectively. In general, these systems describe the solution at the next time-step implicitly. To resolve the implicit description of the solution, the non-linear equations are solved in a fully-coupled manner by means of a damped inexact Newton method. The application of a Newton method requires the Jacobian matrix of the non-linear system in each Newton-step as well as a linear solver to solve the linear system defined by the Jacobian matrix. The details about the chosen Newton method, the linear solvers and preconditioners are described in this Chapter. Furthermore, the choices of finite element spaces and the weights in the time-stepping schemes are given.

In Section 4.1 the chosen finite elements as well as the weights in the time-stepping schemes are described. In the following Section 4.2, the applied Newton method with damping and forcing

strategies is presented. Section 4.3 presents the needed Jacobian matrices for both discussed models. Finally, the linear solvers and preconditioners that are used to solve linear systems with the Jacobian matrices are presented in Section 4.4.

4.1. Discretisation Parameters

In both the Compressible Navier-Stokes model and the Low-Mach model, the unknown functions $\mathbf{v}$, ρ^*, θ_v^* and p^* are discretised in space by means of finite elements. For this purpose, the domain Ω in triangulated admissibly in congruent hexahedrons, see Definition A.21. Based on this triangulation, finite elements (see Definition A.22) of Lagrange type (see Theorem A.23) with trilinear basis polynomials are chosen for all six unknown functions, i.e., a $\mathbb{Q}_1/\mathbb{Q}_1/\mathbb{Q}_1/\mathbb{Q}_1/\mathbb{Q}_1/\mathbb{Q}_1$ discretisation is chosen in space. Expanding all six unknown discrete functions in the nodal basis $\{\psi_i\}_{i=1}^{N_h}$ of this discretisation, i.e.,

$$\begin{aligned}
u_h^{(n)} &= \sum_{i=1}^{N_h} U_i(t_n)\psi_i, \\
v_h^{(n)} &= \sum_{i=1}^{N_h} V_i(t_n)\psi_i, \\
w_h^{(n)} &= \sum_{i=1}^{N_h} W_i(t_n)\psi_i, \\
(\rho_h^*)^{(n)} &= \sum_{i=1}^{N_h} R_i(t_n)\psi_i, \\
\left(\theta_{v,h}^*\right)^{(n)} &= \sum_{i=1}^{N_h} \Theta_i(t_n)\psi_i, \\
(p_h^*)^{(n)} &= \sum_{i=1}^{N_h} P_i(t_n)\psi_i,
\end{aligned} \tag{4.1}$$

each function can be identified with its coefficient vector in the respective expansion. Therefore, the solution tuple $\left(u_h^{(n)}, v_h^{(n)}, w_h^{(n)}, (\rho_h^*)^{(n)}, \left(\theta_{v,h}^*\right)^{(n)}, (p_h^*)^{(n)}\right)$ at any discrete point in time t_n can be identified with the solution vector

$$\mathbf{x}^{(n)} := (\mathbf{U}(t_n), \mathbf{V}(t_n), \mathbf{W}(t_n), \mathbf{R}(t_n), \mathbf{\Theta}(t_n), \mathbf{P}(t_n)) \in \mathbb{R}^N, \quad N := 6N_h. \tag{4.2}$$

Also, all finite dimensional test function spaces are chosen to be defined by the $\mathbb{Q}_1$ discretisation of the domain Ω by hexahedrons.

The implementation of both models is accomplished with the aid of the finite element library HiFlow^3 [41]. HiFlow^3 is a multi-purpose finite element software providing powerful tools for the efficient and accurate solution of a wide range of problems modelled by partial differential equations (PDEs). Based on object-oriented concepts and the full capabilities of C++, the HiFlow^3 project follows a modular and generic approach for building efficient parallel numerical solvers. It provides highly capable modules dealing with the mesh setup, finite element spaces, degrees of freedom, linear algebra routines, numerical solvers, and output data for visualisation. Parallelism – as the basis for high performance simulations on modern computing systems – is

Parameter	θ_1	θ_2	θ_3	θ_4	θ_5	θ_6	θ_7	θ_8	θ_9	θ_{10}	θ_{11}	θ_{12}
Value	0.5	0	0.5	0.5	0	0.5	0.5	1	0.5	0.5	1	0.5

Table 4.1.: Weights in time-stepping scheme

introduced on two levels: coarse-grained parallelism by means of distributed grids and distributed data structures based on the Message Passing Interface (MPI) standard [53], and fine-grained parallelism by means of platform-optimised linear algebra back-ends.

The software package HiFlow^3 offers relevant advantages to the numerical simulation of phenomena from a wide range of research topics: In the field of uncertainty quantification (UQ), HiFlow^3 provides a software module for using Polynomial Chaos expansions to model uncertainties in physical problems by a linear algebra framework. Standard iterative solvers can be employed to solve the associated linear systems of equations. In addition, HiFlow^3 supports mean based preconditioning to accelerate convergence for UQ problems. In the field of Computational Fluid Dynamics (CFD) and Meteorology, HiFlow^3 enables the numerical simulation of various flow phenomena by providing highly scalable preconditioners and solvers for both linear and non-linear systems.

For the time-stepping scheme, the weights θ_j, $j = 1, \ldots, 12$ are chosen as stated in Table 4.1. With these weights, in the momentum equation in both the Compressible Navier-Stokes and the Low-Mach model all terms are treated in a Crank-Nicolson manner except for the pressure part p^*, which is treated in an implicit Euler manner. The continuity equation is in both cases discretised by the implicit Euler scheme in time, whereas the thermodynamic energy equation is discretised by the Crank-Nicolson time-stepping scheme.

4.1.1. Low-Mach model: Operator splitting

In the case of the Low-Mach model, the thermodynamic part of the pressure p_{th} is determined independently via the relation (3.48) as it only depends on time and, therefore, is not discretised by finite elements. Consequently, it is not part of the solution process via Newton's method and needs to be determined on its own.

Instead, an operator splitting applied in order to resolve p_{th} and the dependence of (3.45) and (3.47), respectively, on it:

1. Compute $p_{th}^{\left(n+\frac{1}{2}\right)}$ with an half explicit Euler step of (3.48), i.e., $\theta_{13} = 1$, $\theta_{14} = 0$, with $\Delta t \leftarrow \frac{\Delta t}{2}$.

2. Solve (3.44), (3.45), (3.46), (3.47) via Newton's method with *given constant* value $p_{th}^{(n+1)} \leftarrow p_{th}^{\left(n+\frac{1}{2}\right)}$ and obtain
$$\mathbf{v}_h^{(n+1)}, (\rho_h^*)^{(n+1)}, (\theta_{v,h}^*)^{(n+1)}, (p_h^*)^{(n+1)}.$$

3. Compute $p_{th}^{(n+1)}$ with an half implicit Euler step of (3.48), i.e., $\theta_{13} = 0$, $\theta_{14} = 1$, with $\Delta t \leftarrow \frac{\Delta t}{2}$ and $p_{th}^{(n)} \leftarrow p_{th}^{\left(n+\frac{1}{2}\right)}$.

4.2. Newton's method

The fully discrete systems of both the Compressible Navier-Stokes (Problem 2.15) and the Low-Mach model (Problem 3.11) can be written in residual form

$$F(\mathbf{x}) = 0, \tag{4.3}$$

where, in the following, $F : \mathbb{R}^N \to \mathbb{R}^N$ is assumed to be a non-linear function in $C^1\left(\mathbb{R}^N, \mathbb{R}^N\right)$ with regular Jacobian matrix $J_F(\mathbf{x}) \in \mathbb{R}^{N\times N}$ for any $\mathbf{x} \in \mathbb{R}^N$ and N denotes the number of degrees of freedom in the discretisation. The solution $\mathbf{x}^*$ of (4.3) corresponds in both models to the solution vector $\mathbf{x}^{(n+1)}$ at the new time-step.

In the following, the derivation of Newton's method and its variants is only sketched up to the extend that is needed in order to explain to choices of parameters in Subsection 4.2.3. For a thorough discussion of these methods, including the convergence theory, see [49], for example.

Observe, that (4.3) is equivalent to solve the following optimization problem:

$$\text{Minimise} \quad \|F(\mathbf{x})\| \quad \text{s.t.} \quad \mathbf{x} \in \mathbb{R}^N. \tag{4.4}$$

Therefore, the value $\|F(\mathbf{x})\|$ is taken as criterion for the success of the presented algorithm.

In Newton's method, the function F is replaced by its Taylor series expansion of first order, i.e., F is linearised in the neighbourhood of any fixed $\mathbf{x}_0 \in \mathbb{R}^N$

$$F(\mathbf{x}_0 + \Delta\mathbf{x}) \approx F(\mathbf{x}_0) + J_F(\mathbf{x}_0)\Delta\mathbf{x}, \tag{4.5}$$

where $\Delta\mathbf{x}$ is an arbitrary vector in $\mathbb{R}^N$. Setting $\mathbf{x} := \mathbf{x}_0 + \Delta\mathbf{x}$ and replacing $F(\mathbf{x})$ in (4.3) by its linearisation (4.5) yields the approximation

$$F(\mathbf{x}) \approx F(\mathbf{x}_0) + J_F(\mathbf{x}_0)\Delta\mathbf{x} = 0 \tag{4.6}$$

of (4.3). The solution of (4.6) is given by

$$\tilde{\mathbf{x}} = \mathbf{x}_0 + \Delta\mathbf{x}, \tag{4.7}$$

where $\Delta\mathbf{x}$ is the solution of the linear system of equations

$$J_F(\mathbf{x}_0)\Delta\mathbf{x} = -F(\mathbf{x}_0). \tag{4.8}$$

Taking the solution $\tilde{\mathbf{x}}$ of the linearised system as a new guess for the solution of (4.3) leads to Newton's method as described in Algorithm 4.1.

Algorithm 4.1 (Newton's method)
Let an initial solution $\mathbf{x}_0 \in \mathbb{R}^N$, a relative tolerance $\varepsilon_{rel} > 0$, an absolute tolerance $\varepsilon_{abs} > 0$ and a maximum iteration number $I_{max} \in \mathbb{N}$ be given.

1. Compute initial residual norm $\|F(\mathbf{x}_0)\|$.
2. Set $i \leftarrow 0$.
3. While
$$\frac{\|F(\mathbf{x}_i)\|}{\|F(\mathbf{x}_0)\|} > \varepsilon_{rel} \quad \text{and} \quad \|F(\mathbf{x}_i)\| > \varepsilon_{abs} \quad \text{and} \quad i \le I_{max}:$$
   a) $i \leftarrow i + 1$.
   b) Solve
   $$J_F(\mathbf{x}_{i-1})\Delta\mathbf{x}_i = -F(\mathbf{x}_{i-1}).$$
   c) $\mathbf{x}_i \leftarrow \mathbf{x}_{i-1} + \Delta\mathbf{x}_i$.
   d) Compute residual norm $\|F(\mathbf{x}_i)\|$.

4.2.1. Forcing

The computation of the Newton step $\Delta \mathbf{x}_i$ via (4.8) necessitates the solution of a linear system with the matrix $J_F(\mathbf{x}_{i-1})$. Since the Jacobian matrix for both discussed models is sparse, see Section 4.3, Krylov subspace methods [54, 66, 67] are well-established choices for the solution of (4.8). Typically, the speed of convergence of these methods strongly depends on the condition number of the matrix $J_F(\mathbf{x}_{i-1})$ and, therefore, efficient preconditioning is needed, see Section 4.4, in order to achieve feasible computing times. A further reduction of the computational effort can be achieved, if the influence of the accuracy of the solution of (4.8) on the convergence of Newton's method is analysed, i.e., $\Delta \mathbf{x}_i$ is not computed exactly but only up to an approximate solution. This leads to a class of *inexact* Newton methods. One family of these inexact Newton methods is obtained, if the Newton step $\Delta \mathbf{x}_i$ is asked to satisfy

$$\left\| J_F\left(\mathbf{x}_{i-1}\right) \Delta \mathbf{x}_i + F\left(\mathbf{x}_{i-1}\right) \right\| \leq \eta_{i-1} \left\| F\left(\mathbf{x}_{i-1}\right) \right\| . \tag{4.9}$$

In this context, an approximate step is accepted provided that the relative residual of (4.8) is small. The condition (4.9) is exactly the small linear residual termination condition for the iterative solution of (4.8), so the acceptance of the approximate Newton step is well-motivated. The term η_{i-1} is called *forcing term*. For a convergence analysis of these methods, see [49], Chapter 6.

A possible choice for the forcing term η_i is the so called *Eisenstat-Walker forcing* (see [28]), which is used in the computation of the numerical results in Chapter 6. Given an initial forcing term $\eta_0 \in [0, 1)$ and a maximum forcing term $\eta_{max} \in [0, 1)$, choose

$$\eta_k = \min \left\{ \frac{\left| \left\| F\left(\mathbf{x}_{k+1}\right) \right\| - \left\| F\left(\mathbf{x}_k\right) + J_F\left(\mathbf{x}_k\right) \Delta \mathbf{x}_{k+1} \right\| \right|}{\left\| F\left(\mathbf{x}_k\right) \right\|}, \eta_{max} \right\}, \quad k = 1, 2, \ldots . \tag{4.10}$$

The resulting algorithm, where any appropriate iterative solver for the considered Jacobian matrices can be applied, is as follows:

Algorithm 4.2 (Newton's method with Eisenstat-Walker forcing)
Let an initial solution $\mathbf{x}_0 \in \mathbb{R}^N$, a relative tolerance $\varepsilon_{rel} > 0$, an absolute tolerance $\varepsilon_{abs} > 0$, a maximum iteration number $I_{max} \in \mathbb{N}$, an initial forcing term $\eta_0 \in [0, 1)$ and a maximum forcing term $\eta_{max} \in [0, 1)$ be given.

1. Compute initial residual norm $\left\| F\left(\mathbf{x}_0\right) \right\|$.
2. Set $i \leftarrow 0$.
3. While
$$\frac{\left\| F\left(\mathbf{x}_i\right) \right\|}{\left\| F\left(\mathbf{x}_0\right) \right\|} > \varepsilon_{rel} \quad \text{and} \quad \left\| F\left(\mathbf{x}_i\right) \right\| > \varepsilon_{abs} \quad \text{and} \quad i \leq I_{max} :$$
   a) $i \leftarrow i + 1$
   b) Solve
   $$J_F(\mathbf{x}_{i-1}) \Delta \mathbf{x}_i = -F(\mathbf{x}_{i-1})$$
   with an appropriate iterative linear solver up to the relative tolerance η_{i-1}.
   c) $\mathbf{x}_i \leftarrow \mathbf{x}_{i-1} + \Delta \mathbf{x}_i$.
   d) Compute residual norm $\left\| F\left(\mathbf{x}_i\right) \right\|$.

e) Compute new forcing term

$$\eta_i = \min\left\{\frac{|\|F(\mathbf{x}_i)\| - \|F(\mathbf{x}_{i-1}) + J_F(\mathbf{x}_{i-1})\,\Delta\mathbf{x}_i\||}{\|F(\mathbf{x}_{i-1})\|}, \eta_{max}\right\}$$

Further choices of the forcing terms η_k are discussed in [28, 49], for example.

4.2.2. Damping

The update strategy in step 3c of Algorithm 4.2 does not ensure convergence or even monotonous convergence, because it does not hold

$$\|F(\mathbf{x}_0)\| \geq \|F(\mathbf{x}_1)\| \geq \|F(\mathbf{x}_2)\| \geq \dots \tag{4.11}$$

in general, because, on the one hand, Newton's method does not converge globally and, on the other hand, the step $\Delta\mathbf{x}_i$ can be too large. A remedy to at least the latter problem is to introduce a so called *damping* mechanism to the update step 3c of Algorithm 4.2. In the context of optimization theory, this strategy is known as *line search*. Observe, that there are other techniques to solve the two mentioned problems. For an overview, consider [49, 58] and the references therein.

The basic idea is, that not necessarily the full Newton step $\Delta\mathbf{x}_i$ is taken. If the full step does not lead to a reduction of the non-linear residual, then the size of the step is decreased until a reduction is achieved. Therefore, a step length parameter $\lambda \in (0, 1]$ is introduced. The initial value is $\lambda = 1$. If the new iterate candidate

$$\mathbf{x}_i = \mathbf{x}_{i-1} + \lambda\Delta\mathbf{x}_i \tag{4.12}$$

does not yield a reduction of the non-linear residual, then λ is decreased by a factor $f_d \in (0, 1)$, i.e.,

$$\lambda \leftarrow f_d\lambda.$$

Then, a new iterate candidate is computed by (4.12) and the resulting non-linear residual is checked again for a reduction compared to the last iterate. This procedure is iterated, until a reduction is obtained.

Although this strategy yields a monotonous reduction of the non-linear residual, if a reduction in the search direction $\Delta\mathbf{x}_i$ is possible, it can happen, that the convergence is very slow, because the reduction is very slightly. To remedy this situation, the test for *simple decrease* can be replaced with one for *sufficient decrease*. Instead of checking for the simple decrease of the non-linear residual, the condition

$$\|F(\mathbf{x}_{i-1} + \lambda\Delta\mathbf{x}_i)\| < (1 - \alpha\lambda)\,\|F(\mathbf{x}_{i-1})\| \tag{4.13}$$

needs to be fulfilled in order to accept the step length λ. (4.13) is called *sufficient decrease* of $\|F\|$. $\alpha \in (0, 1)$ is a small, but positive, number, which needs to be chosen such that (4.13) can be as easy as possible satisfied. This strategy is called the *Armijo rule*, see [49]. To prevent an infinite reduction of the step length λ, a minimum step length $\lambda_{min} \in (0, 1)$ is introduced.

Finally, the full Newton method including Eisenstat-Walker forcing and Armijo damping strategies reads as follows:

Parameter	ε_{rel}	ε_{abs}	I_{max}	η_0	η_{max}	f_d	λ_{min}	α
Value	10^{-6}	$5 \cdot 10^{-15} \cdot \lvert\Omega\rvert$	1000	10^{-3}	10^{-3}	$\frac{3-\sqrt{5}}{2}$	10^{-16}	10^{-6}

Table 4.2.: Parameters for Newton's method with Eisenstat-Walker forcing and Armijo damping (Algorithm 4.3). $|\Omega|$ denotes the volume of the computational domain Ω.

Algorithm 4.3 (Newton-Eisenstat-Walker-Armijo method)
Let an initial solution $\mathbf{x}_0 \in \mathbb{R}^N$, a relative tolerance $\varepsilon_{rel} > 0$, an absolute tolerance $\varepsilon_{abs} > 0$, a maximum iteration number $I_{max} \in \mathbb{N}$, an initial forcing term $\eta_0 \in [0, 1)$ and a maximum forcing term $\eta_{max} \in [0, 1)$ be given. Furthermore, let a step length reduction factor $f_d \in (0, 1)$, a minimum step length $\lambda_{min} \in (0, 1)$ and a parameter $\alpha \in (0, 1)$ for sufficient decrease be given.

1. Compute initial residual norm $\|F(\mathbf{x}_0)\|$.
2. Set $i \leftarrow 0$.
3. While
$$\frac{\|F(\mathbf{x}_i)\|}{\|F(\mathbf{x}_0)\|} > \varepsilon_{rel} \quad \text{and} \quad \|F(\mathbf{x}_i)\| > \varepsilon_{abs} \quad \text{and} \quad i \leq I_{max} :$$
   a) $i \leftarrow i + 1$
   b) Solve
   $$J_F(\mathbf{x}_{i-1})\Delta\mathbf{x}_i = -F(\mathbf{x}_{i-1})$$
   with an appropriate iterative linear solver up to the relative tolerance η_{i-1}.
   c) Set $\lambda \leftarrow 1$
      i. $\mathbf{x}_i \leftarrow \mathbf{x}_{i-1} + \lambda\Delta\mathbf{x}_i$.
      ii. Compute residual norm $\|F(\mathbf{x}_i)\|$.
      iii. If
      $$\|F(\mathbf{x}_i)\| < (1 - \alpha\lambda)\|F(\mathbf{x}_{i-1})\| \quad \text{or} \quad \lambda < \lambda_{min}$$
      goto 3d) (*accept the step*), else
      $$\lambda \leftarrow f_d\lambda$$
      and goto 3c)i (*reject the step*).
   d) Compute new forcing term
   $$\eta_i = \min\left\{\frac{|\|F(\mathbf{x}_i)\| - \|F(\mathbf{x}_{i-1}) + J_F(\mathbf{x}_{i-1})\Delta\mathbf{x}_i\||}{\|F(\mathbf{x}_{i-1})\|}, \eta_{max}\right\}$$
   .

4.2.3. Parameters for Numerical Results

Algorithm 4.3 is used for the computation of the numerical results in Chapter 6 with the parameters given in Table 4.2. Observe, that $|\Omega|$ denotes the volume of the computational domain Ω. The given parameters are taken for both the Compressible Navier-Stokes and the Low-Mach model.

4.3. Jacobian matrices

In the following, the Jacobian matrices of both the Compressible Navier-Stokes and the Low-Mach model are derived. The momentum, continuity, thermodynamic energy and ideal gas law equations of Problem 2.15 and Problem 3.11, respectively, can all be written in the form

$$\mathscr{G}\left(\mathbf{v}_h^{(n+1)}, (\rho_h^*)^{(n+1)}, \left(\theta_{v,h}^*\right)^{(n+1)}, (p_h^*)^{(n+1)}\right) = 0. \tag{4.14}$$

Thus, the derivative of $\mathscr{G}$ with respect to $\mathbf{v}_h^{(n+1)}$ in the direction of any $\psi_{\mathbf{v},h} \in (V_h)^3$ is given by

$$\begin{aligned}
&\nabla_{\mathbf{v}_h^{(n+1)}} \mathscr{G}\left(\mathbf{v}_h^{(n+1)}, (\rho_h^*)^{(n+1)}, \left(\theta_{v,h}^*\right)^{(n+1)}, (p_h^*)^{(n+1)}\right) \cdot \psi_{\mathbf{v},h} \\
&\quad = \lim_{h\to 0} \frac{1}{h} \Big[\mathscr{G}\left(\mathbf{v}_h^{(n+1)} + h \cdot \psi_{\mathbf{v},h}, (\rho_h^*)^{(n+1)}, \left(\theta_{v,h}^*\right)^{(n+1)}, (p_h^*)^{(n+1)}\right) \\
&\qquad - \mathscr{G}\left(\mathbf{v}_h^{(n+1)}, (\rho_h^*)^{(n+1)}, \left(\theta_{v,h}^*\right)^{(n+1)}, (p_h^*)^{(n+1)}\right)\Big].
\end{aligned} \tag{4.15}$$

Analogously, the derivatives with respect to the other unknown solution functions can be derived. Since the finite element spaces have finite dimension, it is sufficient to consider the derivatives in the direction of all basis functions of the trial space, where the equations are tested with all basis functions of the finite dimensional finite element test spaces. Therefore, each finite element test function defines one row of the Jacobian matrix and each direction, i.e., trial function, one column of the Jacobian matrix.

The results of the limits in (4.15) are stated in the following Subsections. Observe, that the derivatives for the thermodynamic energy equations are only given once since the discrete formulations are identical for both models.

4.3.1. Momentum equation

4.3.1.1. Compressible Navier-Stokes model

The discrete momentum equation (2.144) depends on $\mathbf{v}_h^{(n+1)}$, $(\rho_h^*)^{(n+1)}$ and $(p_h^*)^{(n+1)}$. Therefore, the derivatives with respect to these variables need to be derived.

The derivative of (2.144) with respect to $\mathbf{v}_h^{(n+1)}$ in the direction of any

$$\psi_{\mathbf{v},h} := (\psi_{u,h}, \psi_{v,h}, \psi_{w,h})^\top \in (V_h)^3$$

is given by

$$
\begin{aligned}
&\nabla_{\mathbf{v}_h^{(n+1)}} \mathscr{G}\left(\mathbf{v}_h^{(n+1)}, (\rho_h^*)^{(n+1)}, (p_h^*)^{(n+1)}\right) \cdot \psi_{\mathbf{v},h} \\
&\quad = \left(\psi_{\mathbf{v},h} + \Delta t \theta_7 \left(\left(\psi_{\mathbf{v},h} \cdot \nabla\right) \mathbf{v}_h^{(n+1)} + \left(\mathbf{v}_h^{(n+1)} \cdot \nabla\right) \psi_{\mathbf{v},h}\right), \varphi_{\mathbf{v},h}\right) \\
&\quad - \left(\Delta t \theta_{10} \left(f\psi_{v,h}, -f\psi_{u,h}, 0\right)^\top, \varphi_{\mathbf{v},h}\right) \\
&\quad + \left(\Delta t \theta_9 \nu_a \nabla \psi_{\mathbf{v},h}, \nabla \varphi_{\mathbf{v},h}\right) \\
&\quad + \sum_{K \in \mathscr{T}_h} \tau_{\mathbf{v},K} \left(\psi_{\mathbf{v},h}, \left(\bar{\mathbf{v}} \cdot \nabla\right) \varphi_{\mathbf{v},h} - \nu_a \Delta \varphi_{\mathbf{v},h}\right)_K \\
&\quad + \sum_{K \in \mathscr{T}_h} \tau_{\mathbf{v},K} \left(\Delta t \theta_7 \left(\psi_{\mathbf{v},h} \cdot \nabla\right) \mathbf{v}_h^{(n+1)}, \left(\bar{\mathbf{v}} \cdot \nabla\right) \varphi_{\mathbf{v},h} - \nu_a \Delta \varphi_{\mathbf{v},h}\right)_K \\
&\quad + \sum_{K \in \mathscr{T}_h} \tau_{\mathbf{v},K} \left(\Delta t \theta_7 \left(\mathbf{v}_h^{(n+1)} \cdot \nabla\right) \psi_{\mathbf{v},h}, \left(\bar{\mathbf{v}} \cdot \nabla\right) \varphi_{\mathbf{v},h} - \nu_a \Delta \varphi_{\mathbf{v},h}\right)_K \\
&\quad - \sum_{K \in \mathscr{T}_h} \tau_{\mathbf{v},K} \left(\Delta t \theta_{10} \left(f\psi_{v,h}, -f\psi_{u,h}, 0\right)^\top, \left(\bar{\mathbf{v}} \cdot \nabla\right) \varphi_{\mathbf{v},h} - \nu_a \Delta \varphi_{\mathbf{v},h}\right)_K \\
&\quad - \sum_{K \in \mathscr{T}_h} \tau_{\mathbf{v},K} \left(\Delta t \theta_9 \nu_a \Delta \psi_{\mathbf{v},h}, \left(\bar{\mathbf{v}} \cdot \nabla\right) \varphi_{\mathbf{v},h} - \nu_a \Delta \varphi_{\mathbf{v},h}\right)_K .
\end{aligned}
\tag{4.16}
$$

The derivative of (2.144) with respect to $(\rho_h^*)^{(n+1)}$ in the direction of any $\psi_{\rho,h} \in Q_h$ is given by

$$
\begin{aligned}
&\nabla_{\left(\rho_h^*\right)^{(n+1)}} \mathscr{G}\left(\mathbf{v}_h^{(n+1)}, (\rho_h^*)^{(n+1)}, (p_h^*)^{(n+1)}\right) \cdot \psi_{\rho,h} \\
&\quad = \left(\Delta t \left(-\theta_8 \frac{\psi_{\rho,h}}{\left(\rho_h^{(n+1)}\right)^2} \nabla \left(p_h^*\right)^{(n+1)} + \theta_{10} \left(0, 0, \frac{g\rho_0}{\left(\rho_h^{(n+1)}\right)^2} \psi_{\rho,h}\right)^\top\right), \varphi_{\mathbf{v},h}\right) \\
&\quad - \sum_{K \in \mathscr{T}_h} \tau_{\mathbf{v},K} \left(\Delta t \theta_8 \frac{\psi_{\rho,h}}{\left(\rho_h^{(n+1)}\right)^2} \nabla \left(p_h^*\right)^{(n+1)}, \left(\bar{\mathbf{v}} \cdot \nabla\right) \varphi_{\mathbf{v},h} - \nu_a \Delta \varphi_{\mathbf{v},h}\right)_K \\
&\quad + \sum_{K \in \mathscr{T}_h} \tau_{\mathbf{v},K} \left(\Delta t \theta_{10} \left(0, 0, \frac{g\rho_0}{\left(\rho_h^{(n+1)}\right)^2} \psi_{\rho,h}\right)^\top, \left(\bar{\mathbf{v}} \cdot \nabla\right) \varphi_{\mathbf{v},h} - \nu_a \Delta \varphi_{\mathbf{v},h}\right)_K .
\end{aligned}
\tag{4.17}
$$

The derivative of (2.144) with respect to $(p_h^*)^{(n+1)}$ in the direction of any $\psi_{p,h} \in P_h$ is given by

$$
\begin{aligned}
&\nabla_{\left(p_h^*\right)^{(n+1)}} \mathscr{G}\left(\mathbf{v}_h^{(n+1)}, (\rho_h^*)^{(n+1)}, (p_h^*)^{(n+1)}\right) \cdot \psi_{p,h} \\
&\quad = \left(\Delta t \theta_8 \left(\frac{1}{\rho_h^{(n+1)}} \nabla \psi_{p,h}\right), \varphi_{\mathbf{v},h}\right) \\
&\quad + \sum_{K \in \mathscr{T}_h} \tau_{\mathbf{v},K} \left(\Delta t \theta_8 \left(\frac{1}{\rho_h^{(n+1)}} \nabla \psi_{p,h}\right), \left(\bar{\mathbf{v}} \cdot \nabla\right) \varphi_{\mathbf{v},h} - \nu_a \Delta \varphi_{\mathbf{v},h}\right)_K .
\end{aligned}
\tag{4.18}
$$

4.3.1.2. Low-Mach model

The discrete momentum equation (3.44) depends on $\mathbf{v}_h^{(n+1)}$, $(\rho_h^*)^{(n+1)}$ and $(p_h^*)^{(n+1)}$. Therefore, the derivatives with respect to these variables need to be derived.

The derivative of (3.44) with respect to $\mathbf{v}_h^{(n+1)}$ in the direction of any

$$\psi_{\mathbf{v},h} := (\psi_{u,h}, \psi_{v,h}, \psi_{w,h})^\top \in (V_h)^3$$

is given by

$$\begin{aligned}
&\nabla_{\mathbf{v}_h^{(n+1)}} \mathscr{G}\left(\mathbf{v}_h^{(n+1)}, (\rho_h^*)^{(n+1)}, (p_h^*)^{(n+1)}\right) \cdot \psi_{\mathbf{v},h} \\
&\quad = \left(\psi_{\mathbf{v},h} + \Delta t\theta_7 \left((\psi_{\mathbf{v},h} \cdot \nabla)\, \mathbf{v}_h^{(n+1)} + \left(\mathbf{v}_h^{(n+1)} \cdot \nabla\right) \psi_{\mathbf{v},h}\right), \varphi_{\mathbf{v},h}\right) \\
&\quad - \left(\Delta t\theta_{10} \left(f\psi_{v,h}, -f\psi_{u,h}, 0\right)^\top, \varphi_{\mathbf{v},h}\right) \\
&\quad + \left(\Delta t\theta_9 \nu_a \nabla\psi_{\mathbf{v},h}, \nabla\varphi_{\mathbf{v},h}\right) \\
&\quad + \sum_{K\in\mathscr{T}_h} \tau_{\mathbf{v},K} \left(\psi_{\mathbf{v},h}, (\bar{\mathbf{v}} \cdot \nabla)\, \varphi_{\mathbf{v},h} - \nu_a \Delta\varphi_{\mathbf{v},h} + \nabla\varphi_{p,h}\right)_K \\
&\quad + \sum_{K\in\mathscr{T}_h} \tau_{\mathbf{v},K} \left(\Delta t\theta_7 \left(\psi_{\mathbf{v},h} \cdot \nabla\right) \mathbf{v}_h^{(n+1)}, (\bar{\mathbf{v}} \cdot \nabla)\, \varphi_{\mathbf{v},h} - \nu_a \Delta\varphi_{\mathbf{v},h} + \nabla\varphi_{p,h}\right)_K \\
&\quad + \sum_{K\in\mathscr{T}_h} \tau_{\mathbf{v},K} \left(\Delta t\theta_7 \left(\mathbf{v}_h^{(n+1)} \cdot \nabla\right) \psi_{\mathbf{v},h}, (\bar{\mathbf{v}} \cdot \nabla)\, \varphi_{\mathbf{v},h} - \nu_a \Delta\varphi_{\mathbf{v},h} + \nabla\varphi_{p,h}\right)_K \\
&\quad - \sum_{K\in\mathscr{T}_h} \tau_{\mathbf{v},K} \left(\Delta t\theta_{10} \left(f\psi_{v,h}, -f\psi_{u,h}, 0\right)^\top, (\bar{\mathbf{v}} \cdot \nabla)\, \varphi_{\mathbf{v},h} - \nu_a \Delta\varphi_{\mathbf{v},h} + \nabla\varphi_{p,h}\right)_K \\
&\quad - \sum_{K\in\mathscr{T}_h} \tau_{\mathbf{v},K} \left(\Delta t\theta_9 \nu_a \Delta\psi_{\mathbf{v},h}, (\bar{\mathbf{v}} \cdot \nabla)\, \varphi_{\mathbf{v},h} - \nu_a \Delta\varphi_{\mathbf{v},h} + \nabla\varphi_{p,h}\right)_K .
\end{aligned} \tag{4.19}$$

The derivative of (3.44) with respect to $(\rho_h^*)^{(n+1)}$ in the direction of any $\psi_{\rho,h} \in Q_h$ is given by

$$\begin{aligned}
&\nabla_{(\rho_h^*)^{(n+1)}} \mathscr{G}\left(\mathbf{v}_h^{(n+1)}, (\rho_h^*)^{(n+1)}, (p_h^*)^{(n+1)}\right) \cdot \psi_{\rho,h} \\
&\quad = \left(\Delta t \left(-\theta_8 \frac{\psi_{\rho,h}}{\left(\rho_h^{(n+1)}\right)^2} \nabla \left(p_h^*\right)^{(n+1)} + \theta_{10} \left(0, 0, \frac{g\rho_0}{\left(\rho_h^{(n+1)}\right)^2} \psi_{\rho,h}\right)^\top\right), \varphi_{\mathbf{v},h}\right) \\
&\quad - \sum_{K\in\mathscr{T}_h} \tau_{\mathbf{v},K} \left(\Delta t\theta_8 \frac{\psi_{\rho,h}}{\left(\rho_h^{(n+1)}\right)^2} \nabla \left(p_h^*\right)^{(n+1)}, (\bar{\mathbf{v}} \cdot \nabla)\, \varphi_{\mathbf{v},h} - \nu_a \Delta\varphi_{\mathbf{v},h} + \nabla\varphi_{p,h}\right)_K \\
&\quad + \sum_{K\in\mathscr{T}_h} \tau_{\mathbf{v},K} \left(\Delta t\theta_{10} \left(0, 0, \frac{g\rho_0}{\left(\rho_h^{(n+1)}\right)^2} \psi_{\rho,h}\right)^\top, (\bar{\mathbf{v}} \cdot \nabla)\, \varphi_{\mathbf{v},h} - \nu_a \Delta\varphi_{\mathbf{v},h} + \nabla\varphi_{p,h}\right)_K .
\end{aligned} \tag{4.20}$$

The derivative of (3.44) with respect to $(p_h^*)^{(n+1)}$ in the direction of any $\psi_{p,h} \in P_h$ is given by

$$\begin{aligned}
&\nabla_{(p_h^*)^{(n+1)}} \mathscr{G}\left(\mathbf{v}_h^{(n+1)}, (\rho_h^*)^{(n+1)}, (p_h^*)^{(n+1)}\right) \cdot \psi_{p,h} \\
&\quad = \left(\Delta t \theta_8 \left(\frac{1}{\rho_h^{(n+1)}} \nabla \psi_{p,h}\right), \varphi_{\mathbf{v},h}\right) \\
&\quad + \sum_{K \in \mathscr{T}_h} \tau_{\mathbf{v},K} \left(\Delta t \theta_8 \left(\frac{1}{\rho_h^{(n+1)}} \nabla \psi_{p,h}\right), \left(\bar{\mathbf{v}} \cdot \nabla\right) \varphi_{\mathbf{v},h} - \nu_a \Delta \varphi_{\mathbf{v},h} + \nabla \varphi_{p,h}\right)_K .
\end{aligned} \tag{4.21}$$

4.3.2. Continuity equation

4.3.2.1. Compressible Navier-Stokes model

The discrete continuity equation (2.146) depends on $\mathbf{v}_h^{(n+1)}$ and $(\rho_h^*)^{(n+1)}$. Therefore, the derivatives with respect to these variables need to be derived.

The derivative of (2.146) with respect to $\mathbf{v}_h^{(n+1)}$ in the direction of any

$$\psi_{\mathbf{v},h} := \left(\psi_{u,h}, \psi_{v,h}, \psi_{w,h}\right)^\top \in \left(V_h\right)^3$$

is given by

$$\begin{aligned}
&\nabla_{\mathbf{v}_h^{(n+1)}} \mathscr{G}\left(\mathbf{v}_h^{(n+1)}, (\rho_h^*)^{(n+1)}\right) \cdot \psi_{\mathbf{v},h} \\
&\quad = \left(\Delta t \theta_{11} \left(\psi_{w,h} \partial_z \rho_0 + \psi_{\mathbf{v},h} \cdot \nabla \left(\rho_h^*\right)^{(n+1)} + (\rho_h^*)^{(n+1)} \text{div } \psi_{\mathbf{v},h}\right), \varphi_{\rho,h}\right) \\
&\quad + \sum_{K \in \mathscr{T}_h} \tau_{\rho,K} \left(\Delta t \theta_{11} \left(\psi_{w,h} \partial_z \rho_0 + \psi_{\mathbf{v},h} \cdot \nabla \left(\rho_h^*\right)^{(n+1)} + (\rho_h^*)^{(n+1)} \text{div } \psi_{\mathbf{v},h}\right), \bar{\mathbf{v}} \cdot \nabla \varphi_{\rho,h}\right)_K .
\end{aligned} \tag{4.22}$$

The derivative of (2.146) with respect to $(\rho_h^*)^{(n+1)}$ in the direction of any $\psi_{\rho,h} \in Q_h$ is given by

$$\begin{aligned}
&\nabla_{(\rho_h^*)^{(n+1)}} \mathscr{G}\left(\mathbf{v}_h^{(n+1)}, (\rho_h^*)^{(n+1)}\right) \cdot \psi_{\rho,h} \\
&\quad = \left(\psi_{\rho,h} + \Delta t \theta_{11} \left(\mathbf{v}_h^{(n+1)} \cdot \nabla \psi_{\rho,h} + \psi_{\rho,h} \text{div } \mathbf{v}_h^{(n+1)}\right), \varphi_{\rho,h}\right) \\
&\quad + \sum_{K \in \mathscr{T}_h} \tau_{\rho,K} \left(\psi_{\rho,h} + \Delta t \theta_{11} \left(\mathbf{v}_h^{(n+1)} \cdot \nabla \psi_{\rho,h} + \psi_{\rho,h} \text{div } \mathbf{v}_h^{(n+1)}\right), \bar{\mathbf{v}} \cdot \nabla \varphi_{\rho,h}\right)_K .
\end{aligned} \tag{4.23}$$

4.3.2.2. Low-Mach model

The discrete continuity equation (3.45) depends on $\mathbf{v}_h^{(n+1)}$. Therefore, the derivative with respect to this variable needs to be derived.

The derivative of (2.146) with respect to $\mathbf{v}_h^{(n+1)}$ in the direction of any

$$\psi_{\mathbf{v},h} := \left(\psi_{u,h}, \psi_{v,h}, \psi_{w,h}\right)^\top \in \left(V_h\right)^3$$

is given by

$$\begin{aligned}
&\nabla_{\mathbf{v}_h^{(n+1)}} \mathscr{G}\left(\mathbf{v}_h^{(n+1)}\right) \cdot \psi_{\mathbf{v},h} \\
&\quad = \left(\frac{\Delta t \theta_{11}}{1-\kappa} \text{div } \psi_{\mathbf{v},h} + \frac{\Delta t \theta_{11}}{p_{th}^{(n+1)} + p_0} \psi_{w,h} \partial_z p_0, \varphi_{p,h}\right) \\
&\quad + \sum_{K \in \mathscr{T}_h} \tau_{\rho,K} \left(\frac{\Delta t \theta_{11}}{1-\kappa} \text{div } \psi_{\mathbf{v},h} + \frac{\Delta t \theta_{11}}{p_{th}^{(n+1)} + p_0} \psi_{w,h} \partial_z p_0, \text{div } \varphi_{\mathbf{v},h}\right)_K .
\end{aligned} \tag{4.24}$$

4.3.3. Thermodynamic energy equation

The discrete thermodynamic energy equations (2.148) and (3.46), respectively, depend on $\mathbf{v}_h^{(n+1)}$ and $\left(\theta_{v,h}^*\right)^{(n+1)}$. Therefore, the derivatives with respect to these variables needs to be derived.

The derivative of (2.148) and (3.46), respectively, with respect to $\mathbf{v}_h^{(n+1)}$ in the direction of any

$$\psi_{\mathbf{v},h} := \left(\psi_{u,h}, \psi_{v,h}, \psi_{w,h}\right)^\top \in (V_h)^3$$

is given by

$$\begin{aligned}
&\nabla_{\mathbf{v}_h^{(n+1)}} \mathscr{G}\left(\mathbf{v}_h^{(n+1)}, \left(\theta_{v,h}^*\right)^{(n+1)}\right) \cdot \psi_{\mathbf{v},h} \\
&\quad = \left(\Delta t \theta_{12} \left(\psi_{w,h} \partial_z \theta_{v,0} + \psi_{\mathbf{v},h} \cdot \nabla (\theta_{v,h}^*)^{(n+1)}\right), \varphi_{\theta,h}\right) \\
&\quad + \sum_{K \in \mathscr{T}_h} \tau_{\theta,K} \left(\Delta t \theta_{12} \left(\psi_{w,h} \partial_z \theta_{v,0} + \psi_{\mathbf{v},h} \cdot \nabla (\theta_{v,h}^*)^{(n+1)}\right), \bar{\mathbf{v}} \cdot \nabla \varphi_{\theta,h}\right)_K .
\end{aligned} \tag{4.25}$$

The derivative of (2.148) and (3.46), respectively, with respect to $\left(\theta_{v,h}^*\right)^{(n+1)}$ in the direction of any $\psi_{\theta,h} \in Q_h$ is given by

$$\begin{aligned}
&\nabla_{\left(\theta_{v,h}^*\right)^{(n+1)}} \mathscr{G}\left(\mathbf{v}_h^{(n+1)}, \left(\theta_{v,h}^*\right)^{(n+1)}\right) \cdot \psi_{\theta,h} \\
&\quad = \left(\psi_{\theta,h} + \Delta t \theta_{12} \mathbf{v}_h^{(n+1)} \cdot \nabla \psi_{\theta,h}, \varphi_{\theta,h,\tau}\right) \\
&\quad + \sum_{K \in \mathscr{T}_h} \tau_{\theta,K} \left(\psi_{\theta,h} + \Delta t \theta_{12} \mathbf{v}_h^{(n+1)} \cdot \nabla \psi_{\theta,h}, \bar{\mathbf{v}} \cdot \nabla \varphi_{\theta,h}\right)_K .
\end{aligned} \tag{4.26}$$

4.3.4. Ideal gas law

4.3.4.1. Compressible Navier-Stokes model

The discrete ideal gas law (2.150) depends on $(\rho_h^*)^{(n+1)}$, $\left(\theta_{v,h}^*\right)^{(n+1)}$ and $(p_h^*)^{(n+1)}$. Therefore, the derivatives with respect to these variables need to be derived.

Define

$$\begin{aligned}
\mathcal{F}_\rho(\rho, \theta) := &-\frac{1}{1-\kappa} \left(-\frac{g\kappa}{R'\theta_z} \ln\left(1 + \frac{\theta_z z}{\theta_0}\right) + 1\right) R' (\theta + \theta_{v,0}) \\
&\cdot \left[\frac{\left(-\frac{g\kappa}{R'\theta_z} \ln\left(1 + \frac{\theta_z z}{\theta_0}\right) + 1\right) R' \rho (\theta + \theta_{v,0})}{p_0} + \frac{\theta + \theta_{v,0}}{\theta_{v,0}}\right]^{\frac{\kappa}{1-\kappa}} .
\end{aligned}$$

Then, the derivative of (2.150) with respect to $(\rho_h^*)^{(n+1)}$ in the direction of any $\psi_{\rho,h} \in Q_h$ is given by

$$\nabla_{(\rho_h^*)^{(n+1)}} \mathscr{G}\left((\rho_h^*)^{(n+1)}, (\theta_{v,h}^*)^{(n+1)}, (p_h^*)^{(n+1)}\right) \cdot \psi_{\rho,h} = \left(\mathcal{F}_\rho\left((\rho_h^*)^{(n+1)}, (\theta_{v,h}^*)^{(n+1)}\right)\psi_{\rho,h}, \varphi_{p,h}\right). \tag{4.27}$$

Define

$$\mathcal{F}_\theta(\rho,\theta) := -\left(\frac{1}{1-\kappa}\left(-\frac{g\kappa}{R'\theta_z}\ln\left(1+\frac{\theta_z z}{\theta_0}\right)+1\right)R'\rho + \frac{p_0}{\theta_{v,0}}\right) \cdot \left[\frac{\left(-\frac{g\kappa}{R'\theta_z}\ln\left(1+\frac{\theta_z z}{\theta_0}\right)+1\right)R'\rho\left(\theta+\theta_{v,0}\right)}{p_0} + \frac{\theta+\theta_{v,0}}{\theta_{v,0}}\right]^{\frac{\kappa}{1-\kappa}}.$$

Then, the derivative of (2.150) with respect to $\left(\theta_{v,h}^*\right)^{(n+1)}$ in the direction of any $\psi_{\theta,h} \in Q_h$ is given by

$$\begin{aligned}\nabla_{(\theta_{v,h}^*)^{(n+1)}} \mathscr{G}\left((\rho_h^*)^{(n+1)}, (\theta_{v,h}^*)^{(n+1)}, (p_h^*)^{(n+1)}\right) \cdot \psi_{\theta,h} \\ = \left(\mathcal{F}_\theta\left((\rho_h^*)^{(n+1)}, (\theta_{v,h}^*)^{(n+1)}\right)\psi_{\theta,h}, \varphi_{p,h}\right).\end{aligned} \tag{4.28}$$

The derivative of (2.150) with respect to $(p_h^*)^{(n+1)}$ in the direction of any $\psi_{p,h} \in P_h$ is given by

$$\nabla_{(p_h^*)^{(n+1)}} \mathscr{G}\left((\rho_h^*)^{(n+1)}, (\theta_{v,h}^*)^{(n+1)}, (p_h^*)^{(n+1)}\right) \cdot \psi_{p,h} = \left(\psi_{p,h}, \varphi_{p,h}\right). \tag{4.29}$$

4.3.4.2. Low-Mach model

The discrete ideal gas law (3.47) depends on $(\rho_h^*)^{(n+1)}$ and $\left(\theta_{v,h}^*\right)^{(n+1)}$. Therefore, the derivatives with respect to these variables need to be derived.

The derivative of (3.47) with respect to $(\rho_h^*)^{(n+1)}$ in the direction of any $\psi_{\rho,h} \in Q_h$ is given by

$$\nabla_{(\rho_h^*)^{(n+1)}} \mathscr{G}\left((\rho_h^*)^{(n+1)}, (\theta_{v,h}^*)^{(n+1)}\right) \cdot \psi_{\rho,h} = \left(\psi_{\rho,h}, \varphi_{\rho,h}\right). \tag{4.30}$$

Define

$$\mathcal{F}_{\theta,LM}(\theta) := \frac{\left(\frac{p_0}{p_{th}^{(n+1)}+p_0}\right)^\kappa p_{th}^{(n+1)}\theta_{v,0} + \left[\left(\frac{p_0}{p_{th}^{(n+1)}+p_0}\right)^\kappa - 1\right]p_0\theta_{v,0} + p_0\theta_{v,0}}{\left(-\frac{g\kappa}{R'\theta_z}\ln\left(1+\frac{\theta_z z}{\theta_0}\right)+1\right)R'\left(\theta_{v,0}+\theta\right)^2\theta_{v,0}}.$$

Then, the derivative of (3.47) with respect to $\left(\theta_{v,h}^*\right)^{(n+1)}$ in the direction of any $\psi_{\theta,h} \in Q_h$ is given by

$$\begin{aligned}\nabla_{(\theta_{v,h}^*)^{(n+1)}} \mathscr{G}\left((\rho_h^*)^{(n+1)}, (\theta_{v,h}^*)^{(n+1)}, (p_h^*)^{(n+1)}\right) \cdot \psi_{\theta,h} \\ = \left(\mathcal{F}_{\theta,LM}\left((\theta_{v,h}^*)^{(n+1)}\right)\psi_{\theta,h}, \varphi_{\rho,h}\right).\end{aligned} \tag{4.31}$$

4.4. Linear solvers and preconditioners

In each iteration of Newton's method (Algorithm 4.3) a linear system needs to be solved. Beside the assembly of the Jacobian matrix and the residual vectors, this is the computationally most expensive step in each Newton iteration. Therefore, efficient linear solvers for the Jacobian matrices are needed, which solve the arising linear systems accurately, fastly and scalably.

The Jacobian matrices of the Compressible Navier-Stokes and the Low-Mach model have different structures and properties. While the Compressible Navier-Stokes model with the described discretisation (see Section 2.3) results in Jacobian matrices, that can be solved by a GMRES method [67] with an appropriately configured black-box preconditioner like incomplete LU factorisation (ILU) [65, 66] or Algebraic Multigrid (AMG) methods [55, 71], for example, the Low-Mach model with the depicted discretisation (see Section 3.3) leads to Jacobian matrices with saddle-point structure, which can also be solved by a GMRES method, but a special preconditioner is needed, that is capable of dealing with the special properties of these matrices like ILU with thresholding [66], multigrid with Vanka smoother [48] or Schur complement techniques [14, 19, 23, 48, 68], for example. Recently, Metsch presented in his Ph.D. thesis [55] an extension of AMG to saddle-point problems.

Therefore, in contrast to the outer Newton iteration, the step of solving the linear system with the Jacobian matrix is model-dependent and different algorithms need to be applied. In Subsection 4.4.1 the solution technique for the Compressible Navier-Stokes model is described. Subsection 4.4.2 covers the algorithm for the Low-Mach model.

4.4.1. Compressible Navier-Stokes equations

4.4.1.1. The linear solver: GMRES

The Jacobian matrix of the Compressible Navier-Stokes model, see Section 4.3, is a regular but not symmetric matrix, which has a sparse structure with the presented finite element discretisation, see Section 4.1. For the approximate and iterative solution of linear systems with these matrix properties the preconditioned GMRES method [67] is a well-established, efficient and robust choice. It belongs to the class of Krylov subspace methods [66]. There are further methods among the Krylov subspace algorithms, that are theoretically suited to solve the arising linear system in the Compressible Navier-Stokes case, e.g., the preconditioned BiCGSTAB algorithm [75], but empirical experience shows, that GMRES is more robust in the scenario presented in Chapter 5.

The GMRES algorithm with Right Preconditioning is stated in Algorithm 4.4. It is given here to allow a clear presentation of the differences to the version used for the solution of the Low-Mach model in Subsection 4.4.2. For a thorough derivation and convergence analysis see [54, 66, 67].

Algorithm 4.4 (GMRES with Right Preconditioning)
Let an initial solution $\mathbf{x}_0 \in \mathbb{R}^N$, a right hand side vector $\mathbf{b} \in \mathbb{R}^N$, a system matrix $A \in \mathbb{R}^{N \times N}$, a relative tolerance $\varepsilon_{rel} > 0$, an absolute tolerance $\varepsilon_{abs} > 0$, a maximum iteration number $I_{max} \in \mathbb{N}$ and a preconditioning matrix $M^{-1} \in \mathbb{R}^{N \times N}$ be given.

1. Compute initial residual $\mathbf{r}_0 \leftarrow \mathbf{b} - A\mathbf{x}_0$

2. If $\|\mathbf{r}_0\| \leq \varepsilon_{abs}$, then END.

3. Set
$$\mathbf{v}_1 \leftarrow \frac{\mathbf{r}_0}{\|\mathbf{r}_0\|}, \quad \gamma_1 \leftarrow \|\mathbf{r}_0\| .$$

4. For $j = 1, \ldots, N$ do:
   a) Set
   $$\mathbf{w}_j \leftarrow AM^{-1}\mathbf{v}_j$$
   b) For $i = 1, \ldots, j$ do:
      i. Set
      $$h_{ij} \leftarrow \mathbf{v}_i^\top \mathbf{w}_j.$$
      ii. Set
      $$\mathbf{w}_j \leftarrow \mathbf{w}_j - h_{ij}\mathbf{v}_i.$$
   c) For $i = 1, \ldots, j-1$ do:
   $$\begin{pmatrix} h_{ij} \\ h_{i+1,j} \end{pmatrix} \leftarrow \begin{pmatrix} c_{i+1} & s_{i+1} \\ -s_{i+1} & c_{i+1} \end{pmatrix} \cdot \begin{pmatrix} h_{ij} \\ h_{i+1,j} \end{pmatrix}.$$
   d) Set
   $$\beta \leftarrow \sqrt{h_{jj}^2 + h_{j+1,j}^2}, \quad s_{j+1} \leftarrow \frac{h_{j+1,j}}{\beta}, \quad c_{j+1} \leftarrow \frac{h_{jj}}{\beta}.$$
   e) Set $h_{jj} \leftarrow \beta$
   f) Set
   $$\gamma_{j+1} \leftarrow -s_{j+1}\gamma_j, \quad \gamma_j \leftarrow c_{j+1}\gamma_j.$$
   g) If
   $$\frac{|\gamma_{j+1}|}{|\gamma_1|} > \varepsilon_{rel} \quad \text{and} \quad |\gamma_{j+1}| > \varepsilon_{abs} \quad \text{and} \quad j+1 \le I_{max} :$$
   set
   $$\mathbf{v}_{j+1} \leftarrow \frac{\mathbf{w}_j}{h_{j+1,j}},$$
   else:
      i. For $i = j, \ldots, 1$ do:
      $$y_i \leftarrow \frac{1}{h_{ii}} \left(\gamma_i - \sum_{k=i+1}^{j} h_{ik} y_k \right).$$
      ii. Set
      $$\mathbf{z} \leftarrow \sum_{i=1}^{j} y_i \mathbf{v}_i.$$
      iii. Set
      $$\mathbf{x} \leftarrow \mathbf{x}_0 + M^{-1}\mathbf{z}.$$
      iv. END.

Parameter	ε_{rel}	ε_{abs}	I_{max}
Value	η_{i-1}	$5 \cdot 10^{-15} \cdot \lvert\Omega\rvert$	1000

Table 4.3.: Parameters of GMRES (Algorithm 4.4) for the Compressible Navier-Stokes model. η_{i-1} denotes the current forcing term in Newton's method and $|\Omega|$ the volume of the computational domain Ω.

Remark 4.5 (GMRES with Right Preconditioning)

1. The matrix $M \in \mathbb{R}^{N \times N}$ denotes an approximation to the system matrix $A \in \mathbb{R}^{N \times N}$, i.e., $M \approx A$, which is chosen such that it can be inverted with low computational costs. In many applications, the matrix M or its inverse are not computed explicitly but an approximate solution with the matrix A is used, e.g., an ILU solve or fixed numbers of Jacobi, Gauß-Seidel or SOR iterations, see [54, 66]. Also fixed numbers of multigrid cycles are possible ([54, 66]). This is done below for the Compressible Navier-Stokes model. In the context of PDE, matrices corresponding to discretisations of a "similar" PDE, that are cheaper to solve in terms of computational costs, are also a popular choice, e.g., discretisations of the Stokes or Oseen equations in the case of the incompressible Navier-Stokes equations, cf. [14, 48, 68]. This approach is chosen for certain parts of the Low-Mach model solver, cf. Subsection 4.4.2.

2. Algorithm 4.4 does not incorporate the possibility to use the GMRES algorithm with restarts, i.e., the so called GMRES(m) algorithm, see [54, 66, 67]. In the test scenario of interacting cyclones, see Chapter 5, the iteration numbers for stable time-step sizes are low such that GMRES can be used without restarts.

The numerical results in Chapter 6 for the scenario described in Chapter 5 are obtained with the GMRES parameters given in Table 4.3. The relative tolerance is given by the current forcing term η_{i-1} of the outer Newton iteration and $|\Omega|$ denotes the volume of the computational domain Ω.

4.4.1.2. The preconditioner: AMG

The GMRES algorithm (Algorithm 4.4) is preconditioned by an Algebraic Multigrid (AMG) method (see, e.g., [31, 33, 55, 71]) in order to solve the linear systems arising in the computation of the Newton steps for the Compressible Navier-Stokes model. AMG algorithms are developed with the aim to provide solution methods that incorporate the convergence behaviour of Geometric Multigrid (GMG) methods, but they are based purely on algebraic considerations, i.e., the structure of the system matrix, and not on the geometry of the discretisation's grid [55]. Lots of efforts have been taken by the AMG community to extend the abilities of these methods in terms of robustness, parallelisation, scalability and applicability to a broad range of applications and matrices, see, e.g., [30, 32, 33, 55, 77, 78] to just name a few. An overview of modern AMG techniques is given in [55].

In the context of this thesis, AMG methods are used as given tools, i.e., this thesis does not provide any contribution to the theory or practical implementation of AMG algorithms. The AMG implementation of the software package *hypre* [20, 34], which is called *BoomerAMG* [38], is chosen for all applications of AMG algorithms within this thesis. The broad applicability of BoomerAMG to discretised PDE problems, its robustness and scalability have been investigated

Parameter	Value	Description
CoarsenType	6	Falgout coarsening
NumFunctions	6	Solution has six component functions
RelaxType	3	hybrid SOR smoother, forward solve
RelaxWt	0.5	Relaxation weight for SOR smoother
InterpType	4	Multipass interpolation
AggNumLevels	5	Number of levels of aggressive coarsening
MaxIter	1	Number of multigrid cycles per preconditioner call
Tol	0.0	Relative tolerance for convergence
StrongThreshold	0.6	Strong threshold for dropping matrix entries

Table 4.4.: Parameters of BoomerAMG for preconditioning GMRES (Algorithm 4.4) in each iteration of Newton's method (Algorithm 4.3) in the case of the Compressible Navier-Stokes model.

and are documented in the literature, see [5–9, 21, 22, 32, 37, 55], for example. For the numerical results in Chapter 6 version 2.10.1 of the hypre library is used.

Due to the amount of implemented options for coarsening and interpolation operators, smoothers, multigrid cycles etc., the number of configurable parameters of BoomerAMG is quite extensive, cf. [44]. The *hypre User Manual* [45] provides introductory hints at the choice of certain parameters for specific problems at hand. For every configurable option BoomerAMG provides a default value and these defaults are documented in the *hypre Reference Manual* [44]. Therefore, only those parameters, which have been altered from the default values, are documented in this Chapter.

The BoomerAMG parameters, which are set to precondition the GMRES algorithm 4.4 for the computation of the Newton step in each iteration of Algorithm 4.3 in the case of the Compressible Navier-Stokes model, are given in Table 4.4. For the meaning of these parameters, see [44]. Observe, that with the default values a V-cycle is performed.

4.4.2. Low-Mach number approximation

4.4.2.1. The linear solver: FGMRES

The Jacobian matrix of the Low-Mach model, see Section 4.3, is a regular but not symmetric matrix, which has a sparse structure with the presented finite element discretisation, see Section 4.1. Additionally, the weak formulation of the Low-Mach model forms a saddle-point problem as it contains the Stokes problem as a special case, see [13], for example, which has to be considered in the construction of an appropriate preconditioner, see [62]. The Schur complement based preconditioning approach, that is presented in Subsection 4.4.2.2, is a well-known and well-suited preconditioning technique for saddle-point problems [48, 62]. It leads to another linear system, the so called Schur complement equation, that itself needs to be solved approximately by an appropriate iterative Krylov subspace method. Therefore, the presented preconditioner is no *fixed* one any more, see [66], and a so called *flexible* variant of the considered Krylov subspace algorithm is needed. Due to the same stability reasons as in the case of the Compressible Navier-Stokes model, see Subsection 4.4.1, GMRES is chosen as iterative linear solver for the linear systems arising in the computation of the Newton steps in Algorithm 4.3, but now in its flexible variant FGMRES [66].

Furthermore, the hydrodynamic part of the pressure p^* is only defined up to an additive constant. Consequently, the coefficient vector of the discrete solution is sought in a subspace S_p of $\mathbb{R}^N$, where the pressure coefficients $\mathbf{P}(t_{n+1})$ have to be such that the corresponding finite element solution incorporates the zero mean value property. It is known, that the convergence of Krylov subspace methods improves the better the obtained basis of the Krylov subspace approximates the problem specific solution space [54, 66]. Therefore, projection steps onto S_p, which ensure, that the corresponding finite element solutions of all iterates incorporate mean value zero in the discrete hydrodynamic pressure, are introduced. Observe, that in this way the FGMRES iteration takes place in the correct subspace S_p of $\mathbb{R}^N$.

The FGMRES algorithm with the described modification for the projection on the subspace S_p is stated in Algorithm 4.6. For a thorough derivation and convergence analysis of FGMRES, see [64, 66].

Algorithm 4.6 (FGMRES with Right Preconditioning and Projection)
Let an initial solution $\mathbf{x}_0 \in \mathbb{R}^N$, a right hand side vector $\mathbf{b} \in \mathbb{R}^N$, a system matrix $A \in \mathbb{R}^{N\times N}$, a relative tolerance $\varepsilon_{rel} > 0$, an absolute tolerance $\varepsilon_{abs} > 0$, a maximum iteration number $I_{max} \in \mathbb{N}$ and preconditioning matrices $M_j^{-1} \in \mathbb{R}^{N\times N}$, $j \in \mathbb{N}$ be given.

1. Project $\mathbf{x}_0$ onto S_p.
2. Compute initial residual $\mathbf{r}_0 \leftarrow \mathbf{b} - A\mathbf{x}_0$
3. Project r_0 onto S_p.
4. If $\|\mathbf{r}_0\| \leq \varepsilon_{abs}$, then END.
5. Set
$$\mathbf{v}_1 \leftarrow \frac{\mathbf{r}_0}{\|\mathbf{r}_0\|}, \quad \gamma_1 \leftarrow \|\mathbf{r}_0\| .$$
6. For $j = 1, \ldots, N$ do:
   a) Set
   $$\mathbf{z}_j \leftarrow M_j^{-1}\mathbf{v}_j.$$
   b) Project $\mathbf{z}_j$ into S_p.
   c) Set
   $$\mathbf{w}_j \leftarrow A\mathbf{z}_j.$$
   d) Project $\mathbf{w}_j$ into S_p.
   e) For $i = 1, \ldots, j$ do:
      i. Set
      $$h_{ij} \leftarrow \mathbf{v}_i^\top \mathbf{w}_j.$$
      ii. Set
      $$\mathbf{w}_j \leftarrow \mathbf{w}_j - h_{ij}\mathbf{v}_i.$$
   f) For $i = 1, \ldots, j-1$ do:
   $$\begin{pmatrix} h_{ij} \\ h_{i+1,j} \end{pmatrix} \leftarrow \begin{pmatrix} c_{i+1} & s_{i+1} \\ -s_{i+1} & c_{i+1} \end{pmatrix} \cdot \begin{pmatrix} h_{ij} \\ h_{i+1,j} \end{pmatrix}.$$

g) Set

$$\beta \leftarrow \sqrt{h_{jj}^2 + h_{j+1,j}^2}, \quad s_{j+1} \leftarrow \frac{h_{j+1,j}}{\beta}, \quad c_{j+1} \leftarrow \frac{h_{jj}}{\beta}.$$

h) Set $h_{jj} \leftarrow \beta$

i) Set

$$\gamma_{j+1} \leftarrow -s_{j+1}\gamma_j, \quad \gamma_j \leftarrow c_{j+1}\gamma_j.$$

j) If

$$\frac{|\gamma_{j+1}|}{|\gamma_1|} > \varepsilon_{rel} \quad \text{and} \quad |\gamma_{j+1}| > \varepsilon_{abs} \quad \text{and} \quad j+1 \leq I_{max} :$$

set

$$\mathbf{v}_{j+1} \leftarrow \frac{\mathbf{w}_j}{h_{j+1,j}},$$

else:

i. For $i = j, \ldots, 1$ do:

$$y_i \leftarrow \frac{1}{h_{ii}} \left(\gamma_i - \sum_{k=i+1}^{j} h_{ik} y_k \right).$$

ii. Set

$$\mathbf{x} \leftarrow \mathbf{x}_0 + \sum_{i=1}^{j} y_i \mathbf{z}_i.$$

iii. Project $\mathbf{x}$ onto S_p.

iv. END.

The main differences between Algorithm 4.4 and Algorithm 4.6 in terms of computational and memory costs are the following:

Remark 4.7 (GMRES vs. FGMRES with projection)

1. The memory costs of FGMRES are approximately twice those of GMRES, because additionally to the Krylov subspace basis $\mathbf{v}_j \in \mathbb{R}^N$, $j \in \mathbb{N}$, the vectors $\mathbf{z}_j \in \mathbb{R}^N$, $j \in \mathbb{N}$, need to be stored.

2. The projection onto the subspace $S_p \subset \mathbb{R}^N$ needs to be computed twice in every FGMRES iteration. In the context of the Low-Mach model each projection step requires the computation of the mean hydrodynamic pressure, i.e., the assembly of a scalar value over the computational domain Ω, and the correction of pressure coefficients, which can be written as a vector-vector addition.

3. Remark 4.5, 2., also holds in the situation of FMGRES and the Low-Mach model.

The numerical results in Chapter 6 for the scenario described in Chapter 5 are obtained with the FGMRES parameters given in Table 4.5. The relative tolerance is given by the current forcing term η_{i-1} of the outer Newton iteration and $|\Omega|$ denotes the volume of the computational domain Ω.

Parameter	ε_{rel}	ε_{abs}	I_{max}
Value	η_{i-1}	$5 \cdot 10^{-15} \cdot \lvert\Omega\rvert$	1000

Table 4.5.: Parameters of FGMRES (Algorithm 4.6) for the Low-Mach model. η_{i-1} denotes the current forcing term in Newton's method and $|\Omega|$ the volume of the computational domain Ω.

4.4.2.2. The preconditioner: nested Schur complement

The FGMRES algorithm (Algorithm 4.6) is preconditioned by an nested Schur complement solver in order to solve the linear systems arising in the computation of the Newton steps for the Low-Mach model. Schur complement techniques are successfully employed to solve the saddle-point problems, that arise in the solution of the incompressible Navier-Stokes equations, see [14, 48, 68], for example. In the following, the Schur complement is extended from the incompressible Navier-Stokes equations to the Low-Mach model by applying two Schur complements in a nested way, i.e., one Schur complement solver is preconditioned by a second one. This approach to precondition the Low-Mach model equations has – to the best of the knowledge of the author – not been reported in the literature so far.

The idea of the Schur complement algorithm is the following: Let a linear system $\mathcal{A}\xi = \mathbf{b}$ in block matrix form

$$\mathcal{A}\xi = \left(\begin{array}{c|c} A & B \\ \hline C & D \end{array}\right) \begin{pmatrix} \mathbf{x} \\ \mathbf{y} \end{pmatrix} = \begin{pmatrix} \mathbf{f} \\ \mathbf{g} \end{pmatrix} \tag{4.32}$$

be given and assume, that A is regular. By performing a block LU decomposition on (4.32), this linear system is equivalent to the following two equations:

$$\left(D - CA^{-1}B\right)\mathbf{y} = \mathbf{g} - CA^{-1}\mathbf{f}, \tag{4.33}$$

$$\mathbf{x} = A^{-1}\mathbf{f} - A^{-1}B\mathbf{y}. \tag{4.34}$$

The matrix $\Sigma := D - CA^{-1}B \in \mathbb{R}^{N_1 \times N_1}$, $0 \leq N_1 \leq N$, is called the *Schur complement* of A in the block matrix $\mathcal{A}$ and (4.33) is called the *Schur complement equation* for y. The strategy to solve equations (4.33) and (4.34), that is considered in the remainder of this thesis, is as following:

Algorithm 4.8 (Schur complement solver)
Let an initial solution $\xi_0 \in \mathbb{R}^N$, a right hand side vector $(f, g)^\top \in \mathbb{R}^N$, a system matrix $\mathcal{A} \in \mathbb{R}^{N \times N}$, a relative tolerance $\varepsilon_{rel} > 0$, an absolute tolerance $\varepsilon_{abs} > 0$, a maximum iteration number $I_{max} \in \mathbb{N}$ and preconditioning matrices $M_j^{-1} \in \mathbb{R}^{N_1 \times N_1}$, $j \in \mathbb{N}$ for the Schur complement matrix Σ be given.

1. Solve Schur complement equation (4.33) for y by FGMRES with Right Preconditioning and Projection (Algorithm 4.6) and the given parameters ε_{rel}, ε_{abs}, I_{max} and M_j^{-1}. The applicability of the projection is described below in Remark 4.11.

2. Compute x via (4.34).

Remark 4.9 (Schur complement solver)
GMRES (Algorithm 4.4) with Right Preconditioning and the BoomerAMG preconditioner (see Subsection 4.4.1.2) are used to compute A^{-1}, wherever it occurs, for the computation of the numerical results in Chapter 6.

In the context of discretisations of PDE, each of the blocks A, B, C, and D corresponds to the couplings between certain variables in the PDE system. The decomposition into those blocks for both applied Schur complement solvers is described next. The Jacobian matrix J_F of the Low-Mach model can be written in variable-wise block matrix form as

$$J_F = \begin{pmatrix} A_{\mathbf{v},\mathbf{v}} & A_{\mathbf{v},\rho} & A_{\mathbf{v},\theta} & A_{\mathbf{v},p} \\ A_{\rho,\mathbf{v}} & A_{\rho,\rho} & A_{\rho,\theta} & A_{\rho,p} \\ A_{\theta,\mathbf{v}} & A_{\theta,\rho} & A_{\theta,\theta} & A_{\theta,p} \\ A_{p,\mathbf{v}} & A_{p,\rho} & A_{p,\theta} & A_{p,p} \end{pmatrix}.$$

$A_{i,j}$ corresponds to the matrix block, where the finite element test functions belong to variable i and the finite element trial functions to variable j.

The first Schur complement solver (Algorithm 4.8) operates on the Schur complement decomposition of the Jacobian matrix J_F of the Low-Mach model and is used as preconditioner for Algorithm 4.6 in the computation of each Newton step. Since this is the outer Schur complement solver, all block matrices etc. corresponding to this instance are denoted by the subscript o. Especially, it holds $\mathcal{A}_o = J_F$. The four block matrices and four block vectors of the outer Schur complement are as follows:

- The matrix A_o corresponds to the block of J_F, where both test and trial functions belong to the temperature θ_v^* and density ρ^* variables, i.e., to the block matrix formed by (4.26), (4.30) and (4.31). Therefore, A_o can be interpreted as the discrete instationary convection operator for θ_v^* and the Jacobian of the ideal gas law for ρ^*.
- The matrix B_o corresponds to the block of J_F, where the test functions correspond to the temperature θ_v^* and density ρ^* variables and the trial functions to the velocity components $\mathbf{v}$ and the hydrodynamic pressure p^*, i.e., to the block matrix formed by (4.25). B_o can be interpreted as the discrete representation of the influences of $\mathbf{v}$ and p^* on θ_v^* and ρ^*.
- Therefore, the block vectors $\mathbf{x}_o$ and $\mathbf{f}_o$ are defined by the test functions of temperature θ_v^* and density ρ^*.
- The matrix C_o corresponds to the block of J_F, where the test functions correspond to the velocity components $\mathbf{v}$ and the hydrodynamic pressure p^* variables and the trial functions to the temperature θ_v^* and density ρ^*, i.e., to the block matrix formed by (4.20). C_o can be interpreted as the discrete representation of the influences of θ_v^* and ρ^* on $\mathbf{v}$ and p^*.
- The matrix D_o corresponds to the block of J_F, where both test and trial functions belong to the velocity components $\mathbf{v}$ and the hydrodynamic pressure p^* variables, i.e., to the block matrix formed by (4.19), (4.21), (4.24). Therefore, D_o can be interpreted as the discrete operator of a perturbed incompressible Navier-Stokes equation system. In contrast to the incompressible Navier-Stokes equations, the density is spatially varying and the continuity equation (3.15) contains additional terms due to the dependence of ρ^* on p_0 and p_{th}.
- Therefore, the block vectors $\mathbf{y}_o$ and $\mathbf{g}_o$ are defined by the test functions of the velocity components $\mathbf{v}$ and the hydrodynamic pressure p^*.

Consequently, the partition of the matrix $\mathcal{A}_o$ for the application of the outer Schur complement can be written in block matrix form as

$$\mathcal{A}_o = \left(\begin{array}{cc|cc} A_{\rho,\rho} & A_{\rho,\theta} & A_{\rho,\mathbf{v}} & A_{\rho,p} \\ A_{\theta,\rho} & A_{\theta,\theta} & A_{\theta,\mathbf{v}} & A_{\theta,p} \\ \hline A_{\mathbf{v},\rho} & A_{\mathbf{v},\theta} & A_{\mathbf{v},\mathbf{v}} & A_{\mathbf{v},p} \\ A_{p,\rho} & A_{p,\theta} & A_{p,\mathbf{v}} & A_{p,p} \end{array}\right).$$

Remark 4.10 (Schur complement as discrete operator splitting)
Based on the interpretation of the four block matrices A_o, B_o, C_o, and D_o, the Schur complement solver can be interpreted as an operator splitting on the discrete level. Observe, that the splitting is only done in the preconditioner of the linear solver, that computes the Newton step. Therefore, the approximate solves of the Schur complement equation (4.33) need only to be accurate enough to provide a Krylov subspace basis in Algorithm 4.6, such that the solution of the linear system can be approximated with sufficient accuracy within a few iterations of Algorithm 4.6.

As described in Algorithm 4.8, the Schur complement equation (4.33) with the system matrix

$$\Sigma_o := D_o - C_o A_o^{-1} B_o \tag{4.35}$$

is solved by Algorithm 4.6. Consequently, efficient preconditioners $M_{j,o}^{-1}$ for Σ_o are needed.

The Schur complement equation (4.33) for the outer Schur complement

$$\left(D_o - C_o A_o^{-1} B_o\right) \mathbf{y}_o = \mathbf{g}_o - C_o A_o^{-1} \mathbf{f}_o \tag{4.36}$$

resolves the Low-Mach model system (3.44)-(3.47) for the velocity $\mathbf{v}_h$ and hydrodynamic pressure p_h^* components. Within this system, equations (3.46) and (3.47) represent the temperature and density propagation, respectively. Keeping $\mathbf{v}$ fixed, (3.46) is an instationary advection equation for the temperature θ_v^* and the density ρ^* depends on the solution functions θ_v^* and p_{th} only, where the latter is resolved separately via an operator splitting approach, see Subsection 4.1. Conversely, (3.44) and (3.45), which describe the propagation of the velocity field $\mathbf{v}$ and the hydrodynamic pressure p^*, only depend on p_{th} and ρ^*. Observe, that θ_v^*, ρ^* and p^* represent small deviations from the reference states only, see Subsection 2.1.5. Therefore, θ_v^* and ρ^* are mainly determined by the convection due to the velocity field $\mathbf{v}$, whereas ρ^* only plays a role in the balance of pressure gradient and gravitational forces in the equations for $\mathbf{v}$ and p^*. Consequently, (3.44) and (3.45) – the disturbed incompressible Navier-Stokes system – form the dominant part in the dynamics of the system (3.44)-(3.47).

In the discrete setting, this dominant part is the one described by the matrices C_o and D_o, but the influence of the part C_o on $\mathbf{v}$ and p^* is small due to the above considerations. Therefore, the matrix $M_{j,o}^{-1}$ with

$$M_{j,o}^{-1} \approx \mathcal{A}_i^{-1} \quad \text{and} \quad \mathcal{A}_i = D_o \tag{4.37}$$

is chosen as preconditioner for Σ_o and $\mathcal{A}_i^{-1}$ is again approximated by a Schur complement solver (Algorithm 4.8), which is referred to as the inner Schur complement and all corresponding block matrices etc. are denoted by the subscript i. The four block matrices and four block vectors of the inner Schur complement are as follows:

- The matrix A_i corresponds to the block of D_o, where both test and trial functions belong to the velocity $\mathbf{v}$ variables, i.e., to the block matrix formed by (4.19) and (4.24) restricted to the test function parts containing $\varphi_{\mathbf{v},h}$. Therefore, A_i can be interpreted as the discrete instationary convection-diffusion-reaction operator for $\mathbf{v}$.

- The matrix B_i corresponds to the block of D_o, where the test functions correspond to the velocity $\mathbf{v}$ variables and the trial functions to the hydrodynamic pressure p^*, i.e., to the block matrix formed by (4.21) restricted to the test function parts containing $\varphi_{\mathbf{v},h}$. B_i can be interpreted as the discrete representation of the influences of p^* on $\mathbf{v}$.

- Therefore, the block vectors $\mathbf{x}_i$ and $\mathbf{f}_i$ are defined by the test functions of velocity $\mathbf{v}$.

- The matrix C_i corresponds to the block of D_o, where the test functions correspond to the hydrodynamic pressure p^* variable and the trial functions to the velocity $\mathbf{v}$, i.e., to the block matrix formed by (4.19) and (4.24) restricted to the test function parts containing $\varphi_{p,h}$. C_i can be interpreted as the discrete representation of the influences of $\mathbf{v}$ on p^*.
- The matrix D_i corresponds to the block of D_o, where both test and trial functions belong to the hydrodynamic pressure p^* variable, i.e., to the block matrix formed by (4.21) restricted to the test function parts containing $\varphi_{p,h}$. Therefore, D_i corresponds to a discrete Poisson problem for the hydrodynamic pressure p^* with Neumann boundary conditions and arises from the grad-div stabilisation.
- Therefore, the block vectors $\mathbf{y}_i$ and $\mathbf{g}_i$ are defined by the test functions of the hydrodynamic pressure p^*.

Consequently, the partition of the matrix $\mathcal{A}_i$ for the application of the inner Schur complement can be written in block matrix form as

$$\mathcal{A}_i = \left(\begin{array}{c|c} A_{\mathbf{v},\mathbf{v}} & A_{\mathbf{v},p} \\ \hline A_{p,\mathbf{v}} & A_{p,p} \end{array}\right).$$

Remark 4.11 (Projection in FMGRES of Schur complement solver)
Since the Schur complement equations with both Σ_o and Σ_i contain the block where the test functions correspond to the hydrodynamic pressure p^*, the projection onto the subspace S_p, see Subsection 4.4.2, is applicable in both cases.

As described in Algorithm 4.8, the Schur complement equation (4.33) with the system matrix

$$\Sigma_i := D_i - C_i A_i^{-1} B_i \tag{4.38}$$

is solved by Algorithm 4.6. Consequently, efficient preconditioners $M_{j,i}^{-1}$ for Σ_i are needed.

The Schur complement equation (4.33) with system matrix Σ_i is the discrete representation of an equation for the hydrodynamic pressure p^*. Another popular approach to solve such an equation for the case of the incompressible Navier-Stokes equations is via the so called *pressure poisson equation (PPE)*, see [69], for example. The idea for preconditioning Σ_i is, to imitate the PPE technique with a regularized version of the matrix D_i, which represents a Poisson problem for the hydrodynamic pressure p^* with Neumann boundary conditions, too, but arises due to the grad-div stabilisation. One advantage is, that the matrix D_i is already at hand and only the mass matrix of the pressure needs to be assembled once in order to regularise D_i. Consequently, no additional assembly of a matrix for the preconditioner of Σ_i is necessary. Therefore, the matrices

$$M_{j,i}^{-1} \approx P_j^{-1} \quad \text{with} \quad P_j = \delta_p \mathcal{M}_p + D_i \tag{4.39}$$

are chosen as preconditioners for the Schur complement Σ_i, where $\mathcal{M}_p$ defined as

$$\mathcal{M}_p := (M_{i,j})_{i,j=1}^{N_h}, \quad M_{i,j} := (\psi_j, \psi_i), \tag{4.40}$$

denotes the mass matrix of the hydrodynamic pressure variable p^* and

$$\delta_p := 10^{-16} \cdot \Delta t \tag{4.41}$$

denotes the regularisation parameter. With this regularisation, the matrices P_j are symmetric and positive definite and, therefore, the inversion is computed by the preconditioned Conjugate

Parameter	ε_{rel}	ε_{abs}	I_{max}
Value	η_{i-1}	0.0	3

Table 4.6.: Parameters of FGMRES (Algorithm 4.6) for the solution of the Schur complement equation (4.36) of the outer Schur complement solver (Algorithm 4.8). η_{i-1} denotes the current forcing term in Newton's method.

Parameter	ε_{rel}	ε_{abs}	I_{max}
Value	10^{-6}	0.0	1000

Table 4.7.: Parameters of GMRES (Algorithm 4.4) for the inversion of the matrix A_o in the outer Schur complement solver (Algorithm 4.8).

Gradient (CG) method (see [39, 54, 66]) and the BoomerAMG preconditioner (see Subsection 4.4.1.2). The presented solution methodology proved to be effective in the scenario of interacting cyclones, see Chapter 5 for the scenario description and Chapter 6 for the numerical results.

The nested Schur complement solvers (Algorithm 4.8) can be configured with a variety of parameters for the occurring (F)GMRES (Algorithms 4.4 and 4.6) solvers and the corresponding preconditioners. The parameters, which are used for the computation of numerical results in Chapter 6, are given in Tables 4.6-4.13. Observe, that the CG algorithm – like (F)GMRES – is an iterative Krylov subspace method and that, therefore, the same convergence criteria can be applied.

Parameter	**Value**	**Description**
CoarsenType	6	Falgout coarsening
NumFunctions	2	A_o represents two solution functions
RelaxType	3	hybrid SOR smoother, forward solve
RelaxWt	0.25	Relaxation weight for SOR smoother
InterpType	2	Classical modified interpolation for hyperbolic PDEs
AggNumLevels	5	Number of levels of aggressive coarsening
MaxIter	1	Number of multigrid cycles per preconditioner call
Tol	0.0	Relative tolerance for convergence
StrongThreshold	0.6	Strong threshold for dropping matrix entries

Table 4.8.: Parameters of BoomerAMG for preconditioning GMRES (Algorithm 4.4) in the inversion of the matrix A_o in the outer Schur complement solver (Algorithm 4.8).

Parameter	ε_{rel}	ε_{abs}	I_{max}
Value	η_{i-1}	0.0	3

Table 4.9.: Parameters of FGMRES (Algorithm 4.6) for the solution of the Schur complement equation (4.33) of the inner Schur complement solver (Algorithm 4.8) with the system matrix (4.38). η_{i-1} denotes the current forcing term in Newton's method.

Parameter	ε_{rel}	ε_{abs}	I_{max}
Value	10^{-6}	0.0	1000

Table 4.10.: Parameters of GMRES (Algorithm 4.4) for the inversion of the matrix A_i in the inner Schur complement solver (Algorithm 4.8).

Parameter	**Value**	**Description**
CoarsenType	6	Falgout coarsening
NumFunctions	3	A_i represents three solution functions
RelaxType	3	hybrid SOR smoother, forward solve
RelaxWt	0.5	Relaxation weight for SOR smoother
InterpType	4	Multipass interpolation
AggNumLevels	5	Number of levels of aggressive coarsening
MaxIter	1	Number of multigrid cycles per preconditioner call
Tol	0.0	Relative tolerance for convergence
StrongThreshold	0.6	Strong threshold for dropping matrix entries

Table 4.11.: Parameters of BoomerAMG for preconditioning GMRES (Algorithm 4.4) in the inversion of the matrix A_i in the inner Schur complement solver (Algorithm 4.8).

Parameter	ε_{rel}	ε_{abs}	I_{max}
Value	10^{-6}	0.0	500

Table 4.12.: Parameters of CG for the inversion of the matrix P_j (4.39) in the inner Schur complement solver (Algorithm 4.8).

Parameter	Value	Description
CoarsenType	6	Falgout coarsening
NumFunctions	1	P_j represents only p^*
RelaxType	6	hybrid SSOR smoother, forward solve
RelaxWt	0.5	Relaxation weight for SSOR smoother
InterpType	0	Classical modified interpolation
AggNumLevels	5	Number of levels of aggressive coarsening
MaxIter	1	Number of multigrid cycles per preconditioner call
Tol	0.0	Relative tolerance for convergence
StrongThreshold	0.6	Strong threshold for dropping matrix entries

Table 4.13.: Parameters of BoomerAMG for preconditioning CG in the inversion of the matrix P_j (4.39) in the inner Schur complement solver (Algorithm 4.8).

5. Cyclone-Cyclone interaction

Contents

A scenario of two interacting tropical cyclones is considered as benchmark problem for the comparison of the Compressible Navier-Stokes and the Low-Mach model in terms of both solution properties and computational performance. It is a challenging and computationally expensive task to forecast the motion and evolution of such an interaction by means of a numerical simulation because physical processes that interact in complex ways on a wide range of spatial and temporal scales need to be considered [11, 12]. The scenario is highly idealised in the sense that exact initial conditions for the velocity field are assumed and that the computational domain is located in the so called *neutral convective mixed layer*. The latter means that no interaction with neither the Earth's surface nor the outer space is considered, and the dynamics are assumed to be purely driven by the fluid flow equations and the initial states of the unknown quantities itself. Therefore, this scenario really allows a comparison of the different model dynamics as influences by means of external forces and complex orographic effects are not present.

The investigation of the interaction of tropical cyclones has a long history in the community of meteorology and reaches back to the 1920s [35, 36]. For an historical overview, see [12, 63], for example. Observe, that it is not the objective of this thesis to provide an in-depth analysis of the results of the two different models by means of meteorological expertise. Rather, the emphasis is on numerical and computational aspects. Therefore, this scenario is considered in order to provide a benchmark problem that has a relevance in numerical weather forecasting. A detailed description of the objectives of the comparison is given in Chapter 6.

In Section 5.1, the computational domain and the initial, idealised velocity field are presented. Based on the given velocity field, appropriate initial distributions for the thermodynamic quantities density, temperature and pressure need to be determined. The exact procedure for this step is given in Section 5.2.

5.1. Domain and initial velocity field

Typically, tropical cyclones have diameters on the scale of several 100 km [12]. In the considered scenario, two cyclones of this type, which interact with each other, are placed in the computational domain with an initial distance of the storm centres of 400 km. Therefore, the horizontal extend of the dynamic evolution of the two cyclones easily reaches the scale of 1000 km. Consequently, the domain Ω needs to be chosen large enough such that the cyclones are still fully contained within the domain on the considered time-interval. For the numerical results in Chapter 6, the domain extends over 4000 km in both horizontal directions, and 13 km in the vertical. Horizontally, the domain is centred around the origin of the coordinate system, i.e., the domain

Ω is defined as

$$\Omega := [-2,000,000; 2,000,000] \times [-2,000,000; 2,000,000] \times [0; 13,000], \tag{5.1}$$

where the boundaries of the intervals are given in meters $[m]$. The origin $(0,0,0) \in \mathbb{R}^3$ is positioned at a northern latitude of $\Phi_0 = 30°$. According to Section 4.1, Ω is triangulated by 400 cells in both horizontal directions and 32 cells in the vertical, which leads to a total amount of $5,120,000$ congruent hexahedrons, where each has the size $10,000\ m \times 10,000\ m \times 406.25\ m$. The size of the cells is chosen such that so called *non-hydrostatic* effects come into account and are – to the scale of the cell size – resolved in the numerical solution [46].

The initial velocity field is idealised as follows: First, the velocity profile is *purely horizontal*, i.e., the vertical component is equal to zero in Ω, $w \equiv 0$. Second, the initial velocity field is *smooth*. A third idealisation is made by assuming, that the two cyclones in their common initial state can be modelled by *linear superposition* of two single storm profiles.

The initial velocity field of one cyclone is defined as follows and is due to [63]: Let a reference velocity $v_{ref} > 0$, $0 < z_l < z_u$, $r_{max}, r_{cut}, r_{wid} > 0$ and $a, b > 0$ be given. Furthermore, let $\mathbf{x}_c := (x_c, y_c)^\top$ denote the horizontal position of the centre of the cyclone, $\mathbf{x} := (x, y)^\top$ the horizontal coordinates and z the vertical coordinate. Then, the initial profile of one cyclone is given as follows. Define

$$\chi(z) := \begin{cases} 1, & 0 \le z \le z_l \\ \frac{1}{2}\left(\cos\left(\pi \frac{z - z_l}{z_u - z_l}\right) + 1\right), & z_l < z \le z_u \\ 0, & \text{else} \end{cases} \tag{5.2}$$

as well as

$$r(\mathbf{x}) := \|\mathbf{x} - \mathbf{x}_c\|_2, \quad s(\mathbf{x}) := \frac{r(\mathbf{x})}{r_{max}}, \tag{5.3}$$

and

$$\xi(\mathbf{x}) := \begin{cases} 1 - \exp\left(-\frac{(r(\mathbf{x}) - r_{cut})^2}{r_{wid}^2}\right), & 0 \le r(\mathbf{x}) < r_{cut} \\ 0, & \text{else} \end{cases}. \tag{5.4}$$

Furthermore, define the *tangential velocity*

$$v_{tan}(\mathbf{x}) := \xi(\mathbf{x}) \cdot v_{ref} \cdot \frac{s(\mathbf{x}) \cdot \left(1 + \frac{6b}{2a} \cdot s^4(\mathbf{x})\right)}{\left(1 + a \cdot s^2(\mathbf{x}) + b \cdot s^6(\mathbf{x})\right)^2} \tag{5.5}$$

and

$$\alpha(\mathbf{x}) := \arctan\left(\frac{y - y_c}{x - x_c}\right). \tag{5.6}$$

Then, the initial velocity field of one cyclone is given by

$$\tilde{\mathbf{v}}_0(x, y, z) := \chi(z) \cdot v_{tan}(\mathbf{x}) \cdot \left(-\sin\left(\alpha(\mathbf{x})\right), \cos\left(\alpha(\mathbf{x})\right), 0\right)^\top. \tag{5.7}$$

The two cyclones are initialized with the parameters given in Table 5.1. The cyclone with centre at $(-200,000; 0)$ is denoted as *western* cyclone and the other with centre at $(200,000; 0)$ is denoted as *eastern* cyclone.

Remark 5.1 (Boundary conditions of initial velocity field)
The initial velocity field (5.7) obviously fulfils the boundary conditions of Problems 2.6 and 3.6 and their discretisations, respectively.

Parameter	Value
v_{ref}	$35.7605\frac{m}{s}$
z_l	$2,000\ m$
z_u	$11,000\ m$
r_{max}	$150,000\ m$
r_{cut}	$1,200,000\ m$
r_{wid}	$500,000\ m$
a	0.3398
b	$5.377 \cdot 10^{-4}$
x_c - western cyclone	$-200,000\ m$
y_c - western cyclone	$0\ m$
x_c - eastern cyclone	$200,000\ m$
y_c - eastern cyclone	$0\ m$

Table 5.1.: Parameters for initial cyclone profiles

5.2. Computation of thermodynamics initial states

The *given* initial velocity field $\mathbf{v}_0$ from the previous subsection describes two idealised tropical cyclones. Based on the velocity field, physically meaningful initial profiles for density, temperature and pressure need to be determined. This is done in two steps.

First, consider Table 2.1 again. The scale analysis given there indicates that for a stable initial state the dominant forces in the momentum equation should be nearly balanced, i.e., the gradient fluxes $(\mathbf{v}\cdot\nabla)\mathbf{v}$, the Coriolis force, the effective gravitational force and the pressure gradient force. Collecting these forces in an equation and using the properties of the reference states for density and pressure, the mathematical task now reads:

Problem 5.2 (Initial density and pressure)
Find $\rho_0^*, p_0^* \in C^1(\Omega)$, such that

$$\rho_0^* \left((\mathbf{v}_0 \cdot \nabla)\, \mathbf{v}_0 + f\mathbf{e}_3 \times \mathbf{v}_0 + g\mathbf{e}_3 \right) + \nabla p_0^* = -\rho_0 \left((\mathbf{v}_0 \cdot \nabla)\, \mathbf{v}_0 + f\mathbf{e}_3 \times \mathbf{v}_0 \right).$$

Of course, Problem 5.2 needs to be equipped with appropriate boundary conditions.

Remark 5.3 (Initial density and pressure)

1. Observe, that in the vertical momentum equation the hydrostatic balance of the reference states is used.

2. Problem 5.2 consists of three equations for two unknown functions. Therefore, Problem 5.2 is over-determined.

Due to the second Remark 5.3, the goal of Problem 5.2 needs to be weakened in order to provide a well-posed problem for the initial density and pressure states. To achieve this, the problem of finding the initial states is reformulated as a least-squares approximation in the L^2 sense, i.e., a least-squares Galerkin approximation is constructed [47].

Let $L : H^1(\Omega) \to L^2(\Omega)$ be an abstract differential operator of first order, $f \in L^2(\Omega)$ and $u \in H^1(\Omega)$. Define the least-squares functional as

$$I(u) := \|Lu - f\|^2_{L^2(\Omega)} = (Lu - f, Lu - f)\,. \tag{5.8}$$

Then, the least-squares problem reads:

$$\text{Minimise } I(u) \text{ subject to } u \in H^1(\Omega). \tag{5.9}$$

The goal functional (5.8) is convex. Therefore, the first-order criterion, i.e., u is a root of the first-order derivative of I, is both a necessary and a sufficient condition for a minimum in (5.9). Deriving the derivative of I with respect to u analogously to (4.15) leads to the following variational problem: Find $u \in H^1(\Omega)$ such that

$$(Lu, L\varphi) = (f, L\varphi) \quad \text{for all } \varphi \in H^1(\Omega). \tag{5.10}$$

Applying (5.10) to Problem 5.2 yields the following least-squares approximation for the initial states of density and pressure. Furthermore, boundary conditions need to be set for ρ_0^* and p_0^*. To fix initial pressure uniquely – it is only determined up to a constant by the partial differential equation as it only occurs with its gradient –, zero Dirichlet boundary conditions are set at the upper boundary $z = z_{max}$ for the pressure. Furthermore, the vertical momentum equation in Problem 5.2 just describes the hydrostatic balance

$$\partial_z p_0^* = -g\rho_0^*,$$

because the vertical component of the initial velocity field is zero. To ensure, that the vertical pressure gradient is zero on the boundary Γ, which is meaningful, because the initial velocity field incorporates zero Neumann boundary conditions on Γ and, therefore, the pressure should not change in the vertical, zero Dirichlet boundary conditions are set for ρ_0^* on Γ.

Problem 5.4 (Initial density and pressure - least-squares formulation)
Find $\rho_0^*, p_0^* \in H^1(\Omega)$, such that

$$\begin{aligned}&(\rho_0^* ((\mathbf{v}_0 \cdot \nabla)\mathbf{v}_0 + f\mathbf{e}_3 \times \mathbf{v}_0 + g\mathbf{e}_3) + \nabla p_0^*, \varphi_\rho ((\mathbf{v}_0 \cdot \nabla)\mathbf{v}_0 + f\mathbf{e}_3 \times \mathbf{v}_0 + g\mathbf{e}_3) + \nabla\varphi_p)\\ =&(-\rho_0 ((\mathbf{v}_0 \cdot \nabla)\mathbf{v}_0 + f\mathbf{e}_3 \times \mathbf{v}_0), \varphi_\rho ((\mathbf{v}_0 \cdot \nabla)\mathbf{v}_0 + f\mathbf{e}_3 \times \mathbf{v}_0 + g\mathbf{e}_3) + \nabla\varphi_p)\end{aligned}$$

holds for all $\varphi_\rho \in H^1(\Omega)$ and all $\varphi_p \in H^1(\Omega)$ as well as

$$\begin{aligned}\rho_0^* &= 0 \quad \text{on } \Gamma,\\ p_0^* &= 0 \quad \text{on } \Gamma_{top} := \{(x, y, z) \in \Gamma : \ z = z_{max}\}.\end{aligned}$$

Discretising Problem 5.4 by means of finite elements analogously to Chapters 2 and 3, respectively, and using the notation introduced there, finally leads to the following discrete problem for the initial density and pressure fields.

Problem 5.5 (Initial density and pressure - discrete)
Let $\Omega \subset \mathbb{R}^3$ be as in (2.94) and $\mathscr{T}_h$ a triangulation of Ω as in (2.116). Define

$$\mathscr{J}(\mathbf{v}) := (\mathbf{v} \cdot \nabla)\mathbf{v} + f\mathbf{e}_3 \times \mathbf{v} + g\mathbf{e}_3$$

Find $(\rho_h^*)^{(0)} \in Q_h$, $(p_h^*)^{(0)} \in P_h$, such that

$$\begin{aligned}&\left((\rho_h^*)^{(0)} \mathscr{J}(\mathbf{v}_0) + \nabla (p_h^*)^{(0)}, \varphi_{\rho,h}\mathscr{J}(\mathbf{v}_0) + \nabla\varphi_{p,h}\right)\\ =&(-\rho_0 ((\mathbf{v}_0 \cdot \nabla)\mathbf{v}_0 + f\mathbf{e}_3 \times \mathbf{v}_0), \varphi_{\rho,h}\mathscr{J}(\mathbf{v}_0) + \nabla\varphi_{p,h})\end{aligned}$$

holds for all $\varphi_{\rho,h} \in Y_h$ and all $\varphi_p \in Z_h$ as well as

$$\begin{aligned}(\rho_h^*)^{(0)} &= 0 \quad \text{on } \Gamma,\\ (p_h^*)^{(0)} &= 0 \quad \text{on } \Gamma_{top} := \{(x, y, z) \in \Gamma : \ z = z_{max}\}.\end{aligned}$$

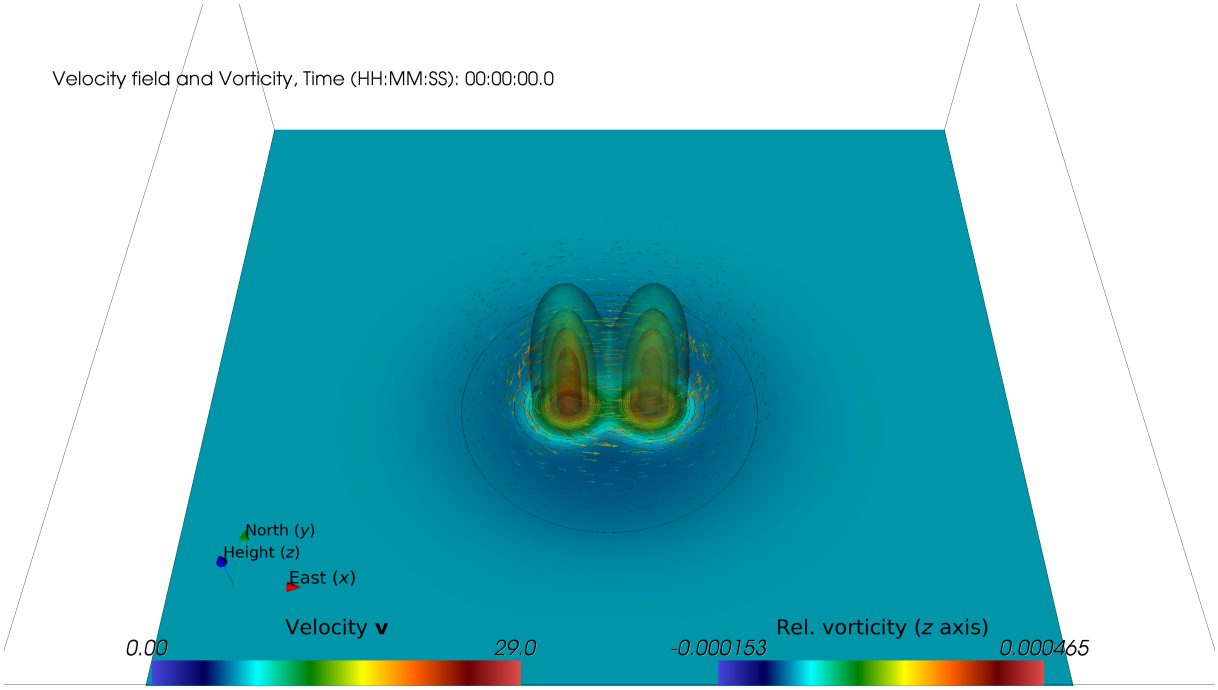

Figure 5.1.: Initial velocity field and vertical vorticity component.

In the second step, the initial temperature field is computed from $(\rho_h^*)^{(0)}$ and $(p_h^*)^{(0)}$ via the ideal gas law (2.98) and (3.9), respectively. In the case of the Low-Mach number approximation, the thermodynamic pressure $p_{th}(0) = 0$ is set. Under the assumption, that the Low-Mach approximation is valid and p_0^* is small compared to the other pressure parts, the initial temperature fields are close to each other. Observe, that the initial pressure p_0^* is not required to have zero mean value as it does not occur in the discrete dynamical system to the chosen time-stepping scheme described in Subsection 4.1.

The initial states are depicted in Figures 5.1-5.5. Observe, that the vertical axis is scaled up by a factor of 100 to allow a clearer visualisation. The initial temperature fields in Figures 5.3 and 5.4, respectively, show a little bit different shapes and a shift in the valuation, but observe, that the field θ_v^* is just the deviation from the reference state $\theta_{v,0}$ which is larger by several orders of magnitude, see Figure 2.1.

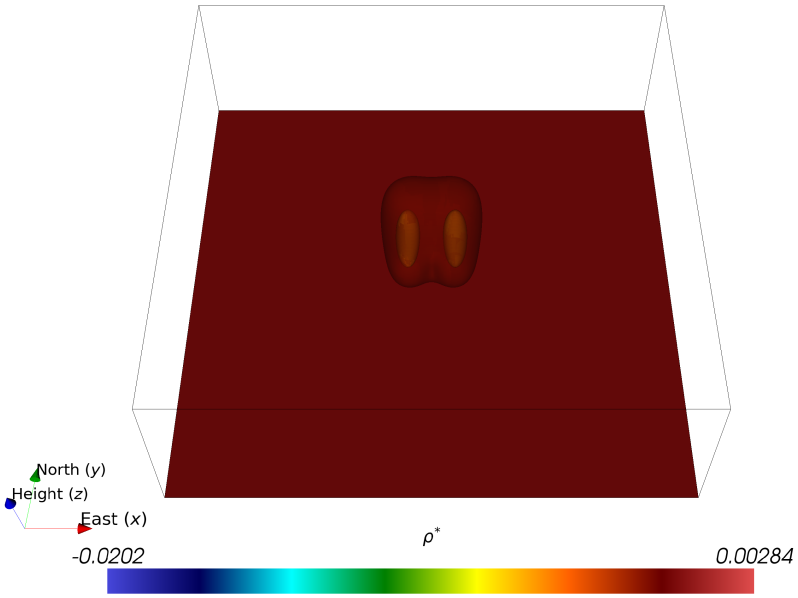

Figure 5.2.: Initial density.

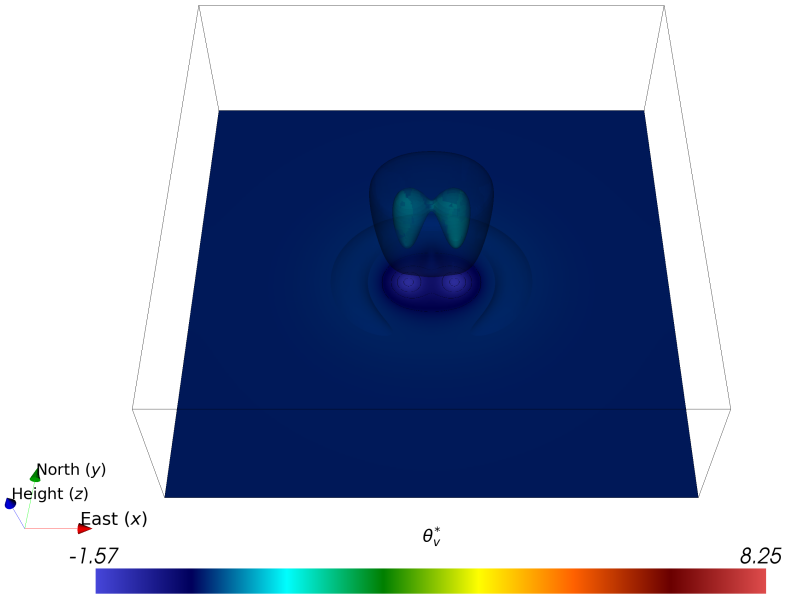

Figure 5.3.: Initial temperature of Compressible Navier-Stokes model.

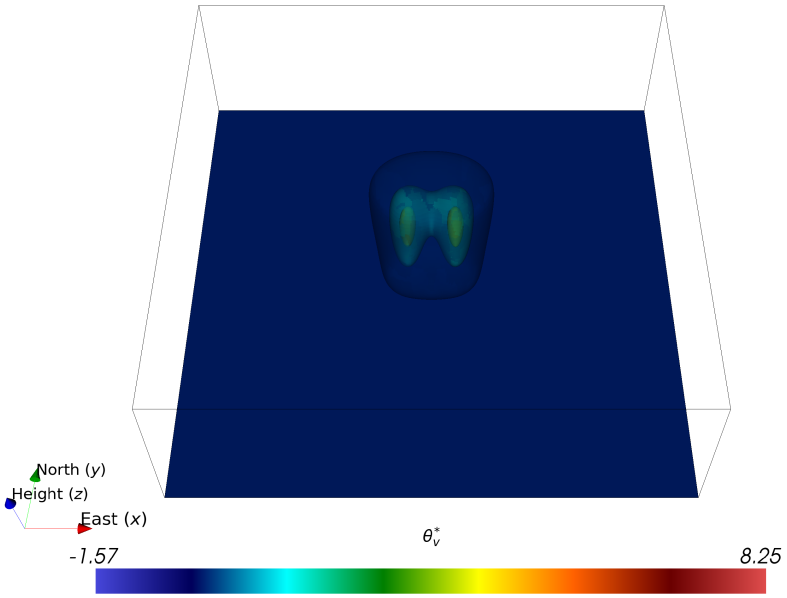

Figure 5.4.: Initial temperature of Low-Mach model.

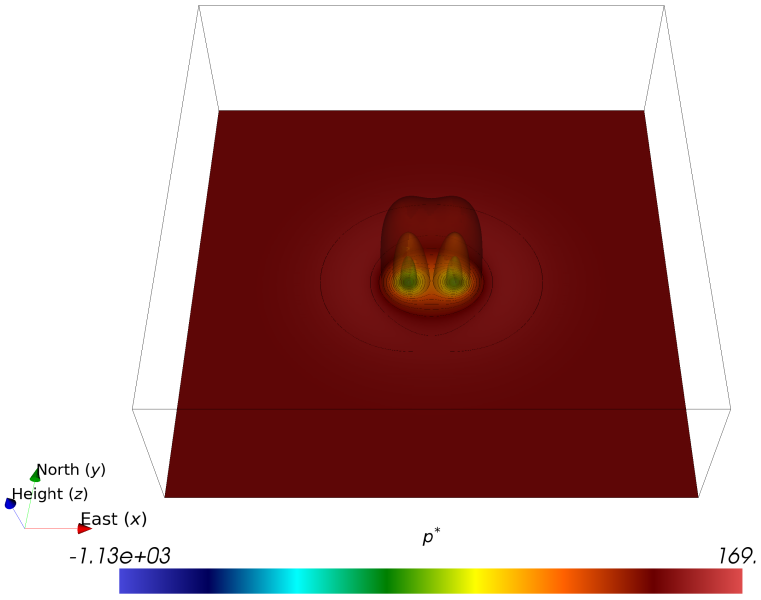

Figure 5.5.: Initial pressure.

6. Numerical results

Contents

In the following, the proposed governing equations, namely the Compressible Navier-Stokes model (see Chapter 2) and the Low-Mach model (Chapter 3), respectively, with their respective discretisations are applied to forecast the evolution of the interacting tropical cyclone scenario described in Chapter 5. It is the main objective to provide comparative measures of numerical properties of the different models. Additionally, basic measures are defined in order to judge the validity of the Low-Mach number approximation in the considered flow regime.

The numerical solution of the cyclone-cylcone interaction problem of Chapter 5 with the discretisations and solvers described in Chapter 4 yields a discrete problem with 31,680,000 *unknowns* or *degrees of freedom (DoFs)* in each time-step. In order to be able to solve these systems in a feasible amount of time and to use the provided computing resources responsibly, the scalability of the solvers proposed in Chapter 4 needs to be investigated and, based on this study, a parallel configuration is chosen for the comparative tests of the two models. A final time of

$$T = 96h = 345,600s \tag{6.1}$$

is chosen, which leads to a forecast of four full days.

In Section 6.1, the results of the proposed scalability study of the solvers are presented. In the following Section 6.2, the comparison of the two models by means of numerical measures and qualitative considerations is depicted.

All tests are run on the bwForCluster MLS & WISO. The abbreviation CNS is used to denote results of the Compressible Navier-Stokes model and the abbreviation LM to denote those of the Low-Mach model.

6.1. Scalability study

An analysis of the memory requirements of both models shows that the Low-Mach model consumes more memory than the Compressible Navier-Stokes Model due to the matrix copies needed in the Schur complement preconditioners. For the described discretisation and the resulting problem size, the memory consumption of the Low-Mach model is approximately 610 GByte in total. As the standard nodes of bwForCluster MLS & WISO are equipped with 64 GByte memory per node, the minimum node number, on which both models can be run, is 10. Considering, that the available 16 processor cores per node are used on 10 nodes and that one parallel MPI process is used per core, the local problem size on each process is approximately 200,000 DoFs, which is quite large. Therefore, the next larger power of 2, which is 256, was chosen as the minimal

Number of processes	**Accumulated time CNS** $[s]$	**Accumulated time LM** $[s]$	**Speed-up CNS**	**Efficiency CNS** [%]	**Speed-up LM**	**Efficiency LM** [%]
256	390.661	2491.286	1	100	1	100
512	207.144	1330.151	1.886	94.30	1.873	93.647
1024	113.158	761.487	3.452	86.309	3.272	81.790
2048	72.843	669.027	5.363	67.038	3.724	46.547

Table 6.1.: Accumulated compute times for the first 10 time-steps without I/O of the two models ranging between 256 and 2048 parallel processes.

configuration for the conduction of the scalability study. A power of 2 is chosen because global reduction operations, as they occur in the computation of scalar products of vectors, are often based on binary trees and, therefore, a number of processes, which is a power of 2, exploits this strategy optimally.

Starting from 256 parallel processes, the scalability to process numbers of 512, 1024 and 2048, which is the maximum number of processors, that can be allocated at once on bwForCluster MLS & WISO, is investigated. In all four configurations, the first ten time-steps of both models are computed and the compute times accumulated in order to filter out deviations in the results that occur due to the scheduling of the underlying operating system.

The accumulated time measurements as well as the resulting speed-up and parallel efficiency for the computation of a whole time-step, i.e., including assembly of matrices and vectors as well as the compute times for the solvers of Chapter 4, without I/O are given in Table 6.1 and those including I/O are given in Table 6.2. Visualisations of the speed-ups are given in Figure 6.1 and of the efficiency in Figure 6.2. Input/Output operations (I/O) include the computation of the vorticity field (see Subsection 6.2), output of the benchmarking quantities such as timings to a Comma Separated Values (CSV) file, writing the solution and the computational mesh to the parallel visualisation toolkit format (PVTU) and writing the solution for checkpointing purposes to a parallel hierarchical data format (HDF5) file. In this context, speed-up and efficiency are defined as follows: Let $P_1, P_2 \in \mathbb{N}$ with $P_1 \leq P_2$ denote two numbers of processors and $T(P_j)$, $j \in \{1, 2\}$, the corresponding compute times. Then the *(incremental) speed-up* from P_1 to P_2 processors is defined as

$$S_{P_1}(P_2) := \frac{T(P_1)}{T(P_2)}. \tag{6.2}$$

In the optimal case it should hold $S_{P_1}(P_2) = \frac{P_2}{P_1}$, which is referred to as the *ideal speed-up*. Consequently, the ratio between actual speed-up and ideal speed-up is measure for efficiency of the compute resources that are consumed additionally and, therefore, the *(parallel) efficiency* is defined as

$$E_{P_1}(P_2) := \frac{\frac{T(P_1)}{T(P_2)}}{\frac{P_2}{P_1}}. \tag{6.3}$$

In the context of the presented scalability study, it holds $P_1 = 256$ and $P_2 \in \{256, 512, 1024, 2048\}$.

The results show that both models scale very well up to 1024 processes and achieve over 80% of parallel efficiency, while the differences between both models are small. For the configuration of 2048 processes, there is a notable decrease in efficiency measure as the speed-up from 1024 to

Number of processes	**Accumulated time CNS** $[s]$	**Accumulated time LM** $[s]$	**Speed-up CNS**	**Efficiency CNS** [%]	**Speed-up LM**	**Efficiency LM** [%]
256	443.582	2547.889	1	100	1	100
512	236.8996	1363.583	1.872	93.622	1.869	93.426
1024	132.970	782.117	3.336	83.399	3.258	81.442
2048	88.620	690.493	5.005	62.568	3.690	46.124

Table 6.2.: Accumulated compute times for the first 10 time-steps with I/O of the two models ranging between 256 and 2048 parallel processes.

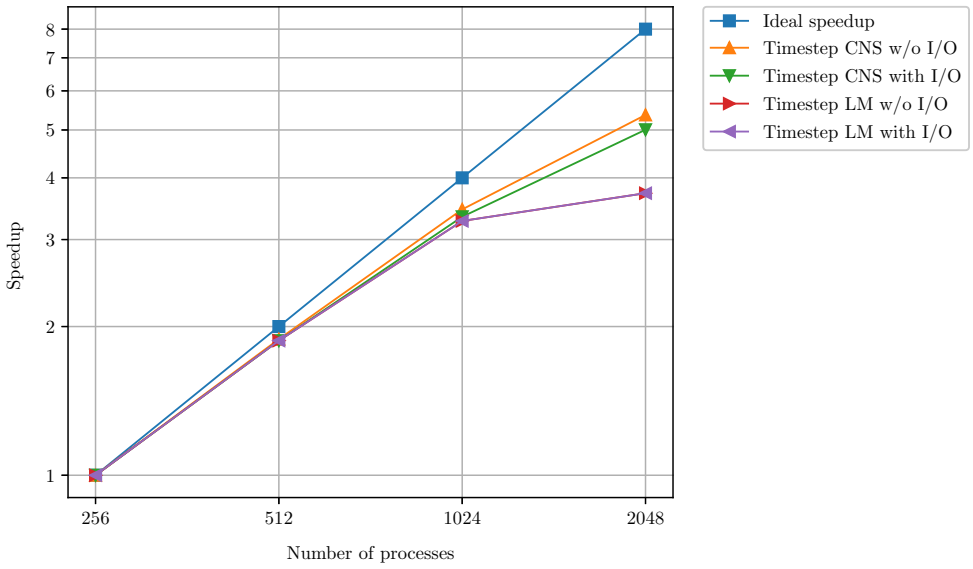

Figure 6.1.: Speedup in strong scaling test for whole time-step on bwForCluster MLS & WISO relative to 256 processes.

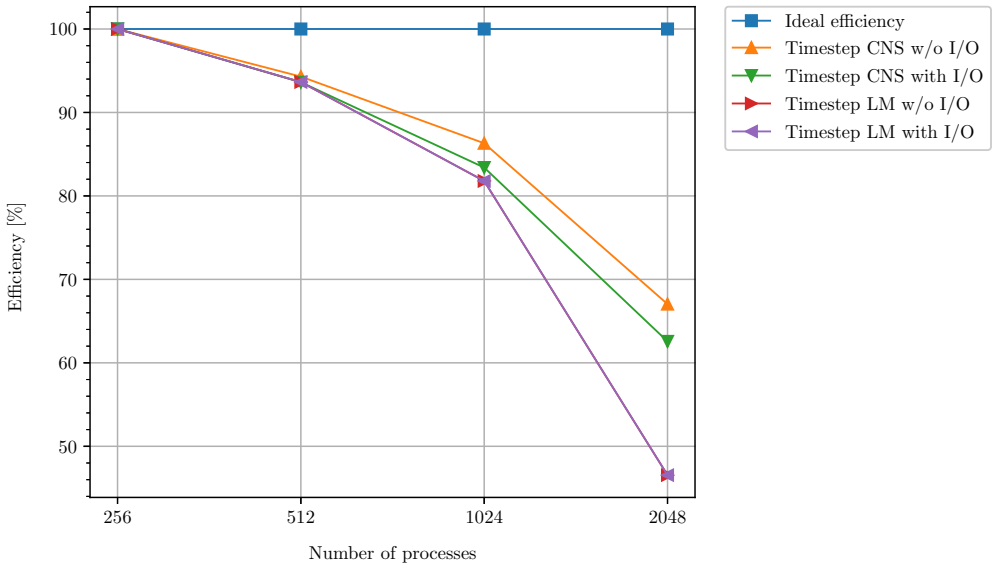

Figure 6.2.: Efficiency in strong scaling test for whole time-step on bwForCluster MLS & WISO relative to 256 processes.

2048 processes is notably smaller than for the lower processor numbers. On 2048 processors, the Compressible Navier-Stokes model performs considerably better by providing an efficiency of over 60%, whereas the efficiency of the Low-Mach model decreases to approximately 45%. Therefore, a process number of 1024 is chosen for the comparative computations in Subsection 6.2, because this configuration provides the best compromise between time-to-solution and efficient usage of the provided hardware resources.

The source of the decrease in efficiency is found in the performance of the linear solvers and preconditioners, respectively. Inspecting the times and scalability measures for the assemblies of residual vectors (Table 6.3) and matrices (Table 6.4) – the numbers for the solvers can be determined by substracting the assembly times from the times given in Table 6.1 – shows that the assembly scales almost perfectly as there is no communication between the different processes needed and, therefore, only the solvers are left as source for the limitation in parallel efficiency. The speed-ups of the assembly are visualized in Figure 6.3 and the efficiency in Figure 6.4. The reason that the Low-Mach model lacks more in efficiency on 2048 processes than the Compressible Navier-Stokes model is due to the fact that the Schur complement preconditioner requires several solves with submatrices of the Jacobian matrix (see Subsection 4.4) and, therefore, the missing scalability of *one* linear system solve is accumulated. One application of a linear solver, more precisely: the AMG preconditioner, does not scale so well to 2048 processors, compared to the configurations with lower process numbers. There are several possible reasons for the behaviour. One possible reason is that, due to the decomposition of the computational domain Ω to more processors, the ratio between local problem size and interface to neighbouring subdomains decreases. As the smoother in the BoomerAMG implementation with standard parameters only works on the local part of the linear system on each processor, the global efficiency of the

Number of processes	**Accumulated time CNS** $[s]$	**Accumulated time LM** $[s]$	**Speed-up CNS**	**Efficiency CNS** [%]	**Speed-up LM**	**Efficiency LM** [%]
256	63.940	65.603	1	100	1	100
512	29.764	30.381	2.148	107.411	2.159	107.967
1024	18.699	18.879	3.419	85.487	3.475	86.875
2048	8.770	8.933	7.291	91.138	7.343	91.793

Table 6.3.: Accumulated assembly times of the residual vectors for the first 10 time-steps of the two models ranging between 256 and 2048 parallel processes.

Number of processes	**Accumulated time CNS** $[s]$	**Accumulated time LM** $[s]$	**Speed-up CNS**	**Efficiency CNS** [%]	**Speed-up LM**	**Efficiency LM** [%]
256	132.562	168.243	1	100	1	100
512	59.633	75.467	2.223	111.148	2.229	111.468
1024	36.603	46.398	3.622	90.549	3.626	90.653
2048	16.67331	21.239	7.951	99.282	7.921	99.017

Table 6.4.: Accumulated assembly times of the Jacobian matrices for the first 10 time-steps of the two models ranging between 256 and 2048 parallel processes.

smoother is decreasing and, consequently, the linear solver needs more iterations to converge to a solution. A further possible source for lacking scalability is the applied coarsening scheme, namely the Falgout coarsening, which is *not* invariant to the number of subdomains, i.e., on different numbers of processors different coarse problems are generated. Therefore, a coarse grid on 2048 processors can be less efficient than the one generated on 1024 processors. A detailed analysis of the sources of the scalability lack on 2048 processors and a general improvement of this behaviour to higher process numbers is a topic of further research, see Subsection 7.2.

6.2. Model comparison

The Compressible Navier-Stokes model and its Low-Mach approximation are compared in two terms. First, numerical properties are analysed and compared in Subsection 6.2.1. Second, aspects in terms of physical properties of the two solutions are investigated in Subsection 6.2.2.

6.2.1. Numerical aspects

The main objective of introducing the Low-Mach approximation to the Compressible Navier-Stokes model is to investigate the gain in the maximum possible time-step size at which the solution can be computed stably as the evolution of phenomena at the speed of sound or even higher is filtered out of the model equations by the Low-Mach assumption. Therefore, these maximal values are determined heuristically by decreasing the time-step size by bisection and,

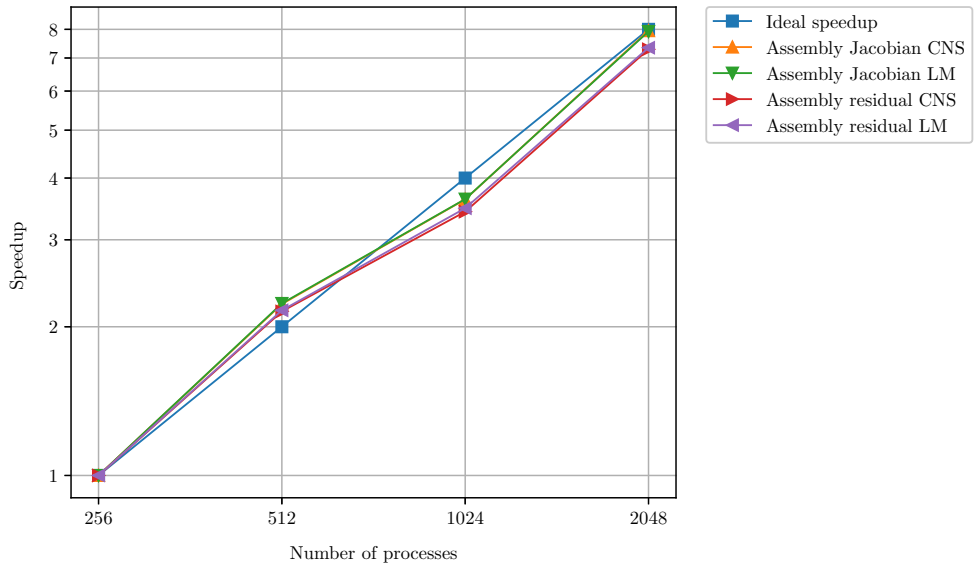

Figure 6.3.: Speedup in strong scaling test for assembly on bwForCluster MLS & WISO relative to 256 processes.

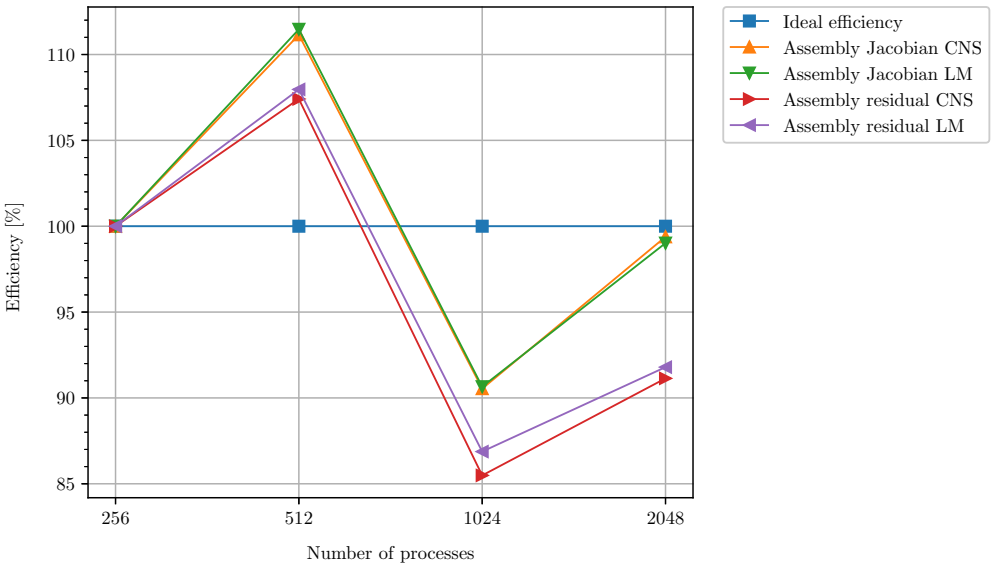

Figure 6.4.: Efficiency in strong scaling test for assembly on bwForCluster MLS & WISO relative to 256 processes.

thereby, constructing nested intervals, starting from the interval $[0s, 60s]$. Via this procedure the following maximal time-step sizes that allow a stable simulation of the cyclone-cyclone interaction scenario are found: The Low-Mach model is able to run stably with a time-step size of

$$\Delta t_{LM} = 10\ s, \tag{6.4}$$

whereas the Compressible Navier-Stokes model needs a time-step size of

$$\Delta t_{CNS} = 0.125\ s \tag{6.5}$$

for stability of the simulation, i.e., the Low-Mach model allows a time-step size that is 80 times larger than the one of the Compressible Navier-Stokes model for the considered scenario. Consequently,

$$M_{LM} = 34,560 \tag{6.6}$$

time-steps of the Low-Mach model need to be computed to simulate the cyclones up to the final time $T = 96\ h$, whereas

$$M_{CNS} = 2,764,800 \tag{6.7}$$

time-steps of the Compressible Navier-Stokes model are needed to complete the simulation.

Based on these findings, both models are run, which leads to the results given in Table 6.5. As several thousands of time-steps need to be computed, the average numbers per time-step are presented here. On average, one time-step of the Compressible Navier-Stokes model takes approximately 9.2 s of computational time, whereas one time-step with the Low-Mach model consumes about 47.5 s. Extrapolating these timings to the full number of intended time-steps, the simulation of the cyclone dynamics consumes approximately *295 days* with the Compressible Navier-Stokes model, whereas the Low-Mach model finishes this task after approximately *19 days*. Because of the infeasibility of the overall compute time with the Compressible Navier-Stokes model, the simulation was stopped after *12:29 (HH:MM)* simulated physical time and all comparative results between the two models are based on this period of simulated time. Also the results of Table 6.5 are based on this time-span.

The accumulated computing times for both models and their ratio are plotted in Figure 6.5. As the Low-Mach model allows 80 times larger time-steps than the Compressible Navier-Stokes model, but one time-step needs approximately a *five times longer* time to compute the solution, the Low-Mach model computes the solution with respect to the physically simulated time approximately *15 times* faster up to the considered time-span.

The non-linear algebraic system of equations of one time-step can be solved with two iterations of Newton's method (Algorithm 4.3) for both models on average. In the very first time-step, the Low-Mach model needs three iterations of Newton's method, but afterwards always two iterations are needed. Therefore, the following comparisons of the linear solvers and the assembly times are representative because the numbers depend directly on the number of Newton iterations.

To compute the Newton steps, the respective linear solver takes approximately 48 iterations on average for the Compressible Navier-Stokes model and between two and three iterations for the Low-Mach model. Therefore, the proposed preconditioning technique of nested Schur complements for the Low-Mach model is very effective for the considered scenario. The five times larger compute time for one time-step of the Low-Mach model results from the fact that within in the Schur complement preconditioner several smaller linear systems need to be solved and the needed compute times for each of these solver applications accumulate.

On average, the assembly of the residual vectors is about 6% *faster* in the Compressible Navier-Stokes model. The assembly of the Jacobian matrices even takes about 25% *less* time.

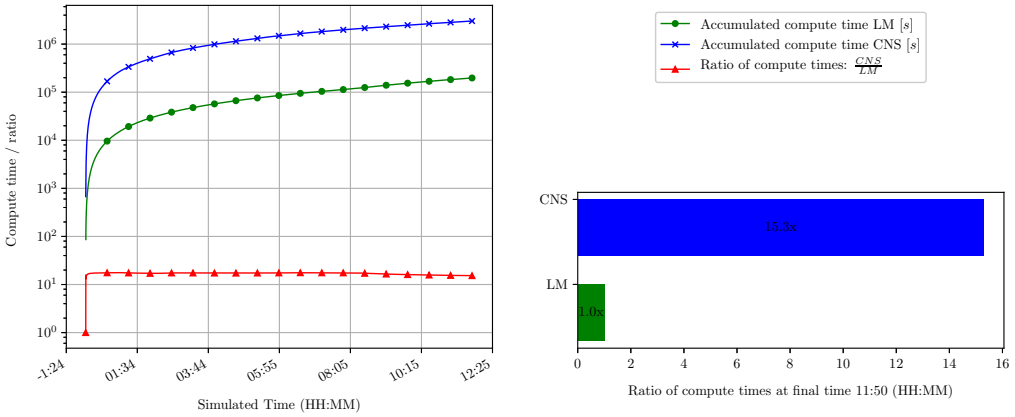

Figure 6.5.: Comparison of compute times.

Model	**Newton iterations**	**Compute time** $[s]$	**Assembly time residual** $[s]$	**Assembly time Jacobian** $[s]$	**(F)GMRES iterations**
LM	2.00023	46.533	1.718	4.437	2.305
CNS	2.0	8.892	1.607	3.342	47.751
Ratio $\frac{CNS}{LM}$	0.99988	0.191	0.935	0.753	20.714

Table 6.5.: Average quantities per time-step compared for both models.

The reason are the additional terms due to the *grad-div* stabilisation of the Low-Mach model that are not present in the case of the Compressible Navier-Stokes model.

The progress of Newton iterations, compute times for one time-step as well as the number of linear solver iterations in the course of the simulated physical time are plotted in Figure 6.6 for the Low-Mach model and in Figure 6.7 for the Compressible Navier-Stokes model, respectively. Observe, that the plot in case of the Low-Mach model covers the whole intended time-interval up to $T = 96\ h$.

6.2.2. Physical aspects

For the comparison of physical aspects of the computed solutions of the two models, both *global* and *local* quantities are taken into account. Whenever the *error* of a quantity $\mathbf{q} \in \mathbb{R}^n$, $n \in \mathbb{N}$ is considered, the *relative error* between the computed quantity $\mathbf{q}_{CNS}$ of the Compressible Navier-Stokes model and the computed quantity $\mathbf{q}_{LM}$ with respect to the Compressible Navier-Stokes model is taken into account, i.e.,

$$e_{\mathbf{q},rel} := \frac{\|\mathbf{q}_{LM} - \mathbf{q}_{CNS}\|_2}{\|\mathbf{q}_{CNS}\|_2}. \tag{6.8}$$

On the global level, the overall *mass of air* in the domain Ω is monitored, which is a measure

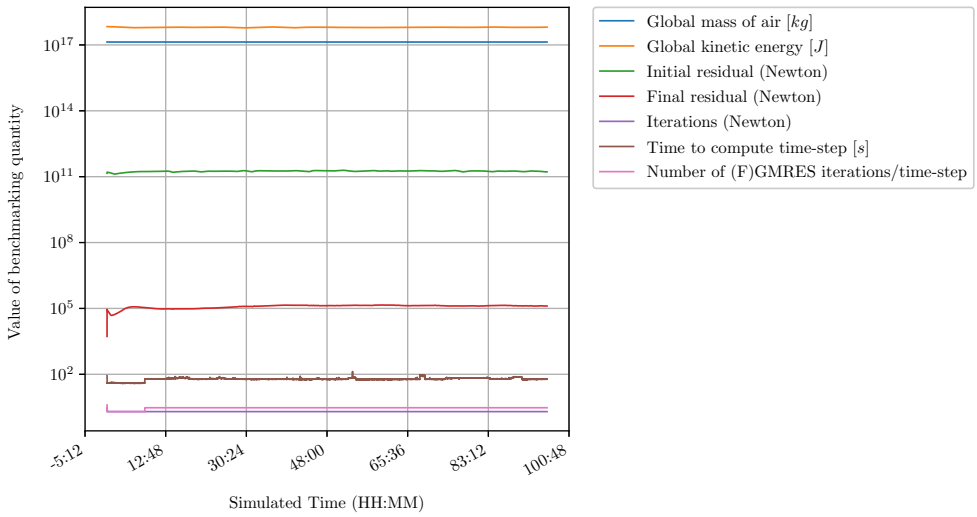

Figure 6.6.: Progress of comparative quantities obtained for the Low-Mach model.

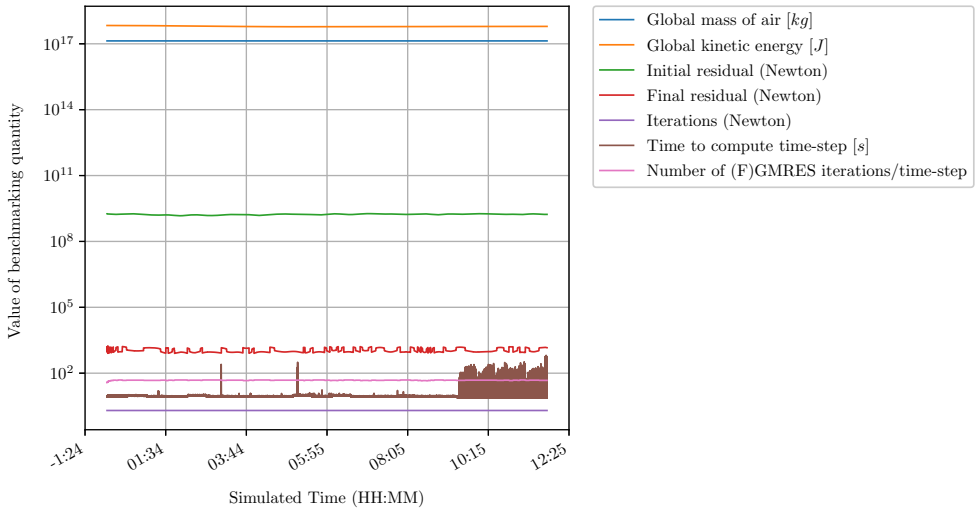

Figure 6.7.: Progress of comparative quantities obtained for the Compressible Navier-Stokes model.

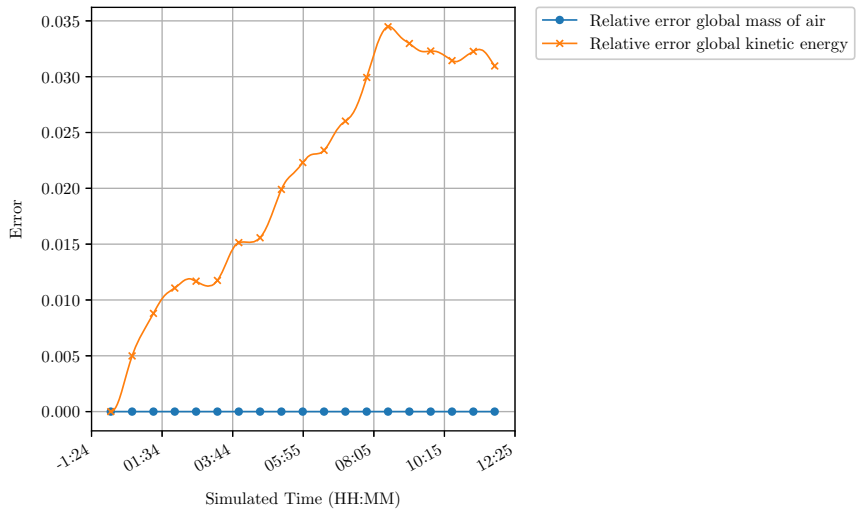

Figure 6.8.: Relative errors global of physical quantities plotted over simulated physical time.

for the conservation of mass, as well as the overall *kinetic energy* in Ω. The global mass of air at any time $t \in [0, T]$ is given by

$$m_\Omega(t) := \int_\Omega \rho(t, \mathbf{x}) \mathrm{d}\mathbf{x}, \tag{6.9}$$

and the global kinetic energy at any time $t \in [0, T]$ is defined as

$$E_{kin,\Omega}(t) := \frac{1}{2} \int_\Omega \rho(t, \mathbf{x}) \, \|\mathbf{v}(t, \mathbf{x})\|_2^2 \, \mathrm{d}\mathbf{x}, \tag{6.10}$$

where $\mathbf{v}$ denotes the velocity field and ρ the density. The relative errors in global mass of air m_Ω and global kinetic energy $E_{kin,\Omega}$ are depicted in Figure 6.8. In the global mass of air there is virtually no difference between the solutions of the two models. Also the global kinetic energy shows very good coincidence between the solutions of the Compressible Navier-Stokes and the Low-Mach model, with the relative error remaining below the 5% bound. Inspecting these two quantities more closely for both models individually, i.e., monitoring the minimum and maximum values of both quantities and comparing them to the initial state, see Table 6.6, it is remarkable that both models show virtually perfect conservation of mass within the considered span of time. The kinetic energy takes its maximum value at the beginning of simulation for both models and obviously decreases first, with the Compressible Navier-Stokes model showing a maximal loss of kinetic energy of approximately 13%, whereas the kinetic energy in the Low-Mach solution has a maximal loss of approximately 11%. The maximal loss occurs 767.5 s later with the Compressible Navier-Stokes model in terms of simulated physical time. It is out of the scope of this thesis to determine, if the energy is really lost or a transformation to another kind of energy causes the decrease in kinetic energy. Answering this question requires expert knowledge in physics or meteorology, respectively, and is a subject of further research, see Subsection 7.2.

On the local level, the following simple measure is applied which on the one hand can be easily computed and on the other hand allows a comparison by means of relative errors. The measure

Quantity	CNS	LM
Initial mass $[kg]$	$1.35495 \cdot 10^{17}$	$1.35495 \cdot 10^{17}$
Time-step	0	0
Minimal mass $[kg]$	$1.35495 \cdot 10^{17}$	$1.35495 \cdot 10^{17}$
Time-step	0	0
Maximal mass $[kg]$	$1.35495 \cdot 10^{17}$	$1.35495 \cdot 10^{17}$
Time-step	0	0
Initial kinetic energy $[J]$	$6.81979 \cdot 10^{17}$	$6.81979 \cdot 10^{17}$
Time-step	0	0
Minimal kinetic energy $[J]$	$5.96013 \cdot 10^{17}$	$6.0834 \cdot 10^{17}$
Time-step	157660	1894
Maximal kinetic energy $[J]$	$6.81979 \cdot 10^{17}$	$6.81979 \cdot 10^{17}$
Time-step	0	0

Table 6.6.: Global physical quantities compared for both models.

is based on the so called *(relative) vorticity* of the velocity field. Vorticity is a local measure of rotation in a fluid and is defined as the curl of velocity [42]. Therefore, the (relative) vorticity is defined as

$$\omega := \nabla \times \mathbf{v}, \tag{6.11}$$

such that in Cartesian coordinates it holds

$$\omega = \begin{pmatrix} \partial_y w - \partial_z v \\ \partial_z u - \partial_x w \\ \partial_x v - \partial_y u \end{pmatrix}. \tag{6.12}$$

In large-scale dynamic meteorology, one is mainly interested in the vertical component

$$\zeta = \partial_x v - \partial_y u \tag{6.13}$$

as it provides a measure for rotation around the vertical coordinate axis and is, therefore, a measure for the large-scale horizontal motions of a fluid, which is air in the considered scenario. For cyclonic storms in the Northern hemisphere is holds $\zeta > 0$ [42], which is exactly valid for the scenario at hand. As ζ takes its maximum at the centre of a cyclone, the *position* of a cyclone is defined as the location of this maximum in the context of this thesis. In the discretisation described in Chapter 4, the hexahedral cells of the triangulation are axis-aligned to the Cartesian coordinate system such that the vertices of the mesh are organised in layers. To provide a position analysis not only at a single point, but along the vertical axis, the two maximum values of ζ and their locations are determined within each of these layers. Ideally, these two positions are separated in each layer such that the locations of both cyclones can be tracked. The resulting positions and the values of ζ are compared for both models.

Remark 6.1 (Vorticity tracking)
Vorticity is a local measure and derivatives of the velocity field are involved. Therefore, it is a derived quantity. Furthermore, due to the Coriolis force the cyclones show different shearing behaviour. Consequently, it can happen, that the determined maximum values of ζ in a layer are within the same cyclone. Additionally, to keep the computation time for the maximal values low,

only the values at the vertices of the triangulation are considered. These reasons lead to noise in the determined vorticity data which is tried to be filtered out the following way: Starting from the initial state where the positions of the maxima of vorticity are known a priori due to the construction of the initial velocity field, in each time-step the determined potential positions are only taken into account if the their distance is larger than six times the horizontal cell diameter. The value of six was determined heuristically. If the positions of one time-step are considered based on the described heuristic approach, their distances to the last "known" position of the cyclone starting more in the west are compared, and the one, which is closer, is assigned to this western cyclone. The other one is categorised as the new position of the eastern cyclone.

Figures 6.9 to 6.12 as well as Figures A.1 to A.29 show the comparisons of cyclone positions as well as vorticity magnitude at these positions in terms of the respective relative error. If the plotted time-line is shorter than the considered span of time, then the cyclones could not be distinguished according to Remark 6.1. Of course, a comparison is done if and only if the cyclones can be distinguished in the forecasting of both models at the same time. Above approximately $10,500\ m$, the maximal value of vorticity is on the order of machine precision and, therefore, the results become more random for both models and a comparison is not possible any more, see Figures A.23 to A.29 in Section A.5. Below, the results show a good coincidence of the predicted storm positions of both models with a maximum deviation of 1.4 cell diameters at a height of $1625\ m$, while the values of vorticity differ at most about 16% at $10,156.25\ m$ height. Below $6500\ m$ of height, the relative errors in vorticity are even constantly below 5%. Therefore, in terms of the predicted cyclone positions as well as the corresponding vorticity values, the Low-Mach model performs very competitively to the Compressible Navier-Stokes model at significantly smaller computational costs. Especially, it can be concluded that the overall vertical profiles of the solutions of both models are very close to each other in the course of the simulated time-span. Therefore, the vertical energy cascade is also very similar in both models which is a further indication for the validity of the Low-Mach approximation in the considered scenario.

The cyclone tracks of the individual models at selected height levels are presented in Figures 6.13 and 6.14, respectively. Observe, that the plots of the Low-Mach model are again for the full time interval up to $96\ h$ of simulated physical time. Furthermore, it can be clearly seen in Figure 6.14 that in the course of the full considered time-span both cyclones merge to a single one, which is moving in north-western direction afterwards due to the Coriolis force.

Finally, the individual model solutions at the last visualisation point of the considered time-span are presented by means of iso-surface and glyph plots, respectively, and analysed. Observe, that the vertical axis is scaled up by a factor of 100 again to allow a clearer visualisation. Figure 6.15 shows the velocity fields (glyph visualisation) as well as the vertical vorticity component (iso-surfaces). The vorticity distributions of the two considered models show slight differences in shape as well as in the global minimal and maximal value, respectively. The velocity fields also look very similar in their distribution and shape over Ω, but the predicted maximal wind speed is about $1.2\frac{m}{s}$ *higher* in the Compressible Navier-Stokes solution compared to the result of the Low-Mach model, which corresponds to a *relative error of approximately* 4.5%. The density fields in Figure 6.16 show very good coincidence both in shape and lower and upper bounds of the predicted variable values. There is a difference in the shape and the bounds of the two temperature fields in Figure 6.17. This is due to the fact that already the initial distributions were different in shape, see Chapter 5, and that, of course, the Low-Mach assumption and, consequently, the Low-Mach approximation affects the overall relations in the modelling of thermodynamics. Observe again, that the presented density, temperature and pressure fields are all deviations from the constant-in-time reference states, which are larger by orders of magnitude. The pressure parts

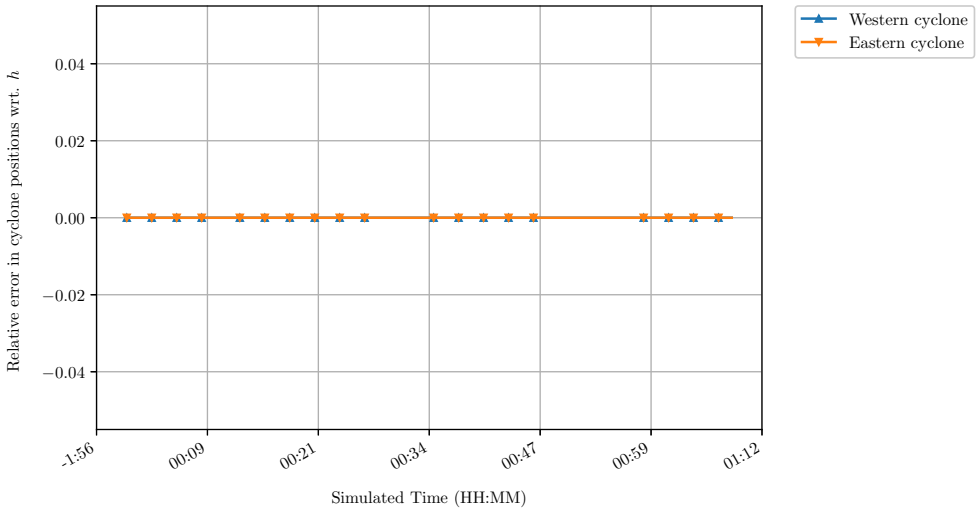

(a) Error in position

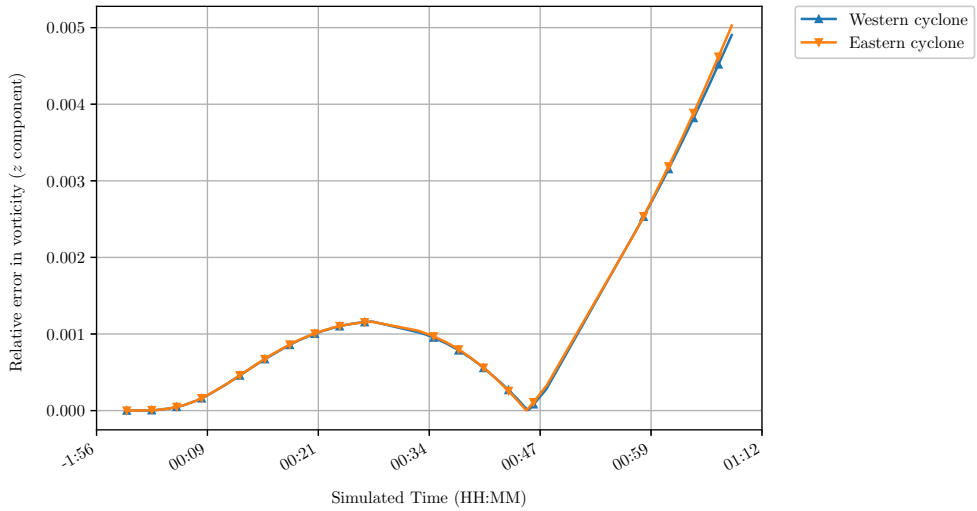

(b) Error in vorticity

Figure 6.9.: Relative error in cyclone positions and corresponding vorticities at $z = 0\ m$.

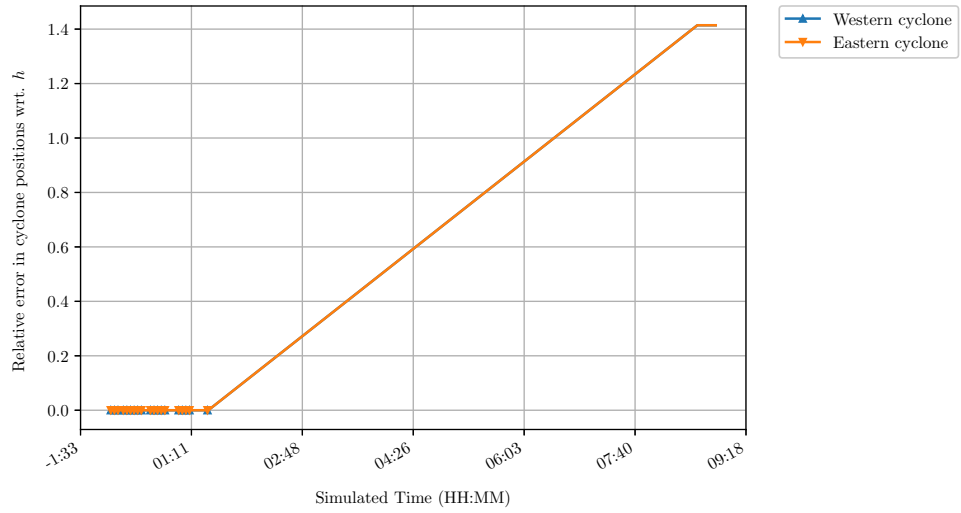

(a) Error in position

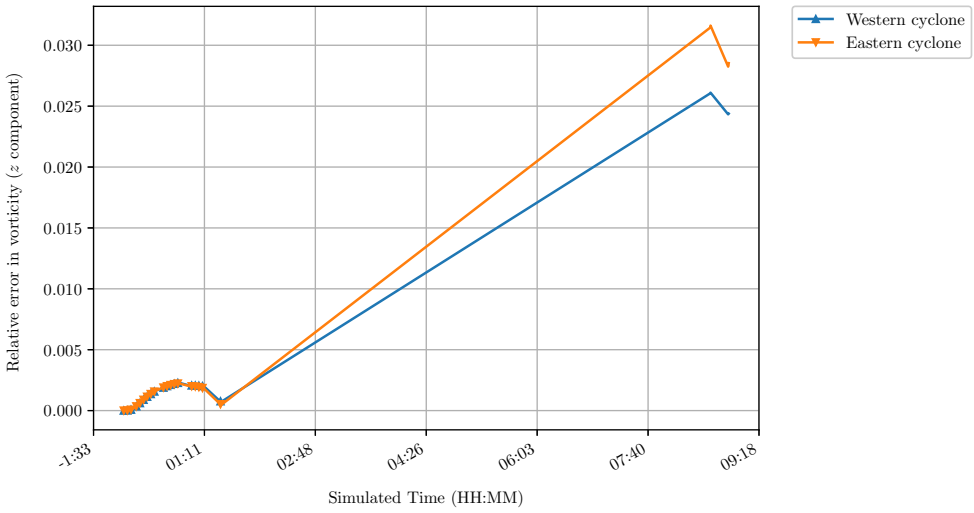

(b) Error in vorticity

Figure 6.10.: Relative error in cyclone positions and corresponding vorticities at $z = 1625\ m$.

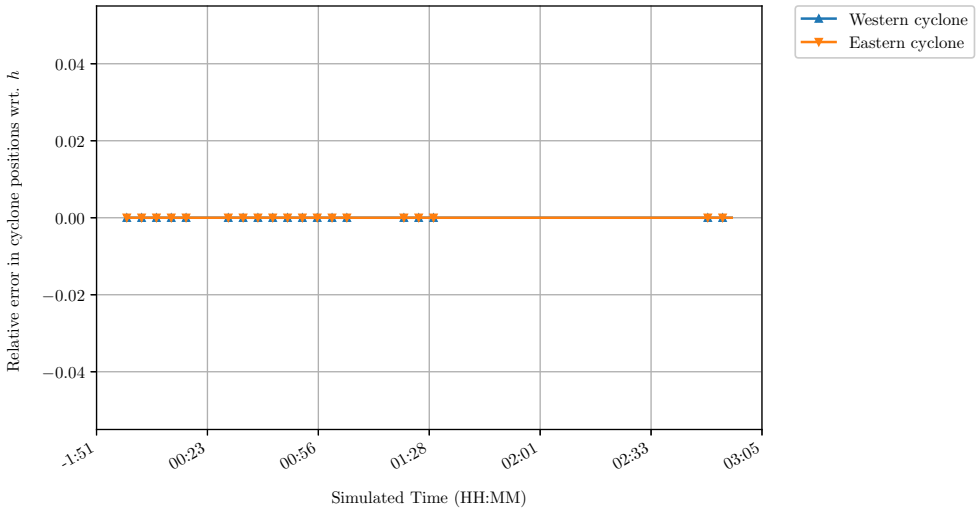

(a) Error in position

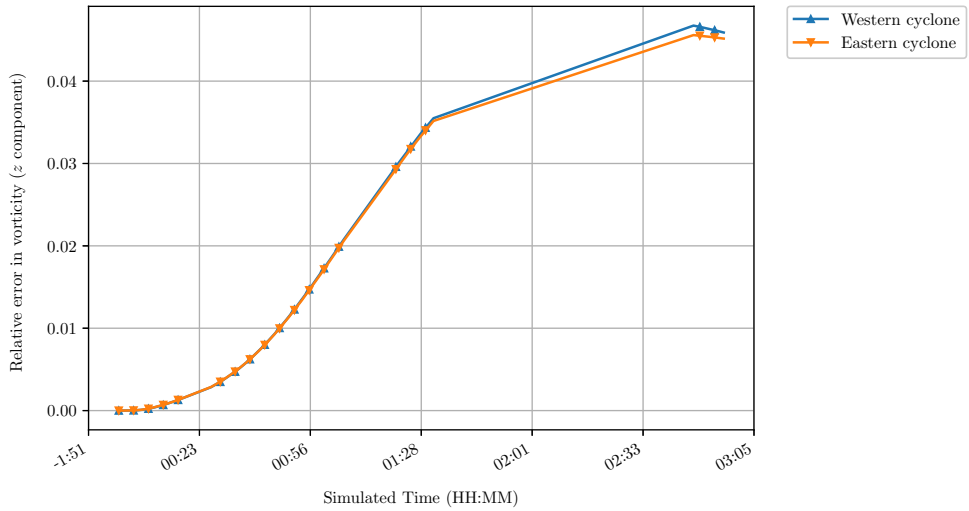

(b) Error in vorticity

Figure 6.11.: Relative error in cyclone positions and corresponding vorticities at $z = 6500\ m$.

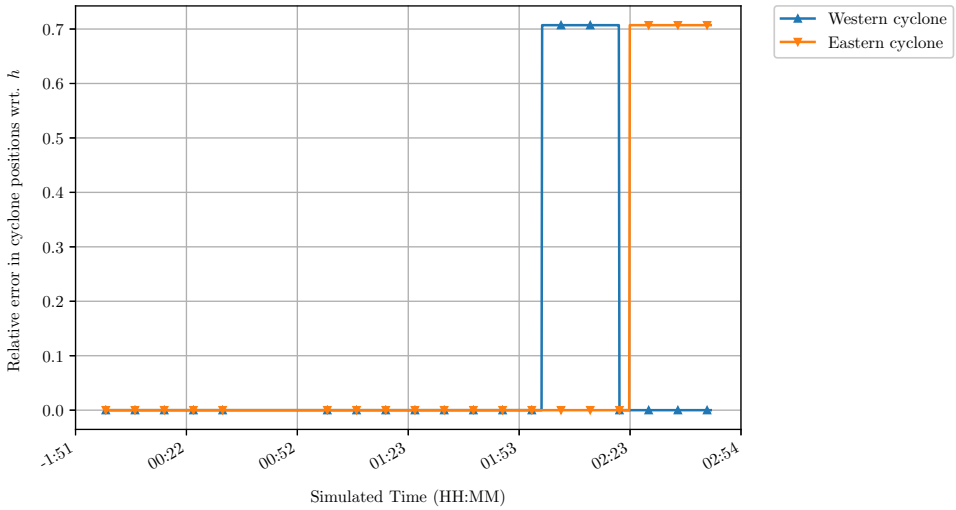

(a) Error in position

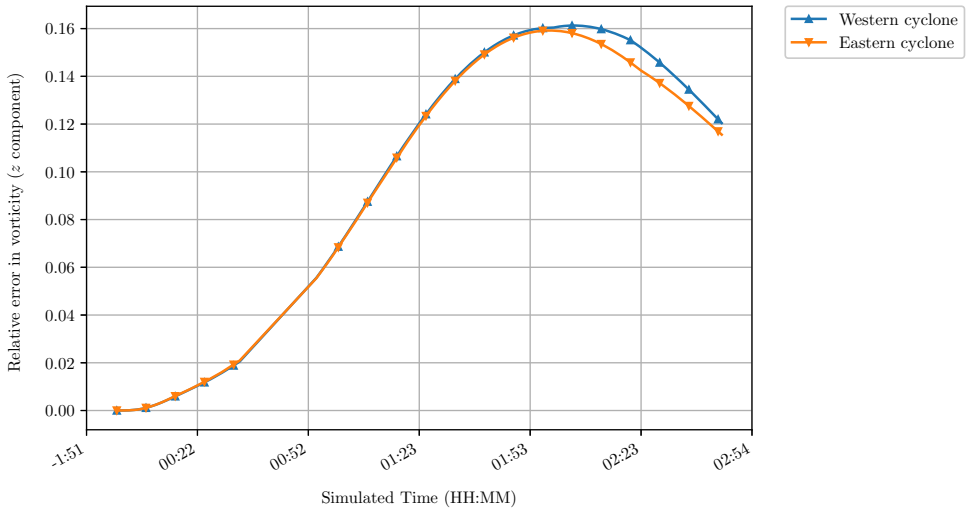

(b) Error in vorticity

Figure 6.12.: Relative error in cyclone positions and corresponding vorticities at $z = 10,156.25\ m$.

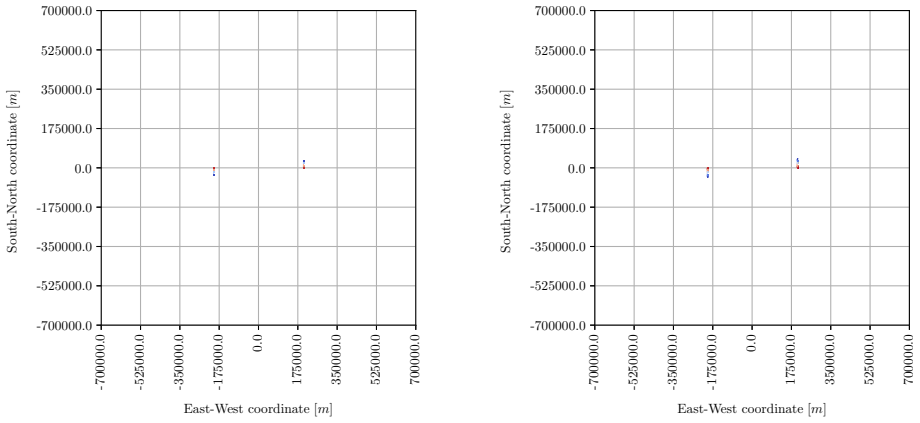

(a) $z = 0\ m$ (b) $z = 812.5\ m$

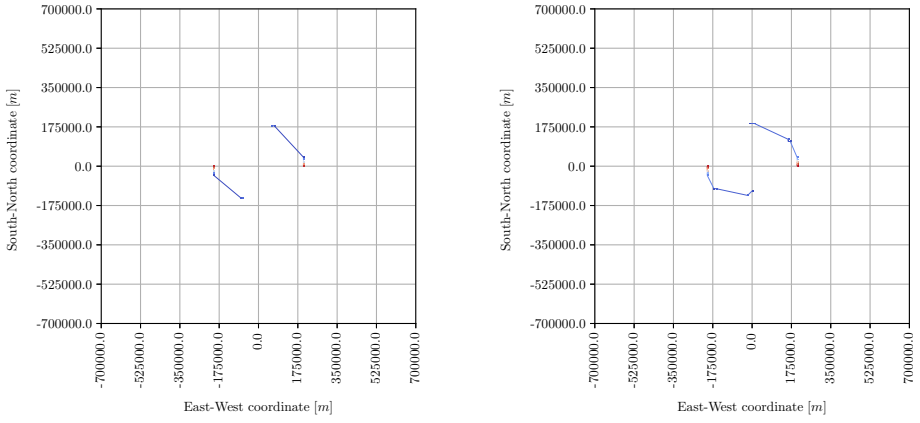

(c) $z = 1625\ m$ (d) $z = 2437.5\ m$

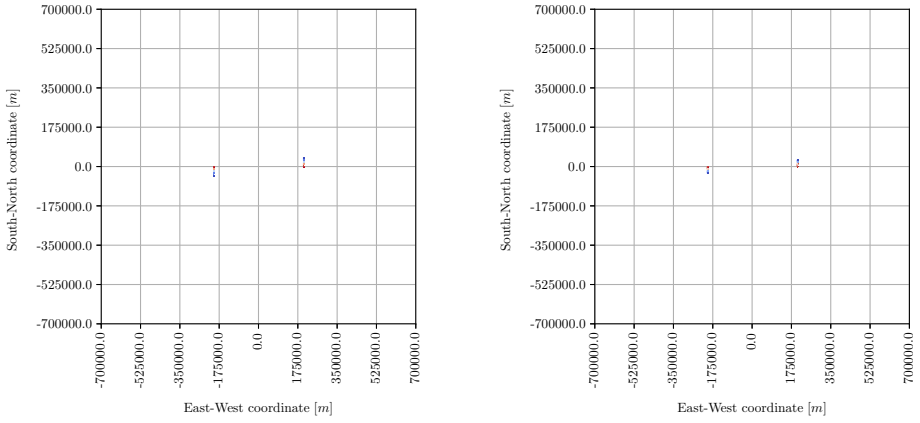

(e) $z = 3250\ m$ (f) $z = 4062.5\ m$

Figure 6.13.: Cyclone tracks of Compressible Navier-Stokes model at selected heights.

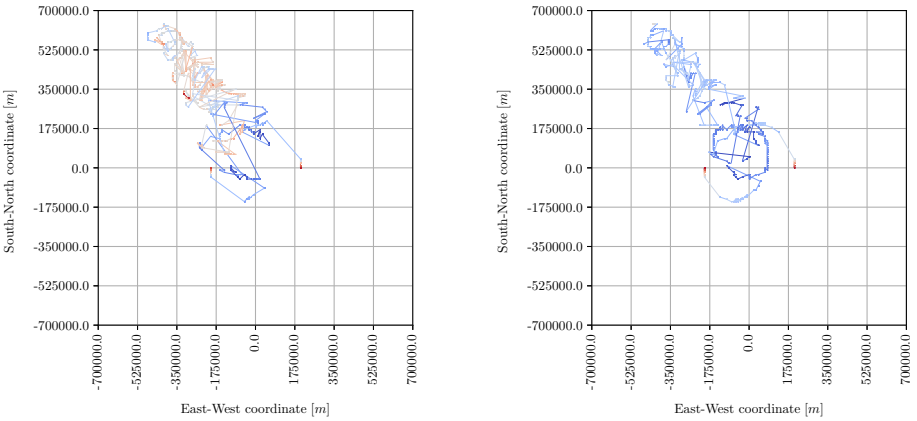

(a) $z = 0\ m$ (b) $z = 812.5\ m$

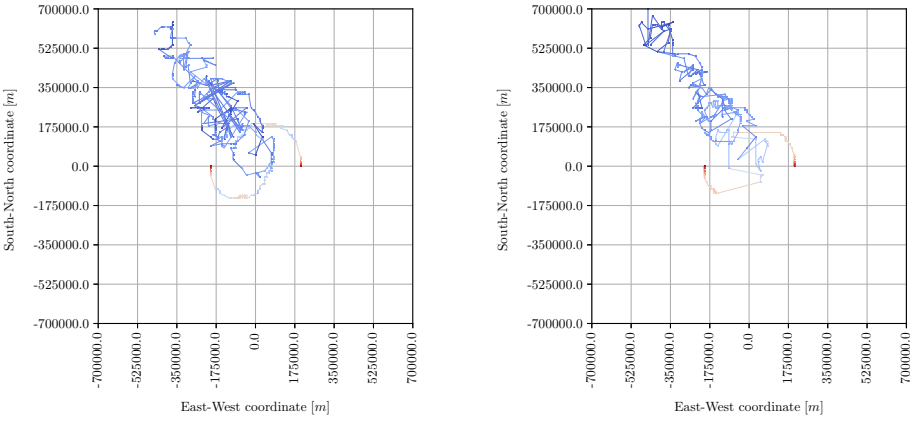

(c) $z = 1625\ m$ (d) $z = 2437.5\ m$

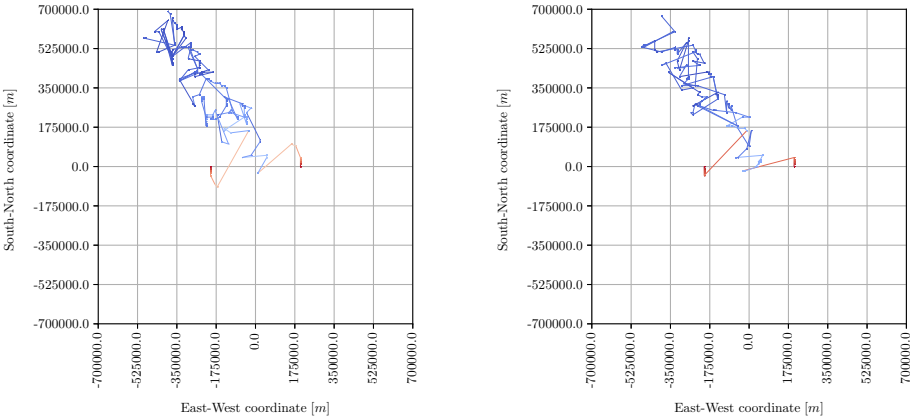

(e) $z = 3250\ m$ (f) $z = 4062.5\ m$

Figure 6.14.: Cyclone tracks of Low-Mach model at selected heights.

p^* look very similar in their shape, only the lower and upper bounds differ due to the Low-Mach approximation. The thermodynamic pressure p_{th} of the Low-Mach solution is plotted over the full time-span up to 96 h in Figure 6.19.

This chapter closes with the presentation of solution of the Low-Mach model at the final time $T = 96\ h$, see Figures 6.23 to 6.26. It can be seen, that in the course of the full considered time-span both cyclones merge to a single one, see Figures 6.20 to 6.22 for the merging process, which is moving in north-western direction afterwards due to the Coriolis force. Consequently, also the locations, where the deviations of density, temperature and pressure, respectively, differ mostly from the reference states, are moving in this direction. Observe, that a former study [11] carried out with a two-dimensional inCompressible Navier-Stokes model showed that the two cyclones do merge only if their initial separation is less or equal to 375 km. For larger initial separations, especially the 400 km considered in this thesis, the results in two dimensions predict that the two cyclones rotate around each other and diverge in different directions afterwards. Therefore, the results obtained in this thesis coincide with the study [63] where the merging was predicted by a simpler three-dimensional hydrostatic model. In contrast to [63], where the two cyclones merged after 6 to 7 h, the merging occurs later in the Low-Mach model after approximately 24 h. This result strongly indicates that the precise prediction of the tracks of the cyclones depends significantly on the model physics and that models with more accurately modelled physical processes are needed. Further possible developments in this direction which are based on this thesis are pointed out in Section 7.2.

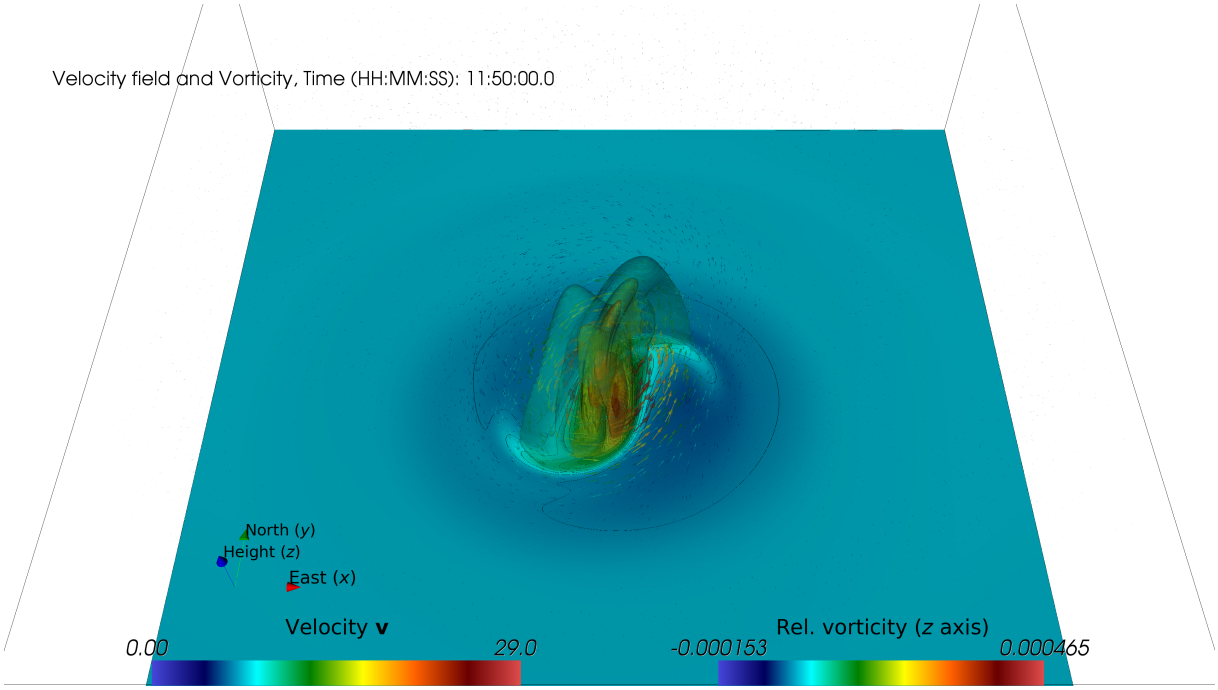

(a) Compressible Navier-Stokes

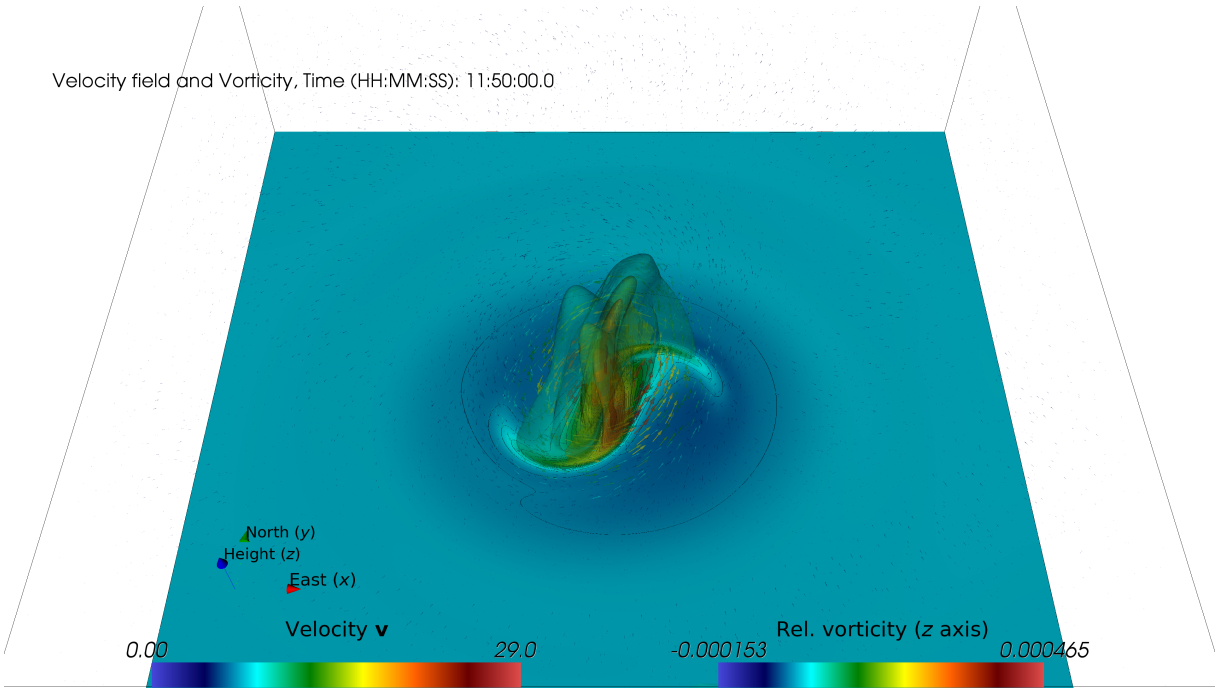

(b) Low-Mach

Figure 6.15.: Velocity field and vertical vorticity component at common final time.

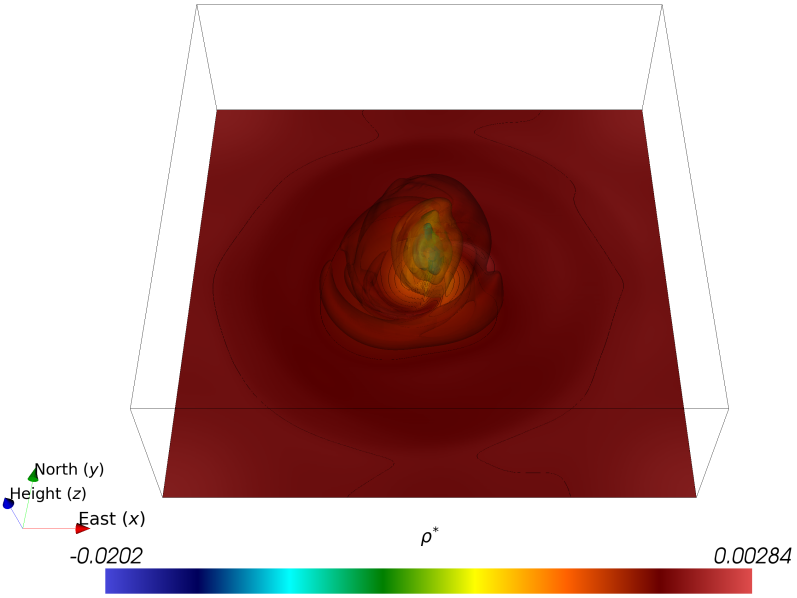

(a) Compressible Navier-Stokes

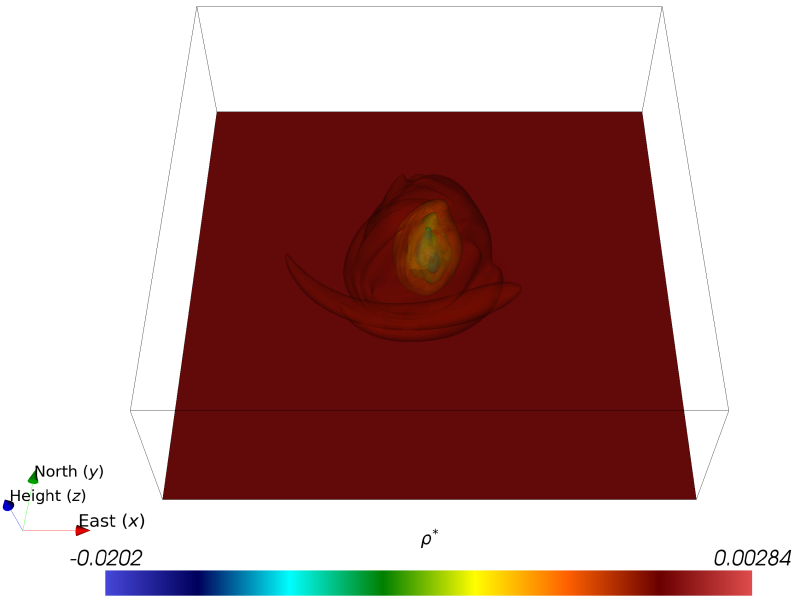

(b) Low-Mach

Figure 6.16.: Density at common final time.

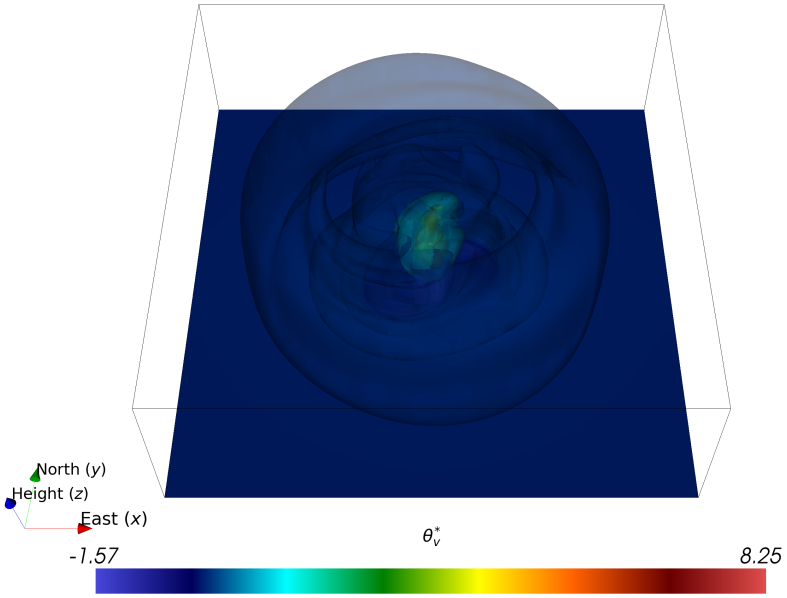

(a) Compressible Navier-Stokes

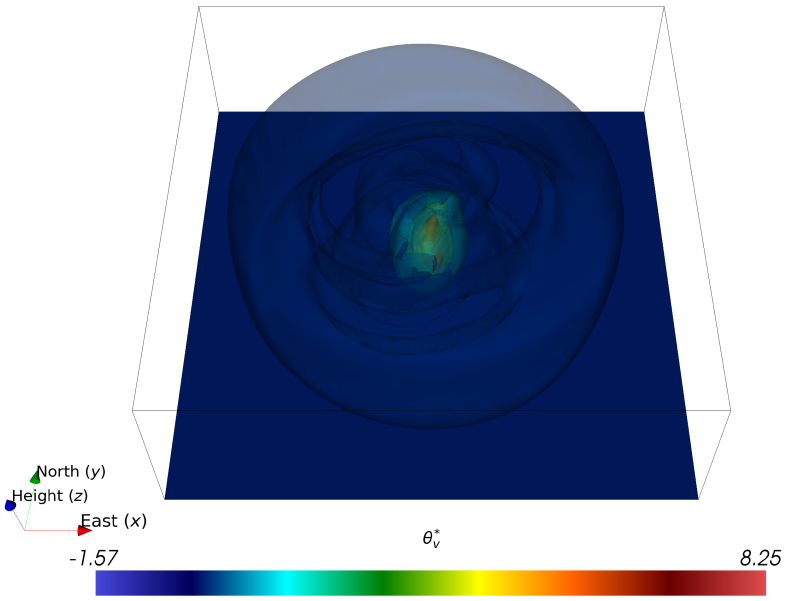

(b) Low-Mach

Figure 6.17.: Temperature at common final time.

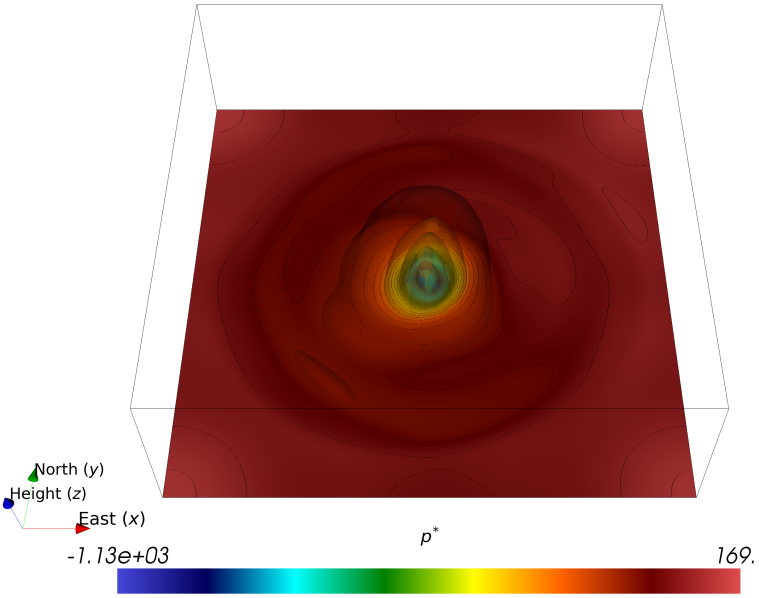

(a) Compressible Navier-Stokes

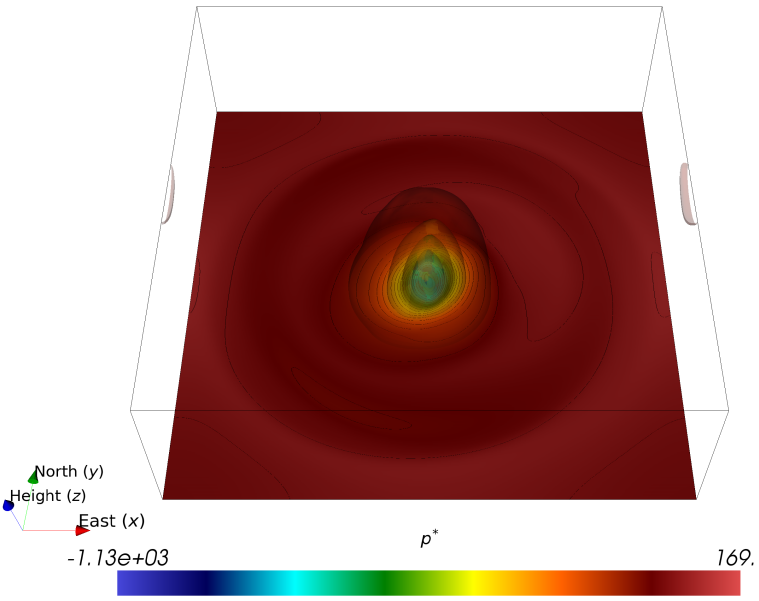

(b) Low-Mach

Figure 6.18.: Pressure at common final time.

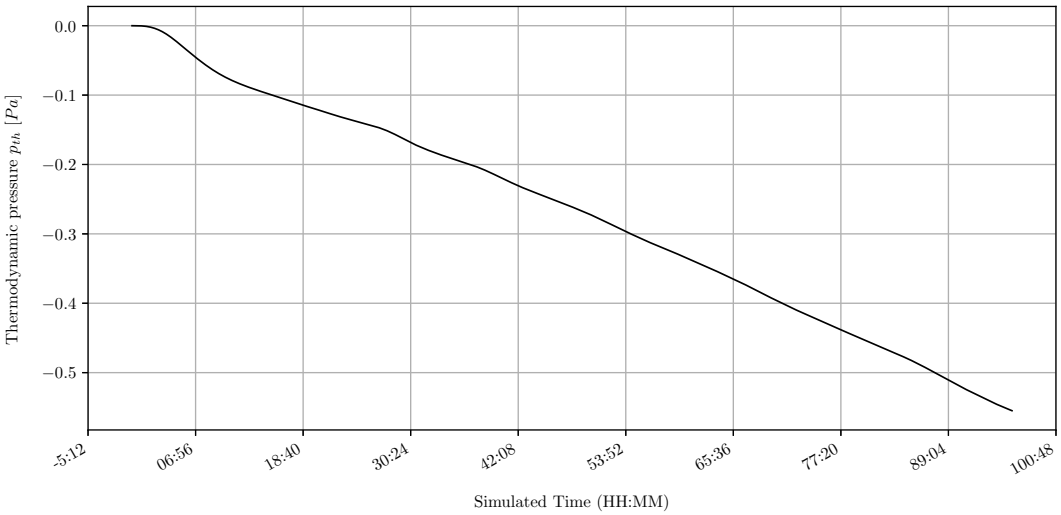

Figure 6.19.: Thermodynamic pressure in the Low-Mach model plotted over time.

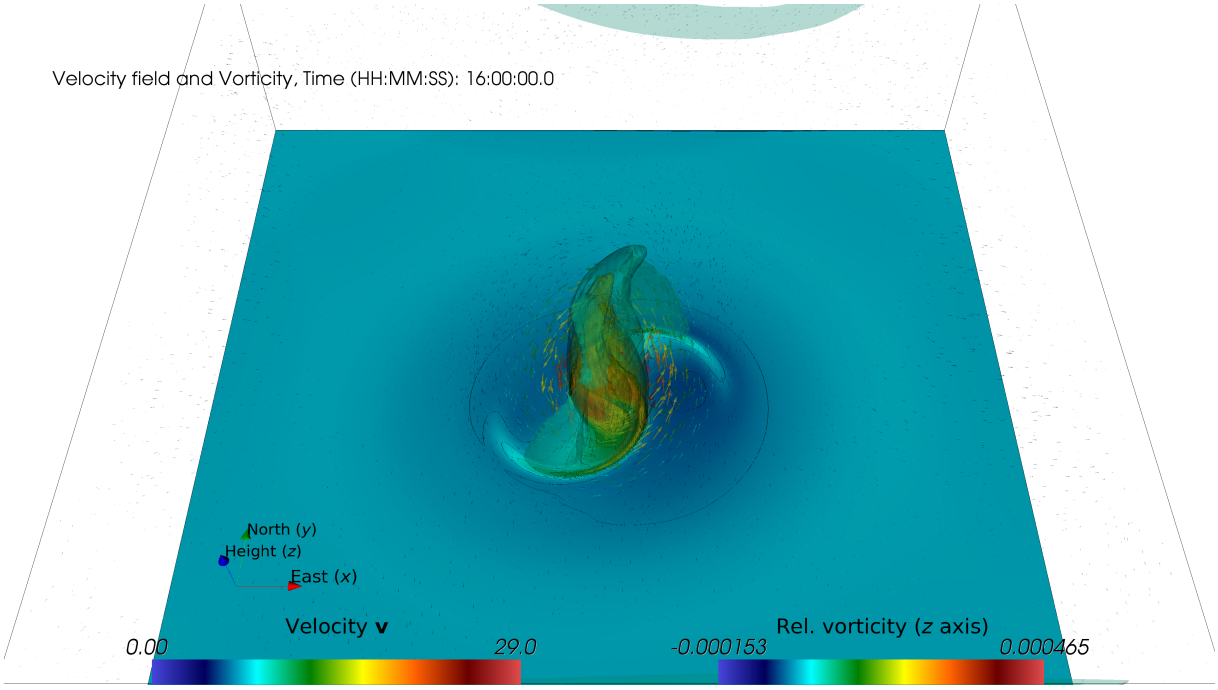

Figure 6.20.: Velocity field and vertical vorticity component at $t = 16\ h$, computed with Low-Mach model.

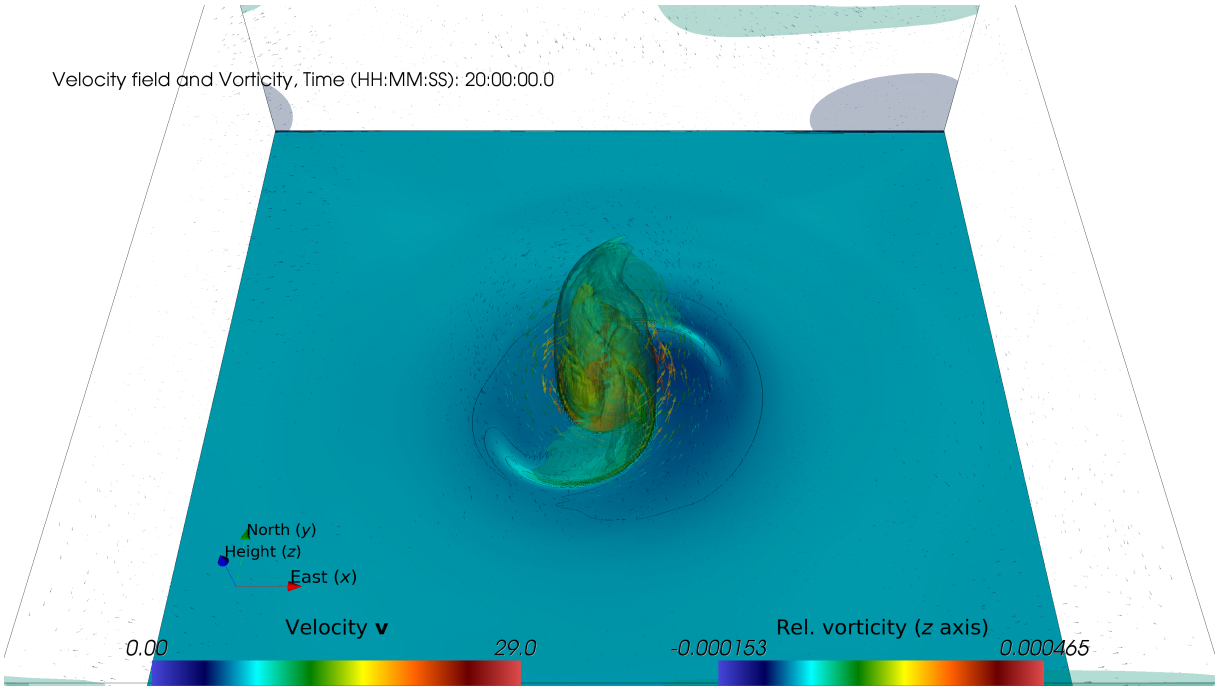

Figure 6.21.: Velocity field and vertical vorticity component at $t = 20\ h$, computed with Low-Mach model.

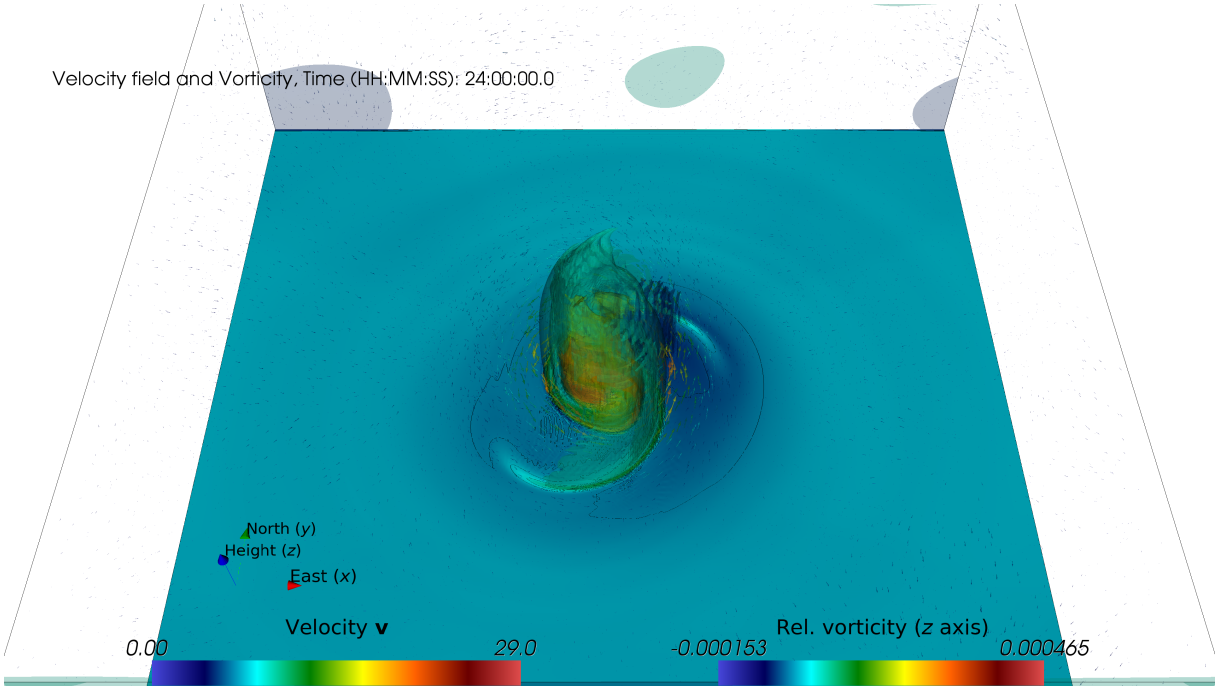

Figure 6.22.: Velocity field and vertical vorticity component at $t = 24\ h$, computed with Low-Mach model.

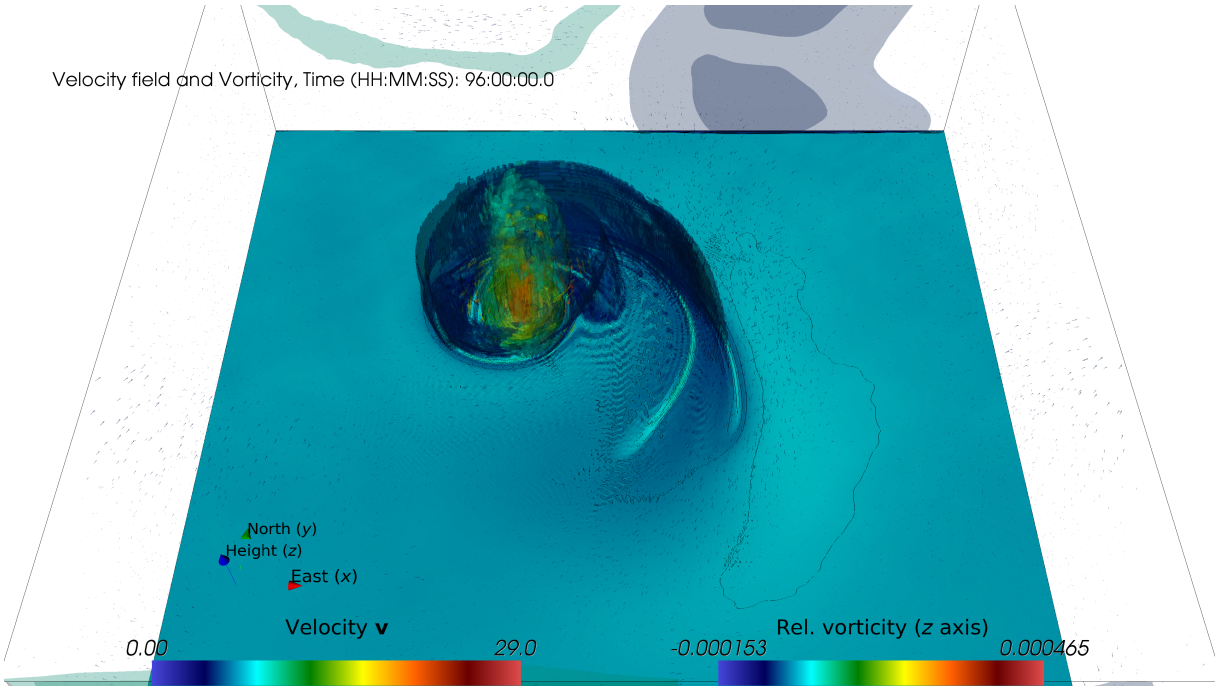

Figure 6.23.: Final velocity field and vertical vorticity component at $T = 96\ h$, computed with Low-Mach model.

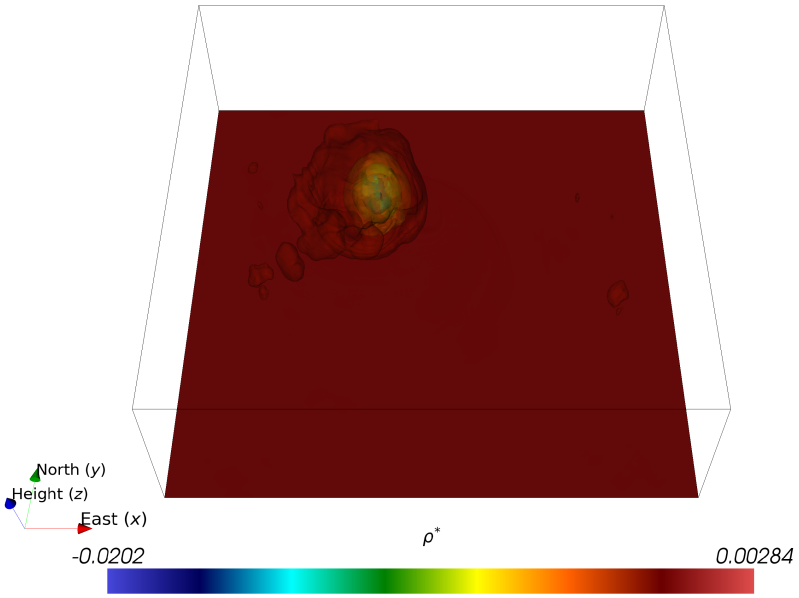

Figure 6.24.: Finale density at $T = 96\ h$, computed with Low-Mach model.

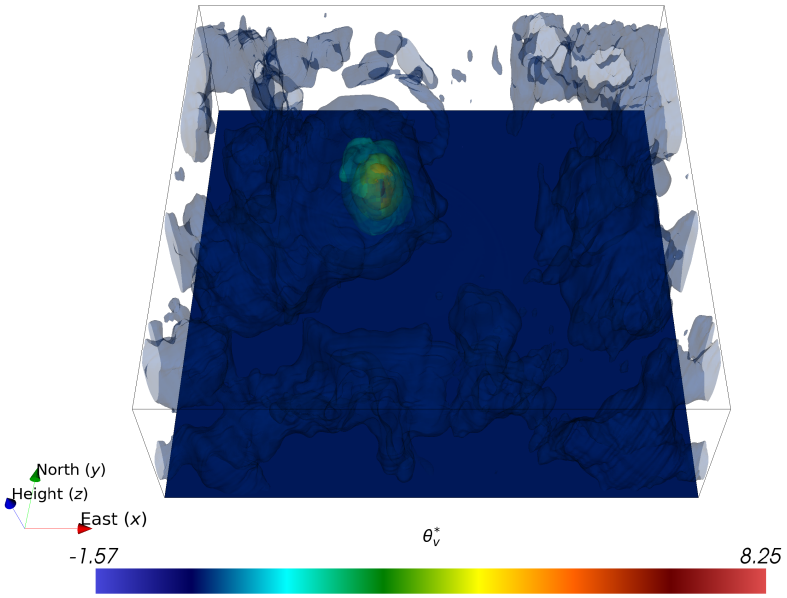

Figure 6.25.: Final temperature at $T = 96\ h$, computed with Low-Mach model.

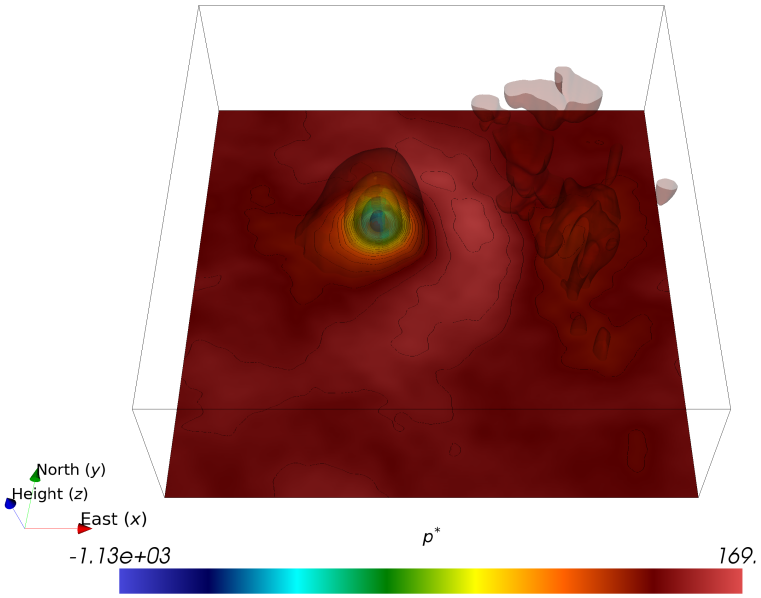

Figure 6.26.: Final pressure at $T = 96\ h$, computed with Low-Mach model.

7. Summary and outlook

Contents

7.1. Summary

In this thesis, the compressible Navier-Stokes equations describing the dynamics of a dry atmosphere were derived. Based on a scale analysis for Low-Mach number flows, the Low-Mach approximation was derived from the compressible Navier-Stokes equations by neglecting the hydrodynamic part of pressure, which is small compared to the hydrostatic and thermodynamic parts, in the ideal gas law. Both models were discretised by finite elements in space and finite differences in time, where all common parameters of the discretisations were chosen identically in order to minimise influences on the discrete solutions due to differences in the respective discretisations. A solution strategy for both models based on an inexact Newton method was presented, where the linear solvers and preconditioners are adapted to the respective model. In case of the Low-Mach model, a preconditioning technique based on nested Schur complement iterations was proposed. A scenario of two interacting tropical cyclones was presented as benchmark problem in order to compare the solutions of the two models in terms of numerical as well as physical properties. The obtained numerical results showed the scalability and robustness of the solution approach and that a fully-coupled solution approach with implicit time-stepping schemes is possible and, in the case of the Low-Mach model, feasible. For the considered scenario, the predicted tracks of the cyclones, which were computed by the Low-Mach model, showed very good coincidence with those of the Compressible Navier-Stokes model at significantly smaller computational costs, such that the Low-Mach approximation can be regarded as valid in this case. Consequently, the Low-Mach model actually allows high-resolution simulations and studies at feasible computational costs compared to the fully Compressible Navier-Stokes model which constitutes a real advantage in the numerical simulation of the considered benchmark scenario. Furthermore, the results obtained with the Low-Mach model over the full considered time-span of 96 h show that the phenomenon of merging cyclones for the chosen model parameters coincides with former studies in this field. In contrast to these studies it was found that the merging occurs to a later point in time than with the simpler models considered in these studies. Therefore, further research on this phenomenon with models including more physical aspects like moisture or radiation, for example, is needed.

7.2. Outlook

The presented results showed a good coincidence between the Compressible Navier-Stokes model and its Low-Mach approximation in terms of the considered comparative measures. Especially

in the area of local quantities, an extension of the considered properties and features promises a more fine-grained benchmark of the models. Methods for tracking certain *features* of dynamic flows in meteorological applications are developed by the meteorological community and form an own area of research, which does not involve physicists only, but also computer scientists. These methods can often be applied in the post-processing steps, such that an analysis of the obtained data is doable without carrying out new simulations.

Furthermore, the comparison was based on idealised models, i.e., moist processes, solar radiation, and multiple chemical reactions, for example, are not represented in the considered sets of equations. In the case of tropical cyclones, especially moist processes represent an important addition as they are a crucial ingredient if also the genesis of cyclones shall be considered in the simulation. Furthermore, moist processes are known to have stabilising effects on the dynamics. Consequently, they could have an effect also on the gap in the time-step sizes between the considered models and, therefore, their effect on the obtained results should be investigated in the future.

The presented comparison is only valid up to a scale of 10 km in the horizontal dynamics and approximately 400 m in the vertical. Effects on smaller scales, like tiny vortices of an extent of a few hundred meters, are not represented directly in the solution, but only their mean effects on the larger scales by means of the applied stabilisation scheme, which can be interpreted as a turbulence or subgrid-scale model. In order to facilitate investigations on the small scales, the scalability of the solvers in terms of both strong – same global problem size computed on more processors – and weak – constant local problem size, but more processors and, therefore, larger global problem size – scaling needs to be improved. Observe, that in the context of this thesis only strong scaling was considered. An ideal weak scalability would enable such simulations within the same time of computation as presented here, if the number of processes is increased at the same ratio as the global problem size grows when considering triangulations with finer cells. An additional improvement of the strong scaling behaviour then allows to obtain the results in a shorter time, if the computation is carried on even more processors. The latter is of exceptional importance, if the Low-Mach model and the proposed solution methodologies are considered as candidates for new numerical models for weather forecasting and climate prediction, respectively, which require the time for computation to be smaller than the simulated time-span.

Another interesting question that was not addressed at all in the context of this thesis is the following: How do the considered models for atmospheric perform, if they are initialised with real data, e.g., from measurements? Real data are not as smooth as the presented ones in case of the idealised tropical cyclones, because, on the one hand, real atmospheric flows – especially on smaller spatial scales – have a much more complex structure and, on the other hand, measured data always contain errors due to technical limitations. How robust are the proposed models to errors in the data and potential lacks of smoothness, that is induced by these errors? How can the answers to these questions be quantified? Methods from the field of *uncertainty quantification* provide a promising approach to tackle these questions. To this end, input data and parameters can be regarded as uncertain and be equipped with a probability distribution of the errors or uncertainties in these data. Based on this modelling, such methods do not compute a single, *deterministic* solution but several solutions of coupled problems which represent stochastic modes of the problem under the considered uncertainties. Consequently, these information can be processed to mean and standard deviation, which are well-understood quantities of probability theory and give an idea, which result can be expected subject to the considered errors and on which scale the results possibly scatter.

A. Appendix

Contents

A.1. Notation

A.1.1. Derivatives

Let $\Omega \subset \mathbb{R}^n$ be a domain, $a, b \in \mathbb{R}$ with $a \leq b$ and $u \in C^p((a,b); C^q(\Omega))$ continuously differentiable with respect to the time variable t and with respect to the space variable x, respectively. Let $x \in \Omega$ and $t \in (a,b)$ and p, q large enough such that the derivatives make sense.

1. We shortly write
$$\partial_t u(t,x) := \frac{\partial}{\partial t} u(t,x)$$
for the time derivative and
2.
$$\partial_i u(t,x) := \frac{\partial}{\partial x_i} u(t,x), \quad i \in \{1, \ldots, n\},$$
for the spatial derivative.

3. Let $\alpha \in \mathbb{N}_0^n$ a multiindex. We define the α^{th}-partial derivative of order

$$|\alpha| := \sum_{i=1}^{n} \alpha_i$$

as

$$\partial^\alpha u(t,x) := \frac{\partial^{|\alpha|} u}{\partial x_1^{\alpha_1} \cdots \partial x_n^{\alpha_n}}(t,x).$$

4. The *Laplace* differential operator Δ is defined as

$$\Delta u(t,x) := \sum_{i=1}^{n} \partial_i^2 u(t,x).$$

5. The *gradient* of u is defined as

$$\nabla u(t,x) := (\partial_1 u(t,x), \ldots, \partial_n u(t,x))^\top \in \mathbb{R}^n.$$

6. Let $u \in C^p((a,b); (C^q(\Omega))^n)$. The *divergence* of u is defined as

$$\text{div } u(t,x) := \sum_{i=1}^{n} \partial_i u_i(t,x).$$

A.2. Calculus

A.2.1. Integration theory

Theorem A.1 (Gauß)
Let $\Omega \subset \mathbb{R}^n$ be an open and bounded subset, where $\partial\Omega$ is C^1. Suppose $u \in C^1(\overline{\Omega})$. Then

$$\int_\Omega \partial_i u(x) \mathrm{d}x = \int_{\partial\Omega} u(s) \boldsymbol{\nu}_i(s) \mathrm{d}s \quad (i = 1, \ldots, n),$$

where $\boldsymbol{\nu} : \mathbb{R}^n \to \mathbb{R}^n$ denotes the outer normal vector field on Ω.

Proof:
See, e.g., [50]. □

A.3. Some functional analysis

This section summarizes the definitions and theorems of functional analysis as they are used throughout this thesis. The definitions and theorems are taken from the textbooks [2, 29, 76]. For further details as well as proofs to the given theorems, refer to these references.

A.3.1. Normed linear, Banach and Hilbert spaces

In this section, the definitions of three fundamental classes of spaces from functional analysis, which are used throughout this thesis, are given.

Definition A.2 (Normed linear space)
Let X a vector space defined on a field $\mathbb{K}$ ($= \mathbb{R}$ or $\mathbb{C}$) and $\|\cdot\|_X : X \to \mathbb{R}$ a mapping. The pair $(X, \|\cdot\|_X)$ is called a *normed linear space* (and the mapping $\|\cdot\|_X$ is called a *norm*), if $\|\cdot\|_X$ fulfils the following properties for all $x, y \in X$ and $\alpha \in \mathbb{R}$:

1. $\|x\|_X \geq 0$ and $\|x\|_X = 0 \;\Leftrightarrow\; x = 0$ (definiteness)
2. $\|\alpha x\|_X = |\alpha| \, \|x\|_X$ (homogeneity)
3. $\|x + y\|_X \leq \|x\|_X + \|y\|_X$ (triangle inequality)

Definition A.3 (Cauchy sequence, completeness, Banach space)
Let $(X, \|\cdot\|_X)$ a normed linear space.

1. A sequence $(x_k)_{k\in\mathbb{N}}$ in X is called *Cauchy sequence*, if $\|x_k - x_l\|_X \to 0$ for $k, l \to \infty$.
2. x is called *limit* of $(x_k)_{k\in\mathbb{N}}$, if $\lim_{k\to\infty} \|x_k - x\|_X = 0$.
3. $(X, \|\cdot\|_X)$ is called *complete* or a *Banach space*, if every Cauchy sequence in X has a limit in X.

Definition A.4 ((Pre-) Hilbert space)

1. Let X a $\mathbb{K}$-vector space. A mapping $(\cdot, \cdot) : X \times X \to \mathbb{K}$ is called *Hermitian sesqui-linear form*, if
   a) $(x, y) = \overline{(y, x)} \;\forall x, y \in X$ (Hermitian)
   b) $(\alpha x, y) = \alpha \, (x, y) \;\forall x, y \in X,\; \alpha \in \mathbb{K}$
   c) $(x, y_1 + y_2) = (x, y_1) + (x, y_2) \;\forall x, y_1, y_2 \in X$
2. The sesqui-linear form is called *positive semi-definite*, if $(x, x) \geq 0 \;\forall x \in X$, and *positive definite*, if $(x, x) \geq 0$ and $(x, x) = 0 \;\Leftrightarrow x = 0$. A positive definite sesqui-linear form is called *inner product*.
3. The pair $(X, (\cdot, \cdot)$ is called pre-Hilbert space, provided $(\cdot, \cdot)$ is an inner product.
4. If X is complete with respect to the induced norm $\|\cdot\|_X := \sqrt{(\cdot, \cdot)}$, X is called *Hilbert space*.

A.3.2. Function spaces

Definition A.5
Boundary regularity Let $U \subset \mathbb{R}^n$ be open and bounded, $k \in \{1, 2, \ldots\}$. We say the boundary ∂U is C^k if for each point $x^0 \in \partial U$ there exist $r > 0$ and a C^k function $\gamma : \mathbb{R}^{n-1} \to \mathbb{R}^n$ such that – upon relabeling and reorienting the coordinate axes if necessary – we have

$$U \cap B\left(x^0, r\right) = \left\{x \in B\left(x^0, r\right) : \quad x_n > \gamma\left(x_1, \ldots, x_n\right)\right\}.$$

Likewise, ∂U is C^∞ if ∂U is C^k for $k = 1, 2, \ldots$, and ∂U is *analytic* if the mapping γ is analytic.

Unless nothing else is stated, let $\Omega \subset \mathbb{R}^n$ be an open, bounded and simply connected domain with boundary $\partial\Omega$ in C^1. For the definition of C^k, see Section A.3.2.1.

A.3.2.1. Spaces of continuous functions

Let $k \in \mathbb{N} \cup \{0, \infty\}$. Then

$$C^k(\Omega) := \{u : \Omega \to \mathbb{R} : \ u \text{ is } k\text{-times continuously differentiable}\}.$$

For $k = 0$, $C(\Omega) := C^0(\Omega)$ is the space of continuous functions on Ω.

In order to have smoothness near the boundary $\partial\Omega$, for $k \in \mathbb{N} \cup \{0, \infty\}$ it is defined

$$C_0^k(\Omega) := \left\{u \in C^k(\Omega) : \quad u \text{ has } \textit{compact support} \text{ in } \Omega\right\}.$$

For dealing with functions, which depend on several variables, which can be separated into variables with respect to time and space, let $p, q \in \mathbb{N} \cup \{\infty\}$ and $a, b \in \mathbb{R} \cup \{-\infty, \infty\}$ with $a \leq b$. Then

$$\begin{aligned} C^p\left((a,b)\,; C^q\left(\Omega\right)\right) := \{u(x,t) : u(\cdot,t) \in C^q(\Omega) \ \forall t \in (a,b), \\ u(x,\cdot) \in C^p((a,b)) \ \forall x \in \Omega\}. \end{aligned}$$

Furthermore, let V be a separable Banach space, then, for $m \in \mathbb{N}$, $C^m([a,b]; V)$ denotes the space of continuous functions defined on $[a,b]$, whose m-th derivative is continuous, and

$$C([a,b]; V) := C^0([a,b]; V).$$

$C^m([a,b]; V)$ becomes a Banach space, if it is endowed with the norm

$$\|f\|_{C^m([a,b];V)} := \max_{t\in[a,b]} \sum_{i=0}^{m} \left\|f^i(t)\right\|_V.$$

A.3.2.2. Lebesgue spaces

Let $1 \leq p < \infty$. The space $L^p(\Omega)$ consists of all real valued function, for which the p-th power is measurable with respect to the Lebesgue measure $\mathrm{d}x := \mathrm{d}x_1 \cdots \mathrm{d}x_n$,

$$L^p(\Omega) := \left\{u : \Omega \to \mathbb{R} : \quad \int_\Omega |u(x)|^p \,\mathrm{d}x < \infty\right\}.$$

Together with the mapping $\|\cdot\|_{L^p(\Omega)} : L^p(\Omega) \to \mathbb{R}$, which is defined as

$$\|u\|_{L^p(\Omega)} := \left(\int_\Omega |u(x)|^p \,\mathrm{d}x\right)^{\frac{1}{p}}$$

and is in fact a norm, the pair $\left(L^p(\Omega), \|\cdot\|_{L^p(\Omega)}\right)$ is a normed space. With the definition

$$\|u\|_{L^\infty(\Omega)} := \operatorname{ess\,sup}_{x\in\Omega} |u(x)|,$$

the definition of $L^p(\Omega)$ can be extended to $p = \infty$ with

$$L^\infty(\Omega) := \{u : \Omega \to \mathbb{R} : \quad \operatorname{ess\,sup}_{x\in\Omega} |u(x)| < \infty\}.$$

For $p = 2$, the space $L^2(\Omega)$ is a Hilbert space endowed with the inner product

$$(u, v)_{L^2(\Omega)} := \int_\Omega u(x)v(x)\mathrm{d}x, \quad u, v \in L^2(\Omega).$$

The dual space of $L^p(\Omega)$ is denoted by

$$(L^p(\Omega))^* := \left\{ f : L^p(\Omega) \to \mathbb{R} : \ f \text{ is linear}, \ \|f\|_{(L^p(\Omega))^*} := \sup_{u \in L^p(\Omega)} \frac{\langle f, u \rangle}{\|u\|_{L^p(\Omega)}} < \infty \right\}.$$

For $1 < p < \infty$, it can be identified with $L^q(\Omega)$, where

$$\frac{1}{p} + \frac{1}{q} = 1.$$

The dual pairing between $L^p(\Omega)$ and its dual space $(L^p(\Omega))^*$ is denoted by

$$\langle f, u \rangle_{(L^p(\Omega))^*, L^p(\Omega)} := f(u).$$

For arbitrary $1 \leq q \leq p \leq \infty$ it holds that

$$L^q(\Omega) \hookrightarrow L^p(\Omega).$$

Furthermore, one defines

$$L^p_{loc}(\Omega) = \{ u : \Omega \to \mathbb{R} : \quad u \in L^p(V), \ V \subset\subset \Omega \},$$

i.e., V is a compact subset of Ω.

Let V a separable Banach space, $a, b \in \mathbb{R} \cup \{-\infty, \infty\}$ with $a \leq b$ and $p \in \mathbb{N}$. $L^p(a, b; V)$ denotes the space of equivalence classes of Bochner integrable functions $u : [a, b] \to V$, i.e.,

$$L^p(a, b; V) := \left\{ u(t) : \ u(\cdot) \in V, \quad \left(\int_a^b \|u(t)\|_V^p \, \mathrm{d}t \right)^{\frac{1}{p}} < \infty \right\}.$$

For $p = \infty$, we have

$$L^\infty(a, b; V) := \left\{ u(t) : \ u(\cdot) \in V, \quad \operatorname{ess\,sup}_{t \in (a,b)} \|u(t)\|_V < \infty \right\}.$$

$L^p(a, b; V)$ is also a Banach space and for $1 < p, q < \infty$ with $\frac{1}{p} + \frac{1}{q} = 1$ the dual space $(L^p(a, b; V))^*$ can be identified with $L^q(a, b; V^*)$, where the dual pairing is given by

$$\langle f, u \rangle_{L^q(a,b;V^*), L^p(a,b;V)} = \int_a^b \langle f(t), u(t) \rangle_{V^*, V} \, \mathrm{d}t.$$

Again, it holds $L^q(a, b; V) \hookrightarrow L^p(a, b; V)$ for arbitrary $1 \leq q \leq p \leq \infty$.

The time derivative $\partial_t u$ of an abstract function $u \in L^2(a, b; V)$ is defined in the sense of distributions: A function $v : [a, b] \to V$, which fulfils

$$\int_a^b u(t) \varphi'(t) \mathrm{d}t = - \int_a^b v(t) \varphi(t) \mathrm{d}t$$

for all test functions $\varphi \in C_0^\infty(a, b)$, is called the (distributional) derivative of u and is denoted by

$$\partial_t u := v.$$

A.3.2.3. Sobolev spaces

If one transfers the above concept of distributional derivatives to the space variables, then the well-known Sobolev spaces are obtained

Weak derivatives

Definition A.6 (Weak derivative)
Suppose $\Omega \subset \mathbb{R}^n$ is open, $u, v \in L^1_{loc}(\Omega)$ and α is a multiindex. We say that v is the α^{th}-*weak partial derivative of* u, written

$$D^\alpha u = v,$$

provided

$$\int_\Omega u D^\alpha \varphi \mathrm{d}x = (-1)^{|\alpha|} \int_\Omega v \varphi \mathrm{d}x$$

for all test functions $\varphi \in C_0^\infty(\Omega)$.

Lemma A.7 (Uniqueness of weak derivatives)
A weak α^{th}*-partial derivative of* u*, if it exists, is uniquely defined up to a set of measure zero.*

Definition of Sobolev spaces and elementary properties

Definition A.8 (Sobolev space)
The Sobolev space $W^{k,p}(\Omega)$ consists of all locally summable functions $u : \Omega \to \mathbb{R}$ such that for each multiindex α with $|\alpha| \leq k$, $D^\alpha u$ exists in the weak sense and belongs to $L^p(\Omega)$.

Remark A.9

1. If $p = 2$, we usually write

   $$H^k(\Omega) = W^{k,2}(\Omega) \quad (k = 0, 1, \ldots).$$

   The letter H is used, since (as we will see) $H^k(\Omega)$ is a Hilbert Space. Note that $H^0(\Omega) = L^2(\Omega)$.

2. We henceforth identify functions in $W^{k,p}(\Omega)$ which agree a.e. (= almost everywhere, i.e., up to a set of measure zero), i.e., the elements of $W^{k,p}$ are equivalence classes.

Definition A.10 (Sobolev norm)
If $u \in W^{k,p}(\Omega)$, we define its *norm* to be

$$\|u\|_{W^{k,p}(\Omega)} := \begin{cases} \left(\sum_{|\alpha|\leq k} \int_\Omega |D^\alpha u|^p \,\mathrm{d}x\right)^{\frac{1}{p}} & (1 \leq p < \infty) \\ \sum_{|\alpha|\leq k} \operatorname{ess\,sup}_\Omega |D^\alpha u| & (p = \infty) \end{cases}$$

It is easily verified, that $\|\cdot\|_{W^{k,p}(\Omega)}$ is indeed a norm.

Theorem A.11 (Sobolev spaces as function spaces)
For each $k = 1, 2, 3, \ldots$ *and* $1 \leq p \leq \infty$*, the Sobolev space* $W^{k,p}(\Omega)$ *is a Banach space.*

Theorem A.12 (Sobolev spaces as Hilbert spaces)
For each $k = 1, 2, 3, \ldots$ *the Sobolev space* $H^k(\Omega)$ *is a Hilbert space endowed with the inner product*

$$(u, v)_{H^k(\Omega)} := \sum_{|\alpha|\leq k} \int_\Omega (D^\alpha u)(D^\alpha v) \mathrm{d}x \quad \forall u, v \in H^k(\Omega).$$

Approximation by smooth functions

Theorem A.13 (Global approximation by smooth functions)
Assume Ω is bounded, and suppose as well that $u \in W^{k,p}(\Omega)$ for some $1 \leq p < \infty$. Then there exist functions $u_m \in C^\infty(\Omega) \cap W^{k,p}(\Omega)$ such that

$$u_m \to u \quad \text{in } W^{k,p}(\Omega).$$

Theorem A.14 (Global approximation by smooth functions up to the boundary)
Assume Ω is bounded and $\partial\Omega$ is C^1, and suppose as well that $u \in W^{k,p}(\Omega)$ for some $1 \leq p < \infty$. Then there exist functions $u_m \in C^\infty(\overline{\Omega})$ such that

$$u_m \to u \quad \text{in } W^{k,p}(\Omega).$$

Traces

Theorem A.15 (Trace Theorem)
Assume Ω is bounded and $\partial\Omega$ is C^1, as well as $1 \leq p < \infty$. Then there exists a bounded linear operator

$$T : W^{1,p}(\Omega) \to L^p(\partial\Omega)$$

such that

1. *$Tu = u_{|\partial\Omega}$ if $u \in W^{1,p}(\Omega) \cap C(\overline{\Omega})$ and*
2. *$$\|Tu\|_{L^p(\partial\Omega)} \leq C \|u\|_{W^{1,p}(\Omega)}$$*

for each $u \in W^{1,p}(\Omega)$, with the constant C depending only on p and Ω.

Definition A.16 (Trace)
We call Tu the *trace* of u on $\partial\Omega$.

Theorem A.17 (Trace-zero functions in $W^{1,p}(\Omega)$)
Assume Ω is bounded and $\partial\Omega$ is C^1. Suppose furthermore that $u \in W^{1,p}(\Omega)$. Then $u \in W_0^{1,p}(\Omega)$ if and only if $Tu = 0$ on $\partial\Omega$.

The space H^{-1}

Definition A.18
The dual space to $H_0^1(\Omega)$ is denoted by $H^{-1}(\Omega)$. $\langle \cdot, \cdot \rangle_{H^{-1}(\Omega), H_0^1(\Omega)}$ denotes the dual pairing between $H^{-1}(\Omega)$ and $H_0^1(\Omega)$.

Definition A.19
If $f \in H^{-1}(\Omega)$, its *norm* is defined as

$$\|f\|_{H^{-1}(\Omega)} := \sup \left\{ \langle f, u \rangle_{H^{-1}(\Omega), H_0^1(\Omega)} : \quad u \in H_0^1(\Omega), \|u\|_{H_0^1(\Omega)} \leq 1 \right\}.$$

Observe, that the space $H_0^1(\Omega)$ is *not* identified with its dual.

Theorem A.20 (Characterisation of H^{-1})

1. *Assume $f \in H^{-1}(\Omega)$. Then there exist functions $f^0, f^1, \ldots, f^n \in L^2(\Omega)$ such that*

$$\langle f, v\rangle = \int_\Omega \left(f^0 v + \sum_{i=1}^{n} f^i \partial_i v \right) \mathrm{d}x \quad \left(v \in H_0^1(\Omega)\right). \tag{A.1}$$

2. *Furthermore,*

$$\|f\|_{H^{-1}(\Omega)} = \inf \left\{ \left(\int_\Omega \sum_{i=0}^{n} \left|f^i\right|^2 \mathrm{d}x \right)^{\frac{1}{2}} : \ f \text{ fulfils (A.1) for } f^0, \ldots, f^n \in L^2(\Omega) \right\}.$$

It follows from A.20The space H^{-1}satz.A.20, that

$$H_0^1(\Omega) \subset L^2(\Omega) \subset H^{-1}(\Omega).$$

A.4. Finite Element theory

Finite Elements are shortly introduced as they are used throughout this thesis. For further details see, e.g., [18].

A.4.1. Triangulation

Let $\Omega \subset \mathbb{R}^3$ be a domain of polygonal shape such that it can be divided in tetrahedrons or hexahedrons.

Definition A.21 (Triangulation)

1. A triangulation $\mathscr{T} = \{T_1, T_2, \ldots, T_M\}$ of Ω in tetrahedrons or hexahedrons, respectively, is called *admissible* if the following properties are fulfilled:
   a) $\overline{\Omega} = \bigcup_{i=1}^{M} T_i$.
   b) If $T_i \cap T_j$ consists of one and only one point, then this point is a vertex of both T_i and T_j.
   c) If $T_i \cap T_j$ consists for $i \neq j$ of more than one point, then $T_i \cap T_j$ is an edge or a facet of both T_i and T_j.
2. We can write $\mathscr{T}_h$ instead of $\mathscr{T}$ if the diameter of each element is at most $2h$.
3. A family of triangulations $\{\mathscr{T}_h\}$ is called *quasi-uniform* if there exists a number $\kappa > 0$ such that every T of $\mathscr{T}_h$ contains a ball of radius ρ_T with

$$\rho_T \geq \frac{h_T}{\kappa},$$

   where h_T is half the diameter of T.
4. A family of triangulations $\{\mathscr{T}_h\}$ is called *uniform* if there exists a number $\kappa > 0$ such that every element T of $\mathscr{T}_h$ contains a ball of radius

$$\rho_T \geq \frac{h}{\kappa}.$$

A.4.2. Finite Element

Definition A.22 (Finite Element)
A Finite Element (FE) is a triple (T, Π, Σ) with the following properties:

1. T is a polyhedron in $\mathbb{R}^d$. (Those parts of the surface ∂T which are located on a hyperplane are called facets.)
2. Π is a subspace of $C(T)$ with finite dimension $\dim \Pi = s$. The functions in Π are called *shape functions*.
3. Σ is a set of s linearly independent functionals on Π. Each $p \in \Pi$ is uniquely determined by the values of the s functionals of Σ.

For the following construction of finite elements the polynomial vector spaces $\mathbb{P}_k, \mathbb{Q}_k \subset \mathbb{R}^d$ are used.

$\mathbb{P}_k$ is the space of polynomials defined in the variables $(x_1, \ldots, x_d)$ with real coefficients, whose overall degree is less or equal to k:

$$\mathbb{P}_k = \left\{ p(x) = \sum_{0 \le i \le k} \alpha_i x^i : \ \alpha_i \in \mathbb{R} \right\}, \qquad \text{if } d = 1.$$

$$\mathbb{P}_k = \left\{ p(x_1, x_2) = \sum_{0 \le i+j \le k} \alpha_{i,j} x_1^i x_2^j : \ \alpha_{i,j} \in \mathbb{R} \right\}, \qquad \text{if } d = 2.$$

$$\mathbb{P}_k = \left\{ p(x_1, x_2, x_3) = \sum_{0 \le i+j+l \le k} \alpha_{i,j,l} x_1^i x_2^j x_3^l : \ \alpha_{i,j,l} \in \mathbb{R} \right\}, \qquad \text{if } d = 3,$$

$$\mathbb{P}_k = \left\{ p(x) = \sum_{|\beta| \le k} \alpha_\beta x^\beta : \ \alpha_\beta \in \mathbb{R}, \ \beta \in \mathbb{N}_0^d, \ x \in \mathbb{R}^d \right\}.$$

It can be shown, that it holds

$$\dim \mathbb{P}_k = \begin{pmatrix} d+k \\ k \end{pmatrix} = \begin{cases} k+1, & d = 1 \\ \frac{1}{2}(k+1)(k+2), & d = 2 \\ \frac{1}{6}(k+1)(k+2)(k+3), & d = 3 \end{cases}.$$

$\mathbb{Q}_k$ is the space of polynomials defined in the variables $(x_1, x_2, \ldots, x_d)$ with real coefficients, whose degree with respect to *one single variable* is less or equal to k:

$$\mathbb{Q}_k = \mathbb{P}_k, \qquad \text{if } d = 1.$$

$$\mathbb{Q}_k = \left\{ p(x_1, x_2) = \sum_{0 \le i,j \le k} \alpha_{i,j} x_1^i x_2^j : \ \alpha_{i,j} \in \mathbb{R} \right\}, \qquad \text{if } d = 2.$$

$$\mathbb{Q}_k = \left\{ p(x_1, x_2, x_3) = \sum_{0 \le i,j,l \le k} \alpha_{i,j,l} x_1^i x_2^j x_3^l : \ \alpha_{i,j,l} \in \mathbb{R} \right\}, \qquad \text{if } d = 3.$$

It can be shown, that it holds

$$\dim(\mathbb{Q}_k) = (k+1)^d.$$

Furthermore, it holds $\mathbb{P}_k \subset \mathbb{Q}_k \subset \mathbb{P}_{kd}$.

A.4.3. Nodal basis

Definition A.23 (Lagrange element)
To a Finite Element space let a set of points be known such that the functions are determined by the values at the points. These functions which differ from 0 at one and only one point of this set of points form a *nodal basis*. Furthermore, we speak in this context of *Lagrange elements*.

In the case of triangles in 2D and tetrahedrons in 3D, the Lagrange finite elements are given by the spaces $\mathbb{P}_k$, whereas in the case of quadrilaterals and hexahedrons they are defined by the spaces $\mathbb{Q}_k$.

A.5. Further figures on cyclone tracking

In this section, additional figures on the tracking of the cyclones in the cyclone-cyclone interaction scenario are given which are not part of the main text for the sake of clarity of the presentation. Figures A.1 to A.29 show the comparisons of the cyclone tracks at those vertical grid levels that have not been shown in Subsection 6.2.2.

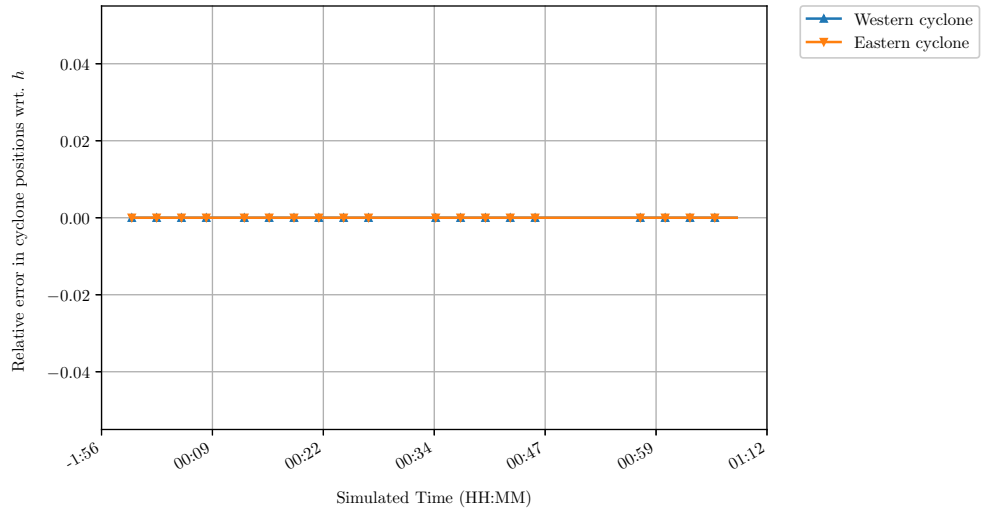

(a) Error in position

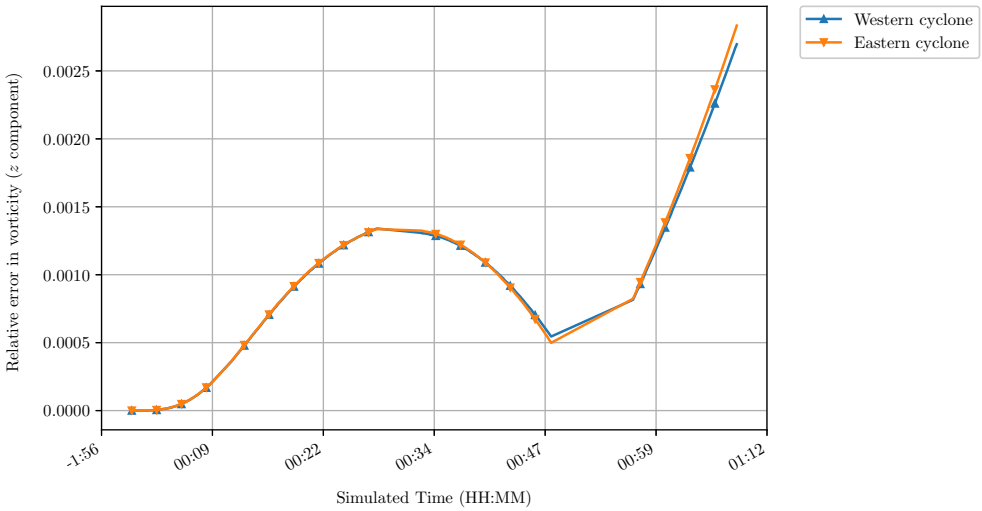

(b) Error in vorticity

Figure A.1.: Relative error in cyclone positions and corresponding vorticities at $z = 406.25\ m$.

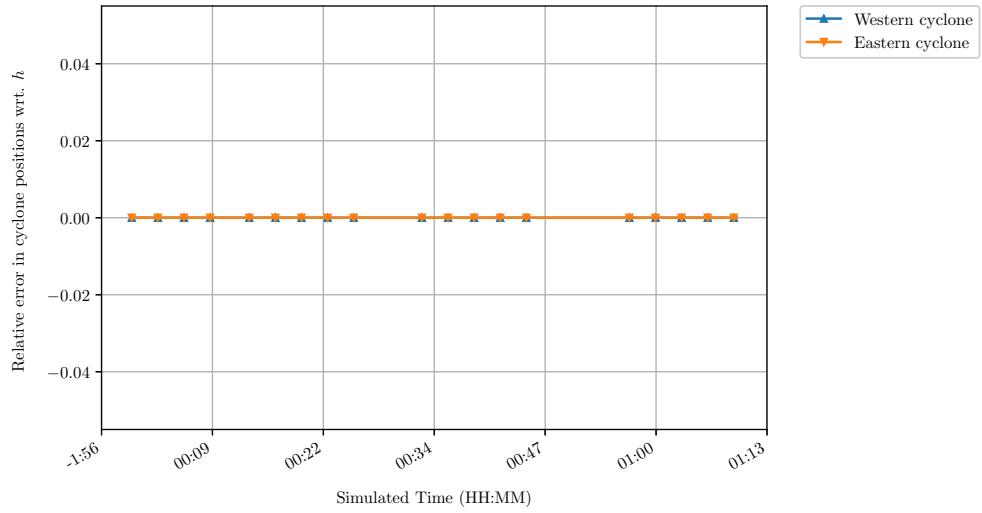

(a) Error in position

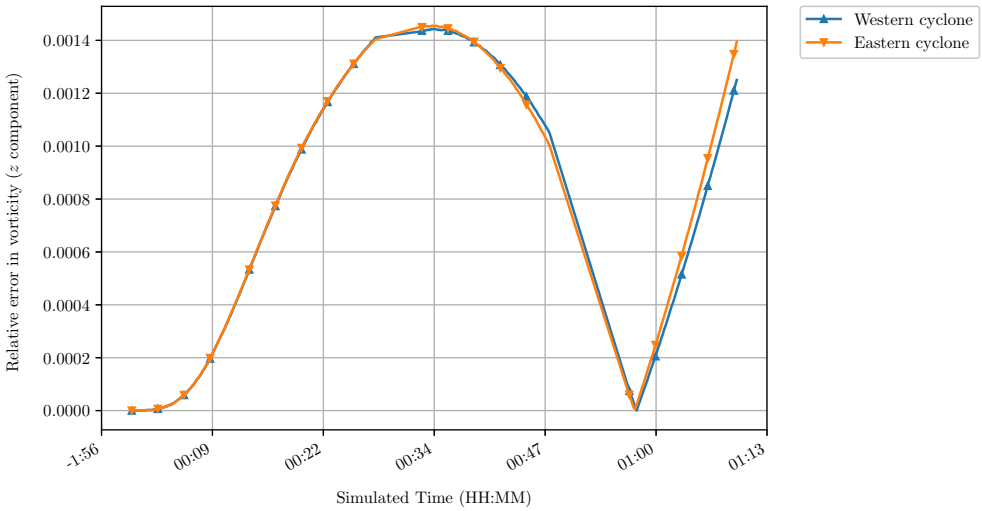

(b) Error in vorticity

Figure A.2.: Relative error in cyclone positions and corresponding vorticities at $z = 812.5\ m$.

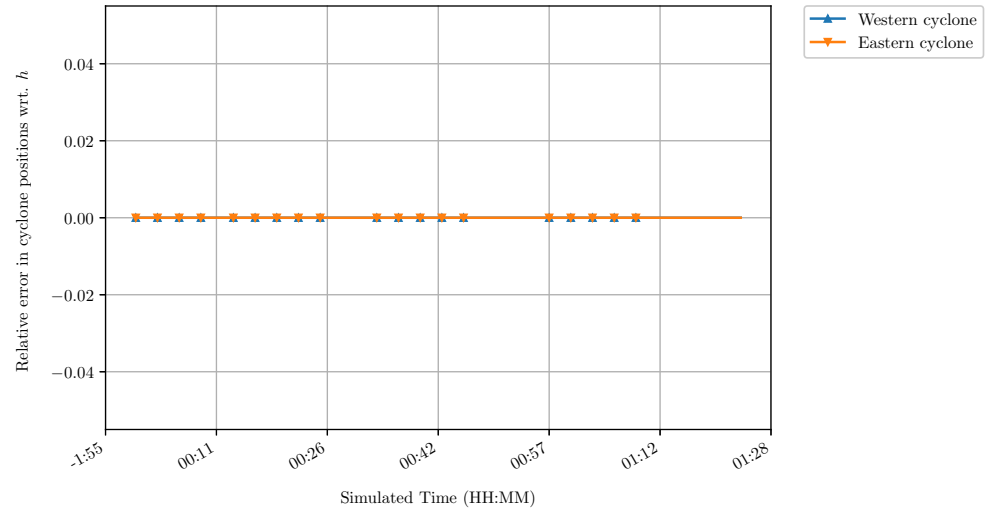

(a) Error in position

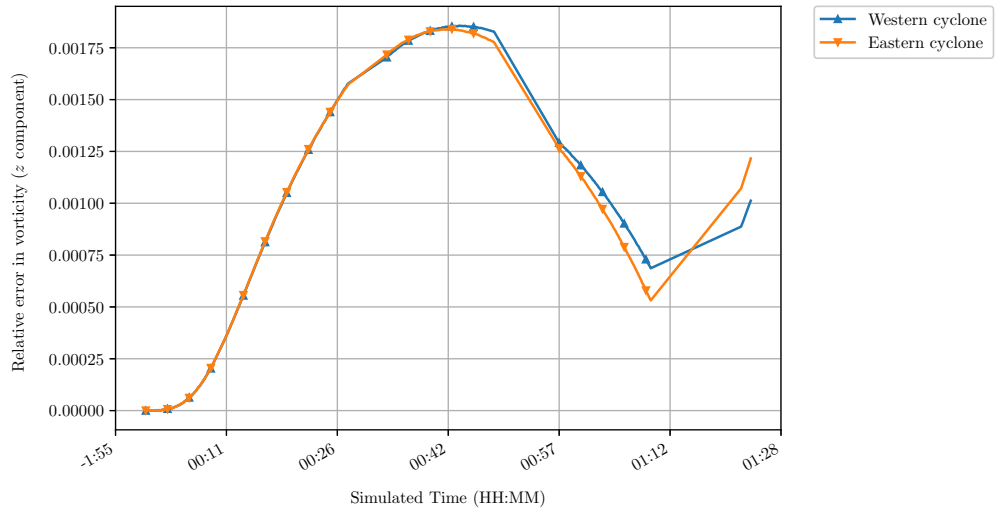

(b) Error in vorticity

Figure A.3.: Relative error in cyclone positions and corresponding vorticities at $z = 1218.75\ m$.

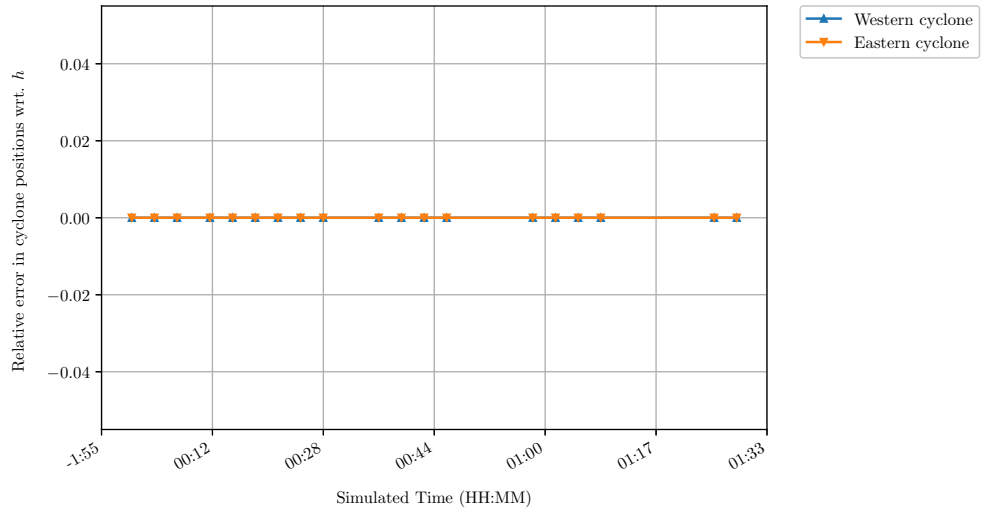

(a) Error in position

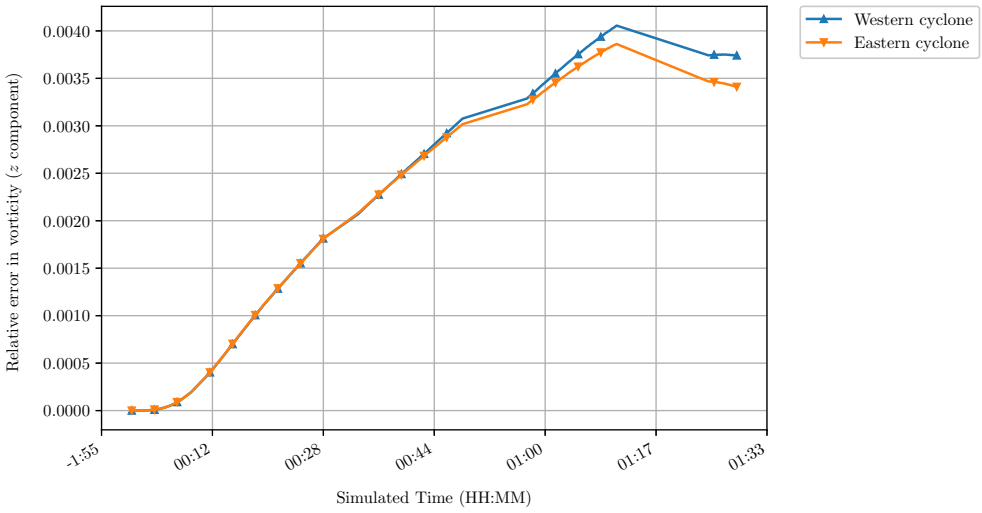

(b) Error in vorticity

Figure A.4.: Relative error in cyclone positions and corresponding vorticities at $z = 2031.25\ m$.

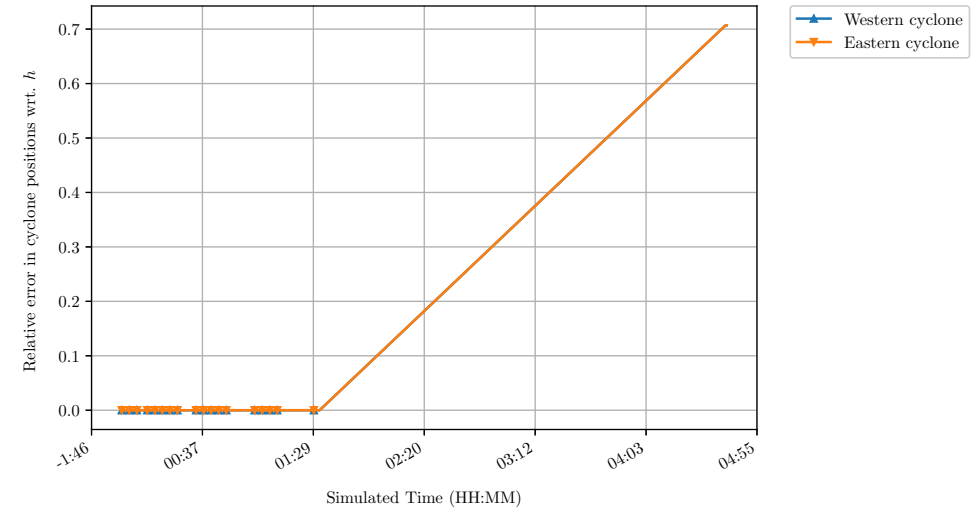

(a) Error in position

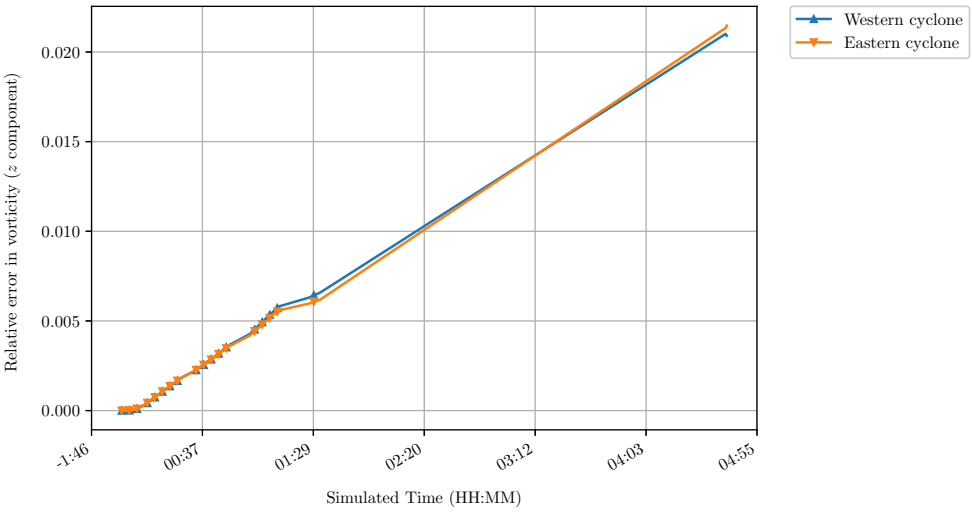

(b) Error in vorticity

Figure A.5.: Relative error in cyclone positions and corresponding vorticities at $z = 2437.55\ m$.

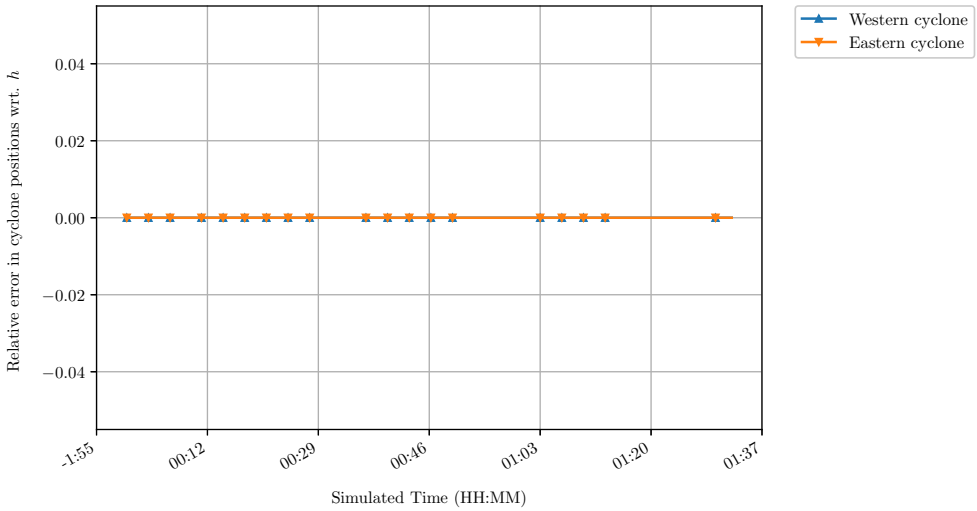

(a) Error in position

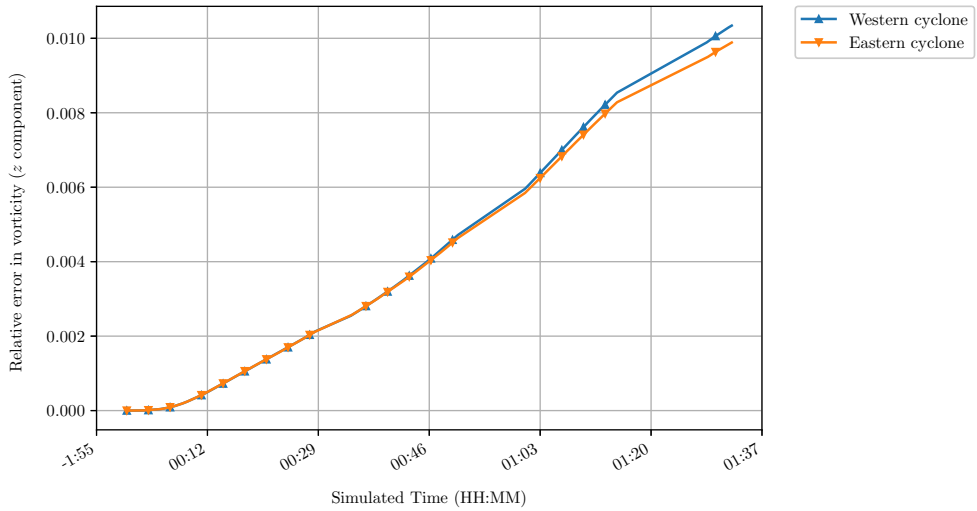

(b) Error in vorticity

Figure A.6.: Relative error in cyclone positions and corresponding vorticities at $z = 2843.75\ m$.

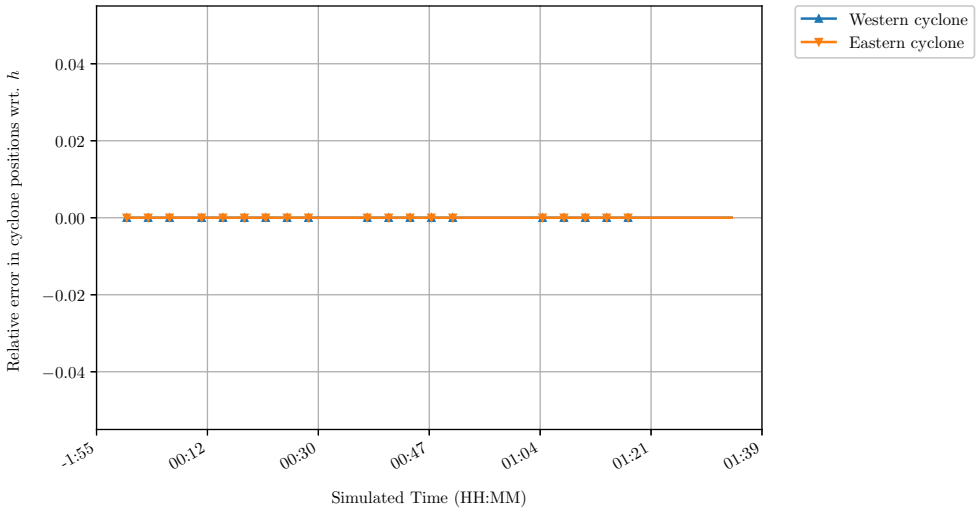

(a) Error in position

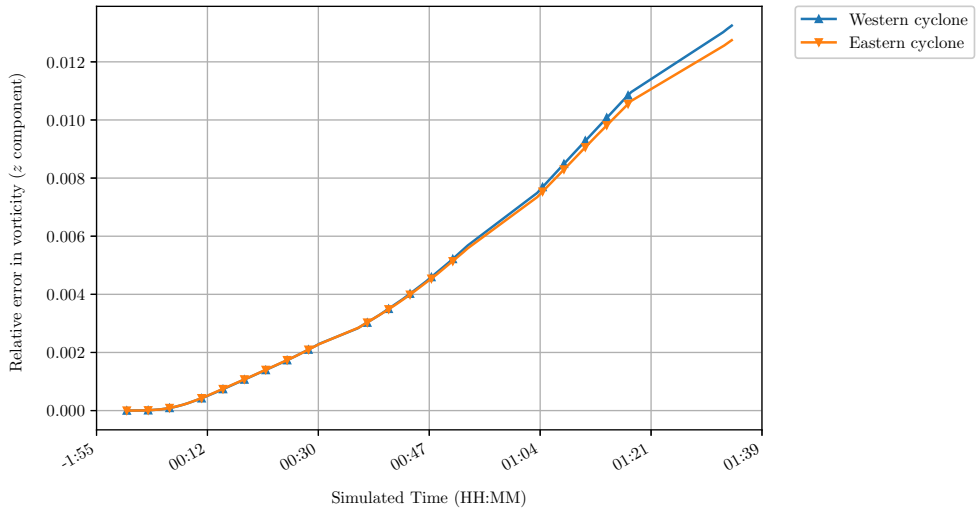

(b) Error in vorticity

Figure A.7.: Relative error in cyclone positions and corresponding vorticities at $z = 3250\ m$.

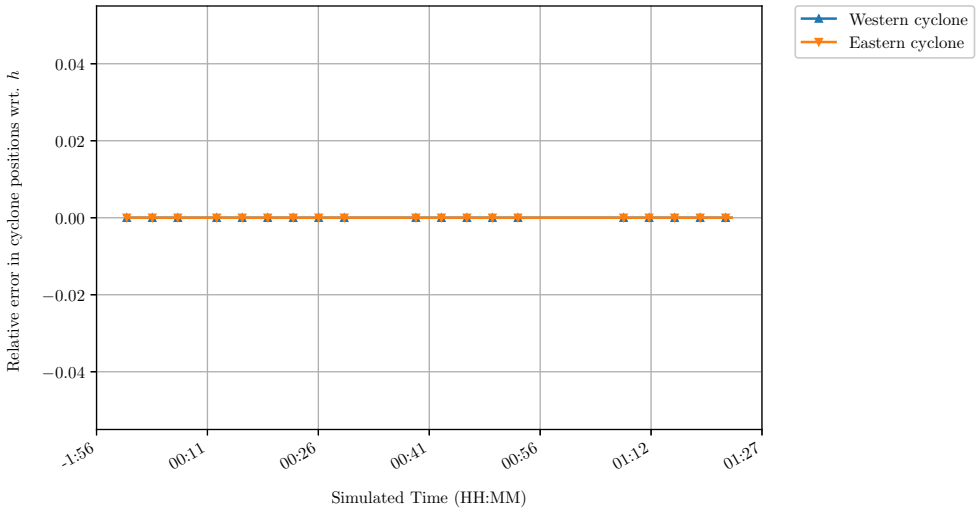

(a) Error in position

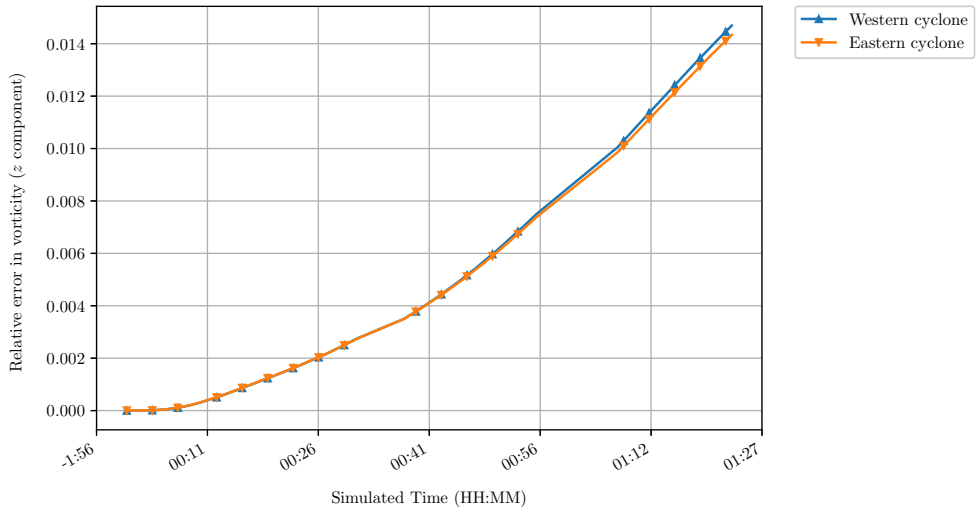

(b) Error in vorticity

Figure A.8.: Relative error in cyclone positions and corresponding vorticities at $z = 3656.25\ m$.

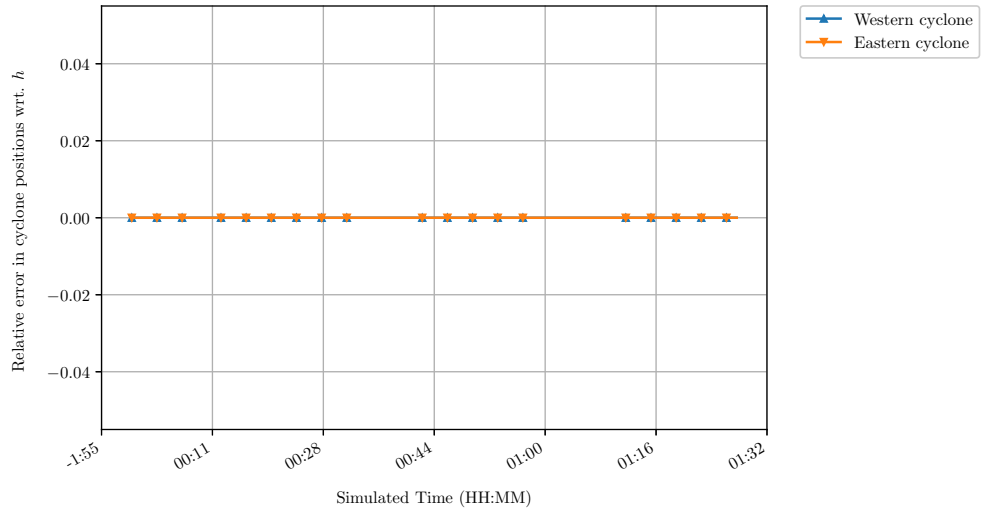

(a) Error in position

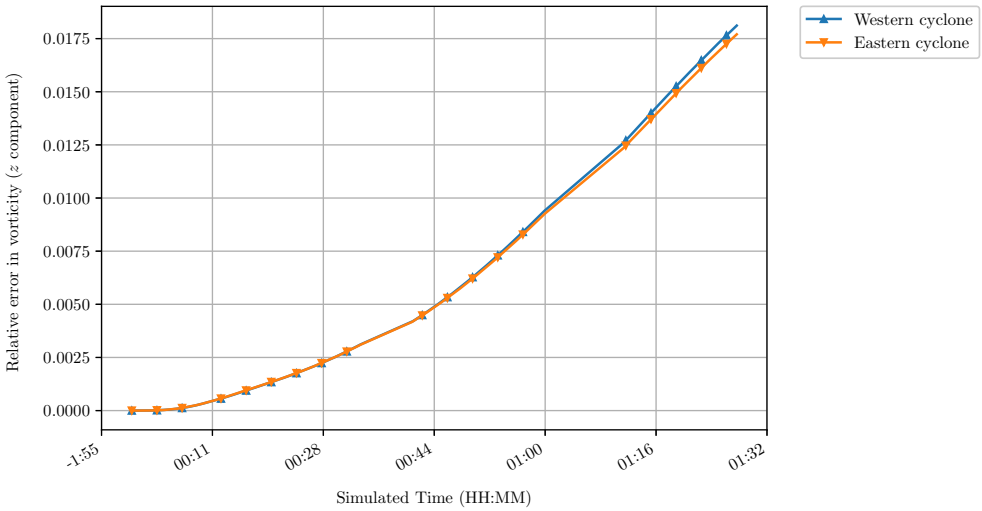

(b) Error in vorticity

Figure A.9.: Relative error in cyclone positions and corresponding vorticities at $z = 4062.5\ m$.

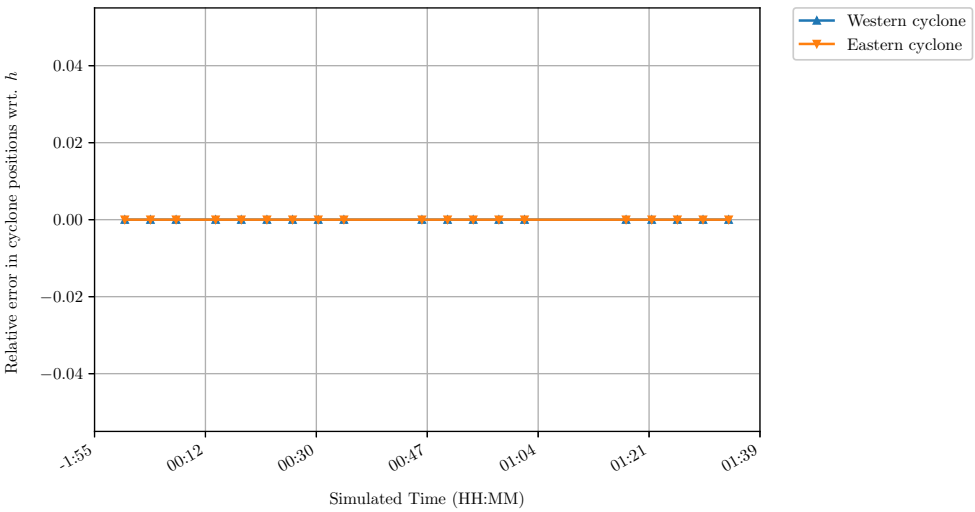

(a) Error in position

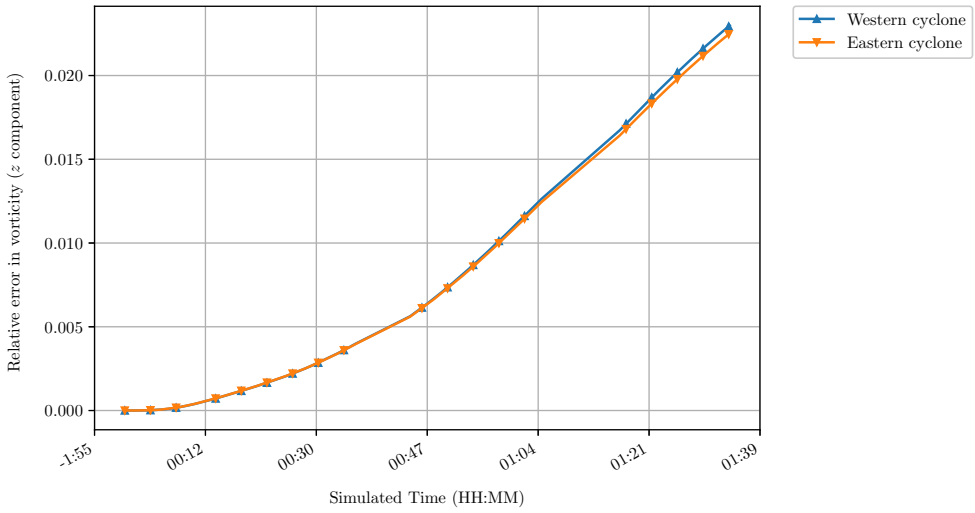

(b) Error in vorticity

Figure A.10.: Relative error in cyclone positions and corresponding vorticities at $z = 4468.75\ m$.

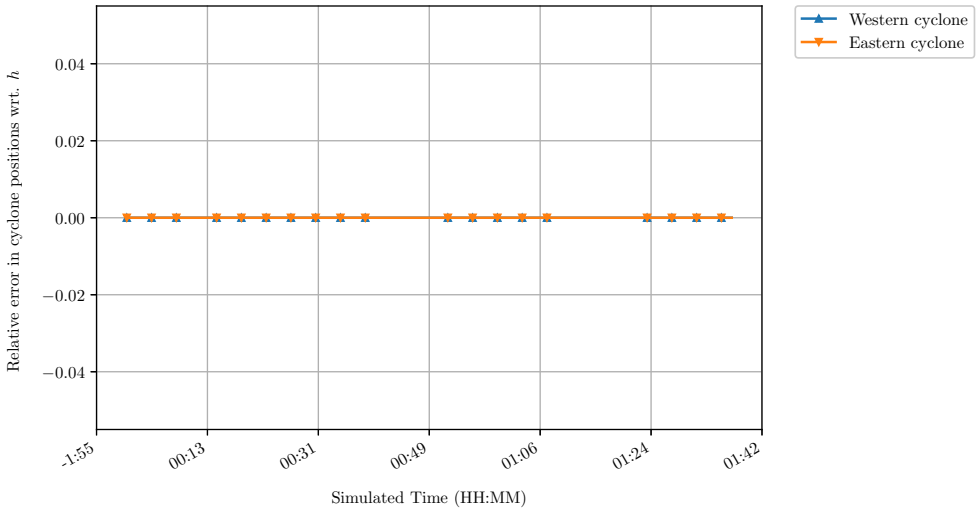

(a) Error in position

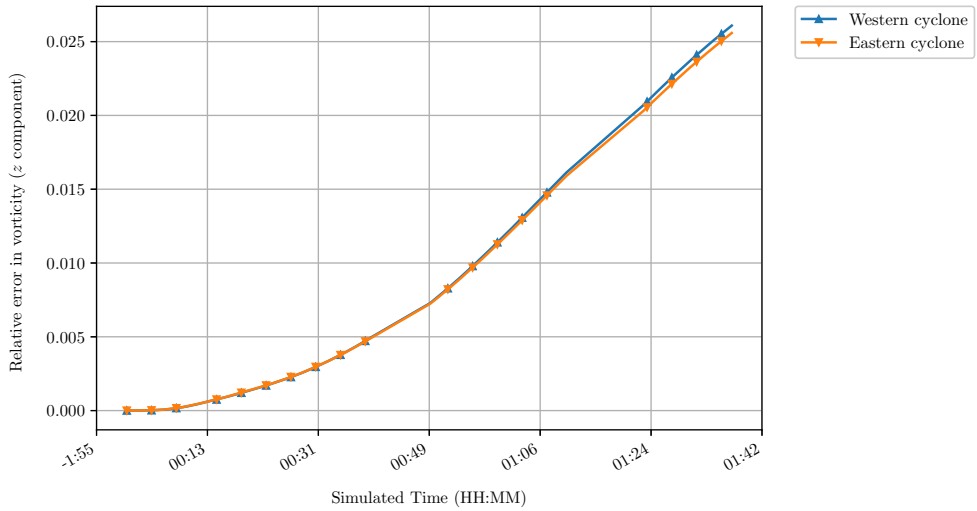

(b) Error in vorticity

Figure A.11.: Relative error in cyclone positions and corresponding vorticities at $z = 4875\ m$.

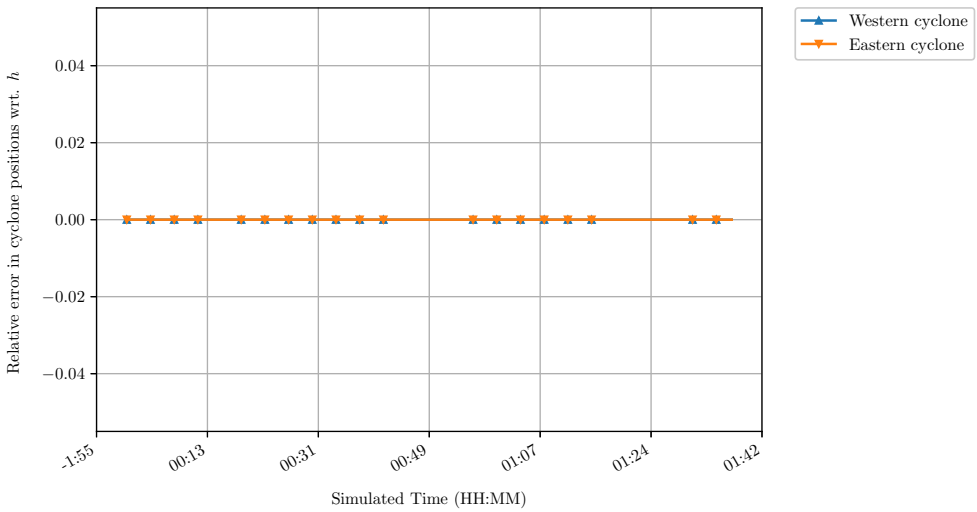

(a) Error in position

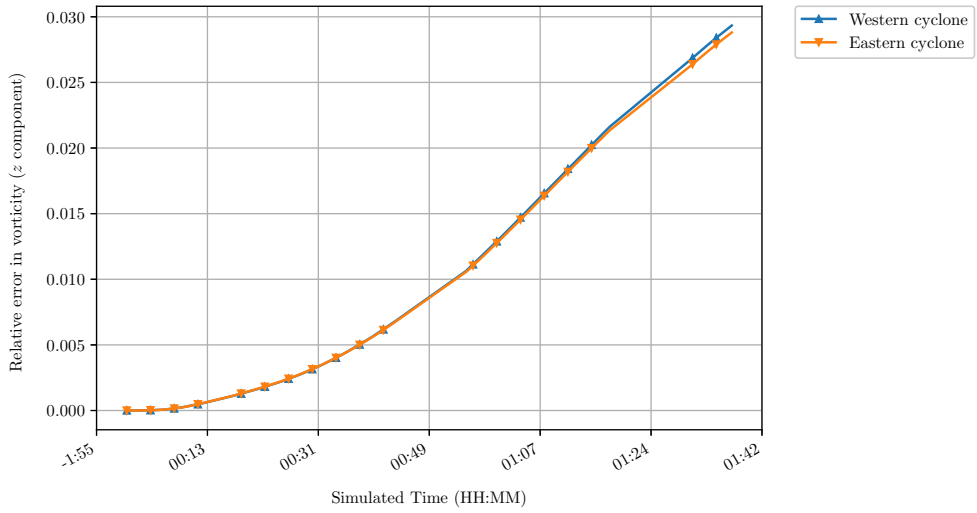

(b) Error in vorticity

Figure A.12.: Relative error in cyclone positions and corresponding vorticities at $z = 5281.25\ m$.

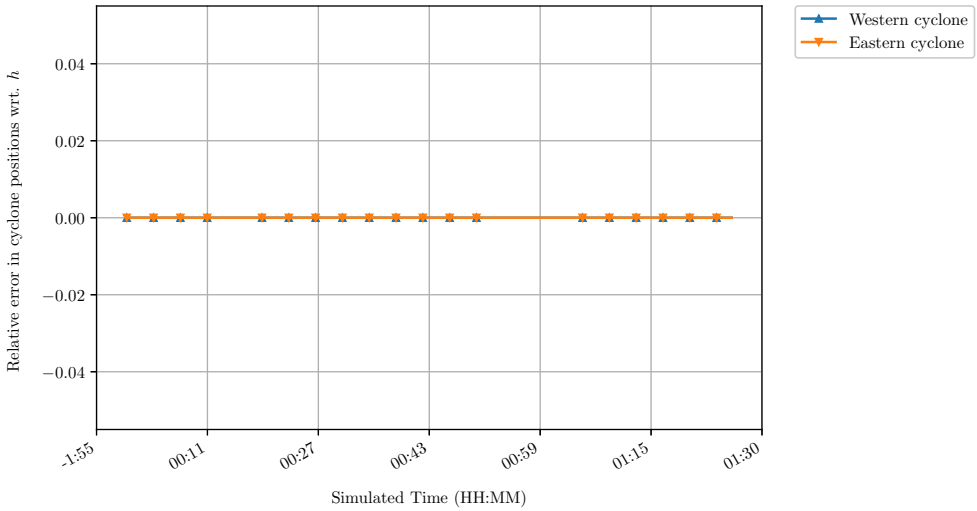

(a) Error in position

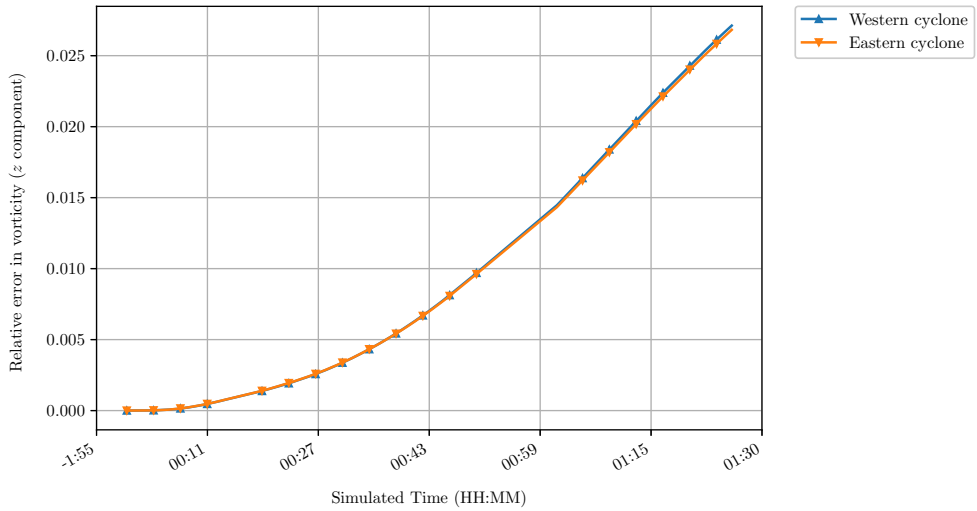

(b) Error in vorticity

Figure A.13.: Relative error in cyclone positions and corresponding vorticities at $z = 5687.5\ m$.

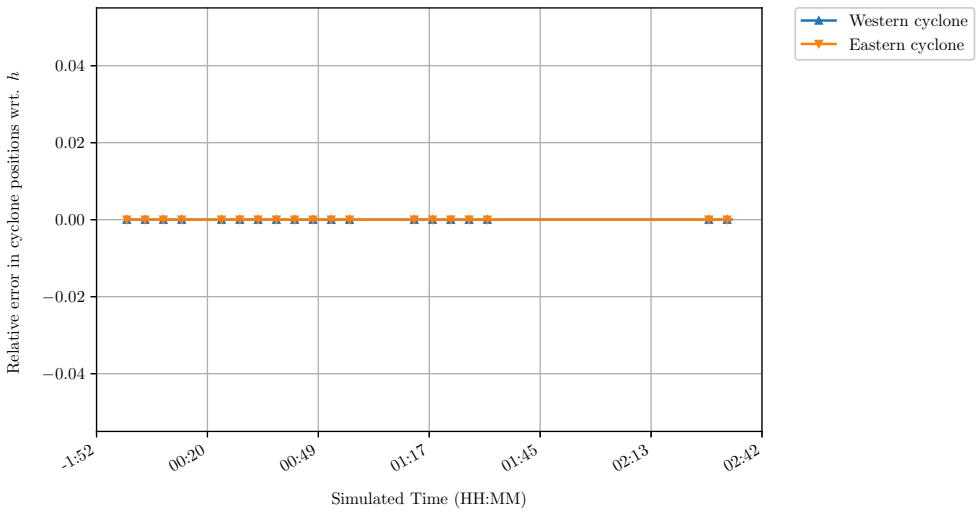

(a) Error in position

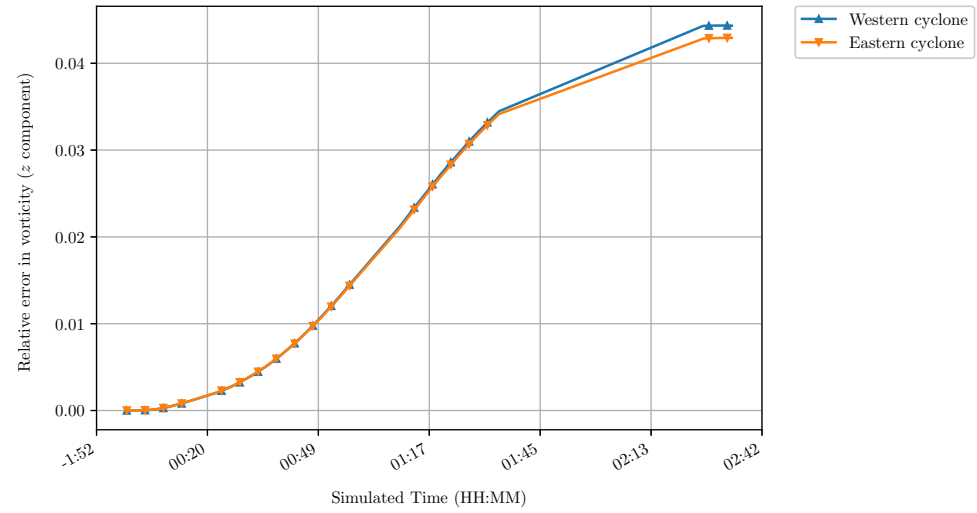

(b) Error in vorticity

Figure A.14.: Relative error in cyclone positions and corresponding vorticities at $z = 6093.75\ m$.

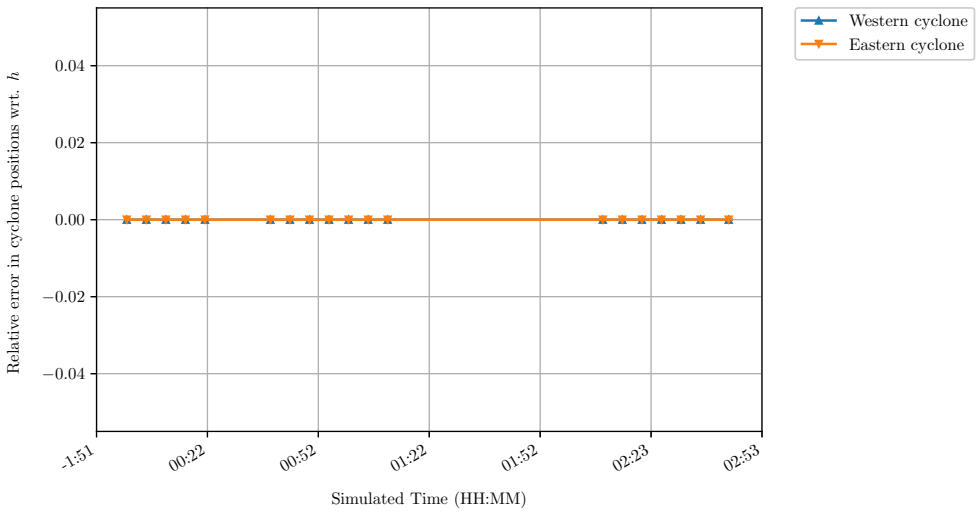

(a) Error in position

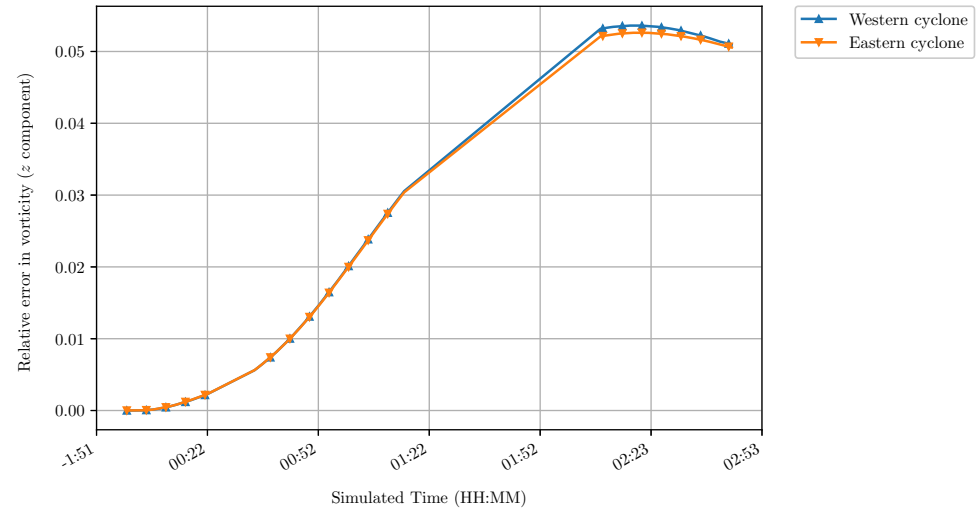

(b) Error in vorticity

Figure A.15.: Relative error in cyclone positions and corresponding vorticities at $z = 6906.25\ m$.

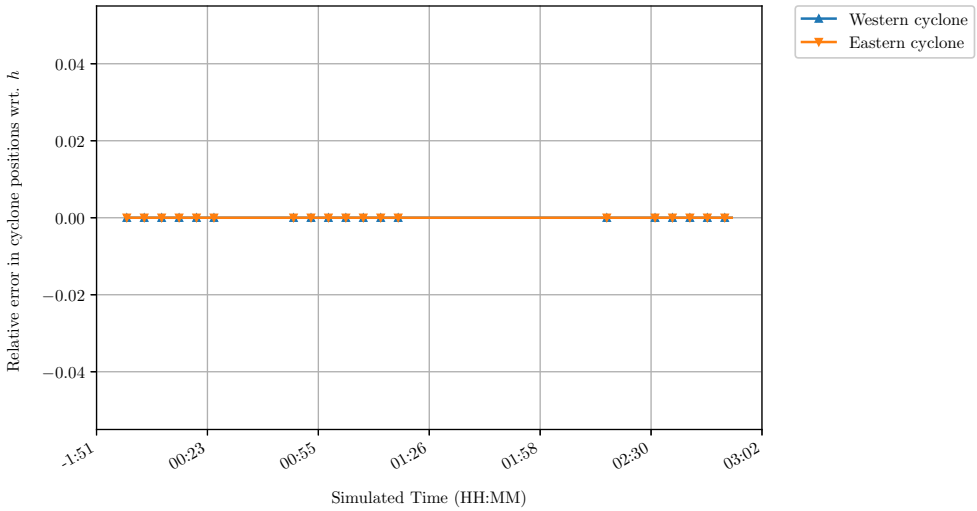

(a) Error in position

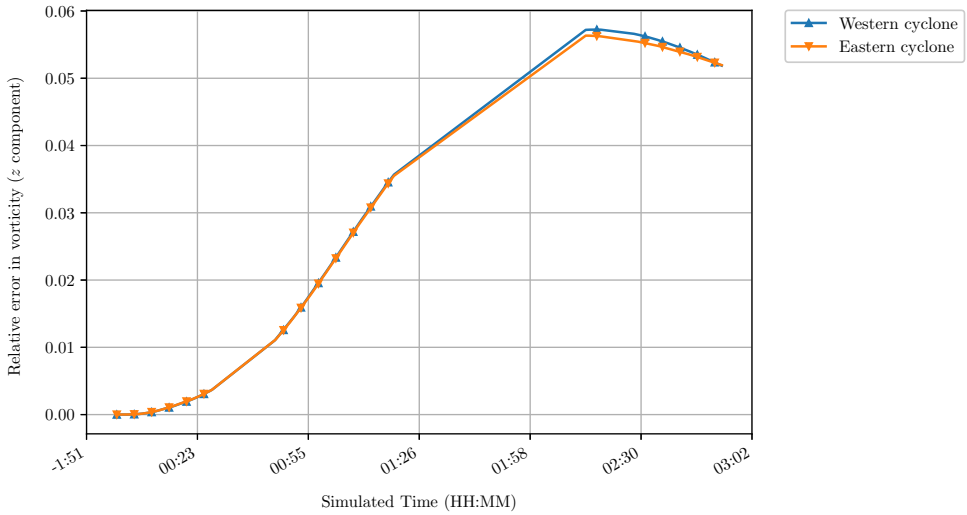

(b) Error in vorticity

Figure A.16.: Relative error in cyclone positions and corresponding vorticities at $z = 7312.5\ m$.

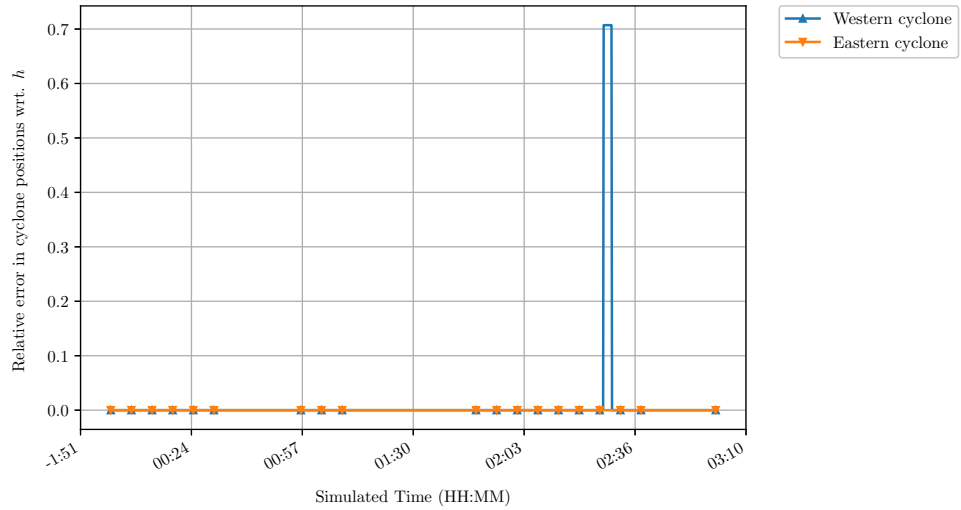

(a) Error in position

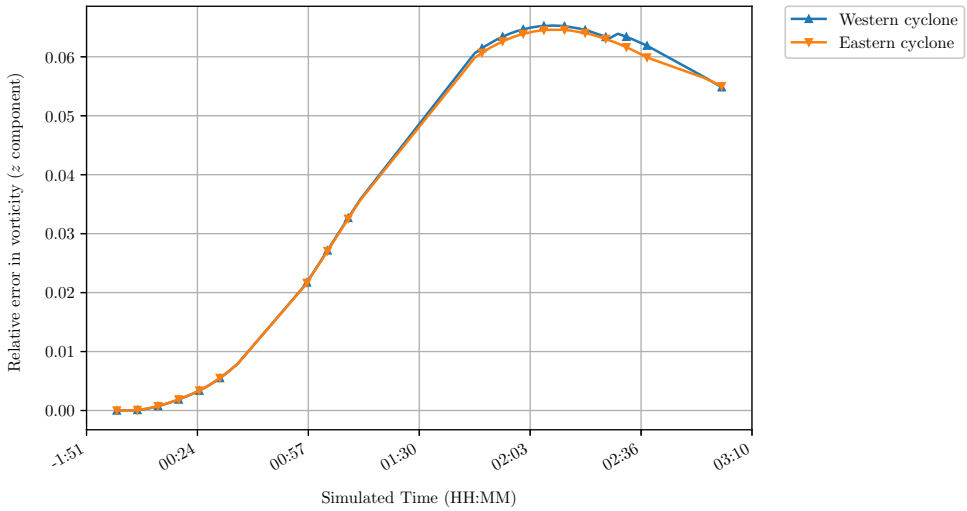

(b) Error in vorticity

Figure A.17.: Relative error in cyclone positions and corresponding vorticities at $z = 7718.75\ m$.

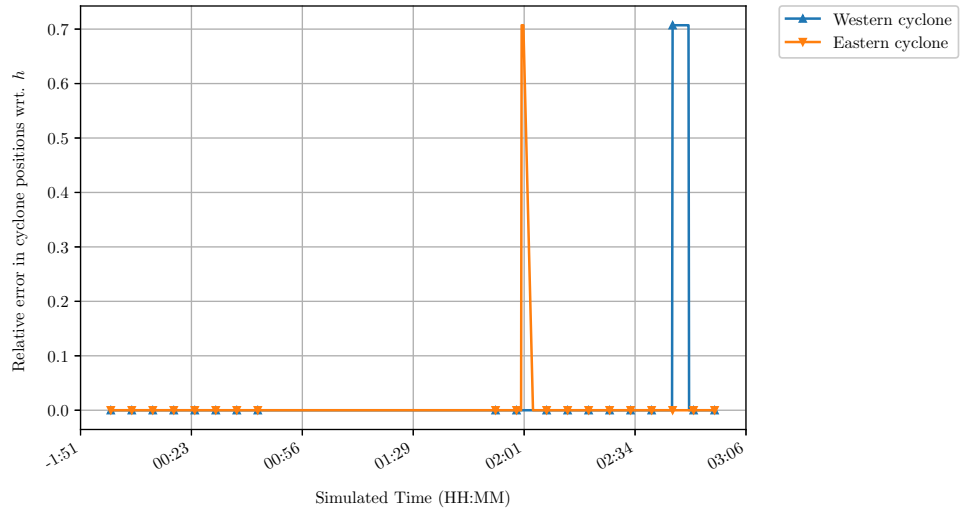

(a) Error in position

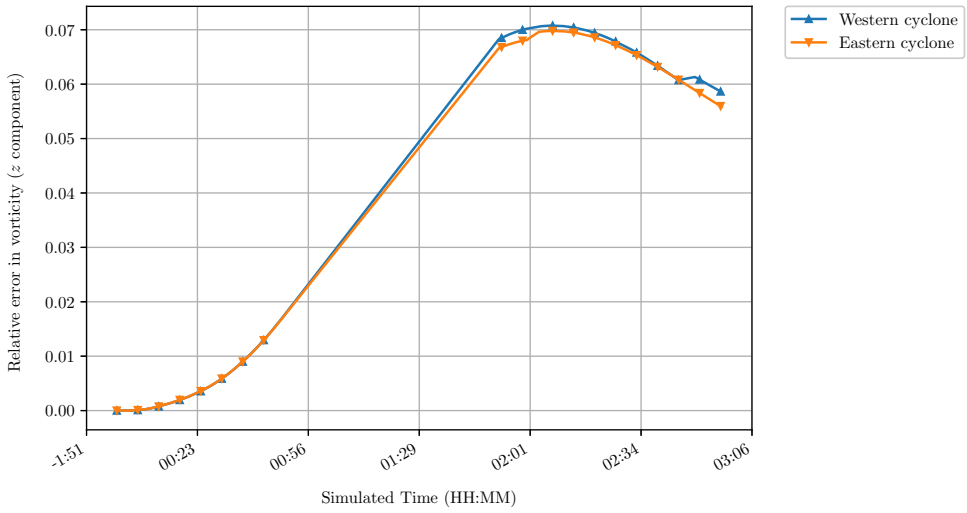

(b) Error in vorticity

Figure A.18.: Relative error in cyclone positions and corresponding vorticities at $z = 8125\ m$.

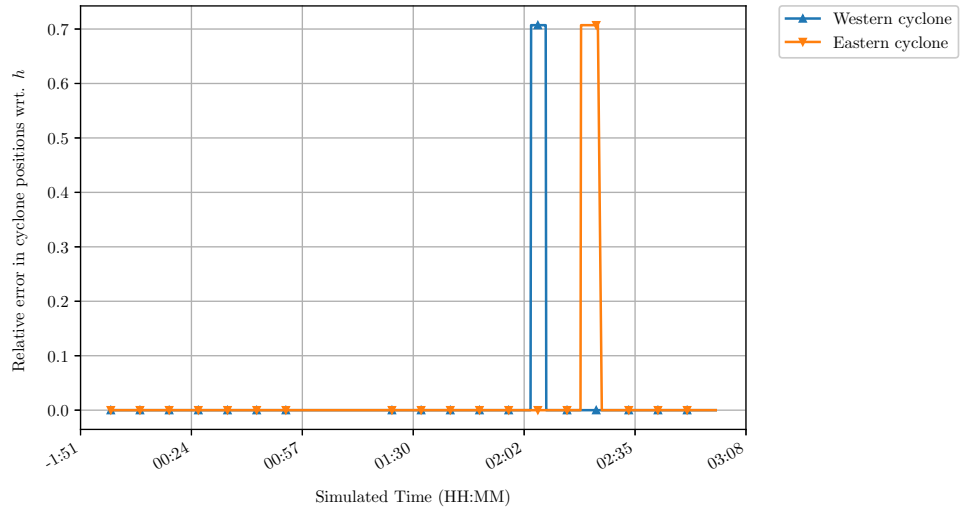

(a) Error in position

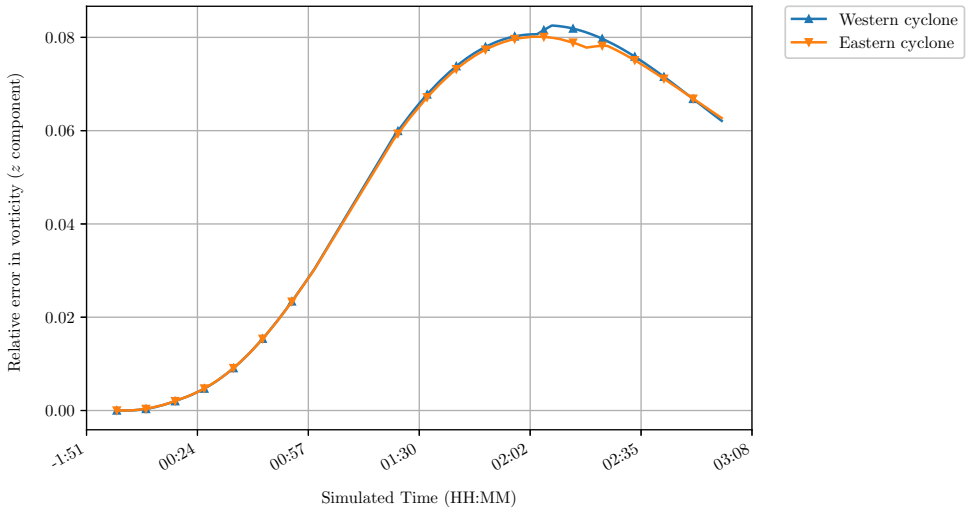

(b) Error in vorticity

Figure A.19.: Relative error in cyclone positions and corresponding vorticities at $z = 8531.25\ m$.

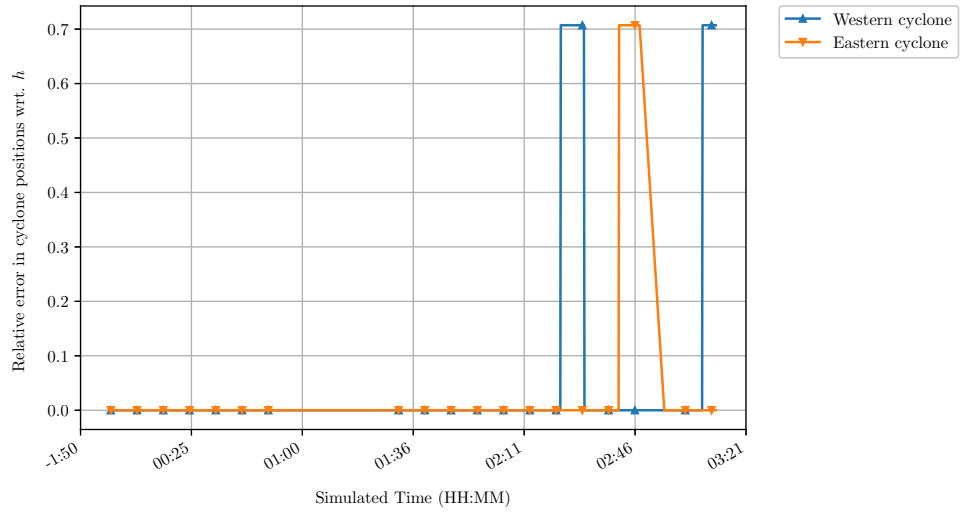

(a) Error in position

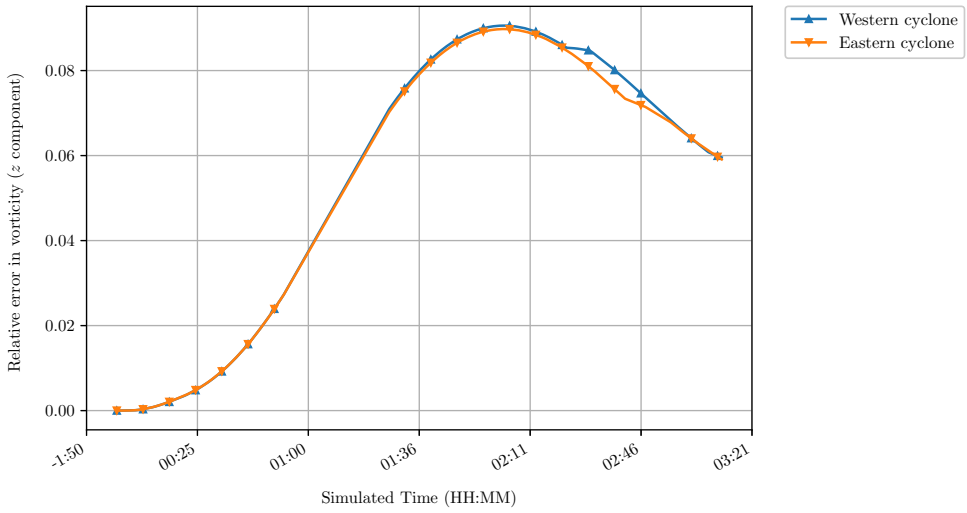

(b) Error in vorticity

Figure A.20.: Relative error in cyclone positions and corresponding vorticities at $z = 8937.5\ m$.

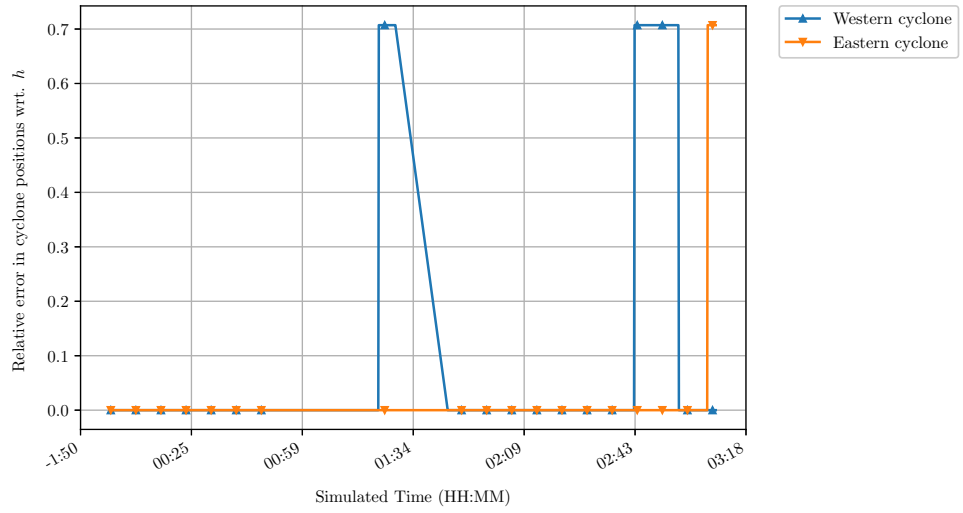

(a) Error in position

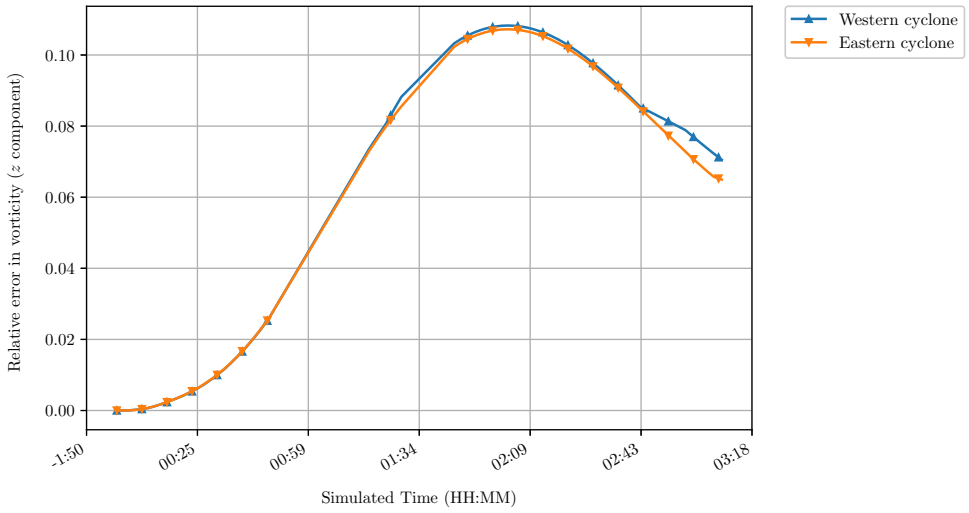

(b) Error in vorticity

Figure A.21.: Relative error in cyclone positions and corresponding vorticities at $z = 9343.75\ m$.

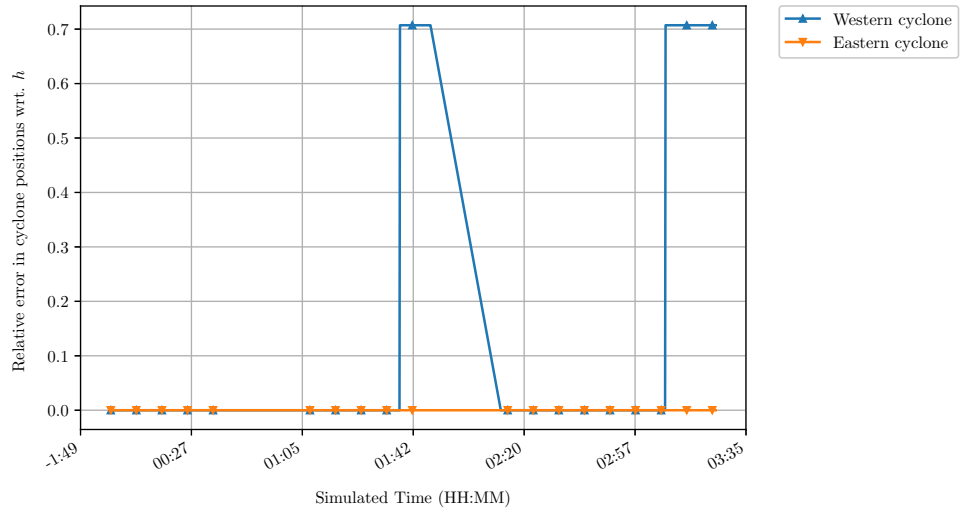

(a) Error in position

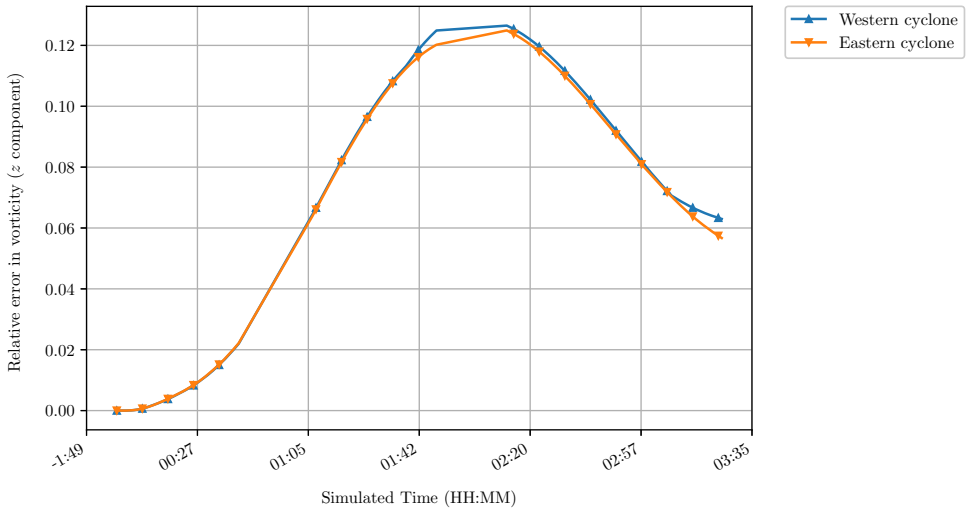

(b) Error in vorticity

Figure A.22.: Relative error in cyclone positions and corresponding vorticities at $z = 9750\ m$.

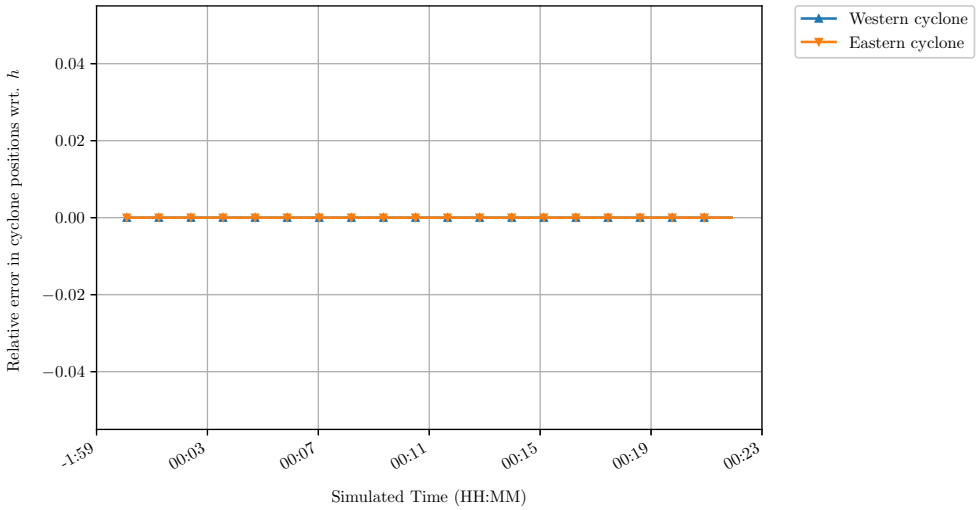

(a) Error in position

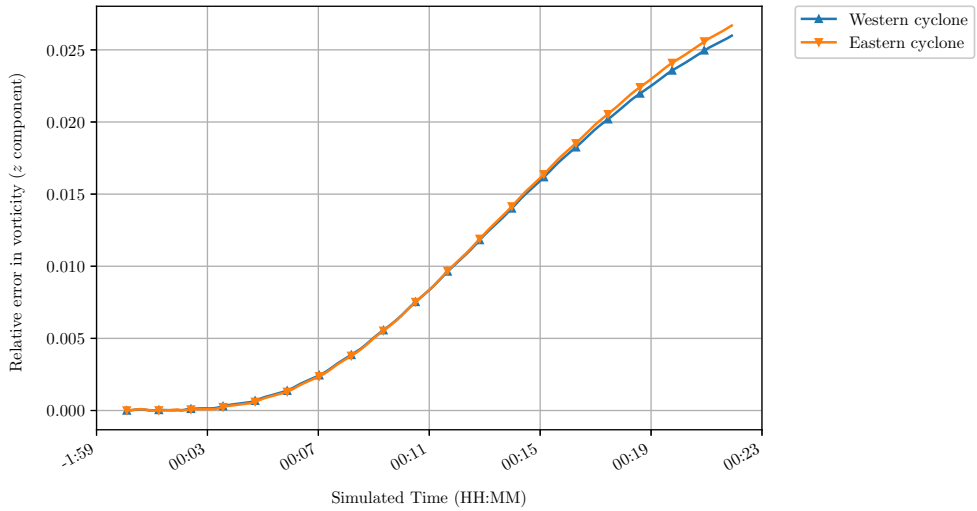

(b) Error in vorticity

Figure A.23.: Relative error in cyclone positions and corresponding vorticities at $z = 10,562.5\ m$.

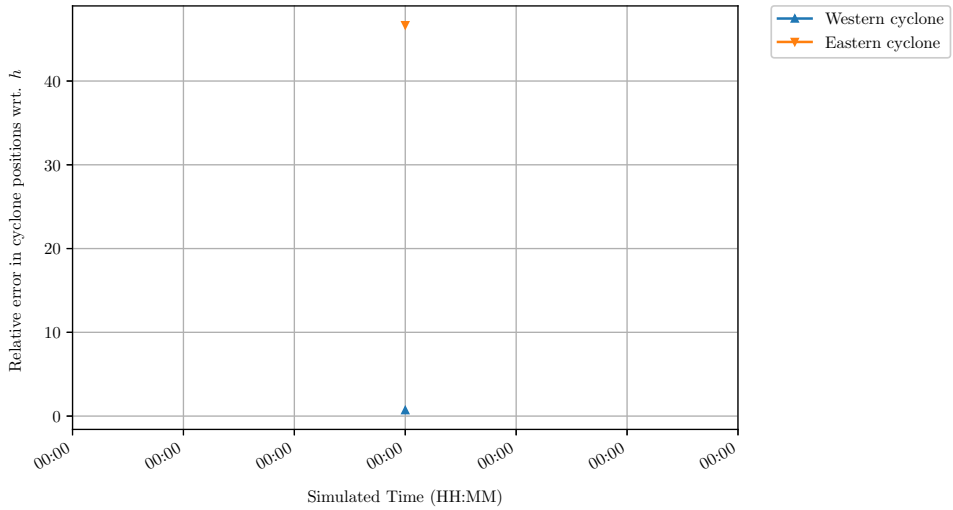

(a) Error in position

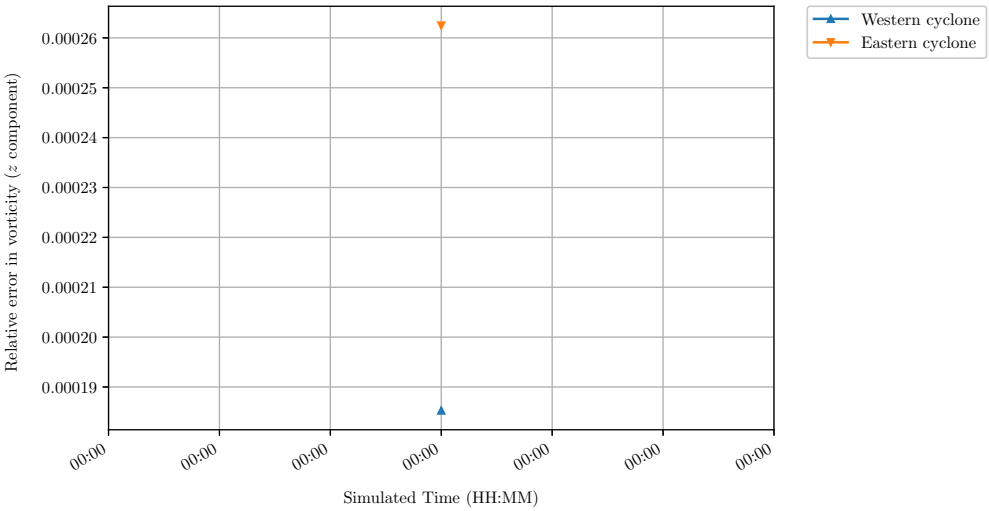

(b) Error in vorticity

Figure A.24.: Relative error in cyclone positions and corresponding vorticities at $z = 10,968.75\ m$.

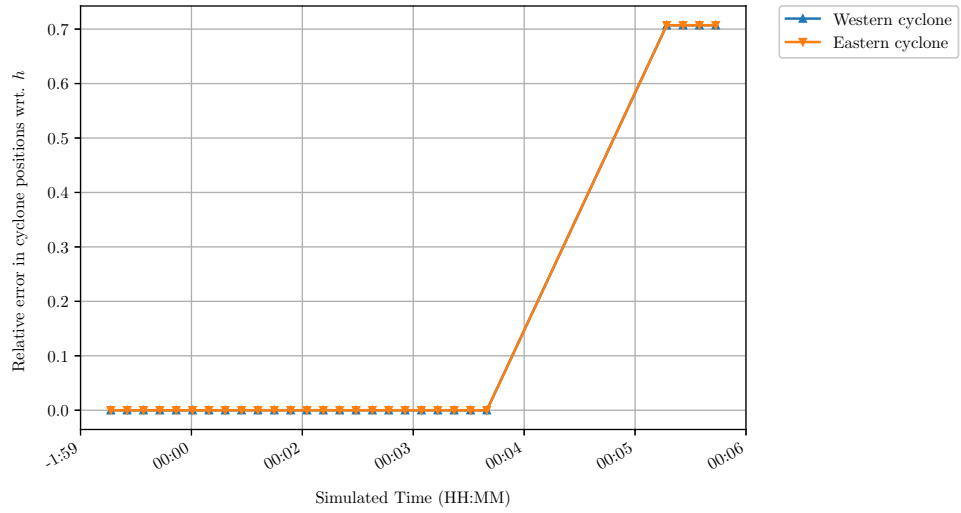

(a) Error in position

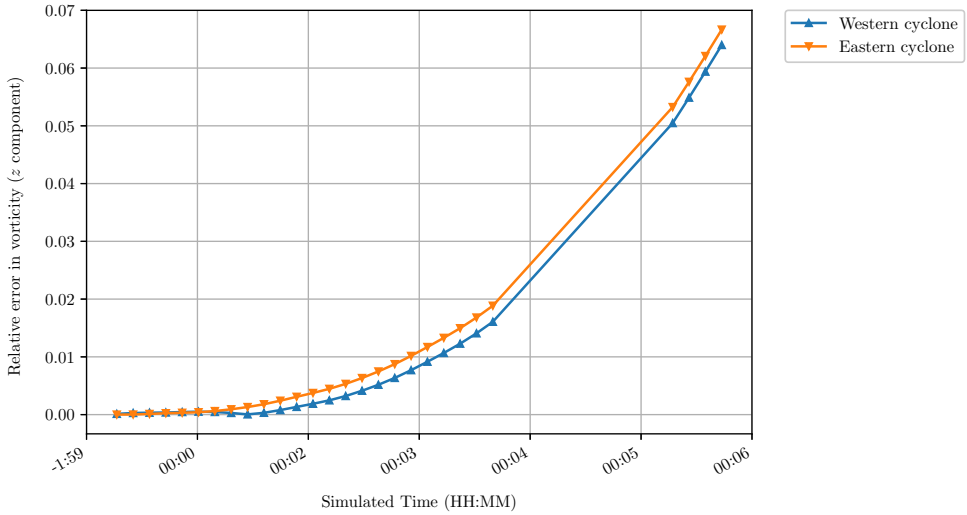

(b) Error in vorticity

Figure A.25.: Relative error in cyclone positions and corresponding vorticities at $z = 11,375\ m$.

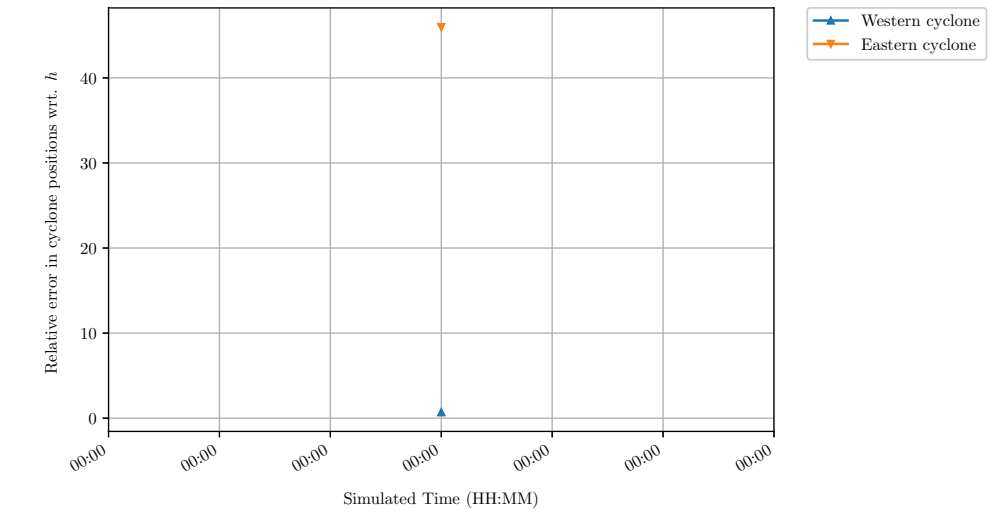

(a) Error in position

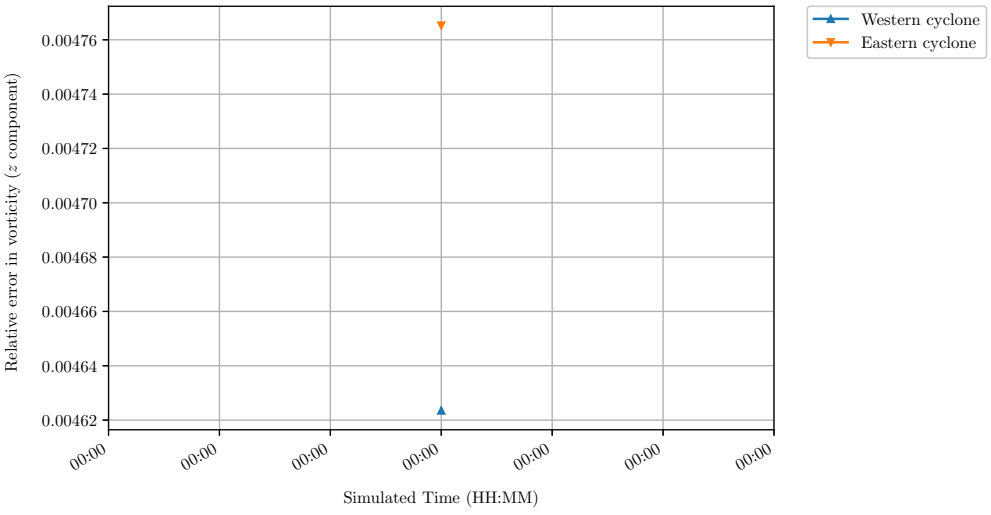

(b) Error in vorticity

Figure A.26.: Relative error in cyclone positions and corresponding vorticities at $z = 11,781.25\ m$.

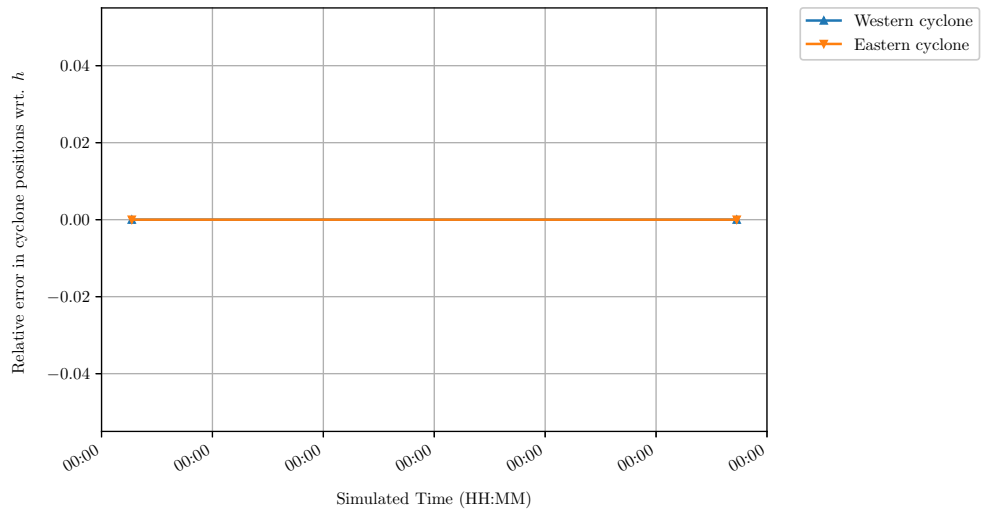

(a) Error in position

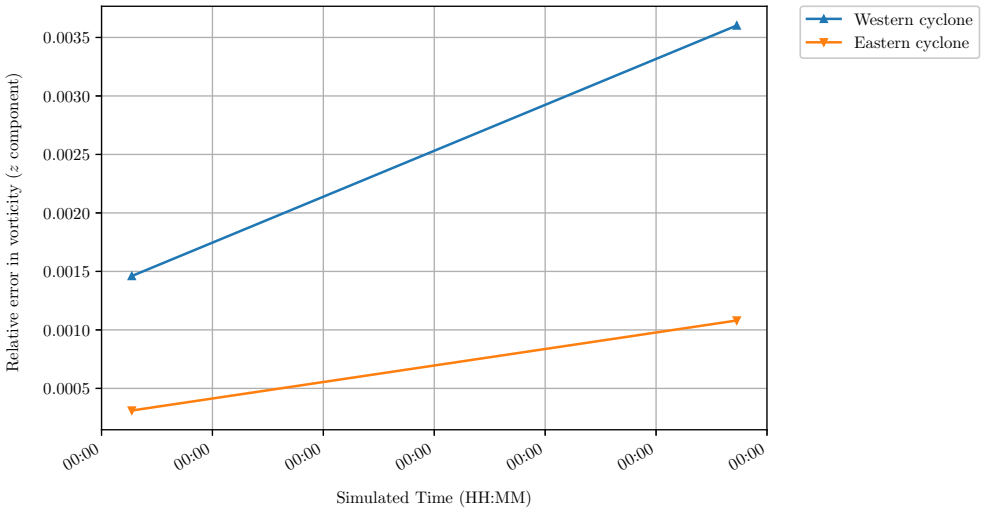

(b) Error in vorticity

Figure A.27.: Relative error in cyclone positions and corresponding vorticities at $z = 12,187.5\ m$.

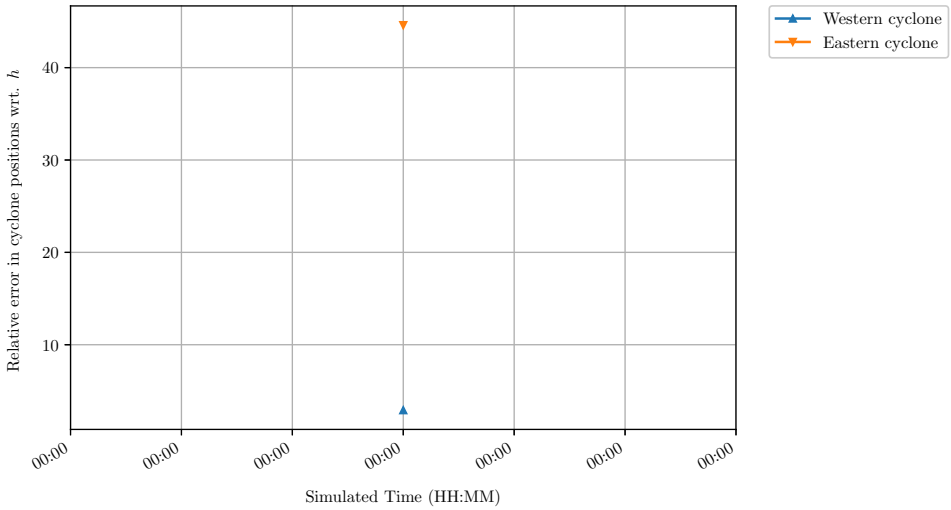

(a) Error in position

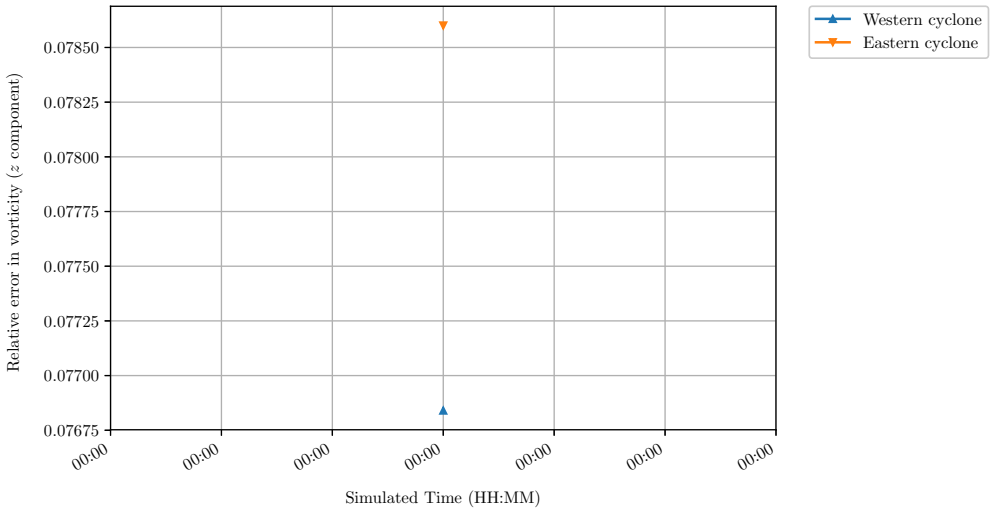

(b) Error in vorticity

Figure A.28.: Relative error in cyclone positions and corresponding vorticities at $z = 12,593.75\ m$.

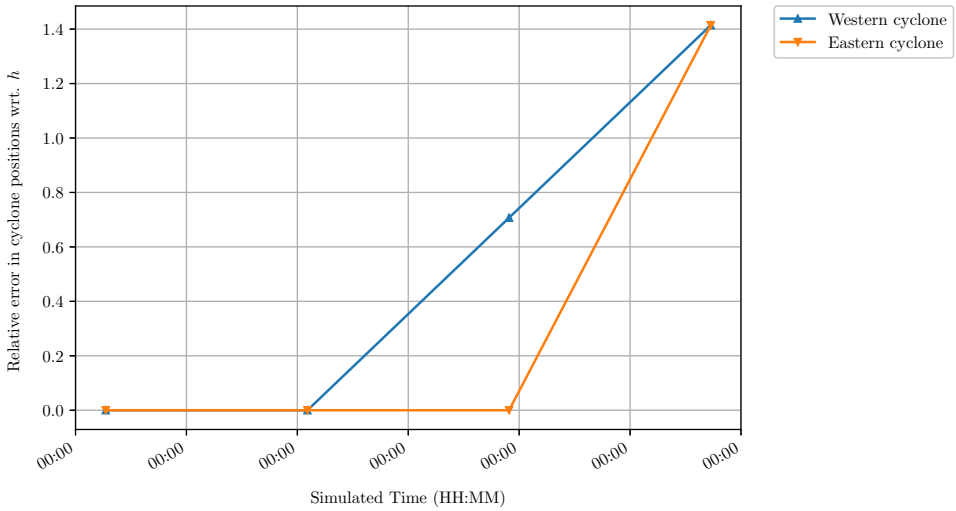

(a) Error in position

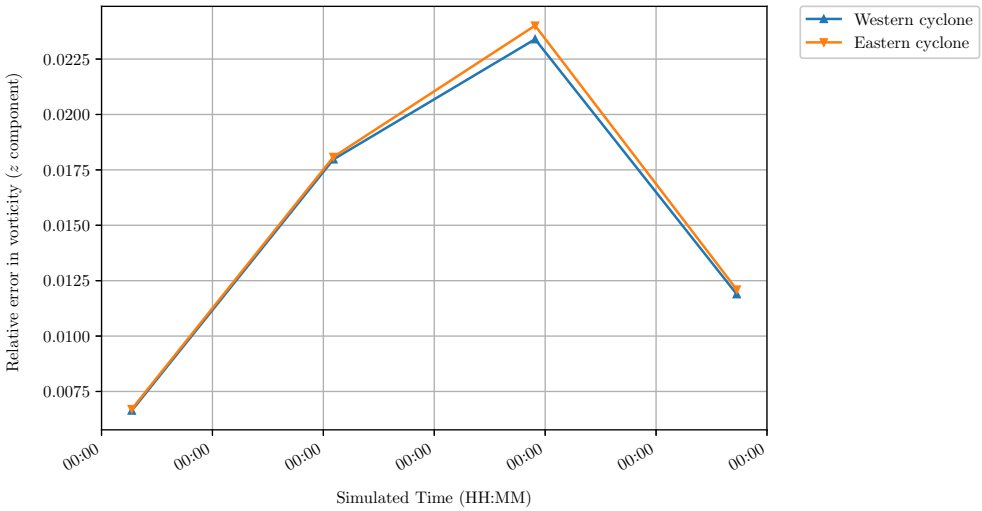

(b) Error in vorticity

Figure A.29.: Relative error in cyclone positions and corresponding vorticities at $z = 13,000\,m$.

Bibliography

[1] J Ed Akin et al. "Stabilization Parameters and Smagorinsky Turbulence Model". In: *Journal of Applied Mechanics* 70.1 (2003), p. 2. ISSN: 00218936. DOI: 10.1115/1.1526569.

[2] Hans Wilhelm Alt. *Lineare Funktionalanalysis*. 6th ed. Springer Berlin Heidelberg, 2012, XIII, 415 S. ISBN: 978-3-642-22260-3. DOI: 10.1007/978-3-642-22261-0.

[3] Matias Avila. "Finite element variational multiscale formulation for low Mach number flows coupled with radiative heat transfer". PhD thesis. Universitat Politècnica de Catalunya, 2012.

[4] Matias Avila, Javier Principe, and Ramon Codina. "A finite element dynamical nonlinear subscale approximation for the low Mach number flow equations". In: *Journal of Computational Physics* 230.22 (Sept. 2011), pp. 7988–8009. ISSN: 00219991. DOI: 10.1016/j.jcp.2011.06.032.

[5] Allison H. Baker, Martin Schulz, and Ulrike M. Yang. "On the performance of an algebraic multigrid solver on multicore clusters". In: *Lecture Notes in Computer Science (including subseries Lecture Notes in Artificial Intelligence and Lecture Notes in Bioinformatics)*. Vol. 6449 LNCS. 2011, pp. 102–115. ISBN: 9783642193279. DOI: 10.1007/978-3-642-19328-6_12.

[6] Allison H. Baker et al. "Challenges of scaling algebraic multigrid across modern multicore architectures". In: *Proceedings - 25th IEEE International Parallel and Distributed Processing Symposium, IPDPS 2011*. Anchorage, AK, USA: Conference Proceedings, IEEE, 2011, pp. 275–286. ISBN: 9780769543857. DOI: 10.1109/IPDPS.2011.35.

[7] Allison H. Baker et al. "Multigrid Smoothers for Ultraparallel Computing". In: *SIAM Journal on Scientific Computing* 33 (2011), pp. 2864–2887. ISSN: 1064-8275. DOI: 10.1137/100798806.

[8] Allison H. Baker et al. "Scaling Algebraic Multigrid Solvers: On the Road to Exascale". In: *Competence in High Performance Computing 2010*. Berlin, Heidelberg: Springer Berlin Heidelberg, 2011, pp. 215–226. ISBN: 978-3-642-24024-9. DOI: 10.1007/978-3-642-24025-6_18.

[9] Allison H. Baker et al. "Scaling hypre's multigrid solvers to 100,000 cores". In: *High Performance Scientific Computing: Algorithms and Applications*. Ed. by Michael W. Berry et al. Springer, 2012. ISBN: 1447124367 9781447124368.

[10] Pavan Balaji et al. "MPI on a Million Processors". In: *Lecture Notes in Computer Science*. Vol. 5759. Springer Berlin Heidelberg, 2009, pp. 20–30. ISBN: 978-3-642-03769-6. DOI: 10.1007/978-3-642-03770-2_9.

[11] Martin Baumann. "Numerical Simulation of Tropical Cyclones using Goal-Oriented Adaptivity". PhD thesis. Karlsruher Institut für Technologie (KIT), 2011.

[12] Martin Baumann et al. "Goal-oriented adaptivity for idealised tropical cyclones: A binary interaction scenario". In: *Meteorologische Zeitschrift* 24.3 (Apr. 2015), pp. 269–292. ISSN: 0941-2948. DOI: 10.1127/metz/2015/0591.

[13] R. Becker, M. Braack, and R. Rannacher. "Numerical simulation of laminar flames at low Mach number by adaptive finite elements". In: *Combustion Theory and Modelling* 3.3 (Sept. 1999), pp. 503–534. ISSN: 1364-7830. DOI: 10.1088/1364-7830/3/3/305.

[14] Michele Benzi, Gene H. Golub, and Jörg Liesen. "Numerical solution of saddle point problems". In: *Acta Numerica* 14 (May 2005), pp. 1–137. ISSN: 0962-4929. DOI: 10.1017/S0962492904000212.

[15] Malte Braack. *Finite Elemente*. Lecture notes. Mathematisches Seminar, Christian-Albrechts-Universität zu Kiel, 2015.

[16] Malte Braack and Thomas Richter. "Stabilized finite elements for 3D reactive flows". In: *International Journal for Numerical Methods in Fluids* 51.9-10 (July 2006), pp. 981–999. ISSN: 0271-2091. DOI: 10.1002/fld.1160.

[17] M. Braack et al. "Stabilized finite element methods for the generalized Oseen problem". In: *Computer Methods in Applied Mechanics and Engineering* 196.4-6 (Jan. 2007), pp. 853–866. ISSN: 00457825. DOI: 10.1016/j.cma.2006.07.011.

[18] Dietrich Braess. *Finite Elemente*. 4th ed. Berlin, Heidelberg: Springer Berlin Heidelberg, 2007, XVIII, 357 S. ISBN: 978-3-540-72449-0. DOI: 10.1007/978-3-540-72450-6. arXiv: arXiv:1011.1669v3.

[19] Jed Brown et al. "Composable Linear Solvers for Multiphysics". In: *2012 11th International Symposium on Parallel and Distributed Computing*. IEEE, June 2012, pp. 55–62. ISBN: 978-1-4673-2599-8. DOI: 10.1109/ISPDC.2012.16.

[20] Edmond Chow, Andrew J. Cleary, and Robert D. Falgout. "Design of the hypre Preconditioner Library". In: *In SIAM Workshop on Object Oriented Methods for Inter-operable Scientific and Engineering Computing*. Ed. by Mike Henderson, Chris Anderson, and Steve Lyons. SIAM, 1998, pp. 106–116.

[21] Edmond Chow et al. "A Survey of Parallelization Techniques for Multigrid Solvers". In: *Parallel Processing for Scientific Computing*. Ed. by M. A. Heroux, P. Raghavan, and H. D. Simon. SIAM Series on Software, Environments, and Tools, 2006. Chap. 10, pp. 179–195. ISBN: 9780898716191.

[22] Andrew J. Cleary et al. "Robustness and scalability of algebraic multigrid". In: *SIAM J. Sci. Comput.* 21.UCRL-JC-130718 (2000), pp. 1886–1908.

[23] Eric C. Cyr, John N. Shadid, and Raymond S. Tuminaro. "Stabilization and scalable block preconditioning for the Navier–Stokes equations". In: *Journal of Computational Physics* 231.2 (Jan. 2012), pp. 345–363. ISSN: 00219991. DOI: 10.1016/j.jcp.2011.09.001.

[24] Anurag Dipankar et al. "Large eddy simulation using the general circulation model ICON". In: *Journal of Advances in Modeling Earth Systems* 7.3 (Sept. 2015), pp. 963–986. ISSN: 19422466. DOI: 10.1002/2015MS000431.

[25] Günther Doms and Ulrich Schättler. *A description of the nonhydrostatic regional model LM, Part I: Dynamics and Numerics*. Tech. rep. Offenbach: Deutscher Wetterdienst, 2002.

[26] Max Duarte, Ann S. Almgren, and John B. Bell. "A Low Mach Number Model for Moist Atmospheric Flows". In: *Journal of the Atmospheric Sciences* 72.4 (Apr. 2015), pp. 1605–1620. ISSN: 0022-4928. DOI: 10.1175/JAS-D-14-0248.1.

[27] Christof Eck, Harald Garcke, and Peter Knabner. *Mathematische Modellierung*. Springer-Lehrbuch. Berlin, Heidelberg: Springer Berlin Heidelberg, 2011. ISBN: 978-3-642-18423-9. DOI: 10.1007/978-3-642-18424-6. arXiv: arXiv:1011.1669v3.

[28] Stanley C. Eisenstat and Homer F. Walker. "Choosing the Forcing Terms in an Inexact Newton Method". In: *SIAM J. Sci. Comput.* 17.1 (1996), pp. 16–32.

[29] Lawrence C. Evans. *Partial Differential Equations*. 2nd ed. American Mathematical Society, 2010. ISBN: 978-0-8218-4974-3.

[30] Robert D. Falgout. "A Note on the Relationship Between Adaptive AMG and PCG". In: *LLNL Technical Report UCRL-TR-205838* (2004).

[31] Robert D. Falgout. *An introduction to algebraic multigrid*. 2006. DOI: 10.1109/MCSE.2006.105.

[32] Robert D. Falgout and Jim E. Jones. "Multigrid on Massively Parallel Architectures". In: *Multigrid Methods*. Ed. by Erik Dick, Kris Riemslagh, and Jan Vierendeels. VI. Vol. 14. Springer-Verlag, 2000, pp. 101–107. ISBN: 978-3-540-67157-2.

[33] Robert D. Falgout and Panayot S. Vassilevski. "On Generalizing the Algebraic Multigrid Framework". In: *SIAM Journal on Numerical Analysis* 42.4 (Jan. 2004), pp. 1669–1693. ISSN: 0036-1429. DOI: 10.1137/S0036142903429742.

[34] Robert D. Falgout and Ulrike Meier Yang. "hypre: A Library of High Performance Preconditioners". In: *Lecture Notes in Computer Science*. Ed. by Peter M. A. Sloot et al. Vol. 2331. Springer Berlin Heidelberg, 2002, pp. 632–641. ISBN: 978-3-540-43594-5. DOI: 10.1007/3-540-47789-6_66.

[35] S. Fujiwhara. "On the growth and decay of vortical systems". In: *Quarterly Journal of the Royal Meteorological Society* 49.206 (Aug. 2007), pp. 75–104. ISSN: 00359009. DOI: 10.1002/qj.49704920602.

[36] S. Fujiwhara. "The natural tendency towards symmetry of motion and its application as a principle in meteorology". In: *Quarterly Journal of the Royal Meteorological Society* 47.200 (Aug. 2007), pp. 287–292. ISSN: 00359009. DOI: 10.1002/qj.49704720010.

[37] Hormozd Gahvari et al. "Systematic Reduction of Data Movement in Algebraic Multigrid Solvers". In: *Proceedings of the 2013 IEEE 27th International Symposium on Parallel & Distributed Processing Workshops and PhD Forum (IPDPSW 2013)* LLNL-CONF-587832 (2013).

[38] Van Emden Henson and Ulrike Meier Yang. "BoomerAMG: A parallel algebraic multigrid solver and preconditioner". In: *Applied Numerical Mathematics*. Vol. 41. 1. 2002, pp. 155–177. DOI: 10.1016/S0168-9274(01)00115-5.

[39] Magnus Rudolph Hestenes and Eduard Stiefel. "Methods of conjugate gradients for solving linear systems". In: *Journal of Research of the Natural Bureau of Standards (NBS)* 49.6 (1952), pp. 409–436. ISSN: 0091-0635. DOI: 10.6028/jres.049.044. arXiv: 1102.0183.

[40] Vincent Heuveline. "On higher-order mixed FEM for low Mach number flows: application to a natural convection benchmark problem". In: *International Journal for Numerical Methods in Fluids* 41.12 (Apr. 2003), pp. 1339–1356. ISSN: 0271-2091. DOI: 10.1002/fld.454.

[41] Vincent Heuveline. "HiFlow^3". In: *Proceedings of the 9th Workshop on Parallel/High-Performance Object-Oriented Scientific Computing - POOSC '10*. New York, New York, USA: ACM Press, 2010, pp. 1–6. ISBN: 9781450305464. DOI: 10.1145/2039312.2039316.

[42] James R. Holton and Gregory J. Hakim. *An Introduction the Dynamic Meteorology*. 5th ed. Academic Press, 2012. ISBN: 9780123848666.

[43] Thomas J. R. Hughes, Guglielmo Scovazzi, and Tayfun E. Tezduyar. "Stabilized Methods for Compressible Flows". In: *Journal of Scientific Computing* 43.3 (June 2010), pp. 343–368. ISSN: 0885-7474. DOI: 10.1007/s10915-008-9233-5.

[44] *hypre Reference Manual - Version 2.10.1*. URL: http://computation.llnl.gov/sites/default/files/public/hypre-2.10.1_ref_manual.pdf.

[45] *hypre User's Manual - Version 2.10.1*. URL: http://computation.llnl.gov/sites/default/files/public/hypre-2.10.1_usr_manual.pdf.

[46] Mark Z. Jacobson. *Fundamentals of Atmospheric Modeling*. 2nd ed. Cambridge University Press, 2005. ISBN: 978-0-521-54865-6.

[47] Bo-Nan Jiang and Louis A. Povinelli. "Least-squares finite element method for fluid dynamics". In: *Computer Methods in Applied Mechanics and Engineering* 81.1 (July 1990), pp. 13–37. ISSN: 00457825. DOI: 10.1016/0045-7825(90)90139-D.

[48] V. John et al. "A comparison of three solvers for the incompressible Navier-Stokes equations". In: *LSSC*. 1999.

[49] C. T. Kelley. *Iterative Methods for Linear and Nonlinear Equations*. Society for Industrial and Applied Mathematics, Philadelphia, Jan. 1995. ISBN: 978-0-89871-352-7. DOI: 10.1137/1.9781611970944.

[50] Konrad Königsberger. *Analysis 2*. 5th ed. Springer-Lehrbuch. Berlin, Heidelberg: Springer Berlin Heidelberg, 2004, p. 459. ISBN: 978-3-540-20389-6. DOI: 10.1007/3-540-35077-2.

[51] William Layton. *Introduction to the Numerical Analysis of Incompressible Viscous Flows*. SIAM, 2008. ISBN: 978-0-898716-57-3. DOI: 10.1137/1.9780898718904.

[52] Andrew Majda. *Compressible Fluid Flow and Systems of Conservation Laws in Several Space Variables*. Vol. 53. Applied Mathematical Sciences. Springer New York, 1984. ISBN: 978-0-387-96037-1. DOI: 10.1007/978-1-4612-1116-7.

[53] *Massage Passing Interface (MPI) Forum*. URL: http://www.mpi-forum.org/.

[54] Andreas Meister. *Numerik linearer Gleichungssysteme*. 5th ed. Wiesbaden: Springer Fachmedien Wiesbaden, 2015. ISBN: 978-3-658-07199-8. DOI: 10.1007/978-3-658-07200-1.

[55] Bram Metsch. "Algebraic multigrid (AMG) for saddle point systems". PhD thesis. Rheinische Friedrich-Wilhelms-Universität Bonn, 2013.

[56] Bernhard Müller. *Computation of Compressible Low Mach Number Flow*. 1996.

[57] Bernhard Müller. "Low-Mach-Number Asymptotics of the Navier-Stokes Equations". In: *Journal of Engineering Mathematics* 34.1/2 (1998), pp. 97–109. ISSN: 00220833. DOI: 10.1023/A:1004349817404.

[58] Jorge Nocedal and Stephen J. Wright. *Numerical Optimization*. 2nd ed. Springer Series in Operations Research and Financial Engineering. Springer New York, 2006. ISBN: 978-0-387-30303-1. DOI: 10.1007/978-0-387-40065-5. arXiv: NIHMS150003.

[59] Antonín Novotný and Ivan Straškraba. *Introduction to the Mathematical Theory of Compressible Flow*. Oxford University Press, New York, 2004. ISBN: 978-0-19-853084-8.

[60] Pavel Plotnikov and Jan Sokołowski. *Compressible Navier-Stokes Equations*. Springer Basel, 2012. ISBN: 978-3-0348-0366-3. DOI: 10.1007/978-3-0348-0367-0.

[61] Alfio Quarteroni and Alberto Valli. *Numerical approximation of partial differential equations*. Vol. 23. Springer Series in Computational Mathematics. Berlin, Heidelberg: Springer Berlin Heidelberg, 2008, 543 S. ISBN: 9783540852674. DOI: 10.1007/978-3-540-85268-1.

[62] Rolf Rannacher. *Numerische Mathematik 3 (Numerik von Problemen der Kontinuumsmechanik)*. 2008.

[63] Andrea D. F. Richter. "Untersuchungen zur Wechselwirkung tropischer Wirbelstürme mit Hilfe eines idealisierten dreidimensionalen numerischen Modells". Diplomarbeit. Karlsruher Institut für Technologie (KIT), 2012.

[64] Youcef Saad. "A Flexible Inner-Outer Preconditioned GMRES Algorithm". In: *SIAM Journal on Scientific Computing* 14.2 (Mar. 1993), pp. 461–469. ISSN: 1064-8275. DOI: 10.1137/0914028.

[65] Yousef Saad. "Parallel iterative methods for sparse linear systems". In: *Studies in Computational Mathematics* 8.C (2001), pp. 423–440. ISSN: 1570579X. DOI: 10.1016/S1570-579X(01)80025-2.

[66] Yousef Saad. *Iterative Methods for Sparse Linear Systems*. 2nd ed. Society for Industrial and Applied Mathematics, 2003. ISBN: 0898715342. DOI: 10.2113/gsjfr.6.1.30. arXiv: 0806.3802.

[67] Yousef Saad and Martin H. Schultz. "GMRES: A Generalized Minimal Residual Algorithm for Solving Nonsymmetric Linear Systems". In: *SIAM Journal on Scientific and Statistical Computing* 7.3 (1986), pp. 856–869. ISSN: 0196-5204. DOI: 10.1137/0907058.

[68] A. Segal, M. ur Rehman, and C. Vuik. "Preconditioners for Incompressible Navier-Stokes Solvers". In: *Numerical Mathematics: Theory, Methods and Applications* 3.3 (2010), pp. 245–275. ISSN: 10048979. DOI: 10.4208/nmtma.2010.33.1.

[69] David Shirokoff and Rodolfo Ruben Rosales. "An efficient method for the incompressible Navier-Stokes equations on irregular domains with no-slip boundary conditions, high order up to the boundary". In: *Journal of Computational Physics* 230.23 (Nov. 2010), pp. 8619–8646. DOI: 10.1016/j.jcp.2011.08.011. arXiv: 1011.3589.

[70] Josef Stoer and Roland Bulirsch. *Numerische Mathematik 2*. 5. Auflage. Springer-Verlag Berlin Heidelberg, 2005.

[71] K. Stüben. "Algebraic multigrid (AMG): an introduction with applications". In: *GMD Report* 70 (1999), pp. 1–127.

[72] Tayfun E. Tezduyar. "Stabilized Finite Element Formulations for Incompressible Flow Computations". In: *Advances in Applied Mechanics*. Vol. 28. C. 1991, pp. 1–44. ISBN: 9780120020287. DOI: 10.1016/S0065-2156(08)70153-4.

[73] Tayfun E. Tezduyar and Yasuo Osawa. "Finite element stabilization parameters computed from element matrices and vectors". In: *Computer Methods in Applied Mechanics and Engineering* 190 (2000), pp. 411–430. ISSN: 00457825. DOI: 10.1016/S0045-7825(00)00211-5.

[74] Tayfun E. Tezduyar and Masayoshi Senga. "Stabilization and shock-capturing parameters in SUPG formulation of compressible flows". In: *Computer Methods in Applied Mechanics and Engineering* 195.13-16 (Feb. 2006), pp. 1621–1632. ISSN: 00457825. DOI: 10.1016/j.cma.2005.05.032.

[75] H. A. van der Vorst. "Bi-CGSTAB: A Fast and Smoothly Converging Variant of Bi-CG for the Solution of Nonsymmetric Linear Systems". In: *SIAM Journal on Scientific and Statistical Computing* 13.2 (Mar. 1992), pp. 631–644. ISSN: 0196-5204. DOI: 10.1137/0913035.

[76] Dirk Werner. *Funktionalanalysis*. 6. Auflage. Springer-Lehrbuch. Springer Berlin Heidelberg, 2011. ISBN: 978-3-642-21016-7. DOI: 10.1007/978-3-642-21017-4.

[77] Ulrike Meier Yang. "On the use of relaxation parameters in hybrid smoothers". In: *Numerical Linear Algebra with Applications* 11.2-3 (2004), pp. 155–172. ISSN: 10705325. DOI: 10.1002/nla.375.

[78] Ulrike Meier Yang. *Numerical Solution of Partial Differential Equations on Parallel Computers*. Ed. by Are Magnus Bruaset and Aslak Tveito. Vol. 51. Lecture Notes in Computational Science and Engineering. Berlin/Heidelberg: Springer-Verlag, 2006, pp. 209–236. ISBN: 3-540-29076-1. DOI: 10.1007/3-540-31619-1. arXiv: arXiv:1011.1669v3.